CONDITION MONITORING OF HELICAL GEAR TRANSMISSIONS BASED ON VIBRATION MODELLING AND SIGNAL PROCESSING

A THESIS SUBMITTED IN PARTIAL FULFILMENT OF THE REQUIREMENT FOR THE DEGREE OF DOCTOR OF PHILOSOPHY AT THE UNIVERSITY OF HUDDERSFIELD

By

KHALDOON F. BRETHEE

M.Sc. University of Anbar, Iraq, 2003.
B.Sc. University of Anbar, Iraq, 2000.

School of Computing and Engineering

University of Huddersfield

UK

August 2017

COPYRIGHT

Copyright statement

i. The author of this thesis (including any appendices and/or schedules to this thesis) owns any copyright in it (the "Copyright") and s/he has given The University of Huddersfield the right to use such copyright for any administrative, promotional, educational and/or teaching purposes.

ii. Copies of this thesis, either in full or in extracts, may be made only in accordance with the regulations of the University Library. Details of these regulations may be obtained from the Librarian. This page must form part of any such copies made.

iii. The ownership of any patents, designs, trademarks and any and all other intellectual property rights except for the Copyright (the "Intellectual Property Rights") and any reproductions of copyright works, for example graphs and tables ("Reproductions"), which may be described in this thesis, may not be owned by the author and may be owned by third parties. Such Intellectual Property Rights and Reproductions cannot and must not be made available for use without the prior written permission of the owner(s) of the relevant Intellectual Property Rights and/or Reproductions.

ABSTRACT

Condition monitoring (CM) of gear transmission has attracted extensive research in recent years. In particular, the detection and diagnosis of its faults in their early stages to minimise cost by maximising time available for planned maintenance and giving greater opportunity for avoiding a system breakdown. However, the diagnostic results obtained from monitored signals are often unsatisfactory because mainstream technologies using vibration response do not sufficiently account for the effect of friction and lubrication. To develop a more advanced and accurate diagnosis, this research has focused on investigating the nonlinearities of vibration generation and transmission with the viscoelastic properties of lubrication, to provide an in-depth understanding of vibration generating mechanisms and hence develop more effective signal processing methods for early detection and accurate diagnosis of gear incipient faults.

A comprehensive dynamic model has been developed to study the dynamic responses of a multistage helical gear transmission system. It includes not only time-varying stiffness but also tooth friction forces based on an elastohydrodynamic lubrication (EHL) model. In addition, the progression of a light wear process is modelled by reducing stiffness function profile, in which the 2^{nd} and 3^{rd} harmonics of the meshing frequency (and their sidebands) show significant alteration that support fault diagnostic at early stages. Numerical and experimental results show that the friction and progressive wear induced vibration excitations will change slightly the amplitudes of the spectral peaks at both the mesh frequency and its sideband components at different orders, which provides theoretical supports for extracting reliable diagnostic signatures.

As such changes in vibrations are extremely small and submerged in noise, it is clear that effective techniques for enhancing the signal-to-noise ratio, such as time synchronous averaging (TSA) and modulation signal bispectrum (MSB) are required to reveal such changes. MSB is preferred as it allows small amplitude sidebands to be accurately characterised in a nonlinear way without information loss and does not impose any addition demands regarding angular displacement measurement as does TSA.

With the successful diagnosis of slight wear in helical gears, the research progressed to validate the capability of MSB based methods to diagnose four common gear faults relating to gear tribological conditions; lubrication shortfall, changes in lubrication viscosity, water in oil, and increased bearing clearances. The results show that MSB signatures allows accurate differentiation between these small changes, confirming the model and signal processing proposed in this thesis.

DECLARATION

This dissertation is submitted for the degree of Doctor of Philosophy at the University of Huddersfield. I hereby declare that the work in this dissertation was carried out in accordance with the Regulations of the University of Huddersfield.

This work is original except where acknowledgement and references are made to the previous work. Neither this nor any substantially similar dissertation has been or is being submitted for a degree, diploma or other qualification at any other university.

Khaldoon F. Brethee

Acknowledgements

All thanks and praise to Almighty **ALLAH** (God) for giving me the strength, knowledge, blessings and the opportunity to undertake this research study in spite of the current situation in my home country of Iraq.

I am deeply indebted to my supervisors, **Prof. Andrew Ball** and **Dr Fengshou Gu**, for their support, encouragement and guidance throughout this research. Their understanding and kindness guided me to perform experimental work to the highest standards and develop a robust theoretical framework in a logical and consistent way. I would like to express my appreciation and deepest gratitude for their motivation to attend conferences and write scientific publications.

I would like to give my grateful acknowledgements to the Higher Committee for Education Development in Iraq (**HCED**) and the University of Anbar for their financial supports during my PhD studies.

I would like to dedicate this work to my family particularly: my mother, the memory of my unforgettable father and brother, my sisters, my wife and my children. They were always supporting me and encouraging me a lot with their best wishes and warm-hearted help in life support.

Also, I would like to extend my gratitude with deeply thankful to all colleagues at the Centre for Efficiency and Performance Engineering (**CEPE**) and staff members of the University of Anbar, especially **Mr. Rashaq Abdullah**, for their helps and support over the last few years. I also highly appreciate the help from **Mr. Dlir Albarzenji** and his family, and all my friends who gave me a help or even advice in my life and research.

May the Almighty God richly bless all of you.

Statement of Originality

I hereby certify that all of the work described within this thesis is the original work of the author. Any published (or unpublished) ideas and/or techniques from the work of others are fully acknowledged in accordance with the standard referencing practices.

(Khaldoon F. Brethee)

PUBLICATIONS

Papers for Journals:

1. Brethee, K., Zhen D. Gu, F. and Ball, A. (2017) 'Helical Gear Wear Monitoring: Modelling and Experimental Validation' *Mechanism and Machine Theory*, 117, pp. 210-229. ISSN: 0094-114X.
2. Brethee, K. Gu, F. and Ball, A. (2017) 'Condition Monitoring of Lubricant Starvation Based on Gearbox Vibration Signatures'. *International Journal of COMADEM*, Special Issue (accepted).
3. Brethee, K., Gu, F. and Ball, A. (2016) 'Frictional effects on the dynamic responses of gear systems and the diagnostics of tooth breakages' *Systems Science & Control Engineering* , 4 (1), pp. 270-284. ISSN 2164-258.

Papers for Conferences:

1. Brethee, K. Gu, F. and Ball, A. (2017) 'Monitoring of Water Contamination in Gearbox Lubricant Based on Vibration Analysis'. *In: COMADEM 2017, the 30th International Congress on Condition Monitoring and Diagnostic Engineering Management, 10th-13th July 2017,* University of Central Lancashire, UK.

2. Brethee, K., Zhang, R., Hamad, N., Gu, F. and Ball, A. (2016) 'Influence of Lubricant Starvation on Gearbox Vibration Signatures for Condition Monitoring'. *In: COMADEM 2016, the 29th International Congress on Condition Monitoring and Diagnostic Engineering Management, 20th-22nd August 2016*, Empark Grand Hotel in Xi'an, China.

3. Brethee, K., Zhou, X., Gu, F. and Ball, A. (2016) 'Frictional Effects on the Diagnostics of Helical Gear Tooth Defects'. *In: IncoME 2016, 30th - 31st August 2016,* Manchester Conference Centre, Manchester.

4. Brethee, K., Gao, J., Ball, A. and Gu, F. (2015) 'Analysis of Frictional Effects on the Dynamic Response of Gear Systems and the Implications for Diagnostics'. *In: Proceedings of the 21st International Conference on Automation and Computing (ICAC'15)* IEEE, University of Strathclyde, Glasgow, UK, 11-12 September 2015, ISBN 978-0-9926801-0-7.

5. Haba, U., Brethee, K., Hassin, O., Gu, F. and Ball, A. (2017) 'Detection and Diagnosis of Reciprocating Compressor Faults Based on Modulation Signal Bispectrum Analysis of Vibrations. *In: COMADEM 2017, the 30th Conference on Condition Monitoring and Diagnostic Engineering Management, 10th-13th July 2017, University of Central Lancashire, UK.* ISBN: 9781909755109

6. Elforjani B., Xu, Y., Brethee, K., Wu Z., Gu, F. and Ball, A. (2017) 'Monitoring Gearbox Using a Wireless Temperature Node Powered by Thermal Energy Harvesting Module'. *In: Proceedings of the 23rd International Conference on Automation and Computing (ICAC'17),* University of Huddersfield, Huddersfield, UK, 7-8 September 2017, (accepted).

7. Hamad, N., Brethee, K., Gu, F. and Ball, A. (2016) 'An Investigation of Electrical Motor Parameters in a Sensorless Variable Speed Drive for Machine Fault Diagnosis'. *In: Proceedings 22nd International Conference on Automation and Computing (ICAC'16)* IEEE, University of Essex, Colchester, UK, 7-8 September 2016, ISBN 9781862181328.

8. Abusaad, S., Brethee, K., Assaeh, M., Zhang, R., Gu, F., & Ball, A. D. (2015, July). 'The detection of lubricating oil viscosity changes in gearbox transmission systems driven by sensorless variable speed drives using electrical supply parameters'. *In Journal of Physics: Conference Series* (Vol. 628, No. 1, p. 012078). IOP Publishing, 2015.

9. Abusaad, S., Benghozzi, A., Brethee, K., Gu, F. and Ball, A. (2014) 'Investigating the Effect of Water Contamination on Gearbox Lubrication based upon Motor Control Data from a Sensorless Drive'. *In: 3rd International Workshop and Congress on eMaintenance, 17th - 18th June 2014*, Lulea, Sweden.

Table of Contents

List of Figures

List of Tables

List of Abbreviations

AM	Amplitude modulation
AE	Acoustic emission
BL	Base line
CB	Conventional bispectrum
CF	Crest Factor
CM	Condition monitoring
DAQ	Data acquisition system
DFT	Discrete Fourier transform
DOF	Degree of freedom
EHL	Elasto-hydrodynamic lubrication
EP	Extreme pressure
FFT	Fast Fourier transform
FM	Frequency modulation
FRF	Frequency response function
GB1	First gearbox
GB2	Second/slave gearbox
GR	Gear ratio
HOS	Higher order spectra
ppm	Parts per million
IEPE	Internal electronic piezoelectric
LH	Left hand helical gear
LOA	Line of action
LL-600	600ml less than the recommended oil level
LL-1100	1100ml less than the recommended oil level
MSB	Modulation signal bispectrum
NDT	Non-destructive testing
ODE	Ordinary differential equation
OLOA	Off line of action
PLC	Programmable logic controller
RH	Right hand helical gear
RMS	Root mean square
SNR	Signal-to-noise ratio
TB	Tooth breakage
TE	Transmission error
TSA	Time synchronous averaged
Subscripts 1 and 2	First and second stages of the gearbox
Subscripts p and g	Pinion and gear

List of Nomenclatures

Symbol	Description	Unit
ω_p	Angular speed of pinion	rad/s
ω_g	Angular speed of gear	rad/s
r_p	Pitch radius of pinion	m
r_g	Pitch radius of gear	m
r_{ap}	Addendum radius of pinion	m
r_{ag}	Addendum radius of gear	m
r_{bp}	Base radius of pinion	m
r_{bg}	Base radius of gear	m
Z_p	Teeth number of pinion	-
Z_g	Teeth number of gear	-
ε_{ratio}	Total contact ratio	m
ε_α	Contact ratio	m
ε_β	Overlap ratio	m
β	Helix angle of helical gear	^{o}
β_b	Helix angle at base radius	^{o}
α_t	Transverse pressure angle	^{o}
p_c	Circular pitch of gear	m
p_b	Circular base pitch of gear	m
P_t	Circular transverse base pitch	m
P_{angle}	Pitch duration angle	^{o}
M_{double}	Meshing region of double pair of teeth	m
M_{single}	Meshing region of single pair of teeth	m
$L_i(t)$	Length of contact lines	m
$L_{ri}(t)$	Length of contact lines on right side of plane of action	m
$L_{li}(t)$	Length of contact lines on left side of plane of action	m
$L_{sum}(t)$	Total length of contact lines during meshing process	m
$DL_{ij}(t)$	Time varying of the length of meshing contact lines for i-contact pair and j-stage of gear meshing	m
n	Maximum number of contact teeth	-
k_o	Mesh stiffness density per unit length	N/m^2
$K_{mi}(t)$	Time-varying mesh stiffness	N/m
$N_{ji}(t)$	Time-varying contact force	N
$C_{mi}(t)$	Damping coefficient	Nm/s
I_p	Moment of inertia of pinion	m^4
I_g	Moment of inertia of gear	m^4
I_e	Equivalent moment of inertia of the meshing gears	m^4

$F_{ji}(t)$	Time-varying friction force	N
F_{p1}, F_{p0}	Friction force components of the pinion contact pairs	N
F_{g1}, F_{g0}	Friction force components of the gear contact pairs	N
$F_{fi}(t)$	Time-varying friction force of i^{th} segment of contact line	N
$T_{fi}(t)$	Time-varying friction torque of i^{th} segment of contact line	Nm
$N_i(t)$	Time-varying of resultant contact force of i^{th} segment line	N
μ	Friction coefficient	-
$\mu_i(t)$	Friction coefficient variation of i^{th} segment of contact line	-
ν_k	Kinematic viscosity of lubricant	m^2/s
ν_o	Dynamic viscosity of lubricant	$N\ s/m^2$
V_s	Relative sliding velocity	m/s
V_r	Gear rolling velocity	m/s
V_e	Entrainment meshing velocity	m/s
R	Combined radius of curvature	m
W'	Unit normal load	N
E'	Effective modulus of elasticity	N/m^2
P_{hx}	Maximum Hertzian pressure	N/m^2
P_{max}	Maximum contact pressure	N/m^2
S	Surface roughness	m
SR	slide-to-roll ratio	-
θ_p	Rotational angle of pinion	rad
θ_g	Rotational angle of gear	rad
$x(t)$	Time waveform signal	V
$X(f)$	Fourier spectrum signal	-
$X^*(f)$	The conjugate of $X(f)$	-
$\|X(f)\|$	Magnitude of Fourier transform	-
$\phi(f)$	Phase of spectrum signal	-
f_r	Shaft frequency	Hz
f_m	Meshing frequency	Hz
f_{rp}	Shaft rotation frequency of pinion	Hz
f_{rg}	Shaft rotation frequency of gear	Hz
f_{sb}	Sideband frequency	Hz
$x_c(t)$	Carrier signal	m/s^2
f_c	Carrier frequency	Hz
A_c	Amplitude of carrier signal	m/s^2
φ_m	Phase angle	rad
$a_m(t)$	Amplitude modulation function	m/s^2
$b_m(t)$	Phase modulation function	rad
$C(f_1, f_2, \ldots, f_{n-1})$	The n^{th} order spectrum	-
$C_n(\tau_1, \tau_2, \ldots, \tau_{n-1})$	Cumulant n^{th} order sequence	-

$E[x_t, x_{t+\tau 1}, \ldots x_{t+\tau m}]$	Cumulant statistical expectation operator	-
$B(f_1, f_2)$	Conventional bispectrum of two frequency components	-
$E[B\|(f_1, f_2)\|]$	Magnitude of conventional bispectrum signal	-
$\varphi_B(f_1, f_2)$	Phase of conventional bispectrum signal	-
$b^2(f_1, f_2)$	Bicoherence index of two frequency components	-
$B_{MS}(f_1, f_2)$	Modulation signal bispectrum of two frequency components	-
$\|B_{MS}(f_1, f_2)\|$	Amplitude of modulation signal bispectrum	-
$\varphi_{MS}(f_1, f_2)$	Phase of modulation signal bispectrum	-
$b_{MS}^2(f_1, f_2)$	Bicoherence of modulation signal bispectrum	-
υ_{40}	Kinematic viscosity at 40 °C	m^2/s
ω_n	Natural frequency	Hz
ξ	Damping ratio	-
F_{Li}, F_{Ri}	Friction forces on left and right sides of plane of action	N
U_a	Axial compressive energy	Nm
U_b	Bending energy	Nm
U_s	Shear energy	Nm
U_h	Hertzian energy	Nm
U_f	Tooth fillet foundation energy	Nm
k_a	Axial compressive stiffness	N/m
k_b	Bending mesh stiffness	N/m
k_s	Shear mesh stiffness	N/m
k_h	Hertzian mesh stiffness	N/m
k_f	Fillet foundation stiffness	N/m
$X_{ri}(t)$	Right arm of friction force segments	m
$X_{pri}(t), X_{gri}(t)$	Right arms of pinion and gear for friction force segments	m
$X_{li}(t)$	Left arm of friction force segments	m
$X_{pli}(t), X_{gli}(t)$	Left arms of pinion and gear for friction force segments	m
$T_{fi}(t)$	Total frictional torque	Nm
f_{ri}	Rotational frequency of i-shaft	Hz
f_{mi}	Gear mesh frequency of i-stage	Hz
m_{pi}	Mass of pinion in i-stage	kg
m_{gi}	Mass of gear in i-stage	kg
k_i	Torsional stiffness of i-shaft	N/m
c_i	Torsional damping of i-shaft	Nm/s
$K_{b\text{-}ij}$	Stiffness of gear supporting bearings (i) in various axes (j)	Nm/rad
$C_{b\text{-}ij}$	Damping coefficients of gear supporting bearings	Nms/rad
T_m	Motor driving torque	Nm
T_L	Generator load torque	Nm
θ_{pi}	Rotational angle of pinion in i-stage	rad
θ_{gi}	Rotational angle of gear in i-stage	rad
θ_{in}	Rotational angle of input driving motor	rad

θ_{out}	Rotational angle of output generator	rad
x_{pi}	Pinion translational response in x-direction of i-stage	m
x_{gi}	Gear translational response in x-direction of i-stage	m
y_{pi}	Pinion translational response in y-direction of i-stage	m
y_{gi}	Gear translational response in y-direction of i-stage	m
z_{pi}	Pinion translational response in z-direction of i-stage	m
z_{gi}	Gear translational response in z-direction of i-stage	m
$[M]$	Mass matrix	kg
$[C]$	Damping matrix	Ns/m
$[K]$	Stiffness matrix	N/s
q	Vibration response vectors	-
δ	Tooth wear width	m
R_w	Amount of wear region	-
C_{ch}	Torque drag or churning losses	Nm
P_{ch}	Power churning losses	Nm/s
C_m	Non-dimensional torque parameter	-
S_m	Submerged gear surface area	m^2
ρ_f	Meshing friction arm	m
Z_{rj}	Gear teeth number of speed reducer gearbox	-
Z_{ij}	Gear teeth number of speed increaser gearbox	-
C	Bearing clearance	m

Chapter 1
Introduction

This chapter presents a general overview of the reasons for choosing this particular topic for research. It then provides a brief description of conventional condition monitoring techniques, in particular gear condition monitoring and fault diagnosis based on vibration signal analysis. Next, it provides an explanation of why vibration monitoring is used for detection and diagnosis of gear faults. Finally, the research aims and the research objectives are given, followed by a description of the thesis structure.

1.1 Background

Online condition monitoring (CM) is a necessary requirement for optimum operation of most industrial electro-mechanical systems. It can be achieved by monitoring physical parameters associated with machinery operation. The purpose is early detection and diagnosis of the presence of faults, their locations and severity levels so that a preventive maintenance plan can be scheduled and appropriate action can be taken before the fault produces a disastrous failure. Various CM techniques including vibration monitoring, thermal monitoring, electric signal monitoring and acoustic emission monitoring have been investigated and examined to improve the reliability and availability of monitoring systems. While each technique has its limitations, when it comes to remote monitoring of the system, it has been found that vibration measurement can provide an immediate indication of incipient faults [1-8].

The vibration signal is a measure of the periodic mechanical movement of the electro-mechanical system. This behaviour (vibration signature) reflects the operating condition of the system, which will change immediately with the introduction of any kind of system abnormality. As a result, vibration monitoring is the most popular method for permanent and intermittent CM and it is considered an efficient method for the CM and fault diagnosis of many industrial applications [9-13]. It has the capability to provide a warning of incipient faults and is suitable for the application of many powerful signal processing techniques which can be applied to extract even very weak indications of a fault [13].

The movement of rotary machine equipment such as bearings, gears and shafts are essential indicators of the condition of a machine. These components often work under harsh and very severe environments such as high load, high temperature, high moisture, in dusty areas, etc. [14]. Gears, in particular, are important components in a variety of industrial applications and play a prominent role in mechanical power transmission, where high speed ratio and high load transmitting efficiency are required. Gear faults can play a critical role in the overall failure modes of a transmission system. Therefore, the detection and diagnosis of gear faults as early as possible can avoid catastrophic failures, saving maintenance costs and improving system availability. Vibration analysis has been extensively used as an effective tool for monitoring and diagnosing gear faults, providing essential information in support of machinery maintenance decisions [15].

1.2 Condition Monitoring Set-up

CM has attracted extensive research interest, particularly to improve the detection and diagnosis of machine faults in their early stages to avoid catastrophic breakdowns and human injuries and minimise maintenance costs. A scheduled maintenance program to ensure long operating availability, is mainly based on the information collected from CM, which has great significance in the business environment due to the following reasons [1, 16, 17]:

- To reduce the cost of maintenance.
- To predict equipment failure.
- To eliminate unscheduled downtime.
- To increase the required expectation of product quality.
- To enhance operator and component reliability.
- To optimize the equipment performance and productivity.
- To improve machine reliability and availability.
- To enhance the expectation of safety performance.

Typically, a maintenance program is determined based on the information collected by CM [18], in which the CM and fault diagnosis process can be achieved through different steps, as shown in Figure 1-1. This involves the evaluation of system health through the analysis and interpretation of signals acquired from sensors and transducers. Moreover, advanced computerised signal processing and data acquisition systems have made monitoring and diagnostic schemes accessible to all industrial production processes.

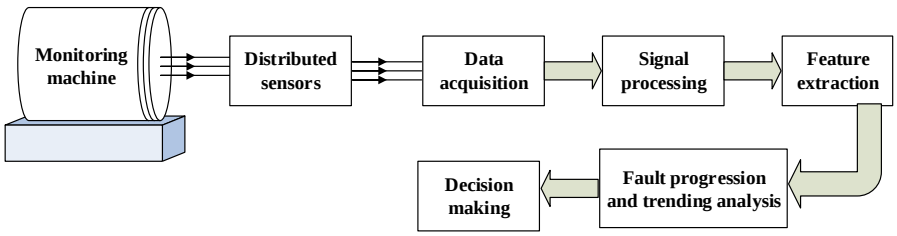

Figure 1-1 Schematic configuration of CM and fault diagnosis process.

1.3 The Concept of Gearbox Condition Monitoring

The monitoring of a gearbox's condition is a vital activity because of its importance in design of transmission systems. A wide range of industrial machines, from wind turbines, to helicopters, to marine power trains and motor vehicles commonly employ gearboxes for power transmission. As these applications are critical for human safety, and reducing

complex repair procedures and high replacement costs, on-line condition monitoring of gears has received increasing attention in recent years [19].

However, according to a number of surveys of wind farms cross Europe and America, the gearbox is the subsystem most likely to be responsible for wind turbine downtime and maintenance cost [6]. Surveys by Wissenschaftliches Mess-und Evaluierungsprogramm and Landwirtschaft-skammer have shown that the gearbox also presents the longest downtime per failure of all the onshore wind turbine components [20]. Figure 1-2 shows a comparison of downtimes of different sub-assemblies of wind turbines in the EU. As most rotating machines use gears in their drive systems, the diagnosis of gear faults as early as possible will improve operational availability and maximize system productivity.

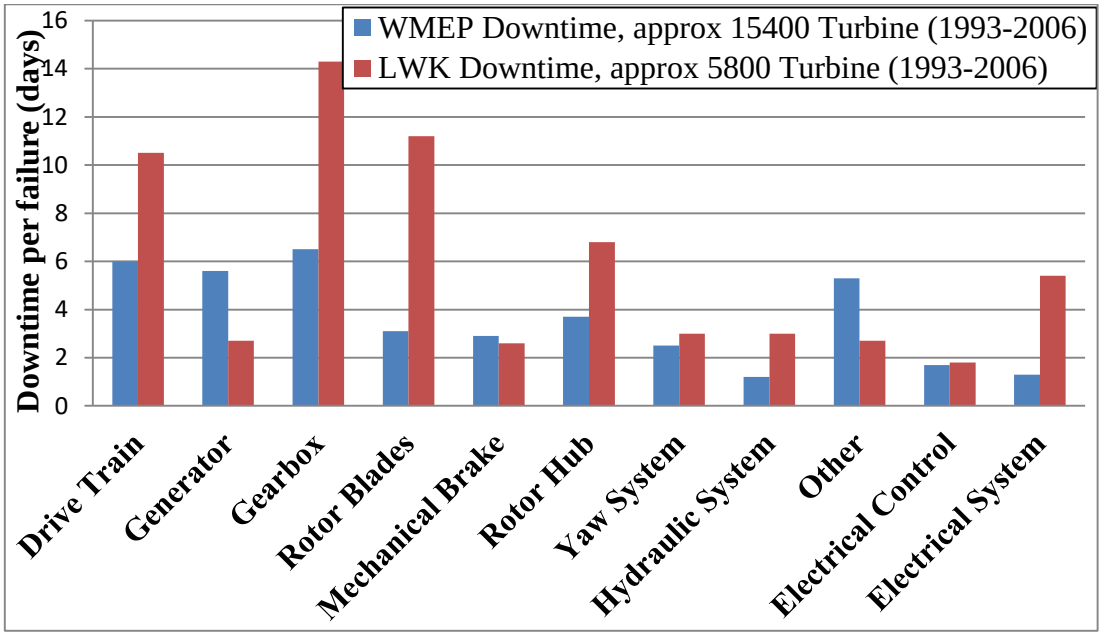

Figure 1-2 Wind turbine sub-assembly downtime per failure from European wind turbines surveys as published in [19, 21].

1.4 Condition Monitoring Techniques

CM has become important in the field of equipment maintenance and industrial products, and has attracted more and more attention worldwide. Due to a wide and increasing variety of systems, components and parts, combined with different forms of production systems, a growing variety of CM techniques are utilized to detect and diagnose faulty operating conditions at an early stage. Understanding the nature of each monitoring technique and the type of measured information will enable better utilization of existing methodology, which is important in a competitive economic environment.

Survey results showing the relative proportions of the various monitoring techniques generally used in CM and non-destructive testing (NDT) [22], are presented in Figure 1-3. The survey indicated the techniques most widely used are Vibration Analysis, Oil Analysis, Infra-red Thermography, and Human Senses. The results are similar to those obtained by the Plant Maintenance Resource Centre in a survey carried out in 2002 [23].

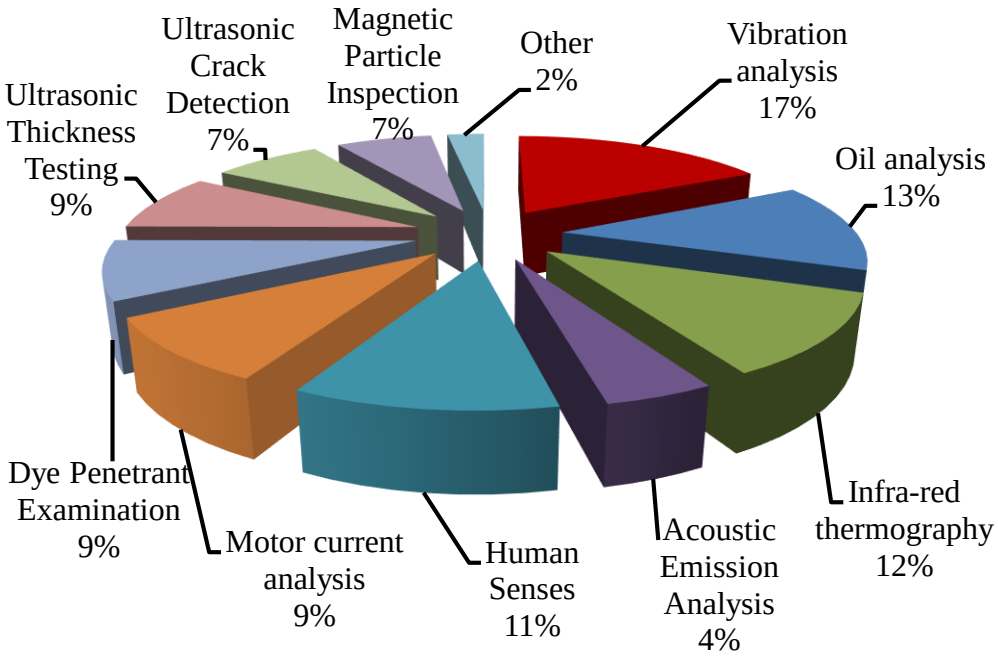

Figure 1-3 Relative usage of common condition monitoring techniques [22].

CM techniques should be used as part of a comprehensive predictive maintenance program [24]. A high reliability and optimal processing capability should be taken into account when selecting the most effective CM method. The monitoring method chosen need to [3]:

1. Measure the output quality and quantity values of the system variations.
2. Measure the system's input/output relationship.
3. Measure and simultaneously compare the output parameters within a set of standard operating conditions.

There are numerous CM techniques, which are viable for monitoring rotating machinery. Selection depends on their individual capabilities and limitations in detecting early changes in characteristic parameters and trends. The following techniques are generally used and need to be considered when selecting the best sets of signal features [25-29]:

1.4.1 Lubricant Analysis

The reliability of any mechanical drive depends largely on the protective properties of the lubrication oil used for its drive train, which can provide advance warning of abnormal machine conditions. The purpose of lubrication oil CM is to determine whether the oil has deteriorated to such a degree that it no longer performs its protective function, and to provide early warning of the possibility of total failure [30]. Lubricant analysis measures certain of the physical properties of the oils effected by contamination, including water content, soot/carbon content, the presence of metallic particles and oxidation status. The main tests generally used in the oil analysis process are [31]:

- Viscosity analysis,
- Oxidation analysis,
- Water content or acid content analysis,
- Particle count analysis,
- Machine wear analysis, and
- Temperature.

However, the online health monitoring of lubrication oil has some limitations e.g. it uses expensive instrumentation and cannot detect failures outside the gearbox [32]. Moreover, it does not localize the failure in complicated gearboxes [33]. For these reasons, off-line monitoring is often used with oil analysis but the time needed to take a sample and carry out the analysis and accessibility remain problematic.

1.4.2 Acoustic Emission

Acoustic Emission (AE) is becoming an increasingly significant tool in the field of CM of machinery [34]. Machines normally, generate noise and create vibration due to the contact of materials in motion. AE detects high-frequency signals in rotating machinery, which are picked up by means of special AE microphones, and the acoustic and/or noise waveforms received can be used to detect faults. AE sources include contact, cyclic fatigue, friction, turbulence, material loss, cavitation, leakage, etc. [35].

However, a high cost of AE, only a few types of faults occur in the high-frequency range and the attenuation of the signal as well as a practical constraint in applying the AE sensor, which has to be close to its source, are the main drawbacks with AE technique [36-38]. In addition, AE required a very high sampling frequency because of high frequency signal

output from its sensors. Moreover, high data volume and complicated features of AE signal make the data processing extremely difficult [39].

1.4.3 Motor Current Monitoring

Motor current monitoring is based on measuring and analysing the electric drive motor's supply current, for detecting and locating a fault. Its computation is mainly based on measuring the stator phase currents, using three AC current sensors, which can offer a useful information on gear tooth surface damage [40]. The motor current can change corresponding to mechanical load variations. These variations can be detected and monitored remotely and their analysis used for machine CM.

This technique can be used effectively for mechanical and electrical fault detection in induction machines, especially for low but it is difficult to detect high frequencies [41, 42]. Moreover, the dominant components of the electrical signals are the supply frequency components, where some mechanical faults are somewhat hard to obtain.

1.4.4 Thermal Monitoring

Thermal monitoring is a quick observation technique recognized as useful for CM, because temperature can be a key parameter for monitoring the performance and condition of machines. The degradation of electrical equipment can cause excessive overheating, which can lead to the eventual failure of the equipment [43]. Heat is one of the biggest failure modes in mechanical systems, which can be generated by friction, cooling loss or material loss. An excessive amount of friction can be caused by wear, misalignment, and over-or under-lubrication.

Thermal imaging improves the ability to predict equipment failure and plan corrective action before a costly shutdown or equipment damage. One of the disadvantages of this technique is that attention must be given to the environment of the working instrument. Any change in factors such as atmospheric temperature or density of airborne particles can have to a great effect on the reliability and accuracy of the measurements [44].

1.4.5 Vibration Analysis for Condition Monitoring

Vibration analysis is one of the most widespread methods used in CM [45]. It has become an important method for fault detection and identification in gearing systems. The concept of the vibration signature is to examine and analyze changes in machine vibration to detect

damage occurrence. All machines generate vibrations, including those in good condition. The vibration is generated by shaft rotation and gear meshing. Machine components generate characteristic vibration signals that separate them from the other components and distinguish their health conditions. CM systems based on vibration analysis can monitor all parts of gearboxes, for example the gears themselves, bearings and shafts [15, 46-49] .However, sensitivity to the installation location and need to sometimes mount vibration transducers in inaccessible places, are the main drawbacks of vibration measurement [40, 42]. Despite these drawbacks, vibration characteristics have been widely used to detect and monitor at least the following causes of faults in rotating machinery [45, 50]:

- Misalignment and/or damage to gear teeth and bearings.
- Unbalance and thermal dissymmetry in rotating machinery.
- Pits and cracks in component parts.
- Misalignment and cracks in shafts.
- Loose parts including excessive wear in bearings.
- Resonance of rotating components.
- Deterioration due to a wide range of sources: broken parts, corrosion, erosion, rubbing, etc.,

The different vibration frequencies in rotation machines are related to the structure geometry and the speed of the machine. An increase or modification in these vibrations can be an indication of the presence of failure, or of an upcoming failure. By using vibration monitoring, the causes of the problems can be found and the remaining useful life of the components can be estimated. Data acquisition, data processing and failure pattern recognition are the main stages of vibration-based fault detection processes, the vibration signal can be collected experimentally (or simulated) for analysis and feature extraction to assess the machine's condition [51]. Since vibrations analysis is a powerful diagnostic tool, there are a number of different techniques that have been developed for general use [52], see Sec. 1.5 below.

1.5 Why Vibration Signature Analysis Is Used?

Implementing a successful CM system provides useful and reliable information for the necessary maintenance program and thereby brings significant cost benefits to industry

[53]. This allows the machinery to operate at full capacity by reducing unnecessary scheduled maintenance and minimizing unplanned downtime. Vibrations signature analysis is the most common and popular monitoring technique used to measure and predict the condition of a rotating machinery and is generally considered as an important predictive tool in most maintenance programs [7, 8, 45, 50].

The vibration signals contain valuable information about the mechanical condition of the various parts involved, as well as reflecting the overall course of operation of the system assembly [24, 54]. The vibration signals are directly related to the periodic movement of the machine components and are very sensitive to any abnormality in the moving components, whether a bent rotating shaft or a damaged tooth on a gear. Measurement and analysis of the vibration response give essential fault diagnosis information relevant to the conditions of the different components of the machines [55]. Vibration measurement has the capability of monitoring all the parts of a gearbox, for example gearing, bearings and shafts and provides a warning of incipient faults. Furthermore, many powerful signal processing techniques can be applied to extract even very weak fault indications from the measured vibration signal [13].

Vibration analysis has the ability to provide a quick, economical, and reliable monitoring technique in an industrial environment. However, vibration monitoring cannot provide all the information required for a condition based maintenance program. Nevertheless, vibration analysis can be considered as an effective tool for gear fault diagnosis due to the following advantages [15]:

1. Vibration signal is non-destructive and sensitive to a wide range of defects.
2. The frequency and amplitude of the vibration spectrum are directly linked to the source of vibration,
3. Different signal processing techniques can be applied to the vibration signal,
4. Fast and easy measurement can be obtained by accelerometers, which are non-intrusively mounted on the external surfaces of a machine.
5. The measuring instruments are becoming inexpensive due to the rapid development of electronics and manufacturing efficiency.
6. Vibration signals provide diagnostic information regarding the precise nature of malfunctioning machinery with a minimum use of transducers,
7. Very sensitive to system abnormality,

8. Increased machine availability, reduced breakdown time,
9. No risk involved in data collection, hence safety improved,
10. Gives improved ability to manage maintenance procedure and make cost savings,
11. Can be used in different places for more conventional measurement methods in the oil industry.

1.6 Research Motivation

Gearboxes are fundamental and critical mechanical parts for power transmissions in a wide range industrial machines. Gearbox lubrication has a strong influence on damage formation and gear failures but despite the fact that many problems are caused by lubrication failure, little work has been undertaken to examine the possibility of employing vibration analysis for detecting lubrication status.

Generally, lubricant deterioration leads to greater friction between the meshing contact surfaces and has a significant effect on the dynamic characteristics of gears, which can be observed in different ways, including strong nonlinearities in dynamic behaviour, noise and vibration.

Gear defects such as wear, tooth breakage, spalling and fatigue, produce repetitive impacts during rotary motion. These failures lead to significant modulation effects induced by the resonance frequencies of the system; rotation of the shaft and dynamic meshing forces. Thus, the periodic and modulation characteristics of fault mechanisms need to be extracted effectively for the implementation of reliable fault detection and diagnosis of the health of gearbox components.

In addition, vibration analysis based CM of gearbox components has previously been examined only from a signal processing point of view. Little focus has been applied to the use of mathematical models to understand the physical interaction of meshing gears and the effect of tooth faults on the vibrational behaviour of the gear system. For successful implementation of gearbox health monitoring, a baseline dynamic model of a gearbox needs to be established, then robust signal processing techniques can be applied for fault diagnostics.

To develop more advanced and accurate diagnosis, this research has focused on the investigation of the non-linearities in vibration transmission and viscoelastic properties of lubrication, so that it enables an in-depth understanding of the vibration mechanism and

hence the development of effective signal processing methods for early detection and accurate diagnosis of gear incipient faults. In addition, effective signal processing is required for de-noising and reliable feature extraction from nonlinear impulsive effects and modulation characteristics of fault mechanisms. The major concerns of this research work includes:

1. Use of an experimental test rig, consisting of driving motor, two gearboxes and load.
2. Simulation of different faults in the gearbox components and production of tooth surface wear in a realistic way.
3. Construction of a comprehensive dynamic model to study the influence of different tooth surface faults on gear dynamic response, with the inclusion of time-varying stiffness and tooth friction based on EHL principles.
4. Use of an effective method such as TSA (time synchronous averaging) and MSB (modulation signal bispectrum), to reduce background noise and to increase the possibility of using vibration signals for monitoring different gearbox lubricant deteriorations.
5. Evaluation of the performance of the MSB for monitoring excessive bearing clearance due to gear wear.

1.7 Research Aims and Objectives

1.7.1 Research Aims

- To develop a non-linear dynamic model for gear interaction including frictional effects to better understand the gear vibration responses under different operating conditions.
- To implement advanced signal modelling and data analysis techniques capable of enhancing vibration signatures to achieve more accurate detection and reliable diagnosis of different lubricant deteriorations.

Achieving these aims and experimentally verifying the noise reduction, signal analysis and feature optimisation, will provide for more efficient fault detection and diagnosis for the monitoring of multistage gearboxes.

1.7.2 Research Objectives

In order to fulfil this research, a number of objectives have been identified as follows:

Objective 1. To review existing condition monitoring techniques and assess the performance of the most common techniques used for online CM and early fault detection of gearboxes.

Objective 2. To review the main sources of gear vibration to obtain an in-depth understanding of the dynamic interactions between transmission components.

Objective 3. To design and construct a mechanical transmission test rig for the evaluation of industrial gearboxes under different operating conditions, which allow different faults to be introduced into the gearbox components, enabling subsequent system behaviour to be characterised.

Objective 4. To develop numerical dynamic model with the help of MATLAB, and compute the periodic mesh stiffness variation of helical gears as a function of the contact position of the meshing teeth. Also, to characterise the vibration signature changes, enabling more reliable diagnostics under different operating conditions.

Objective 5. To calibrate the linear and nonlinear responses of the dynamic model and evaluate the model for different frictional modes with progressive tooth breakages.

Objective 6. To develop an efficient computation and stable analysis of the dynamic responses of a tooth surface worn in a two-stage helical gearbox using a run-to failure experimental test and a comprehensive dynamic model including EHL friction effects.

Objective 7. To investigate nonlinearities in vibration transmission and viscoelastic properties of gearbox lubrication, and hence develop effective signal processing methods for online monitoring and diagnosis of different gearbox oil deterioration conditions under different gear operating conditions, and any constraints on its usage that should be considered.

Objective 8. To develop guidelines for future research activity relating to this field.

1.8 Structure of the Thesis

The thesis is divided into nine chapters including the current chapter. A brief synopsis of each subsequent chapter is as follows:

Chapter 2–This chapter presents an overview of gearbox transmission theory with the principal sources of vibration and noise induced during the gear meshing process. It also

explains gear failure modes, the status of gearbox lubrication and the conditions for lubricant deterioration.

Chapter 3 -This chapter gives an introduction to vibration analysis techniques commonly used for CM and fault diagnostics of the gear system. It starts with main characteristics of time and frequency domain analysis followed by an explanation of TSA and the effect of modulation. After that, higher order spectra analysis methods are introduced due to their ability to suppress background noise and improve the gear fault detection and diagnosis.

Chapter 4 –This chapter explains the test facility and fault simulation used in this study. It describes the gearbox test rig components and control systems that are used to carry out the investigation with the vibration measurement specifications. Fault simulation and data collection procedure are discussed at the end of this chapter.

Chapter 5 -This chapter presents a numerical dynamic model of a two-stage helical gearbox with the inclusion of time-varying friction based on the EHL model. An in-depth calculation of helical gear mesh stiffness is also developed including the dynamics of the system under various possible failure conditions. In addition, different tooth breakage (TB) severities have been simulated to evaluate the model performance under different tooth stiffness excitation models.

Chapter 6 -This chapter illustrates parameter identification and validation of the numerical model with the experimental results for the purpose of CM. It examines the gear dynamic responses from both experimental and numerical studies with increasing tooth surface wear from its earliest phase. A description of the experimental setup of a run-to-failure test arrangement is developed. The numerical model is developed to simulate time-varying mesh stiffness, coupled with an EHL frictional model and tooth wear characteristics.

Chapter 7 - This chapter defines the diagnostic relationship between vibration signature and lubrication status of the gearbox. Different lubrication problems such as contamination with water, starvation and change in oil viscosity have been simulated under different operating conditions. To establish online health monitoring of the gearbox oil condition based on vibration signal analysis, effective analysis methods have been used to normalise the condition indicator and investigate any measurable changes correlated with the variation of gearbox oil condition for future preventive maintenance.

Chapter 8 - This chapter evaluates the performance of the MSB method for monitoring excessive bearing clearance based on vibration analysis in the presence of gear wear. Three bearings with different standard clearances have been used to investigate the effect of bearing clearance variations on the characteristics of helical gear vibration characteristics.

Chapter 9 – This chapter draws conclusions based on the key findings of the research. The objectives are reviewed and a summary of the author's contribution to knowledge and the novel aspects of the research are presented. This chapter also gives suggestions and recommendations for future work in related research areas.

Chapter 2
Gearbox Overview

This chapter presents a brief overview of gear transmission theory. The critical sources of gear vibration and noise are also presented with an in-depth analysis and explanation of the interactions of sources during the teeth meshing process. In addition, the most common failure modes in gear transmission systems that relate to the tribological condition are provided at the end of this chapter.

2.1 Introduction

Gears are the key components for most power transmission systems for increasing speed ratios and efficiently transmitting high torques. Gears are used in every industry; e.g. textiles, automobiles, aerospace, shipping, and agriculture. A wide variety of industrial machines including wind turbines, marine power trains, gas turbines for power generation and automotive transmissions all employ gears. These applications often function in very severe environments; high temperature, high humidity, high loads, dusty areas, etc. [14]. Thus, CM of rotating machinery components has attracted extensive research, in which detection and diagnosis of faults as early as possible was the object.

Gear faults play a significant role in the overall failure modes of the transmission system. The common gear faults are mainly related to gear tooth irregularities, i.e., the chipped tooth, tooth breakage, root cracking, spalling, pitting and surface damage, which are typically localized faults [40, 56]. Excessive applied load, insufficient lubrication or installation problems such as misalignment are the main reasons for gear failure. To detect and correctly diagnose an imminent gear failure, understanding the gear failure mode, and the collecting and quantitative analysing of data are essential.

Gear fault detection was traditionally carried out by monitoring the vibration signal and extracting certain statistical parameters. These extracted features were known to be correlated with particular faults within the gearbox. Such an approach was intended to minimise maintenance cost, avoid catastrophic failures and improve systems' availability.

2.2 Transmission Gear Theory

Gears are the key components inside the transmission train commonly used to provide motion control and vary the torque transmitted between rotating shafts. The power transmission often includes a gear system which can be used to increase the output torque or output speed, but not both simultaneously. A gear system invariably produces a change in torque, creating a mechanical advantage and transmitting a synchronous motion through the gears. Standard gears consist of a common number of teeth in relationship to their diameter. The circular pitch (p_c) is represented this relationship as [57]:

$$p_c = \frac{2\pi r}{Z} = \frac{2\pi r_p}{Z_p} = \frac{2\pi r_g}{Z_g} \tag{2.1}$$

Where Z is the number of teeth, r represents the pitch radius of the gear and the subscripts p and g symbolize the pinion (driver) and the gear (driven) respectively.

The mechanical advantage of power transmission gears is given by gear ratio (**GR**), the input power (P_p) to the output power (P_g), as presented in Eq. (2.2). This equation assumes zero frictional losses between the two mating gears. The **GR** can be expressed in terms of gear radii, teeth numbers or the rotational speeds of the pinion (ω_p) and gear (ω_g) (Eq. 2.2).

$$\mathbf{GR} = \frac{P_g}{P_p} = \frac{r_g}{r_p} = \frac{Z_g}{Z_p} = \frac{\omega_p}{\omega_g} \tag{2.2}$$

To understand the geometric and kinematic contact throughout the gear meshing cycle, a schematic drawing of a transverse section of a pair of gears is shown in Figure 2-1. For uniform gear rotation, the meshing teeth always develop contact points along the action line **CF**, passing through the pitch point (**P**). The tangent to the gear base circles at points **A** and **B** is named the line of action (LOA).

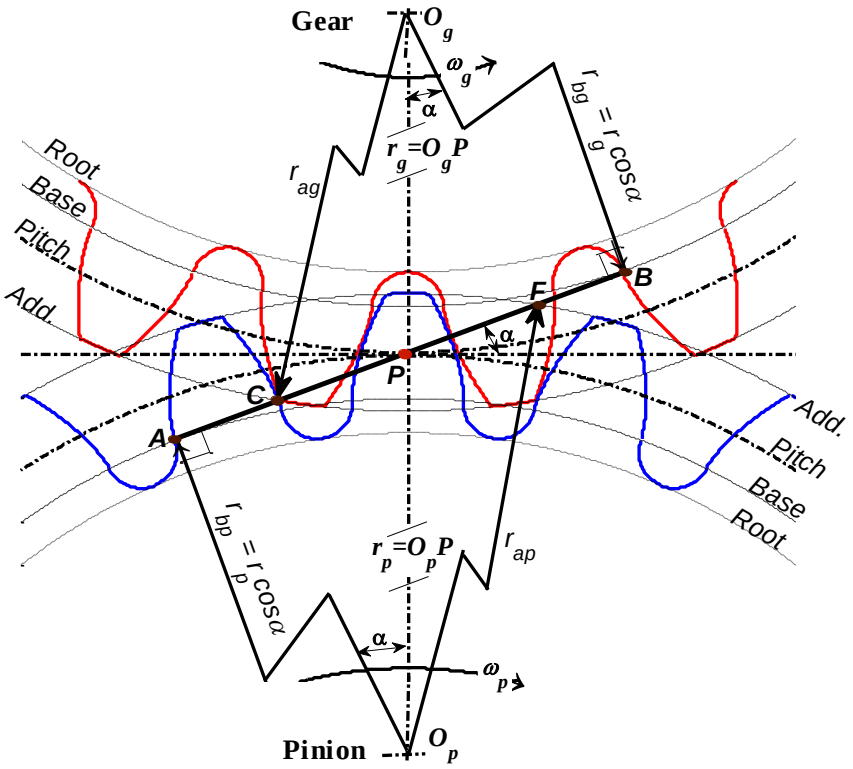

Figure 2-1 Gear meshing process of a transverse section of a pair of gears in contact

At the point **P**, the line **LOA** crosses the gear centreline, $\mathbf{O_pO_g}$, at an angle (90-α) where α is the pressure angle. The effective length of the line of action (**CF**) can be calculated as:

$$LOA = \sqrt{r_{ap}^2 - r_{bp}^2} + \sqrt{r_{ag}^2 - r_{bg}^2} - (r_p + r_g)\sin\alpha \tag{2.3}$$

where, r_{ap}, r_{bp}, r_{ag} and r_{bg} are the addendum and base radii of the pinion and gear respectively.

2.3 Gear Classification

An increasingly wide range of gear designs is being produced due to the expanding demands of industrial applications. Gears are available in many different sizes, capacities and speed ratios. Transmitting a synchronous motion and power directly between shafts are the main purpose of gears but gears can serve in a range of functions. Gears are classified by the relationship of the relative position of the gearing shaft axes, in which the axes of connecting shafts may be parallel, intersecting, or neither parallel nor intersecting [58]. A brief list of the common gear forms is shown in Figure 2-2.

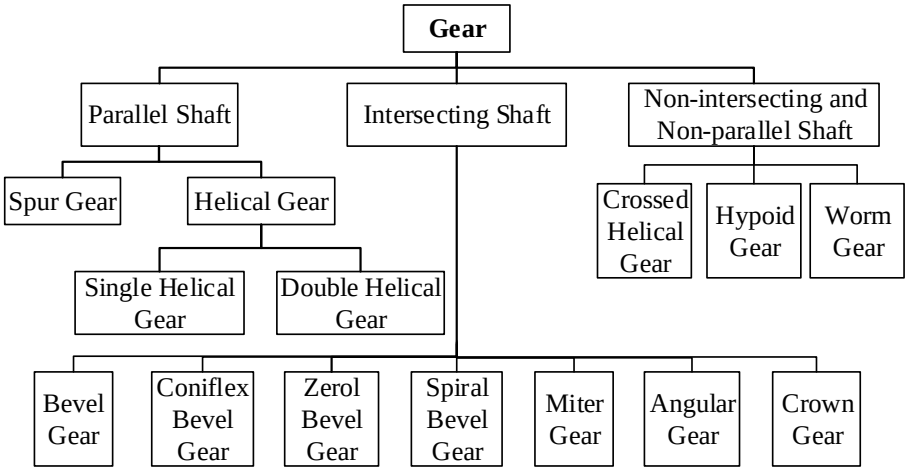

Figure 2-2 Gear classification relating to the shaft axes [59]

2.4 Spur and Helical Gears

For efficient transmission of high power rotary motion between parallel shafts, spur and helical type gears are used. Spur gears are easier to design and manufacture. However, helical gears are preferred for higher power applications due to their larger tooth contact ratio, greater strength, and where low noise and smoother engagement of tooth meshing is required. Due to the presence of the helix angle, the contact lines of the helical gears run diagonally across the tooth face [60], which can distribute the transmitted load more evenly and more quietly.

Figure 2-3 shows spur and helical gear configurations. The helical design shows teeth angles to the left and right of the rotational axis. This angle creates axial thrust, but means

helical gears provide a smoother and quieter run, making them the better choice for large load transmission at high operational speeds, whereas the spur gears are suitable for slower speed applications [60, 61].

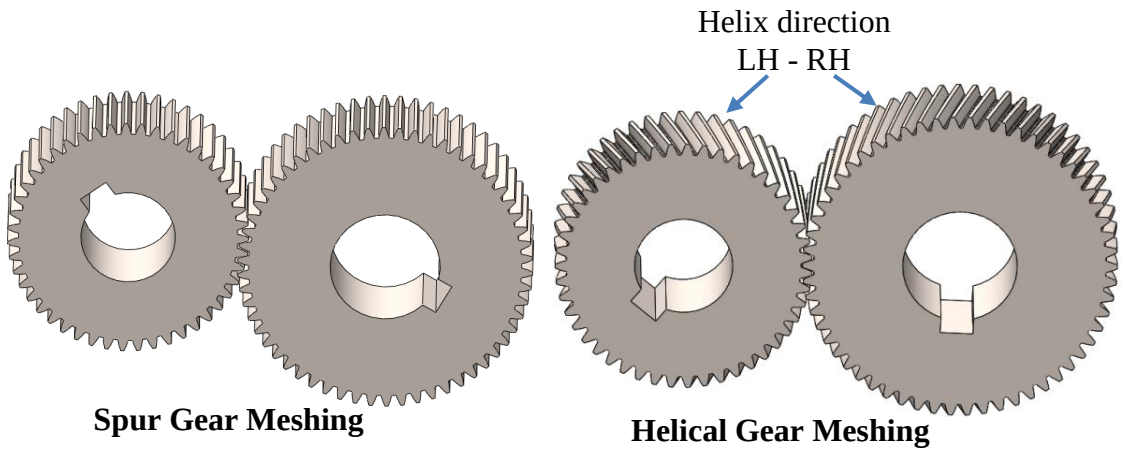

Figure 2-3 Illustration of spur and helical gears

2.5 Principal Sources of Gear Vibration and Noise

Gears are the main transmission components, and with the growing need for greater power transmission, the gear drive assembly tends to become more complex. Gear vibration and noise remain a source of intense annoyance, which has been of wide concern for many years, but it can be used usefully to monitor the condition of the gearbox [9, 11, 35].

To understand and control gear vibration, it is necessary to have knowledge of gear vibration sources, and let it be remembered, sound/noise is a vibration that typically propagates as an audible wave in the frequency range roughly 20 Hz to 20 kHz [62]. Of course, it is always good to reduce noise as that will improve working conditions and even enhance the capability of the transmission system. Nevertheless, there are also many sources of excessive vibration in gears, which have a strong influence on instabilities in the overall dynamics of the gearing applications [9, 12, 63-66]. These sources include:

2.5.1 Mesh Stiffness Variation

The variation of tooth mesh stiffness is a principal source of internal dynamic forces that cause parametric instabilities and severe excitations in gear systems [67, 68]. The internal excitations occur between the contact tooth surfaces during their relative motion and act on both surfaces with the same intensity but in opposite directions. The major variations in gear stiffness are caused by changes in the number of engaged tooth pairs.

For identical spur gears, the teeth in contact during the meshing process vary alternately between a single pair and double pair [69]. Thus, normal spur gears have a contact ratio of ($1 < \varepsilon_{ratio} < 2$) [70], i.e. the meshing pair number is in the range between 1.0 and 2.0 [71, 72]. Figure 2-4 clarifies the various positions of spur gear meshing events and the time-variation of gear mesh stiffness from teeth engagement to separation.

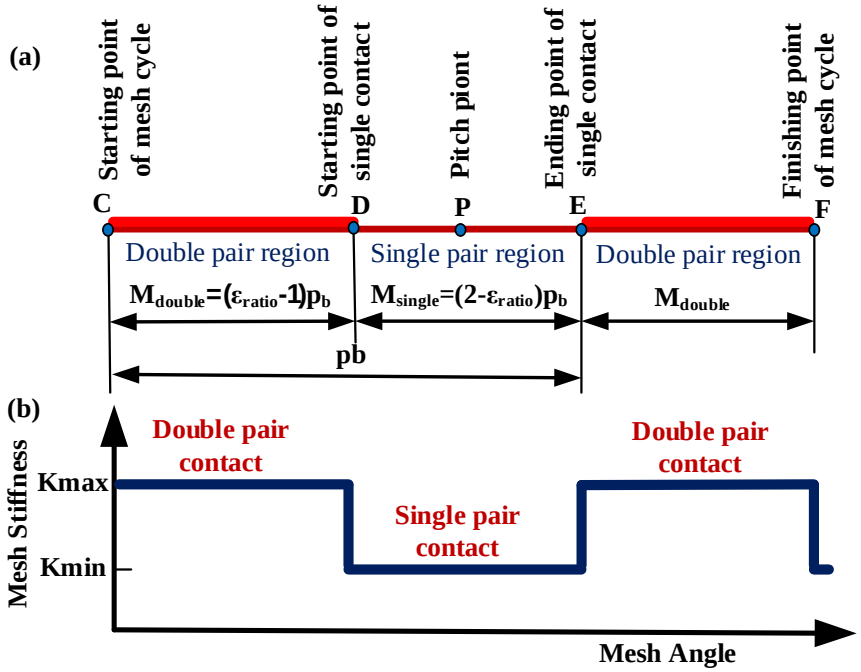

Figure 2-4. Mesh stiffness regions of meshing gear pair in one period; where pb is the base pitch, M refers to the mesh event, εα is the contact ratio

The mesh contact cycle starts at a tooth root, point **C** (the intersect point of the **LOA** with the addendum circle diameter of the driven gear), which varies between a single and double tooth pair along the length of the tooth profile passing through **P** and terminates at the tooth tip, point **F** (the intersect point of the **LOA** with the addendum circle diameter of the driver gear). The average number of tooth pairs in contact is represented by the contact ratio $\boldsymbol{\varepsilon_\alpha}$, which is defined by Eq. (2.4).

$$\varepsilon_\alpha = \frac{LOA}{p_b} \tag{2.4}$$

where p_b is the base pitch of the gear tooth curve and can be calculated by Eq. (2.5).

$$p_b = \frac{2\pi r_b}{Z} = \frac{2\pi r_{bp}}{Z_p} = \frac{2\pi r_{bg}}{Z_g} \tag{2.5}$$

In the case of helical gears, the contact variations between the teeth are smoother because their contact lines are oblique due to the existence of the helix angle, β [73, 74]. Thus, the overlap due to the helix angle β needs to be taken into account by introducing the overlap ratio ε_β, which is defined as:

$$\varepsilon_\beta = \frac{b \tan \beta_b}{p_b} \tag{2.6}$$

The sum of the contact ratio and the overlap ratio is defined as the total contact ratio $\varepsilon_{ratio} = \varepsilon_\alpha + \varepsilon_\beta$. Thus, the contact ratios are the key factor that affects the fluctuating value of the length of the contact-line. The mesh stiffness is fluctuating continuously with this variation of length and number of contact lines and is closely related to the load variations on these lines. The mesh stiffness of a helical gear is roughly proportional to the sum of the lengths of the contact lines of all the tooth pairs in contact [75]. The length and the number of the contact lines vary across the plane of action of the helical gear tooth face, starting at point **C** and travelling obliquely to finish at point **F**, as shown in Figure 2-5.

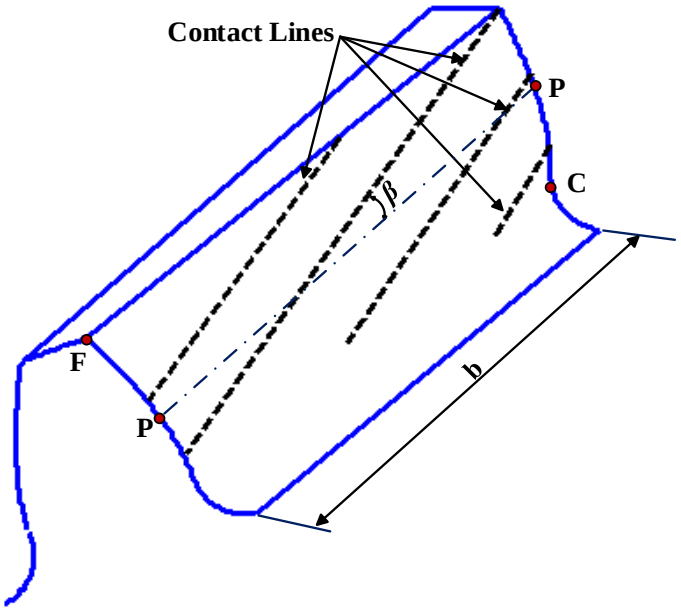

Figure 2-5 Contact lines patterns on a helical tooth face

The overall stiffness function ($K_{mi}(t)$) is defined as a combination of the total length of contact lines $L_i(t)$, and a constant mesh stiffness density per unit length (k_o) along the contact lines, is given in ISO 6336 standard [76, 77], see Eq. (2.7). The subscript *i* refers to the number of contact tooth pairs. This variation in the gear mesh stiffness is one of the

most important parameters determining gear tooth excitation and thus, a primary source of vibration and noise in gear drives.

$$K_{mi}(t) = k_0 \, L_i(t) \tag{2.7}$$

2.5.2 Friction

Friction force and resulting nonlinear excitations are another considerable source of vibration [78]. Friction is considered one of the main sources of energy dissipation and an important excitation parameter to gear dynamic instabilities. It shows as time-varying parametric excitations that affects the system performance and leads to large vibrations and audible noise [79].

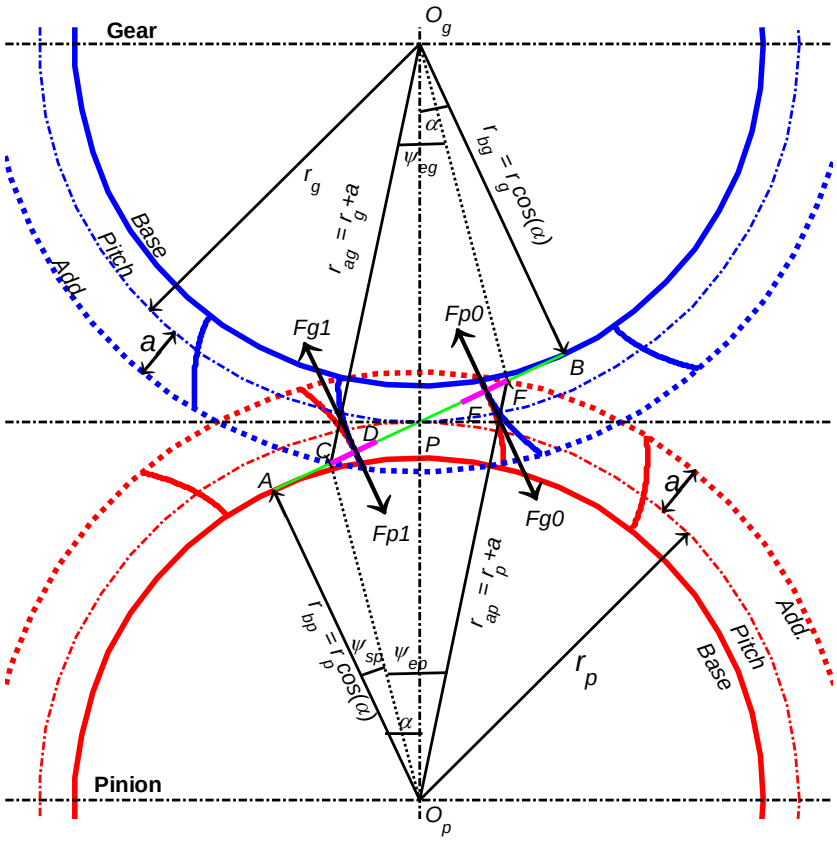

Figure 2-6 Effect of friction forces during gear mesh process [80]

Previous studies have been reported that significant torque variations are induced due to changes in friction forces around the pitch point [81, 82]. As shown in Figure 2-6, the effects include moments about the gear centre from friction forces perpendicular to the **LOA**, F_{p1}, F_{p0}, F_{g1}, F_{g0} (affecting gear rotation), excitation of off-line-of-action (**OLOA**) gear translations and nonlinear dependence of friction on gear sliding velocity [79]. Based

on Coulomb's law of friction, the friction force (F_{ji}) in the *i*th meshing pair is defined by Eq. (2.8).

$$F_{ji}(t) = \mu N_{ji}(t) \tag{2.8}$$

Where *i* refers to the contact tooth pair of the mesh cycles, *j* denotes the variety of pinion and gear, $N_{ji}(t)$ is the time-varying contact force of the *i*th meshing pair along the **LOA** and μ is the friction coefficient experienced due to the tribological conditions existing between tooth contact surfaces.

The change in friction conditions can be described by fluctuations in the friction coefficient during the mesh process, which have great influence on dynamic response of the gear system and its running status. Many parameters affect the friction coefficient and researchers have proposed different empirical formulae developed experimentally and based on the curve fitting to estimate the friction coefficient [83], see Table 2-1.

Table 2-1 Empirical formulas used to calculate friction coefficient

Published Author	Empirical Formulae
Misharin (1958)	$\mu = 0.325\left[V_s V_r v_K\right]^{-0.25}$
Benedict and Kelley (1960)	$\mu = 0.0127\left[\frac{50}{50-S}\right]\log_{10}\left[\frac{3.17\times10^{8}W}{v_0 V_s V_r^2}\right]$
ISO TC60	$\mu = 0.12\left[\frac{WS}{RV_r v_0}\right]^{0.25}$
O'donoghue and Cameron (1966)	$\mu = \frac{0.6(S+22)}{35}\left[v_0^{\frac{1}{8}} V_s^{\frac{1}{3}} V_r^{\frac{1}{6}} R^{\frac{1}{2}}\right]^{-1}$
Drozdov and Gavrikov (1967)	$\mu = \left[0.8\sqrt{v_k}V_s + V_r\varphi + 13.4\right]^{-1}$ $\varphi = 0.47 - 0.13\times10^{-4}P_{\max} - 0.4\times10^{-3}v_K$
Kelley and Lemanski (1967)	$\mu = \frac{C_1}{1-C_3R_q}\log_{10}\left[\frac{C_2W}{v_0V_sV_t^2}\right]$
Hai Xu et al. (2005)	$\mu = e^{f(SR,P_h,v_0,S)}P_h^{b2}\left\|SR\right\|^{b3}V_e^{b6}v_0^{b7}R^{b8}$ $f\left(SR,P_h,v_0,S\right) = b1 + b4\left\|SR\right\|P_h\log_{10}\left(v_0\right) + b5e^{-\left\|SR\right\|P_h\log_{10}(v_0)} + b9e^{S}$

In these formulae, v_k and v_o are the kinematic and dynamic viscosities of lubricant, V_s is the relative sliding velocity, V_r is the sum of the rolling velocities, R is the combined radius of

curvature, W is the unit normal load, P_{max} is the maximum contact pressure and S is the surface roughness parameter, i.e.

$$\mu = f\left(v_k, v_o, V_s, V_r, R, W, P_{\max}, S, \ldots\right) \tag{2.9}$$

These empirical formulae for μ are valid within certain ranges of key system parameters. They are not general and often represent certain lubricants, operating temperatures, speed and load ranges, and surface roughness conditions of roller specimens that might differ from those of the actual gear pair of interest [83]. Generally, the theoretical friction coefficients are derived from EHL and tribological theory.

2.5.3 Lubricant Entrapment

The major functions of gear lubrication are separating contact surfaces, reducing friction and dissipating heat. However, gear lubricating conditions also have some influence on gear vibration, especially under low oil temperature or high viscosity [84]. During the gear mesh process, the lubrication is trapped and squeezed, the engaging teeth entrap oil and force it out of the gear teeth regions. Squeezing lubricant between gear teeth and pressurizing it to eject in the axial direction contributes to gear oil splashing, which can be considered as one of the main sources of gear vibration.

2.5.4 Transmission Error

In most literature, transmission error (TE) is the deviation of the driven gear from "perfect" conjugate action, and is usually the result of geometric errors and/or mesh stiffness variation, as such it will be time-dependent and relative to the respective position of the gear teeth in contact [85]. The geometric errors are mainly due to errors in the manufacture of the gear teeth and assembly errors within systems that result in profile and tooth spacing errors. However, TE results not only from manufacturing inaccuracies, such as profile errors, tooth pitch errors and run-out but also from bad design [49]. Figure 2-7 demonstrates the effect of TE during the gear mesh process, in which the total TE comprise the tooth profile variation and accumulated pitch variation [46].

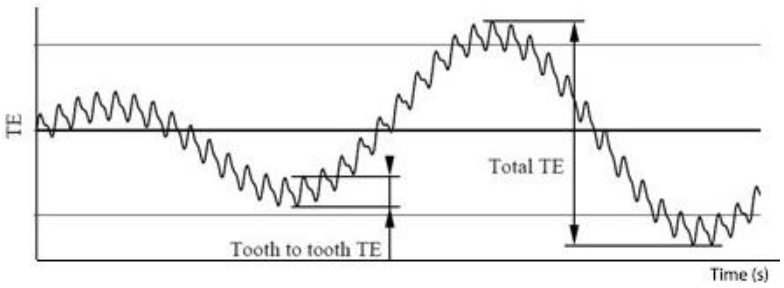

Figure 2-7 Gear transmission error signal

TE is considered to be one of significant vibration excitation sources in the gear structure [86], and can be used to measure the smoothness of the drive. For a simple gear set, TE can be evaluated by:

$$\mathbf{TE} = (\theta_p - \frac{Z_g}{Z_p}\theta_g)r_g \tag{2.10}$$

where Z_p, Z_g are teeth numbers of the pinion and gear respectively, θ_p, θ_g are the angles of rotation of the gears of interest and r_g is the radius of the driven gear.

2.5.5 Variation of Contact Load

The dynamic variation of tooth contact force during the engagement cycle is another primary cause of vibration generation in gear systems. The contact load distribution varies in amplitude with direction or position of the contact points over the tooth profile, in turn this can cause dynamic excitation between the meshing gears. In general, the speed-torque characteristics vary with operational conditions, which produces a slight fluctuation in gear speed with variation of the transmitted load. The load variation is mainly caused by the following factors:

- The alternating engagement number of the contact pairs of teeth.
- The variation of the mesh stiffness along the **LOA**.
- The deviation in the involute tooth profile.

2.5.6 Backlash

Backlash is the clearance between two mating gear teeth, which is required for smooth operation. A gear pair is bound to have some backlash to prevent mating gears from grinding contact on both sides, and allows lubrication to enter the contact regions. However, backlash can result in additional dynamic forces and can cause excessive

vibration levels due to its double-sided impacts. The effect of vibration due to backlash can cause tooth separation and loss in contact between the teeth, the nonlinear backlash force *f(x, b)* can be expressed as in Eq. (2.11) [87, 88].

$$f(x,b)=\begin{cases} x-b & (x>b) \\ 0 & (-b\le x\le b) \\ x+b & (x<-b) \end{cases} \qquad 2.11$$

As a consequence of contact loss, the linear gear stiffness will have a piecewise characteristic. The discontinuation represents the backlash, whereby the impact in a gear system is not observed when the displacement *x* lies in the region ($-b \le x \le b$), see Figure 2-8. This makes for a strong nonlinear effect, causing complex behaviour and intense vibration [89].

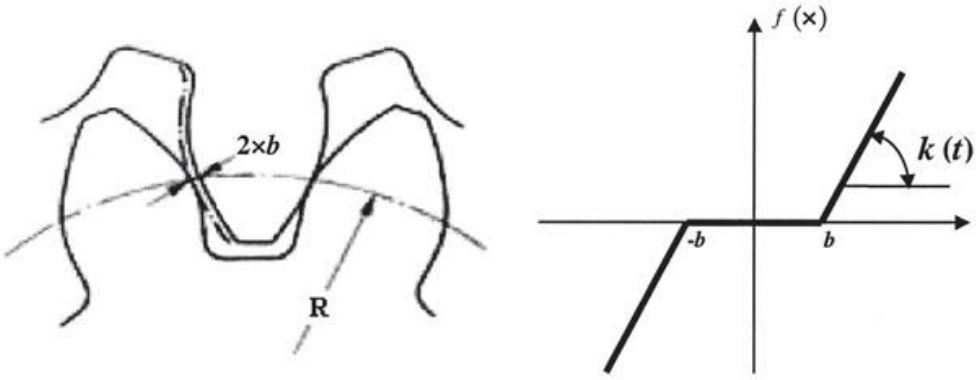

Figure 2-8 Nonlinear expression of gear backlash [89]

2.5.7 Machining Error

Deviation in the mean running surface of the teeth profile tends to cause vibration in gears with strong instabilities in the overall dynamics of the geared system. The difference between the perfect involute surface and the actual one will influence the load sharing characteristics. Various gear errors will occur due to an incorrect profile on the gear cutting tool or errors in positioning the tool in relation to the work during the generating operation.

Heat treatment can result in deformation and distortions of the gears. Run-out of the gear surface results in accumulated pitch variation, which generates non-uniform motion and transmission error. These manufacturing error significantly influence the gear vibration and enhance the amplitudes of the tooth meshing harmonics.

2.5.8 Resonance

To understand and control gear vibration, it is important to have knowledge not only about the gears but also about the complex behaviour of the assembly. The dynamics of the gear system basically consist of a wide range of meshing gears, shafts, bearings and gearbox casing. Because each gear tooth meshes with an impact, structural resonance may be excited by operating speeds in the gears, shafts and housing [90]. Resonance in the gearbox should be monitored because it can amplify vibration to a level beyond the intended design limits and accelerate system failure.

2.6 Failure Modes of Gears

For gear systems or gear trains a high efficiency and low levels of noise and vibration are the main requirements. Any failure in the gearing components will alter the normal operating conditions and may lead to total system failure. Gears can fail in service for a variety reasons including poor design, inappropriate application and manufacturing error. The physical causes of most gear damage are [91]:

- Overload or shock loading,
- Bending fatigue,
- Contact fatigue,
- Wear and scuffing, and
- Cracking.

Gear damages can be divided into geometrical defects and teeth errors. In which, geometrical defects include manufacturing defects and installation errors, while teeth errors are the defects that affect the working surfaces of the gear teeth and occur during its running. According to ISO 10825 standard [92], these defects can be classified as shown in Figure 2-9.

In general, gear faults can be categorized into localized faults and distributed faults. Local faults are those that affect a small area such as a cracked or chipped tooth or spalling, but these can rapidly increase in area once initiated, and if not detected early will spread until they are distributed faults over a large area of the gear surface. Distributed faults may also be due to wear and fatigue and will spread over a large area and damage the working surfaces of the gear teeth.

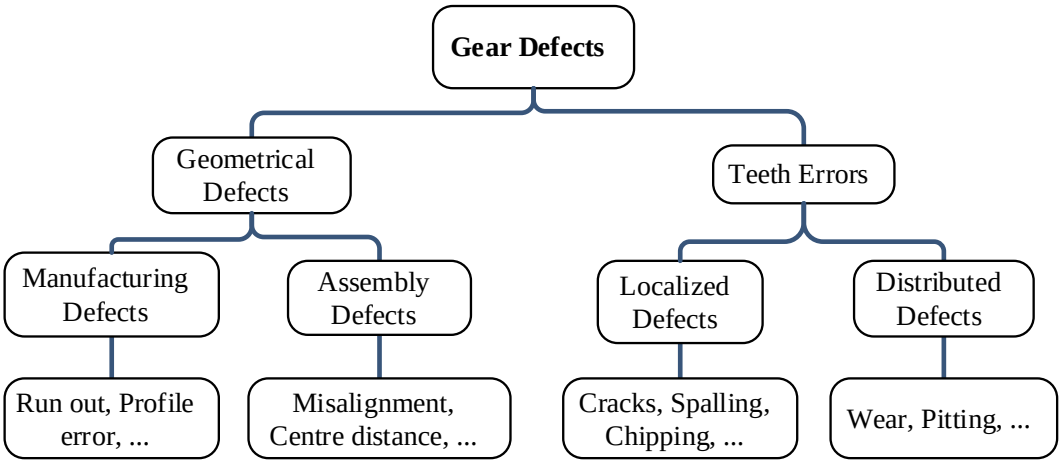

Figure 2-9 Classification of gear defects [93]

2.7 Gear Lubrication

Lubrication has a strong influence on the damage formation of typical gear failures. Many researchers have applied a wide range of approaches and much effort to improve the application of lubrication in the mechanical engineering industry. Gear lubrication significantly affects the health of the transmission system.

During operation, gears will experience rolling, sliding, vibration and shock-loading, and the useful life of the gears may be shortened or terminated by pitting, abrasive wear, fracture, etc. [94]. Lubrication is essential for extending gear life and protecting the surfaces in contact from the tribological processes which cause failure [95].

Adequate lubrication is necessary for the successful and efficient operation of gear transmission systems. Therefore, lubricants with extreme pressure (EP) additives are carefully designed and produced to minimise unwanted reactions between the mating tooth surfaces [94]. Suitable gear lubricants must have the following essential properties [94, 96]:

- High adhesive quality to maintain the required boundary films and remain on the gear teeth under heavy loads. This enables the tooth contact surfaces to resist centrifugal force and the pressures created by the tooth meshing forces.
- A viscosity such that the lubricant is thin enough to flow into the contact mesh regions to support the tooth mesh load and create the necessary boundary films at different operating temperatures.

- Frictional characteristics that will eliminate any stick–slip condition and chatter when rotation first starts.
- Remain unaffected chemically by heat, resist oxidation and be capable of dissipating any heat caused by friction or churning as quickly as possible.

2.8 Gearbox Lubrication Status

Gearbox oil lubricant is important in preventing premature wear and friction between gear teeth surfaces, which reduces gear vibration and increases the lifetime of the gears. The main function of lubrication is to maintain a lubrication film between two moving metal surfaces, which improves machine availability and efficiency through minimizing friction, reducing wear and preventing a temperature rise between the parts in contact. However, various circumstances influence the performance of the gearbox oil, including:

2.8.1 Lubricant Contamination

Oil lubricant is subject to many contaminants such as water, sulphur, etc. [97]. High water content can destroy both physical and chemical properties of the lubricant and cause corrosion and oxidation. Emulsion may be present due to the water content, and emulsion has a lower load carrying capacity which results in damage failure to the operating surfaces [98]**.** There are various ways for water present in the surrounding air as rain or humidity, may ingress lubrication systems; e.g. through condensation of air in oil or through defective seals or leaky gaskets or reservoir covers that have been damaged.

Water contamination causes undesirable mechanical effects such as change in viscosity and lubricant degradation, cavitation in pumps, and chemical reactions with anti-wear additives and oxidation inhibitors to generate solid precipitates [99].

2.8.2 Lubricant Viscosity

Viscosity is one of the parameters that can accurately reflect oil performance and has been used as a standard feature to monitor the state of the lubrication oil. The gear oil viscosity has a significant impact on the gear lubrication function. Viscosity will normally increase as a result of lubricant oxidation and degradation or contamination with higher grade oil, which result in a thicker lubricant film that improves anti-wear and damping behaviour. However, the proper gear lubricant, matching its properties to the particular application, is important to long-term and efficient operation; if the oil's viscosity is too high, churning

and shearing losses will increase, meaning more energy is required to turn the gears and there will be an increase in heat generated [100].

2.8.3 Lubricant Volume

Loss of lubrication or lubrication starvation could lead to critical failure of many gears and bearing systems. Insufficient lubrication of a gearbox, can increase friction, temperature and material wear, increase scuffing, pitting and micro-pitting, and will ultimately lead to a failure of components that are essential to the continued functioning of the system [101], [102, 103].

The oil immersion depth is the major influenced on drag and churning losses in the gears, these must be balanced against the detrimental effects of increased gear bulk temperatures and scuffing failure if the oil level is too low [103, 104].

2.9 Gear Faults Related to Lubrication

The gear tooth surfaces roll over and slide against each other, and it combines rolling and sliding motion which generate the various common gear failures. The sliding motion and variation in friction tends to generate additional stress in the region of the contact band, which result in cracks and plastic flow on tooth contact surfaces subject to heavy loads [105]. The distribution of the stress resulting from combined rolling and sliding is shown in Figure 2-10, and it can be seen the maximum influence of shear stress is located very close to the contact interface [106].

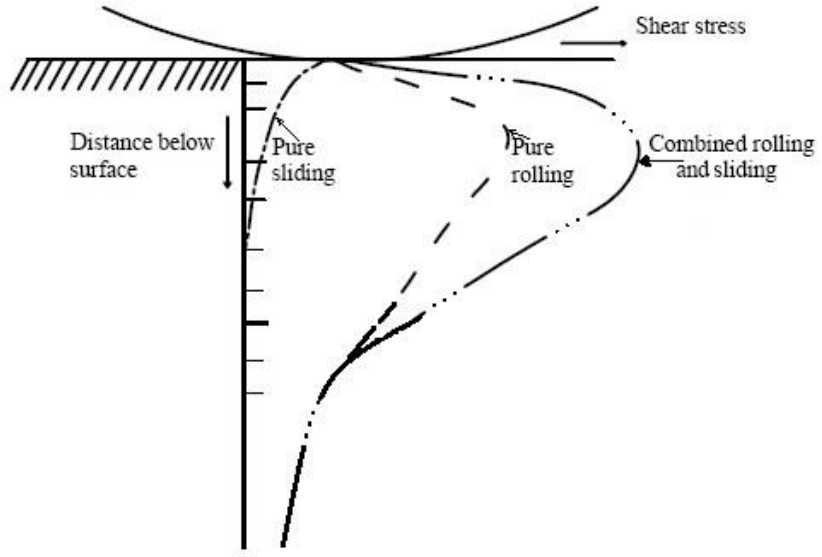

Figure 2-10 Stress distribution between the contacting surfaces under sliding-rolling [106]

A complex mixture of rolling and sliding are excited during the meshing process of tooth pairs, which vary along the profile of each tooth, as depicted in Figure 2-11. The gear teeth initially come into contact at point **C**, where the tip of the gear engages near the root of the pinion. There is a combination of rolling and sliding, whereby the directions are the same in the addendum while the sliding (friction) direction is opposite at the tooth root. The sliding rate changes continuously during the meshing process and undergoes a reversal in direction at the pitch line. It is only zero at the pitch point **P**, at which there is, only momentarily, a pure rolling effect.

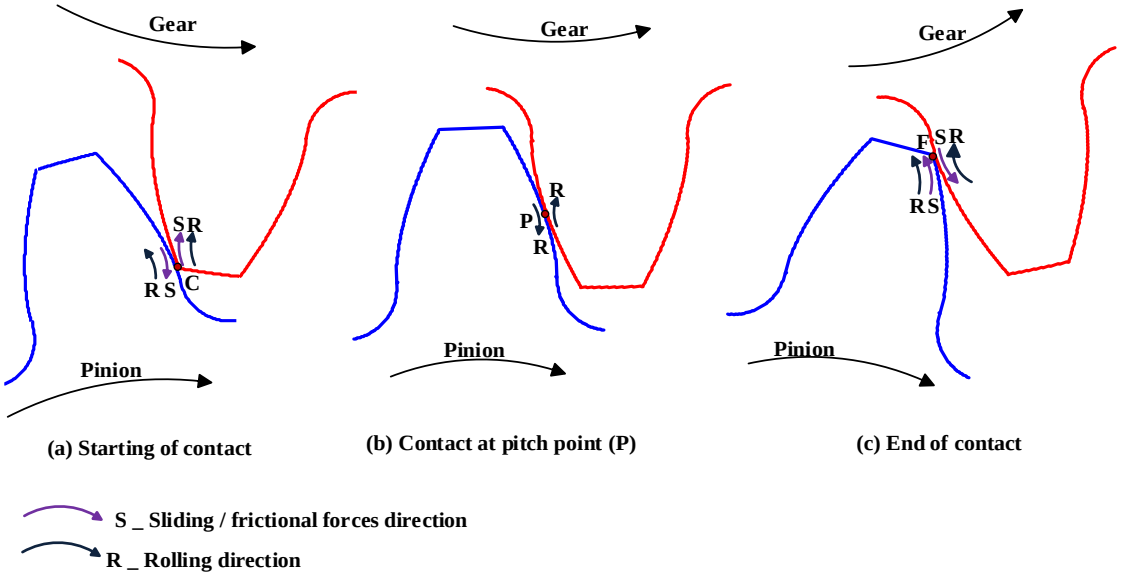

Figure 2-11 Sliding and rolling combination for gear tooth contact [106, 107]

The friction forces between the contact surfaces are produced due to the sliding action. These forces always act away from the pitch line of the pinion teeth, whereas the effect on the driven gear teeth is towards the pitch line. Based on the relative velocities of the contact surfaces, rolling and sliding occur in the same directions or in opposite directions. For opposite directions of rolling and sliding, the effect is rolling the surface material in one direction, and pushing (sliding) in another, which results in higher stresses than when both rolling and sliding have the same direction. Therefore, contact fatigue and pitting are more likely to be initiated in the dedendum [106, 108].

Hence, sliding is continuously present within the gear mesh process and the presence of a lubricant is crucial for the survival of any set of gears, especially if heavily loaded. The continued presence of the lubricant depends mainly on the lubricant service conditions. The most common gear faults due to lubrication failure are:

2.9.1 Tooth Surface Wear

Gear wear is the undesired removal of material that continuously alters the surface geometries of the contacting teeth due mechanical meshing, and results in loss of gear tooth profile and thickness together with changes in load distributions and contact stresses, which accelerate the occurrence of other failure modes such as pitting and scoring [109-111].

Tooth surface wear occurs over a relatively long period of time, with the breakage-off of small particles from both contact surfaces, and may range from excessive wear to catastrophic breakage. Wear accumulation has a significant effect on gear dynamic behaviour such as decreasing meshing stiffness, larger transmission error, and an increasing backlash. Thus, it can influence the functioning of a gear pair and change the tooth contact patterns [109, 112-114]. As a result, the vibration characteristics in terms of vibration amplitudes, harmonic content and the degree of nonlinear behaviour will be changed [112, 114].

The major types of tooth surface wear are:

- ***Abrasive Wear***

Generally abrasive wear is categorized as the cutting or removing of small distorted fragments from the contact surface due to the presence of foreign material such as fine abrasive particles in the lubricant [108], and radial scratch marks or grooves will commonly be present on the contact surface. Abrasive wear progresses very quickly and shows as a distortion in the tooth profile and more gear backlash, which influence the dynamic behaviour of the meshing process and greater levels of noise and vibration are expected.

- ***Adhesive Wear***

Adhesive wear arises by gradual removal of adhered fragments during frictional interactions and transfer of material from the contact surface of one tooth to that of another. It is characterized by high wear rates and the heat that is generated by unstable friction, in which the sliding motion may be prevented due to very large coefficients of friction. The adhesive wear is mainly related to a breakdown in the lubricant's basic function of providing some degree of separation between the sliding surfaces [115].

- ***Corrosive Wear***

Oxidative wear is often referred as corrosive wear, which occurs when oxygen in the environment interacts with the contact surfaces. High sliding, high contact pressure and

asperity interaction activity result in a continuous oxidation layer being formed and removed from the contact surfaces [116].

- ***Contact Fatigue Wear***

Fatigue wear is mainly caused by cyclic and repetitive loading, which is widely observed on rolling contact machine elements such as gears and bearings. As a result of material surface fatigue, contact fatigue wear reflects this process under alternating contact stress with a peak level. As a result of contact stress fatigue, fragments of pits or cavities in the contacting surfaces are removed under continued rolling and sliding. Since fatigue is initiated by shear stresses, several types of fatigue failure occur in rolling/sliding elements due to variations in rolling and sliding contact along with the variation of metallurgical and geometrical variables [108].

2.10 Key Findings

- Helical gears are widely used in different industrial applications due to high transmission power applications requiring low noise operation and smooth meshing engagement.
- Gears often work under harsh conditions in severe environments in which monitoring and diagnosing of gear faults as early as possible is essential.
- Understanding the sources of gear vibration and noise can improve the selection of gears for given working conditions and enhance the capability of the transmission systems.
- Friction between tooth contact surfaces is an important excitation parameter in gear dynamic instabilities that can lead to large nonlinearity excitations.
- The lifetime and healthy operation of gear transmission system are significantly influenced by the lubrication conditions.
- Various gear failures are frequently related to the combination of rolling and sliding motions during the meshing process.
- Detecting and diagnosing gear wear in its early stage can reduce the risk of occurrence of failure modes such as pitting, scoring and tooth breakages.

Chapter 3

Gearbox Fault Detection and Diagnosis Techniques Based on Vibration Analysis

This chapter presents those signal processing techniques most widely used for fault detection and condition monitoring of gear systems, based on vibration measurements. The suitability of relevant vibration analysis techniques is briefly discussed in association with the process of obtaining effective diagnostic features for detecting and identifying different gearbox defects. Especially, their mathematical backgrounds and physical explanations are developed to assist the understanding of the results presented in the following chapters of this thesis.

3.1 Introduction

Geared machines generate vibration even when operating in a healthy condition, this is due to the meshing of the gear stages and shaft rotation. Machine components generate their own characteristic vibration signals that separate them from the other components and distinguish their health conditions [14].

Much work has been undertaken with the aim of finding a reliable monitoring strategy for gear transmission and bearing support systems [9, 35, 117]. Vibration analysis is one of the most common and effective techniques for online health monitoring of machinery components to avoid breakdowns and, possibly, even catastrophic failures of a system [118]. The main advantage of vibration signature analysis is that the vibration signal can be readily collected experimentally (or predicted theoretically) for analysis and feature extraction to assess the machine condition [51]. Different techniques and fault identification procedures can be applied to the vibration signal to extract signatures which provide useful diagnostic information, enabling all parts of rotating machinery to be monitored [45, 50].

3.2 Fault Detection Techniques Based on Vibration Signal

To detect and correctly diagnose an imminent failure, suitable methods for detecting, analysing and assessing any abnormal condition of the rotating machinery are required. Vibration monitoring is the most popular monitoring technique for detecting gear faults. It does this by extracting certain statistical parameters which are known to be correlated with particular faults. However vibration signals are often contaminated by noise and require suitable signal processing to extract useful information for determining the condition of the system [8, 119].

Gearbox faults such as wear, tooth breakage, spalling, unbalance shafts and other abnormal conditions generally produce repetitive impacts, which result in a modulation phenomenon in the vibration signals. Hence, sidebands will appear near the resonance frequency or gear mesh frequencies, so that demodulation is an important element in the signal processing for gearbox condition monitoring and fault diagnosis. The most popular vibration based diagnosis techniques, because of ease of implementation, include: Waveform analysis, Fast Fourier Transform (FFT), Spectral analysis, Order Analysis and Time Synchronous Averaging (TSA) [120].

In feature extraction of gearboxes, much research and problem solving has been required due to the complicated nature of machine structures and the many different types of signal interference that can occur. Feature extraction techniques can locate specific components, and detect vibration signatures in vibration signals using appropriate analytical techniques [119].

To do this successfully it is critical to reduce the random noise and enhance the signal-to-noise ratio (SNR) for more reliable feature extraction. To this end, vibration signal processing techniques have attracted extensive research, particularly the detection and diagnosis of machine faults in their early stages, leading to the development of many useful techniques in condition monitoring and fault diagnosis.

The main techniques applied to vibration signals for gearbox fault diagnosis are:

3.2.1 Time Domain Waveform Analysis

Time domain analysis of the waveform data is a well-known CM technique. Generally, this technique extracts information based on a statistical measurement of the vibration signal as a function of time. Conventional techniques include several time features: peak values (PV), root mean square (RMS), crest factor and kurtosis are the most common statistical parameters that have been applied to diagnosing bearing and gear faults [121]. In addition, the use of TSA has made time domain analysis more effective in detecting faults, especially in gearboxes.

The time-domain signal is a visual representation of the instantaneous acceleration compounding all individual frequency components. The procedure used to perform the analysis of the time domain signal is either visual inspection or, more usually, to analytically interrogate the time-domain using statistical parameters [122]. The time domain signal can indicate the existence of faults, as when periodic impulses and high levels of vibration over wide frequency bands are observed, but it can be difficult to diagnose the source of the faults.

Typical vibration waveforms of different gearbox tests are shown in Figure 3-1. The waveforms show the anomalous behaviour between the healthy and faulty gearbox due to the presence of different faults (tooth-breakage and tooth surface wear).

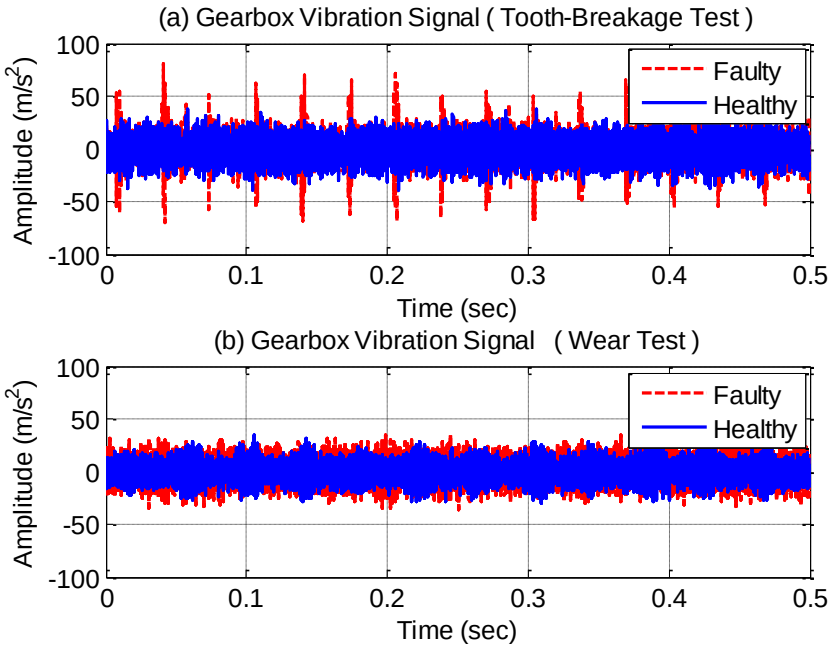

Figure 3-1 Raw data of vibration acceleration signals for different gearbox tests.

In Figure 3-1 it is possible to detect changes in the vibration signature due to the presence of faults; the large amplitude periodic impulses and higher vibration levels resulting from the gear faults can be identified easily. However, diagnosis of a fault from the observed symptoms (vibration waveform) can be a difficult task if the variation in the waveform is small [120]. Statistical parameters are often used to quantify the time signal but the specific fault condition of the system may not be predicted accurately.

3.2.1.1 *Root Mean Square*

The root mean square (RMS) value of a vibration signal is a time analysis feature that measures the power content in the vibration signature [119]. It is the best-known of the time -domain parameters used to detect faults in rotating machines. This feature is good for tracking the overall vibration level, and can be very effective in detecting any major out-of-balance in rotating systems, but it is not sensitive enough to detect incipient faults in particular, or provide any information on which component is failing [48].

RMS can be calculated by normalizing the second statistical moment of the signal, see Eq. (3.1):

$$RMS_x = \sqrt{\frac{1}{N}\sum_{n=1}^{N}\left(x(n)-\bar{x}\right)^2} \tag{3.1}$$

$$\bar{x} = \frac{1}{N}\sum_{n=1}^{N} x(n) \tag{3.2}$$

Where *N* is the number of samples in the recorded signal, *x(n)* is the amplitude of the signal for the nth sample and $\bar{x}$ is the mean value of the *N* amplitudes.

In general, the RMS of a vibration signal is a very good descriptor of the overall system condition. In addition, the vibration level of the machine can be monitored using change of RMS, typically the vibration level will increase more rapidly when gear damage happens. The RMS is also sensitive to operational condition changes [33].

3.2.1.2 *The Crest Factor (CF)*

This feature is useful for the early stage detection of defects in bearings and gears. It is the ratio of the peak level of the raw time-domain signal to the RMS value for the same signal, as explained in Eq. (3.4) [123]. The higher the largest peaks in the signal, the larger the crest factor. For gear vibration signals, the CF ranges between 2 and 6 for normal condition [48], so if the value of the CF exceeds the upper limit that should be taken to mean the presence of a defect.

$$Crest\ Factor = \frac{Peak\ level}{RMS} \tag{3.3}$$

$$Peak\ level = Max\ |x(t)| \tag{3.4}$$

Where *x(t)* is the time waveform signal.

For more explanation, Figure 3-2 depicts the CF value, peak and RMS level of a vibration signal with an impulsive source such as gear tooth breakage. Based on Eq. (3.3), the CF can be a sensitive and a reliable indicator only in the presence of significant impulsiveness [124], in which the peak value increases while no significant change in the RMS value of the vibration signal occurs [33]. However, RMS increases with damage progression and the corresponding CF value decreases. Thus it is difficult to use CF to diagnose the damage severity for established faults.

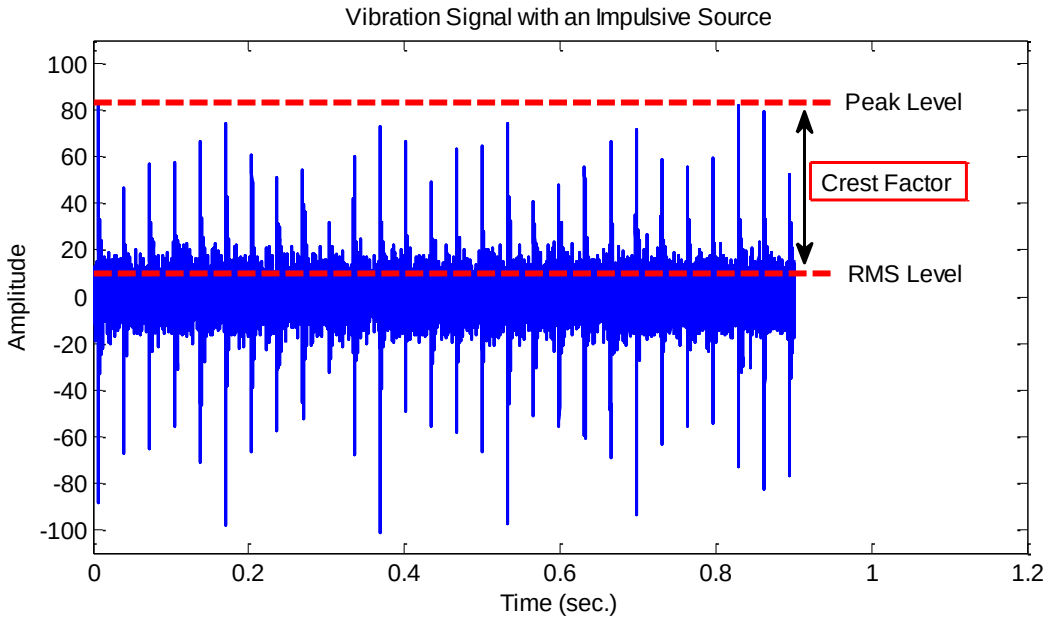

Figure 3-2 Crest Factor, peak and RMS levels with an impulsive source such as gear tooth breakage (CF exceeds the limit)

3.2.1.3 *Kurtosis*

Kurtosis is defined as the fourth moment of the distribution of the signal. It provides a measure of the impulsive nature of the signal. The use of the fourth power makes Kurtosis very sensitive to the peakedness or flatness of the signal. The fourth power of the signal effectively amplifies the contribution of isolated peaks in the signal [124]. Kurtosis provides a measure of the major peaks in a set of data but it has the same weakness as CF. In the initial stages of gear breakage this feature will be high and is a sign of a fault, but as the fault grows in magnitude and extends, the relative amplitude of the peaks decrease. The equation for kurtosis is:

$$kurtosis = \frac{\frac{1}{N}\sum_{n=1}^{N}\left(x(n)-\bar{x}\right)^4}{\left[\frac{1}{N}\sum_{i=1}^{N}\left(x(n)-\bar{x}\right)^2\right]^2} \tag{3.5}$$

3.2.2 Time Synchronous Averaging (TSA)

TSA is a signal processing technique that eliminates the influence of noise by extracting periodic waveforms or repetitive signals from noisy data. It can be used to enhance the SNR by resampling the vibration data synchronously, say, shaft rotation [125]. TSA is an effective technique in the time domain used widely in vibration monitoring and fault

diagnosis in order to suppress components which are asynchronous with the ones of interest [126]. It has been successfully applied in the area of diagnosis of early defect detection in gears and bearings [127-129].

The TSA is well suited for gearbox analysis, in which it enables the vibration signature of the gear under analysis to be separated from other gears and noise sources in the gearbox. It can show the pattern of the tooth meshing vibration over one revolution, including any modulation effect [12]. The noise components include electrical noise, bearing vibrations and vibrations related to other shafts or nearby machinery, which can confuse the periodicity of fault impulses and affect the accuracy of fault diagnosis.

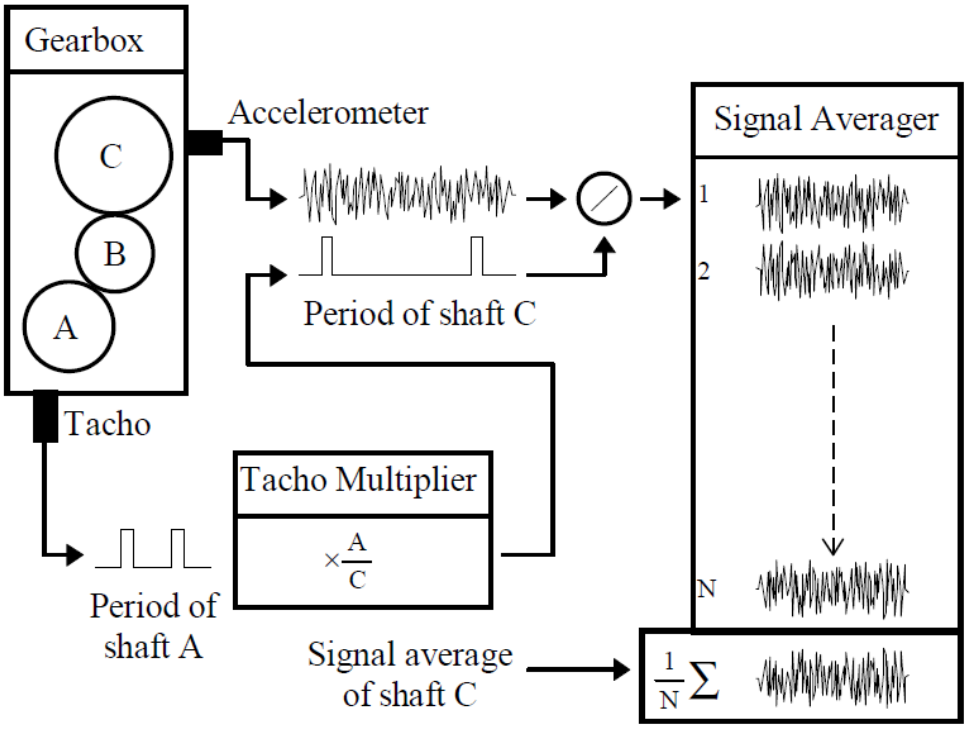

Figure 3-3 Synchronous averaging process of a gearbox vibration signal [130].

The TSA is applied based on knowing the rate at which the component part of interest is rotating. It requires an external time trigger so that each sample of the signal is over the same period, and must accommodate variations in shaft speed. This can be accomplished by using a shaft encoder (or tacho multiplier) which ensures the samples taken all begin at the same point in the rotation cycle and for the same period of time, say one rotation of the shaft. The time domain of the vibration signal is divided into segments according to the period of revolution of the rotating shaft, and all the segments are summed, so that random noise and asynchronous components cancel out. Figure 3-3 depicts how the main TSA

process is performed on a continuous time signal of a gearbox, using a tacho multiplier to provide the trigger signal of each rotational period of the given shaft.

Generally, vibration signals from rotating machinery are a combination of periodic signal with random noise. Assuming a signal $x(t)$ consists of a periodic signal $x_T(t)$ and a noise component $n(t)$. If $x_T(t)$ is spaced at intervals T_o with a fundamental frequency $f_o=1/T_o$, then the signal can be expressed as [131].

$$x(t) = x_T(t) + n(t) \tag{3.6}$$

The vibration signal $x(t)$ is divided into segments according to the interval T_o, then all the segments are added together for averaging, which can be expressed as:

$$y(t) = \frac{1}{N}\sum_{i=0}^{N-1} x(t + iT_o) \tag{3.7}$$

Where N is the number of the averaged segments and $y(t)$ is the averaged result.

The number of the averages is an important parameter that affects the accuracy of $y(t)$ [132]. After performing a sufficient number of averages, only frequencies at exact multiples of the trigger frequency f_o are passed, which can be viewed in the frequency domain. Analysis of the synchronously averaged signals enables extraction of the features of interest [128].

However, more computational intensive of measurement and calculation time are required by increasing the number of averages [133]. The main drawback of TSA is that it needs additional instrumentation (sensor, encoder/tacho), which is sometimes difficult to install. In addition, it may suppress some important information, spectral frequency components that are not in the same integer harmonics with the shaft frequency, these could include bearing frequencies.

3.2.3 Frequency Domain Analysis

A spectrum or frequency-domain signal is a plot of the amplitude of a signal as a function of frequency. It can show how the signal's energy is distributed over a range of frequencies. Spectral analysis is commonly used with vibration analysis for condition monitoring in geared transmission systems and has proved a valuable tool for detection and diagnosis of faults in different rotating machinery systems [2].

The advantage of frequency-domain analysis over time-domain analysis is its ability to easily identify and isolate frequency components of interest, and the repetitive nature of

the vibration signal is clearly displayed as peaks in the frequency spectrum [90]. The vibration signal of a machine is generated by both the individual components and by their assembling and installation. Each component in a working machine generates a specific identifiable frequency, thus a given frequency spectrum can often be attributed directly to corresponding machine components [134]. As shown in Figure 3-4, the gearbox characteristic frequencies such as shaft frequency f_r, meshing frequency f_m, sideband frequency f_{sb} and their harmonics can be identified easily.

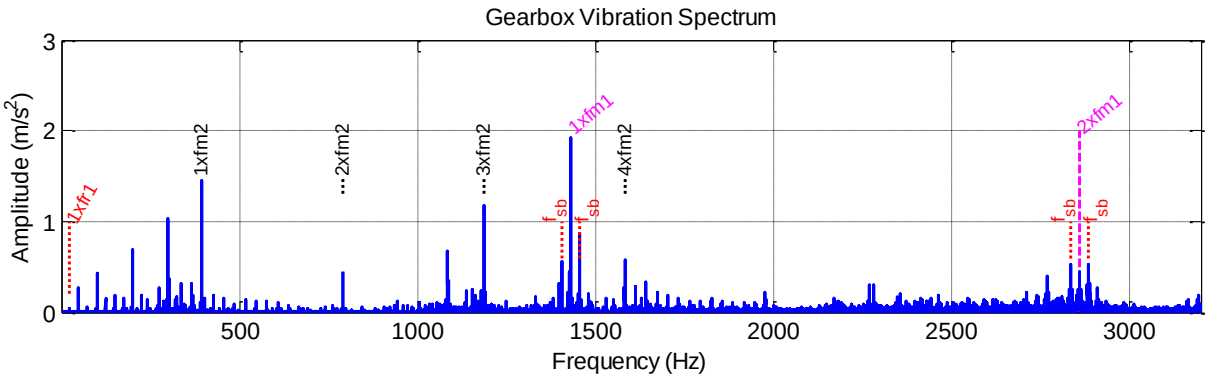

Figure 3-4 Vibration spectrum characteristics of industrial gearbox.

The main idea of spectrum analysis is to look at the whole spectrum, identify frequency components of interest and extract features from the signal for the purpose of effective and accurate fault detection [135]. Frequency domain methods include the Fast Fourier Transform (FFT), Hilbert Transform and Power Cepstrum, etc. The difference in power spectral density due to the presence of a gear and/or bearing fault is used by these methods to detect and identify the damaged elements [18].

The most widely used conventional method for spectrum analysis is the FFT, which is implemented as the Discrete Fourier Transform (DFT) with considerable savings in computational time. The Fourier transform is defined by the following equation:

$$X(f) = F\{x(t)\} = \frac{1}{T}\int_{-T/2}^{T/2} x(t)e^{-j2\pi ft}dt \tag{3.8}$$

Where *x(t)* is the time domain signal with a periodicity of *T, and X(f)* is the FFT of the main signal and *f* is the induced frequency.

Frequency domain features are generally more consistent in the detection of abnormal change and diagnosis of gearbox condition [136]. It offers the possibility of displaying the repetitive nature of the vibration signals and isolating them as frequency components

related to specific machine parts or faults [18]. Different techniques based on Fourier spectrum analysis are explained in more detail in [13, 137].

However, although the spectral analysis method is very well recognised and widely used for CM of machines, it is somewhat unsuitable for the extraction of information from a non-stationary signal [138]. In general, faults occurring on machinery components generate non-stationary signals, and these non-stationary components contain vital information related to the machines' faults [138]. Hence, it is critical for fault diagnosis to process these non-stationary signals.

3.2.3.1 *Mesh Frequency Characteristics*

Examination of the amplitude of the vibration frequency spectra often provides useful information about the source of failure. In gear systems, the meshing frequency is the dominant excitation feature of the vibration signals [2, 7, 120, 139-141] . The changes in the spectral amplitudes of the meshing frequency components usually indicate the potential condition of the gear system. Each gear set generates a unique profile of frequency components which should be monitored consistently [142]. The gear-mesh frequency (f_m) and its harmonics can be calculated by multiplying the gear teeth number (Z) by the rotational speed (ω) or rotation frequency (f_r) of the same gear.

$$f_{m,i} = i \times (\frac{Z_p \omega_p}{60}) = i \times (\frac{Z_g \omega_g}{60}) \tag{3.9}$$

or:

$$f_{m,i} = i \times Z_p f_{rp} = i \times Z_g f_{rg} \tag{3.10}$$

Where i is an integer number referring to the ordinal harmonic of the corresponding mesh frequency. Z_p, Z_g are the number of teeth on pinion and gear respectively. ω_p , ω_g are rotational speeds in (rpm) of the pinion and gear respectively, and f_{rp} , f_{rg} are shaft rotation frequencies in (Hz) of the pinion and gear respectively.

With gears, special attention must be given to any changes that occur in the peaks produced at the meshing frequencies. Randall has claimed that the first three gear meshing harmonics and their sidebands provide sufficient information for both the successful identification of the presence of a gear fault and its condition [143]. Therefore, by observing the changes in these features, the progression of gear faults can be monitored and a good indicator of gear failure sources provided.

3.2.3.2 *Shaft Frequency*

Vibration of shafts and their associated couplings occur at machine rotational frequencies. These vibrations are dominant and, therefore, their amplitudes are assumed to be a function of angular speed. Generally, different faults, such as unbalance, misalignment and shaft bending can, most easily, be detected by monitoring the amplitude and phase of rotational speed components [144, 145].

For a gearbox operating at constant speed, the variation in the rotational frequency is due to the fluctuations in transmitted load/torque between the gear shafts. However, this variation is assumed to be negligible in relation to the dynamic response of the mean rotational frequency. The shaft frequencies of each of the pinion (f_{rp}) and gear (f_{rg}) can be calculated in terms of the rotational speeds (ω_p and ω_g) as:

$$f_{rp} = \frac{\omega_p}{60}, \quad f_{rg} = \frac{\omega_g}{60} \tag{3.11}$$

3.2.3.3 *Sideband Characteristics*

In the frequency spectrum, sidebands appear due to the repetitive impacts of faults. Gearbox defects usually result in modulation phenomenon in the vibration signals, which appear as families of sidebands around the gear mesh frequency components. The modulations effect in the gearbox's vibrations are caused by eccentricities, varying gear-tooth spacing, pitch errors, varying load, etc. [146].

Local gear faults, such as cracked or broken gear teeth can also excite a number of sidebands around the mesh frequency harmonics, with spacing equal to the rotation speed of the faulty gear. Analysis of sideband components can give a clear indication as to the nature of gear faults and provide useful information on the detection and diagnostic capabilities of gear defects.

Any differences in the gear vibration responses may cause changes in the sidebands across the fundamental and harmonics of the gear mesh frequency. Each gear set generates a series of modulations/sidebands around the harmonics of the fundamental gear mesh frequency, where the sideband frequencies can be written as [143]:

$$\begin{aligned} f_{sb,ij} &= f_{m,i} \pm j \times f_{rp} \\ f_{sb,ij} &= f_{m,i} \pm j \times f_{rg} \end{aligned}, \quad i = 1, 2, 3..., \quad j = 1, 2, 3... \tag{3.12}$$

Where: j is an integer number of the sideband frequency component.

3.2.3.4 *Modulation Effects*

The components of the gear mesh frequency are the dominant features of the gear transmission spectrum. However, the signal is subjected to modulation when a non uniformity is induced into the gear mesh period, which result in sidebands around the harmonics of the gear mesh frequency. Demodulation is necessary to extract the main signal and the modulating or carrier signal, and both of them provide valuable information for CM of the system. Demodulation is extraction of the data signal by removing the carrier signal from the modulated signal.

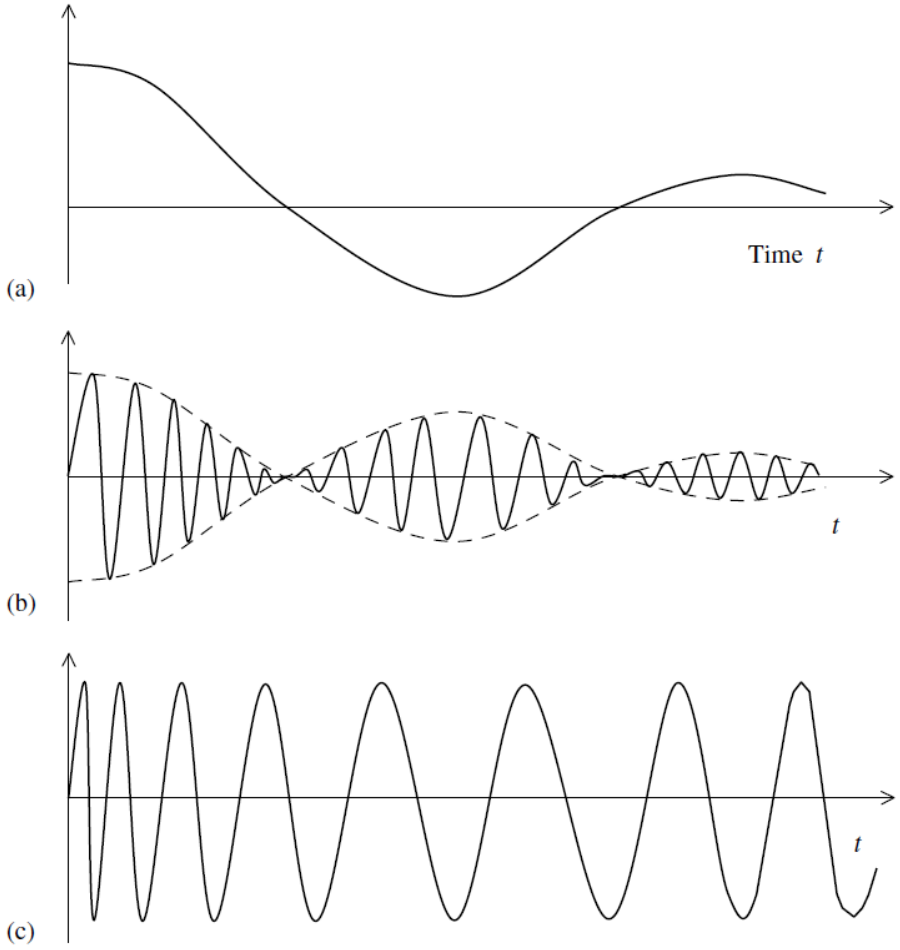

Figure 3-5 (a) Modulating signal; (b) amplitude-modulated (AM) signal; (c) frequency modulated (FM) signal [4].

Amplitude modulation (AM) and frequency modulation (FM) are the most common forms of signal modulation [4]. A transient signal shown in Figure 3-5(a) is used as modulating signal. For AM, the amplitude of a periodic carrier signal is varied according to the amplitude of the modulating signal, whereas the frequency of the carrier signal is kept

constant, as shown in Figure 3-5(b). AM can be useful in the applications of fault detection and diagnosis in rotating machinery [4].

The carrier signal amplitude remains constant in FM, whilst the carrier signal frequency is varied proportionally based on the amplitude of the modulating signal, as illustrated in Figure 3-5(c). FM is less susceptible to noise than AM.

3.2.3.4.1 Amplitude Modulation

The principle use of AM is particularly important in the practice of using mechanical vibration for fault detection and diagnosis of rotating machinery [4]. Randall states that the amplitude of a gearbox casing vibration, induced by the meshing of the gears, is modulated by the variability of torque load [143]. Because vibration amplitude is sensitive to tooth loading it is expected that the vibration amplitude will be modulated accordingly. This amplitude modulation causes sidebands to occur in the vibration spectrum, and several types of machine problems can be detected by monitoring the evolution of these sidebands [4, 147-149].

In the case of gearboxes, a number of gear faults can enhance the amplitude modulation due to the individual impacts generated by defect impulses [13, 18, 124, 150]. The eccentricity of a gear gives a continuous modulation by a frequency corresponding to the instantaneous rotational frequencies of the gearbox components. Local defects such as a cracked or spalled tooth will also cause irregular tooth meshing and result in modulation of the mesh frequency at the shaft rotational speed, with consequent sidebands around the harmonics of the gear mesh frequency.

AM can be achieved by multiplying the modulating signal $x(t)$ by a high frequency carrier signal $x_c(t)$, resulting in a signal $x_a(t)$ that is described by [4]:

$$x_a(t) = x(t)\, x_c(t) \tag{3.13}$$

The carrier is a high-frequency signal that could be any periodic signal, sinusoidal, square or triangular. A vibration signal with a carrier frequency f_c, and an amplitude A_c, can be expressed as:

$$x_c(t) = A_c \cos(2\pi f_c t) \tag{3.14}$$

The Fourier spectrum of the product signal is simply the Fourier spectrum of the original signal shifted through the frequency of the sinusoidal signal. In which, the Fourier spectrum

$X_a(f)$ of the amplitude-modulated signal $x_a(t)$, can be obtained from the definition of Fourier integral as:

$$X_a(f) = A_c \int_{-\infty}^{\infty} x(t)\cos(2\pi f_c t)\exp(-2\pi j f t)\,dt \tag{3.15}$$

Since,

$$\cos(2\pi f_c t) = \frac{1}{2}\left[\exp(2\pi j f_c t) + \exp(-2\pi j f_c t)\right] \tag{3.16}$$

the modulated waveform is given by:

$$X_a(f) = \frac{A_c}{2}\int_{-\infty}^{\infty} x(t)\exp[-2\pi j(f - f_c)t]\,dt + \frac{A_c}{2}\int_{-\infty}^{\infty} x(t)\exp[-2\pi j(f + f_c)t]\,dt \tag{3.17}$$

By assuming a linear process and extracting the common factors, the mathematical statement of the modulation theorem yields [4]:

$$X_a(f) = \frac{A_c}{2}[X(f - f_c) + X(f + f_c)] \tag{3.18}$$

The carrier frequency could be the gear mesh frequency, multiples of the bearing ball pass frequency, resonant frequency of a machine component/structure, or the resonant frequency of an accelerometer, whereas the sidebands are either the shaft rotational speed or one of its multiples [151].

3.2.3.4.2 Frequency Modulation

The gearbox vibration signal may contain amplitude and phase modulations that are periodic, with the rotation frequency of the gear. Variations in the rotational speed of the gears and/or variations in the tooth spacing will produce FM of the tooth-meshing frequency [130]. In fact, the fluctuations in the contact force between the meshing teeth not only give rise to AM, but also result in variations of angular velocity that give a FM at the gear meshing frequency. These modulations make vibration signatures for the diagnosis of gear faults much more complex in both time and frequency domains.

Under ideal operating conditions, the vibration from a pair of two perfect gears can be considered as a sinusoid with predominant frequency peaks at the gear meshing harmonics [152]. Including phase angles, the time-domain average of the gear meshing vibration $x(t)$, at time t, can be expressed as:

$$x(t) = \sum_{m=1}^{M} X_m \cos(2\pi m f_m t + \varphi_m) \quad , \quad m = 1, 2, 3... \tag{3.19}$$

Where, X_m is the vibration amplitude of a mesh frequency harmonic, m is the harmonic order of the gear mesh frequency f_m, and φ_m is the phase angle of the harmonic.

When a discrete gear fault (such as a tooth crack) occurs in a gearbox, this equation is modified by the introduction of periodic amplitude or phase modulations into the vibration signal. With these amplitude and frequency modulations present, the modulated signal $x_a(t)$, can be written as [153]:

$$x_a(t) = \sum_{m=1}^{M} X_m (1 + a_m(t)) \cos(2\pi m f_m t + \varphi_m + b_m(t)) \tag{3.20}$$

Where: $a_m(t)$ and $b_m(t)$ are the amplitude and phase modulation functions respectively, which produce sidebands around the mesh harmonics in the frequency domain.

3.2.4 Higher Order Spectra (HOS)

Inconsistencies in the analysis of the spectrum could be a result of noise inclusion. To obtain more consistent and accurate results, new signal processing methods have been developed with the aim of enhancing the SNR to enable more efficient diagnosis. HOS of discrete-time signals is a useful method for signal-processing and is used widely in data analysis [154-157]. HOS has the ability to reconstruct and preserve both magnitude and phase information.

In general, HOS (also known as polyspectra [158]) functions may contain different information about the signals, which can be classified as shown in Figure 3-6. The HOS are defined in terms of cumulants, as a set of *n* real random variables with their cumulant order. The n^{th} order spectrum $C(f_1, f_2, \ldots, f_{n-1})$ of the $x(t)$ is defined as the Fourier transform of its n^{th} order cumulant sequence $C_n(\tau_1, \tau_2, \ldots, \tau_{n-1})$ [158].

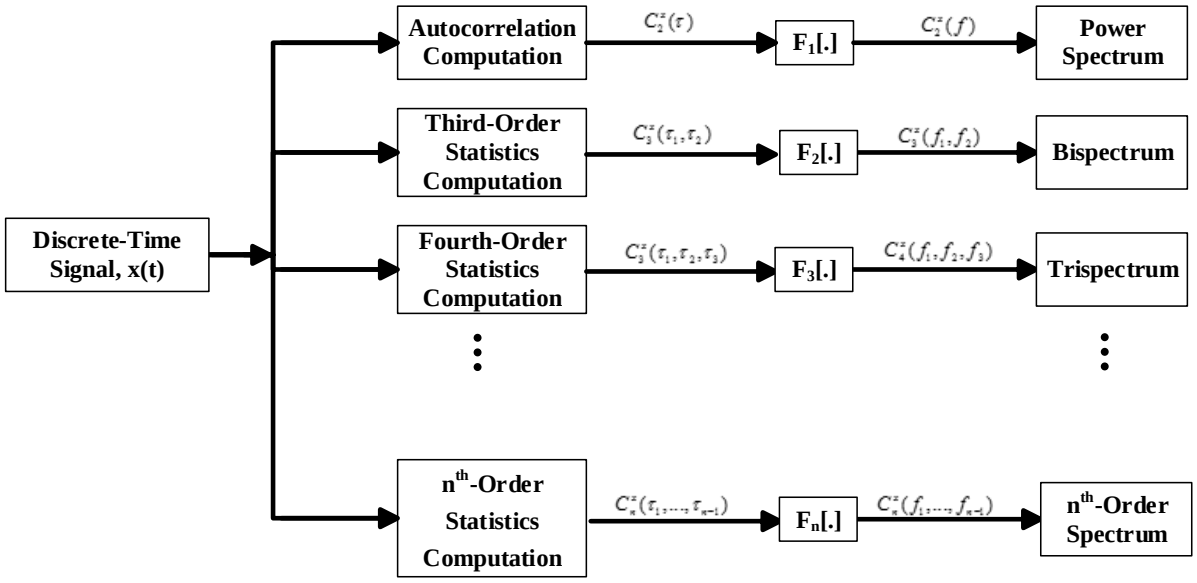

Figure 3-6 The higher-order spectra classification [159]

The generalised concept of HOS was introduced by Tukey and Brillinger in the early 1960s [160], and this method has attracted a large number of researchers in many areas. The HOS consist of higher-order moment spectra, which are very useful in the analysis of transient and periodic signals, and cumulant spectra for random processes, which is important in the analysis of stochastic signals. The general motivations behind the use of HOS in digital signal processing are [159, 161]:

1. To suppress the Gaussian noise of unknown power spectra.
2. To reconstruct and identify the phase coupling in the signals as well as the magnitude response of signals.
3. To detect and characterize nonlinear properties in the data.
4. To extract information due to deviation from Gaussianity and system nonlinearity.

3.2.4.1 *Power Spectrum (PS)*

The power spectrum is a real positive quantity which gives a measure of the harmonic power as a function of frequency. It can be defined based on its order spectrum, *n=2*. The DFT of the vibration signal *x(t)*, is defined as:

$$X(f) = \sum_{t=-\infty}^{\infty} x(t)\, e^{-j2\pi ft} \tag{3.21}$$

Which can be rewritten in the format of its magnitude *X(f)* and phase $\phi(f)$:

$$X(f) = |X(f)| \exp[j\varphi(f)] \tag{3.22}$$

The power spectrum of the signal *x(t)* is defined as the square of the magnitude of the Fourier transform of the signal

$$X(f) = \sum_{\tau_1=-\infty}^{\infty} C_2(\tau_1)\, e^{-j2\pi f\tau_1} = \left| \int_{-\infty}^{\infty} C_2(\tau_1)\, e^{-j2\pi f\tau_1} \right|^2 \tag{3.23}$$

Which can be written as the first-order cumulant:

$$PS(f) = E[X(f).X^*(f)] \tag{3.24}$$

Where $|X(f)|$ is the magnitude of the Fourier transform of the cumulant signal $C_2(t)$, $X^*(f)$ is the complex conjugate of $X(f)$ and $E[\ ]$ is the cumulant statistical expectation operator. It shows that a statistical averaging is necessary for the spectrum estimation process. However, no phase information can be measured by the power spectrum and certain types of phase coupling that could be associated with system nonlinearities cannot be correctly identified.

3.2.4.2 *Bispectrum Analysis*

Bispectrum is a higher order spectrum of the third order statistic, that can be used to suppress the effect of noise processes and search for evidence of nonlinear interactions in signals. It has the ability to recover the observed signal by estimating the magnitude and the phase information of the original signal [162]. It can also extract further phase information by detecting phase relationships between the frequency components. The bispectrum of a signal *x(t)*, is formally defined as:

$$X(f_1, f_2) = \sum_{\tau_1=-\infty}^{\infty} \sum_{\tau_2=-\infty}^{\infty} C_3(\tau_1, \tau_2)\, e^{-j2\pi f_1\tau_1} e^{-j2\pi f_2\tau_2} \tag{3.25}$$

Where, $C_3(\tau_1, \tau_2)=E[x_t, x_{t+\tau 1}, x_{t+\tau 2}]$ is the third order cumulant sequence of the signal *x(t)*.

3.2.4.2.1 Conventional Bispectrum (CB)

The third order estimation spectrum or the conventional bispectrum $B(f_1, f_2)$ can be expressed mathematically using the Fourier transform of a discrete time domain signal, which represents the contribution to the mean product of three Fourier components, in which one frequency is equal to the sum of the other two frequencies:

$$B(f_1, f_2) = E[X(f_1)X(f_2)X^*(f_1 + f_2)] \tag{3.26}$$

Where f_1, f_2 and f_1+f_2 are three individual frequency components.

The main properties of this third-order measurement are explained in [163], in which $B(f_1,f_2)$ is a complex quantity (containing both magnitude and phase), see Eq. (3.27); is biperiodical, see Eq.(3.28); symmetrical, see Eq. (3.29); and is capable of detecting and quantifying phase coupling. To show these properties, Eq. (3.26) is rewritten as [158, 163]:

$$B(f_1, f_2) = E[|B(f_1, f_2)| \exp[j\varphi_B(f_1, f_2)] \tag{3.27}$$

$$B(f_1, f_2) = E[B(f_1 + 2\pi, f_2 + 2\pi)] \tag{3.28}$$

Which can be expanded as:

$$\begin{aligned} B(f_1, f_2) &= E[B(f_2, f_1)] = E[B^*(-f_2,-f_1)] = E[B^*(-f_1,-f_2)] = E[B(-f_1 - f_2, f_2)] \\ &= E[B(f_1,-f_1 - f_2)] = E[B(-f_1 - f_2, f_1)] = E[B(f_2,-f_1 - f_2)] \end{aligned} \tag{3.29}$$

For each independent component of f_1, f_2 and f_1+f_2, statistically independent random phases will be characterized and distributed over $(-\pi, \pi)$. Upon statistical averaging denoted by the expectation operator $E[]$ in Eq. (3.29), the bispectrum will tend towards zero due to the random phase mixing effect. In this way random noise can be suppressed significantly [147].

To make the bispectrum independent of the energy content at the bifrequencies, another parameter called bicoherence is used which is a normalized form of the bispectrum. The bicoherence is used extensively for the detection and quantification of quadratic phase coupling in the bispectrum estimation detection of quadratic phase coupling. a squared bicoherence is chosen because it is bounded between 0 and 1, and is defined as [164, 165]:

$$b^2(f_1, f_2) = \frac{|B(f_1, f_2)|^2}{E[|X(f_1)X(f_2)|^2]E[|X(f_1 + f_2)|^2]} \tag{3.30}$$

The bicoherence normalises the estimated bispectrum in order to reduce the influence of the signal's power spectrum, which results in a clear illustration of the true nature of the signal. Thus a frequency pair where phase coupling has occurred, 100% degree of nonlinear interactions among frequency combinations, f_1, f_2 and f_1+f_2, will be shown by a bicoherence index $b^2(f_1, f_2)$ close to unity, while an absence of phase coupling will produce a near-zero value of $b^2(f_1, f_2)$ [158]. Zero values of the bicoherence index suggests that the components are produced independently from the system. Therefore, based on the amplitude of the

bicoherence index, quadratic nonlinear interactions can be detected and the degree of interaction between the coupling components can be also measured [166].

3.2.4.2.2 Modulation Signal Bispectrum

The bispectrum presented in Eq. (3.26) can only include the presence of nonlinear interactions between frequency combinations, f_1, f_2 and f_1+f_2. It omits the possibility of the occurrence of quadratic phase coupling at f_1-f_2, which may be important due to the nonlinearity between f_1, f_2. Because of this, the conventional bispectrum it is not adequate to describe modulation signals such as those representing gearbox vibration, see Eq. (3.27). To improve the performance of CB in characterising the gearbox vibration signals, a modulation signal bispectrum (MSB) has been developed as a new AM detector in [166] [147, 167]:

$$B_{MS}(f_1, f_2) = E[X(f_2 + f_1)X(f_2 - f_1)X^*(f_2)X^*(f_2)] \tag{3.31}$$

Where its magnitude and phase are as follows [165]:

$$|B_{MS}(f_1, f_2)| = E[|X(f_2 + f_1)||X(f_2 - f_1)||X(f_2)||X(f_2)|] \tag{3.32}$$

$$\varphi_{MS}(f_1, f_2) = \varphi(f_2 + f_1) + \varphi(f_2 - f_1) - \varphi(f_2) - \varphi(f_2) \tag{3.33}$$

If there is coupling between f_1 and f_2, their phases are related by

$$\begin{aligned} \varphi(f_2 + f_1) &= \varphi(f_2) + \varphi(f_1) \\ \varphi(f_2 - f_1) &= \varphi(f_2) - \varphi(f_1) \end{aligned} \tag{3.34}$$

By substituting Eq. (3.34) into Eq. (3.33), it can be seen that the total phase of the MSB will be zero and the MSB amplitude will be the product of the four magnitudes. Therefore, a bispectral peak will appear at (f_1, f_2), which are interacting, and which will also produce sideband components at (f_1 - f_2) and (f_1 + f_2). On the other hand, if there is no phase coupling between any of the components, the AM detector will not exhibit a peak at (f_1, f_2) and the expectation operator will then cause the value of $B_{MS}(f_1, f_2)$ to approach zero. This estimator will also correctly produce only one bispectral peak that appears at bifrequency $B_{MS}(f_1, f_2)$ per occurrence of AM. This is a more accurate way of representing the sideband characteristics of the modulation signals [166].

Similar to the conventional bicoherence, a normalised form of MSB or modulation signal bicoherence is used to measure the degree of coupling between the three components as [147, 167]:

$$b_{MS}{}^{2}(f_1, f_2) = \frac{\left|B_{MS}(f_1, f_2)\right|^2}{E[\left|X(f_2)X(f_2)X^*(f_2)X^*(f_2)\right|^2]E[\left|X(f_2+f_1)X(f_2-f_1)\right|^2]} \quad (3.35)$$

Moreover, the MSB signal degrades to the power spectrum in case of $f_1=0$, and Eq. (3.31) can be written as:

$$B_{MS}(0, f_2) = E[X(f_2)X^*(f_2)X(f_2)X^*(f_2)] \quad (3.36)$$

Which is close to Eq. (3.24) in term of:

$$PS(f) = \sqrt{B_{MS}(0, f_2)} = E[X(f_2)X^*(f_2) \quad (3.37)$$

3.3 Key Findings

- Different vibration based diagnosis techniques can be applied to extract useful information for online health monitoring of the system conditions.
- Time domain analysis is the simplest form of signal processing for measuring and recording the incoming raw signal. It extracts valuable information based on a statistical measurement of the raw signal as a function of time.
- TSA is an effective technique that is widely used in vibration monitoring and fault diagnosis by extracting repetitive signals from noisy data. However, it requires an external time sampled trigger signal provided by an additional instrumentation sensor, and it may suppress some important information in its order spectra.
- Machinery faults typically generate non-stationary components in the signal, which contain information vital for fault diagnosis.
- Although spectral analysis is the most widely used method for CM of machines, it is critical to process the non-stationary signals for fault diagnosis.
- Most gear defects cause irregular tooth meshing, which results in modulation of the mesh frequency by shaft rotational speed, resonant frequencies of the system and dynamic meshing forces.
- MSB analysis allows random noise and aperiodic components in the vibration signals to be suppressed effectively, whereby the nonlinear modulation components can be decomposed and revealed more clearly.

Chapter 4

Experimental Test Rig

This chapter describes the test facilities used in this study. It details the main mechanical equipment and the measuring instrumentation employed for the experimental investigation of a multistage gearbox transmission system. The data acquisition system used to record the experimental data is also explained in this chapter. Finally, the chapter describes how the gear mechanical faults and the different lubrication status were simulated, in which the experimental procedures and steps used to appreciatively obtain the vibration signals from the testing gearbox, for healthy and faulty gear conditions are explained.

4.1 Introduction

To assess the effectiveness of using vibration signals for online condition monitoring of helical gearboxes (gear fault detection and diagnosis), experimental work was carried out on a laboratory rig transmission system. Depending on the measurement system used, a test bench provides multiple ways of monitoring the health of an industrial two-stage helical gearbox. This gearbox was developed to the highest standard of accuracy and reliability in a variety of industrial applications, which is superior in transmission higher load-carrying capacity.

Sufficient experimental studies are essential for developing and evaluating an effective technique to be used extensively. The test rig was designed based on a real industrial mechanical transmission system. It was designed to perform repeatable, deterministic test runs under controlled conditions. The aim of the experiments was to introduce fault condition into a two-stage helical gearbox in order to detect and correlate the abnormal condition indices with real fault data.

4.2 Test Rig Construction

For this research, a purpose-built experimental test bench was utilised to perform extensive experimental monitoring of different gear failure modes. The test rig comprises back-to-back gearboxes, in which the first gearbox (GB1) acts as a speed reducer while the second, slave, gearbox (GB2) acts as a speed increaser. An induction motor and load generator are connected in series with both gearboxes via flexible couplings, see Figure 4-1. This arrangement allows different load conditions to be imposed on the test gearboxes. The test rig assembly is powered by an AC motor (15 kW, 1460 rpm) while the DC generator was used to apply different load conditions on the system.

An electronic Optima Control System was used to provide full control of operating conditions (varying speeds and loads) via a touch screen monitor interface. It was used for setting up the required working conditions in terms of run-time, speed, load and the number of operating sets. The control panel is connected to the test rig as shown in the schematic diagram of the test rig setup, Figure 4-2. A data acquisition and measurement system was connected to measure electric (current and voltage), rotational speed and vibration signals through suitable sensors in order to manipulate and save the required data to a PC via a USB cable.

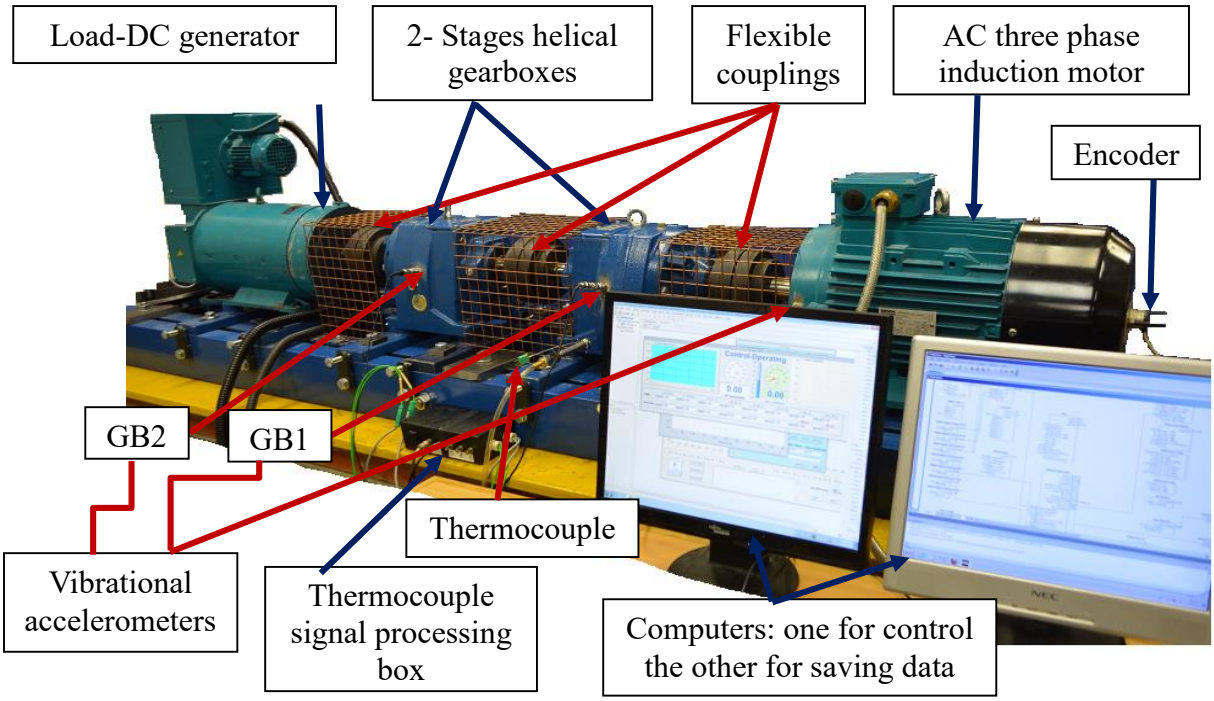

Figure 4-1 Test rig construction

4.3 Test Rig Facilities

The experimental test rig was designed to conduct various test-runs under controlled conditions where simulated faults could be introduced when required. Figure 4-2 shows a schematic diagram of the gearbox test rig configuration.

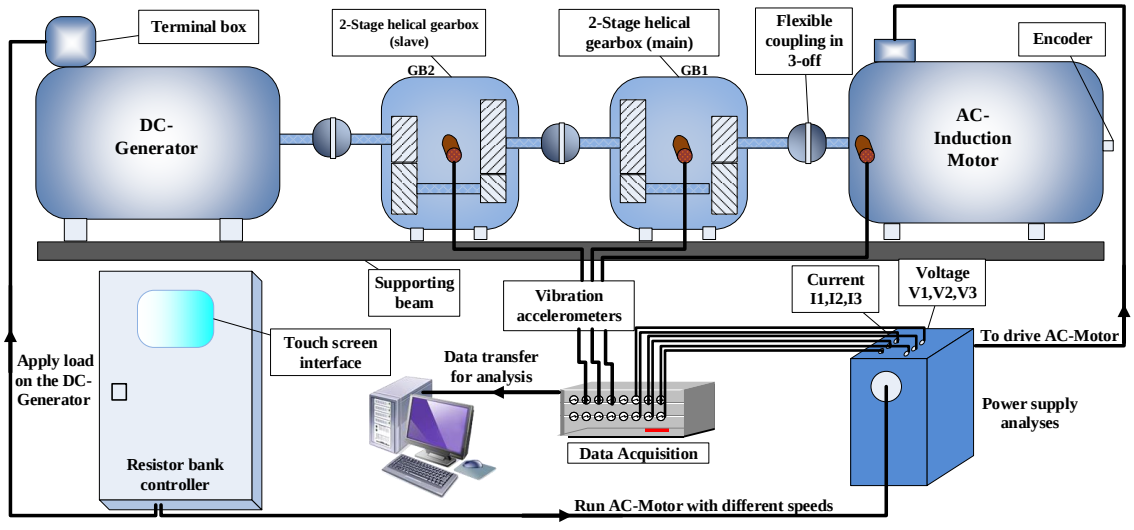

Figure 4-2 A schematic diagram of the test rig setup

The test parameters were selected to assess detection and monitoring procedures for simulated typical gear faults under various operating conditions, to determine the health

status of the gearbox. This requires developing appropriate data analysis methods to extract useful information for early fault detection and diagnosis.

4.4 Mechanical/Electrical Components

The test rig was intended to monitor the health of a two-stage helical gearbox using traditional techniques: vibration, temperature, speed and electrical (motor voltage and current) signals. The rotating components of the test rig were mounted on a double U-beam, which was attached to a concrete base. The beam was designed to allow the assembled components to be removed and reassembled easily. The test rig components were connected via flexible couplings at three junctions; the connection of the AC motor to the input shaft of the test gearbox, where the two gearboxes were inter-connected, and where the DC generator was connected to the output shaft of the slave gearbox, see Figure 4-2. A summary of the main test rig components is given in Sec. 4.4.1 to 4.4.5.

4.4.1 Two-Stage Helical Gearbox

A two-stage helical gearbox manufactured by Radicon Transmission UK Limited was used for the experimental work of this study. Using such a commercial gearbox allows the extracted signals to be more realistic and more reliable for verification and implementation. A schematic diagram of the structure of the gearbox is shown in Figure 4-3. The component model shows the type of gears in each stage inside the gearbox which are meshed with a reduction ratio depend on their teeth number. The rotational frequency of each shaft inside the gearbox and the gear mesh frequencies are also shown, which can be determined by:

$$\left.\begin{aligned} f_{r1} &= \frac{\omega_1}{60} \\ f_{r2} &= f_{r1} * \frac{z_1}{z_2} \\ f_{r3} &= f_{r1} * \frac{z_1}{z_2} * \frac{z_3}{z_4} \end{aligned}\right\} \tag{4.1}$$

where: ω_1 refers to the input shaft speed in rpm (speed of AC motor), f_{r1}, f_{r2} and f_{r3} refer to the rotational frequency of the input, intermediate and output shafts respectively.

$$\left.\begin{aligned} f_{m1} &= f_{r1}\, z_1 \\ f_{m2} &= f_{r2}\, z_3 \end{aligned}\right\} \tag{4.2}$$

where, f_{m1} and f_{m2} refer to the mesh frequency of each stage. The overall reduction ratio of the gearbox is 3.678, as explained in Table 4-1.

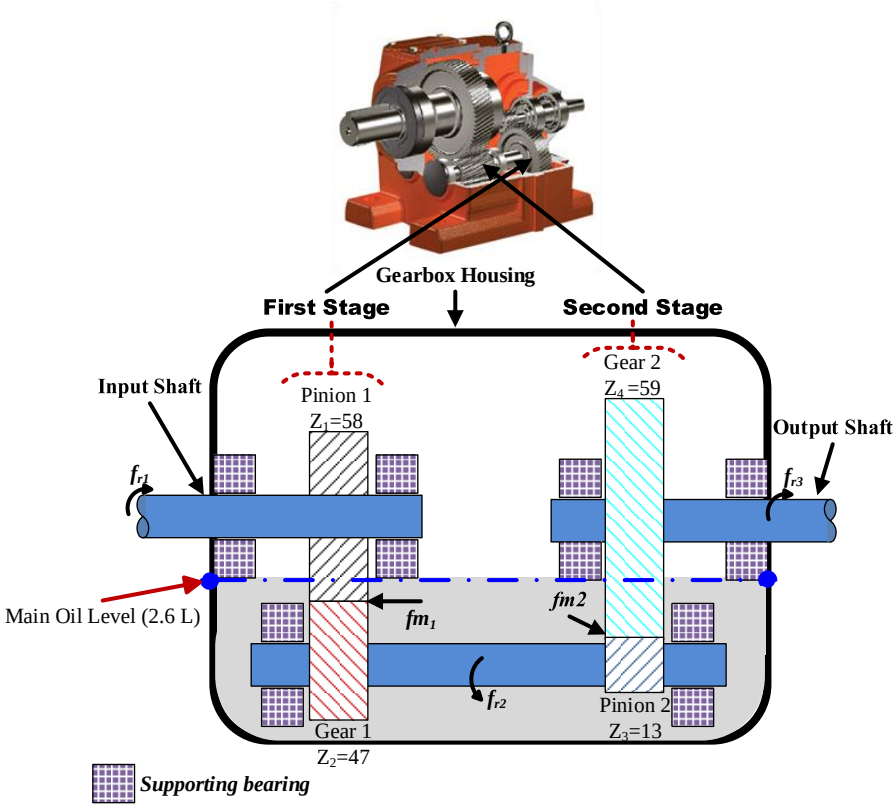

Figure 4-3 A photograph and schematic structure of two-stage helical gearbox

Table 4-1. Design parameters of the two stage helical gearbox

Description	First Stage		Second Stage	
	Pinion	Gear	Pinion	Gear
Number of teeth	Z_1=58	Z_2=47	Z_3=13	Z_4=59
Ref. circle diameter (mm)	81.369	65.937	26.684	121.1
Shaft diameter (mm)	28.0	24.0	25.0 (gear shaft)	39.5
Rotation speed (Hz)	f_{r1}	f_{r2}	f_{r2}	f_{r3}
Meshing frequency	f_{m1}		f_{m2}	
Reduction ratio	0.8103		4.5385	
Overall reduction ratio	$\frac{f_{r1}}{f_{r3}} = \left(\frac{Z_2}{Z_1}\right)\left(\frac{Z_4}{Z_3}\right) = 3.678$			
Manufacturer	Radicon			
IT TYPE	M07223.6BRC-1-----			
Input power (kW)	13.1			
Output torque (Nm)	306 Nm @1450rpm			
Overhung load (kN)	3.50			
Oil type	EP 320 (mineral oil)			
Oil volume (L)	2.6			

For the purposes of lubrication, MILLGEAR 320 EP was used with specifications detailed in Table 4-2. Use of the proper industrial gear lubricant is important for long-term and

efficient operation. According to AGMA 9005-E02, the choice of the appropriate lubricant depends on matching its properties to the particular application. The higher the speed of the gear drive, the lighter the viscosity needs to be. The selection of lubricant viscosity must be based on the lowest and highest operating and/or ambient temperatures experienced [168].

Table 4-2 Physical properties of Millgear 320 EP industrial lubricating oil [169]

Industrial Gear Oil	**MILLGEAR 320 EP**
Specific Gravity @ 15°C (kg/l)	0.901
Kinematic Viscosity @ 100°C (cSt)	23.5
Kinematic Viscosity @ 40°C (cSt)	320
Viscosity Index (AGMA 9005-E02)	92

An empirical equation for determining the required viscosity was detailed by Davis (2005) [170]:

$$\upsilon_{40} = \frac{500}{V^{0.5}} \tag{4.3}$$

Where υ_{40} is the lubricant kinematic viscosity at 40 °C (in cSt) and V is the operating pitch line velocity (in m/s), which is given by:

$$V = \frac{2\pi}{60}\omega r = 0.0524\omega d \quad (m/s) \tag{4.4}$$

Where d is the operating pitch diameter of the pinion (in metres) and ω is the pinion speed (in rpm). According to Eq. (4.3), the required kinematic viscosity for gearbox application should be υ_{40}=322 cSt, and the recommended grade for this value is ISO VG 320 as established by BS 4231:1992 and ISO 3448:1992 [171]. which is provided by Millgear 320 EP lubricating oil.

4.4.2 AC Driving Motor

A three-phase electric motor manufactured by Brook Crompton type T-DA160LA as shown in Figure 4-4, was coupled to the input shaft of GB1 via a flexible coupling. It was used to drive the test rig with power 15 kW (20 hp) at a maximum speed of 1460rpm, within voltage range of 380-415V and electric supply frequency 50 Hz. It provided full load torque 98.1 Nm with a rotor inertia of J=0.129 kg.m^2 and shaft diameter 42 mm. The motor is fully controlled by a programmable logic controller (PLC) via a touch screen user interface

to set up the requested test profile. In addition, an electric measuring unit was used to analysis the power supply (see Figure 4-2) and to measure the required current and voltage signals of each phase driving the motor.

Figure 4-4 AC Induction motor (Brook Crompton) [172]

4.4.3 DC Generator

A Brook Hansen DC generator was attached to the test rig as a torsional loader, which provides different loads to the system. The magnitude of the load is expressed in percentage of the maximum power of the DC generator (15 kW at a full speed of 2100 rpm, armature voltage 460 V and field current of 37.5 A). The DC generator can be designed to provide different torque load conditions, such as sinusoidal load or variable step load, through the PLC controller.

4.4.4 Flexible Coupling

A flexible coupling, type HRC150H manufactured by Fenner, was used at each of the three connecting points to link the mechanical components of the test rig, see Figure 4-2. These provide flexible connections that accommodate any slight misalignment between the shafts, and transmit power without slip or disconnection. The coupling is a three jaw type, manufactured from a hard rubber with a size of 150mm and a transmission power up to 100 kW at 1600 rpm. An elastic type of flexible spider rubber coupling was implanted between the two jaws of the coupling. These flexible rubber spiders allow only the torque to be transmitted between the shafts. Figure 4-5 shows the flexible coupling system, which consists of two half couplings and an intermediate flexible component.

Figure 4-5 Hard rubber coupling

4.4.5 Speed and Load Controller

The test rig is controlled by a PLC SIEMENS, SIMATIC S67-200, see Sec. 6.2.2, which was developed by Optima Control Solutions Ltd. The PLC is easy to use and has the ability to deliver the required torque and speed accurately. It is equipped with a touch screen to enter the test profile and to monitor the key variables during the run-up of the system (see Figure 4-6). Different parameters can be controlled by the system via the touch screen interface, such as: time duration of the operation, driving speed of the AC motor (% of full speed, 1460 rpm) and the applied load of the DC generator (% of full load, 15 kW).

Figure 4-6 Control panel of the test rig

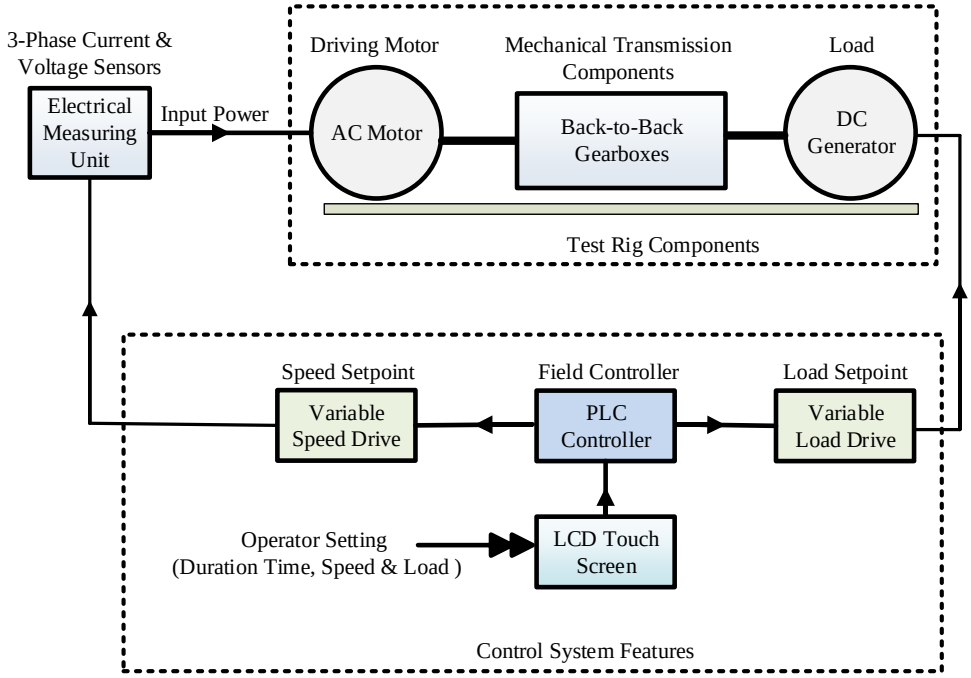

Figure 4-7 Block diagram of the experimental test rig control system

The control system controls the speed of the AC motor via the variable speed drive, and simultaneously applies the required torque load on the DC generator via the variable load drive, as illustrated in Figure 4-7. The PLC controller transmits the required supply parameters as entered by the operator via the LCD touch screen, to run the test rig under the required operating condition.

4.5 Measurement Instrumentations

For this series of experiments, the measurement system was set to measure three acceleration signals, two thermocouple signals, one encoder signal and one power supply measuring signals for the online condition monitoring of the gearbox under different fault and operational conditions. The acquired data signals were recorded and transferred to a computer for analysis. The system has the potential to be used simultaneously to measure the three-phase electric signals. The measuring devices used during the operational test runs are presented in Sec. 4.5.1- 4.5.4.

4.5.1 Vibration measurements

The piezo-electric accelerometer is the most common transducer used for vibration measurement, to convert the mechanical motion into a measurable electrical voltage signal. It is a low cost and low maintenance device that is ideal for use with either portable data

collectors/analysers or as part of online machine protection systems [173]. It can be used effectively for measuring dynamic changes in mechanical variables including shock and vibration over a wide frequency range, up to 20 kHz [174].

4.5.1.1 *Piezo-Electric Accelerometer*

Piezo-electric accelerometers offer a wide frequency range with different sensitivities, masses, sizes and shapes [175]. Typically, the vibration signal is measured by accelerometers placed at suitable points on the system. Based on the magnitude and frequency of the vibration signal to be measured on the test rig, and the operating temperature, three piezo-electric accelerometers were chosen with different voltage sensitivities of (10.22, 5.012 and 4.980 mV/ms^{-2}). These transducers are suitable for vibration measurements within a range between 1 Hz to 10 kHz and do not require any additional signal conditioning apart from their standard charge amplifiers.

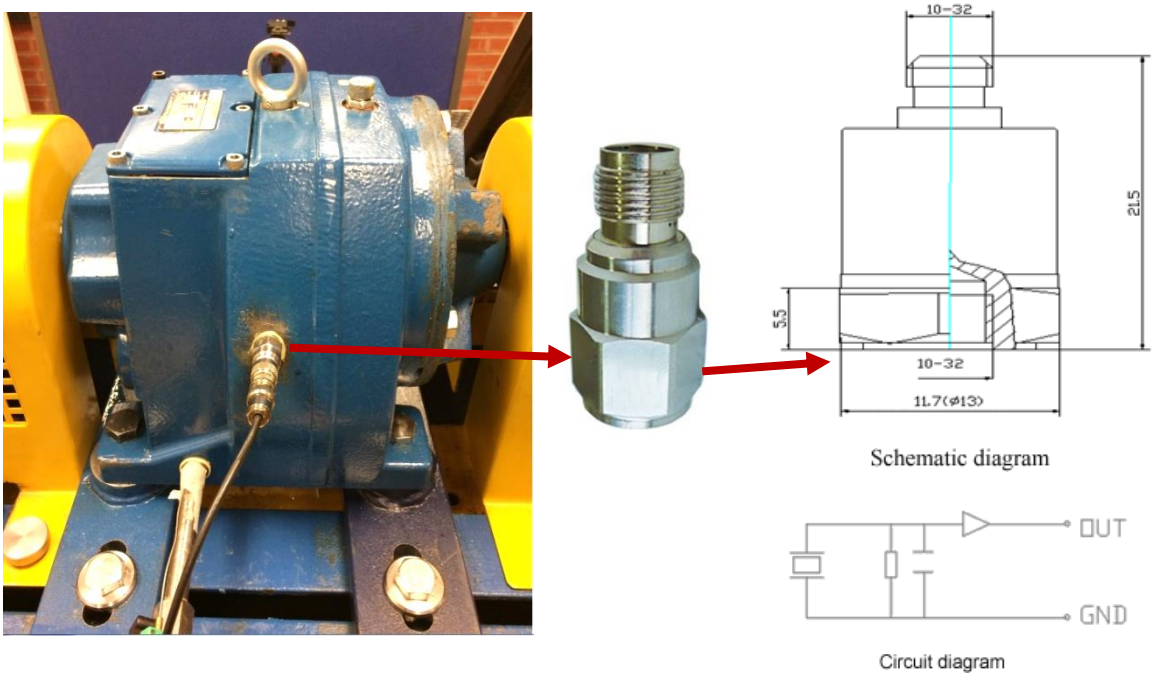

Figure 4-8 IEPE accelerometer model: CA-YD-185TNC

The accelerometer was mounted horizontally on the gearbox housing using a threaded aluminium stud, as shown in Figure 4-8. This method of attaching the accelerometer complies with the IEPE (Internal Electronic Piezoelectric) standard. The accelerometer was connected directly to the data acquisition system and then to the computer via a USB port. The mounting point was chosen so that the accelerometer was placed very close to the

impact of the line of action of each stage, whereas the mesh gear vibration of each stage can be measured by one sensor.

4.5.1.2 *Accelerometer Theory*

The piezo-electric accelerometer generally consists of two elements; a mass to generate an inertial force and a piezoelectric crystal to produces an electrical charge that is related to the force exerted upon it, see Figure 4-9 [176].

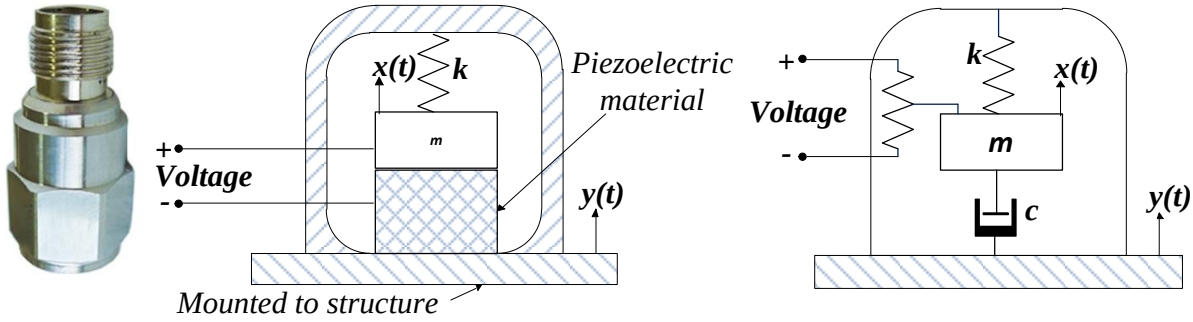

Figure 4-9 Schematic of an accelerometer mounted on a structure and a photograph of commercial available version (CA-YD-185TNC)

The accelerometer model is based on the damped mass-spring system as depicted in Figure 4-9. The force is governed by Newton's second law of motion; $F = ma$. Based on force balance, the equation of motion of the mass, m, is:

$$m\ddot{x} + c(\dot{x} - \dot{y}) + k(x - y) = 0 \tag{4.5}$$

Where *x(t)* is the displacement of mass and *y(t)* is the structural motion that is being measured, which can be assumed to undergo a motion of the form $y = Y\cos\omega t$. The relative displacement between mass and base is $z(t) = x(t) - y(t)$, is directly proportional to the compression of the piezoelectric element. Thus, the equation of the motion yields [176]:

$$m\ddot{z} + c\dot{z} + kz = m\omega^2 Y\cos\omega t \tag{4.6}$$

The steady state solution to Eq. (4.6) is:

$$z(t) = \frac{\omega^2 Y}{\sqrt{(\omega_n^2 - \omega^2)^2 + (2\xi\omega_n\omega)^2}}\cos\left(\omega t - \tan^{-1}\frac{2\xi\omega_n\omega}{\omega_n^2 - \omega^2}\right) \tag{4.7}$$

Where ω and *Y* are frequency and amplitude of the base structure motion, *y(t)*, ω_n is the natural frequency of the accelerometer and ξ is its damping ratio. It can be seen that *z(t)* has the same frequency and the same input acceleration amplitude as the base, especially when $\omega_n > \omega$. However, there is a phase shift between the two movements of $\tan^{-1}(2\ \xi\ \omega_n$

$\omega/(\omega^2_n - \omega^2)$). The working frequency range of the accelerometer with excellent linearity is limited to well below its resonant frequency.

4.5.2 Shaft Speed Measurement

An incremental optical encoder manufacturer by Hengstler; Type: RS32-O/100ER was used to measure the angular speed of the AC motor shaft and its position. It can be used for different industrial processes and control systems, and is an established electrical engineering standard.

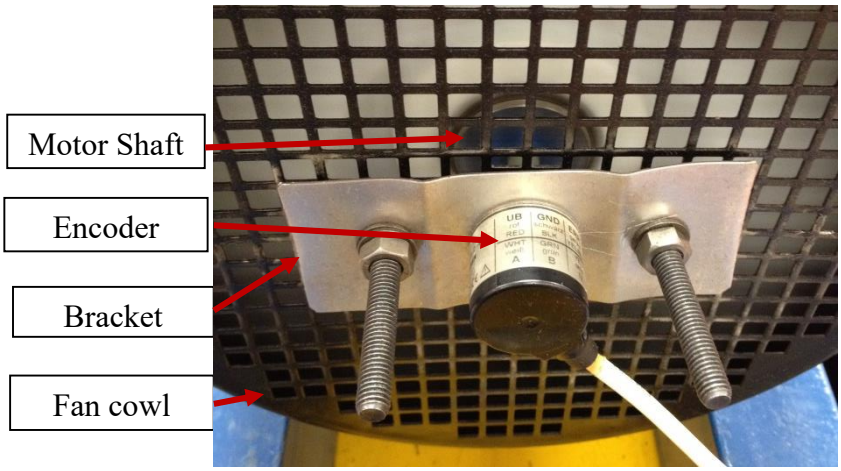

Figure 4-10 Encoder fitted at the end of the AC-motor shaft

The encoder is fitted to the end of the induction motor shaft via a bracket mounted on the fan cowl (see Figure 4-10). The device is powered by 10V dc-supply, and connected to the computer via the data acquisition system, without any amplification. The encoder produces a rectangular pulse shape, and 100 pulses per revolution of the motor shaft, which give a suitably accurate shaft position. The time samples are synchronized with the trigger pulses for every complete revolution, which are used to measure the angular shaft speed.

4.5.3 Data Acquisition System (DAQ)

A data acquisition system (DAQ) is a tool designed to interface any test rig to a PC by acquiring data as electrical signals which can be transformed into a digital format for processing, analysis and storage by a computer. The DAQ generally has hardware and data acquisition software, which are used with sensors and field wiring to monitor different conditioning signals such as acceleration, speed, temperature, sound level, force, etc.

Figure (4-11) shows the high-performance data acquisition system (Sinocera YE6232B) from Global Sensor Technology with card PD2-MF-16-500/16L PCI used in the laboratory

for capturing and analyzing the experimental data at a sampling frequency of 96 kHz. It has 16 analog input channels, which are used to convert the analog signals acquired from the transducers (e.g., accelerometers) to digital signals and then transfer them to the computer for analysis. The technical specifications of the DAQ used in this study are shown in Table 4-3.

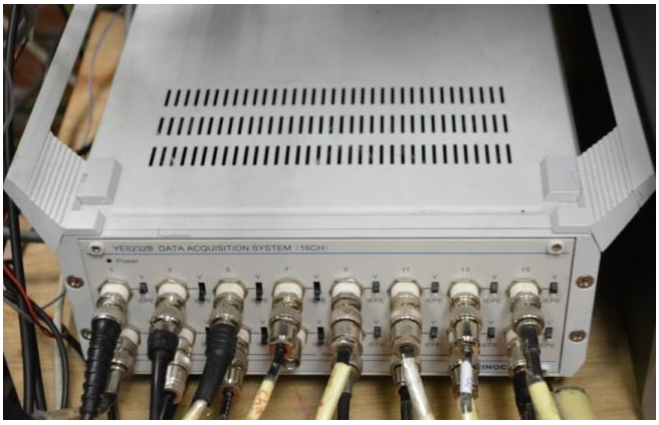

Figure 4-11 Global Sensor Technology YE6232B of the DAQ

Table 4-3 Technical Specifications of the DAQ

DAQ system manufacturer	**Global Sensor Technology YE6232B**
Company: SINOCERA	Piezotronics, INC. Version 1.2
Number of Channels	16 (selectable)
A/D Conversion resolution	24 bit
Sampling rate (maximum)	96kHz per channel, Parallel sampling
Maximum sampling	1.5 MHz
Input range	±10 V
Gain	×1, ×10, ×100
Filter	Anti-aliasing
Internal acquisition card	USB 2.0
Software	YE7600

YE76000 software was used to record the input data and support the DAQ. This software can also be used to give the user a clear visible overview on a real time display of all the channels used, see Figure 4-12. The data collection can be manipulated to ensure the accuracy and reliability of the signals. The DAQ has the capability to set parameters for acquiring data for efficient data storage and fast data conversion to a Matlab format for all 16 channels.

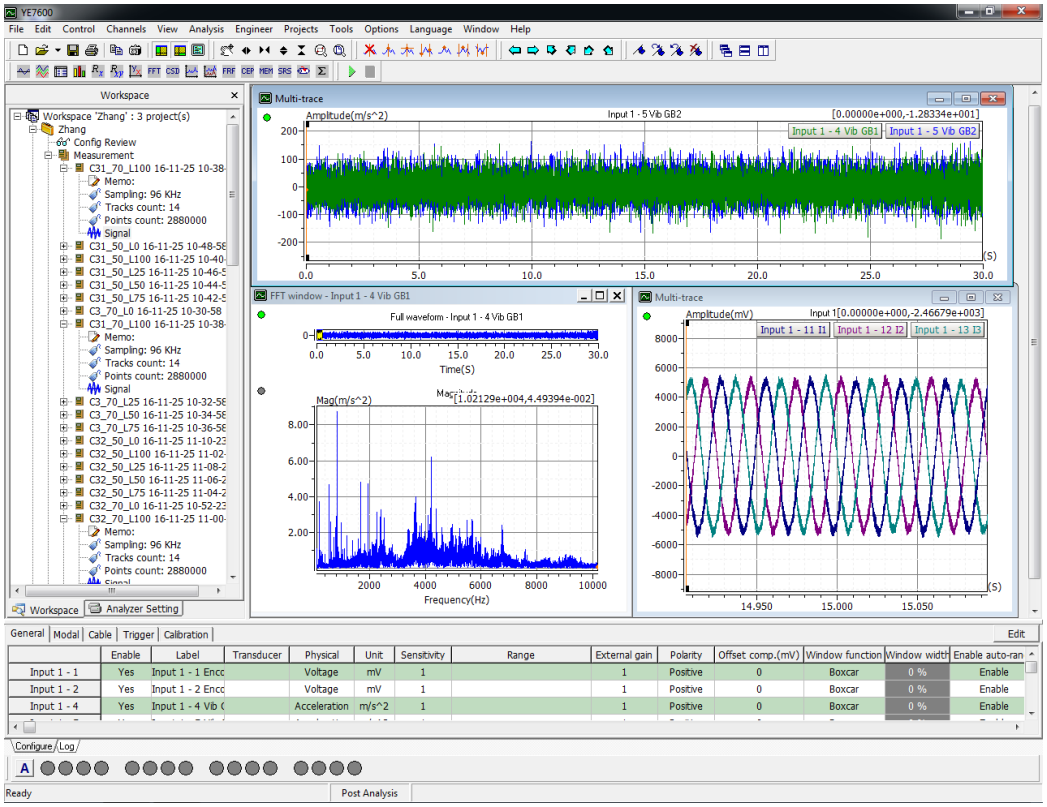

Figure 4-12 Real-time display and data collection in progress

4.5.4 Thermocouple

A Pro K-type 316 stainless steel thermocouple of 3 mm diameter from RS, as shown in Figure 4-13, was used to measure the oil temperature inside the two gearboxes. Pro K-types are widely used in research and industry to provide temperature measurements over a wide range. The temperature detected by the thermocouple is presented as a voltage signal which is taken as a measure of the temperature. The signal is sent to the temperature processing unit for filtering and amplification. Then the DAQ reads the signal and records it at 96 kHz sampling rate.

Figure 4-13 Thermocouple type K mineral insulated probe

4.6 Fault Simulation

During normal operation, due to long-term running, transmission torque and rotational motion of the gears, a variety of faults can occur which detrimentally affect gearbox

performance. Gearboxes have limits for their vibration levels, exceeding this limit will have a detrimental effect on the whole system. The detection of common gearbox faults using an effective signal processing technique is the main focus of this study.

The common gear faults are mainly related to gear tooth irregularities, i.e., tooth breakage, wear and surface damage. Such faults are exacerbated if there are deficiencies in lubrication. These faults can lead to a potentially catastrophic failure of the transmission system if undetected. To help develop reliable and accurate detection and diagnosis, seeding faults in a real system is an effective way to investigate likely consequences in more realistic situations.

There are two approaches used by researchers for experiment simulation of defects in the gearbox. Either to intentionally cause a specific defect, and then compare the system response to the healthy condition, or by a run-to-failure approach monitoring system response until a defect forms naturally. In this study, both approaches have been employed to examine the use of gear vibration signature to diagnose various fault conditions. The simulated faults are as follows:

4.6.1 Tooth Breakage

Tooth breakage (TB) is a common fault that can occur in helical gears due to high contact ratio, shock or overloading, and which weakens the metal and finally results in failure by fatigue. To develop successful diagnostic techniques, TBs of different severities were simulated intentionally in the first stage of the test gearbox (GB1), as shown in Figure 4-14. The vibration signatures under different TBs were analysed to produce a realistic feature for detection and diagnosis of this fault. Note: 20% tooth breakage is where 20% of the length of the tooth was removed. Similarly, for 40% TB.

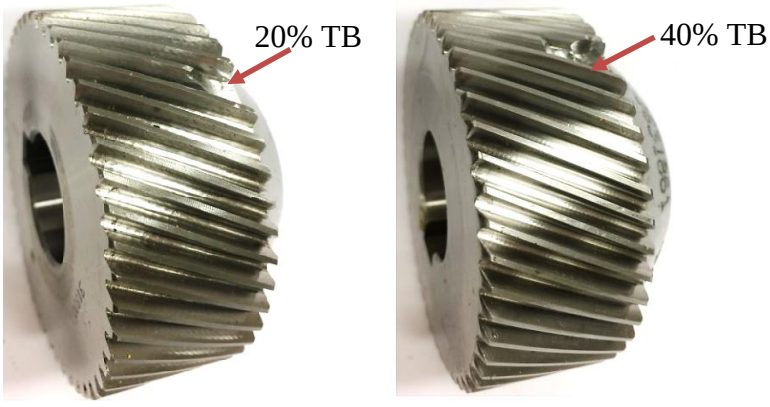

Figure 4-14 Simulated tooth breakage fault

4.6.2 Wear

Tooth surface wear is a common failure mode that occurs after relatively long periods of service. It affects reliability and hence the availability of gear drives. To identify an effective indicator of tooth surface wear, a run-to-failure test was performed by driving the test rig under sinusoidal and step torque loads with variable rotational speeds. The wear fault was developed naturally, but the time taken to the occurrence of the fault was minimised by including shock loading when changing the load. The gearbox vibration signal was monitored throughout the test scenario. By the end of the test, the tooth surface deterioration had developed as shown in Figure 4-15, in which the wear was still at an early stage.

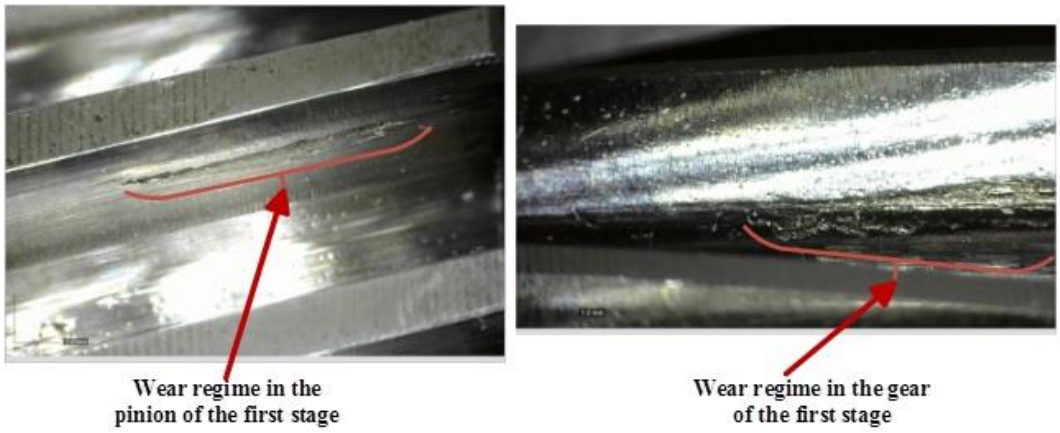

Figure 4-15 Gear wear fault from a run-to-failure test

4.6.3 Gear Lubricant Deterioration

Lubrication is a very important factor influencing the performance of gearboxes; lubricant failure causes equipment failure. The major duties of lubrication are dissipating the generated heat and reducing friction and wear between contacting surfaces. Failure in lubrication due to the presence of dust, contamination with water, or degradation due to being used for an extended period of time, may lead to catastrophic breakdown of the gearbox and large maintenance bills. Vibration signal monitoring should be an effective and reliable method for cost-effective, online health monitoring of gearbox lubricant condition and gearbox lubricant deterioration.

The different tests completed in this research, are tabulated in Table 4-4.

Table 4-4 Different tests of gearbox oil lube condition

Defect Types	Test Severity	Operating Condition	
		Speed	Load
Water Contamination (kppm)	0 (baseline), 2 kppm, 4 kppm, 7 kppm, 20 kppm, 30 kppm, 60 kppm, 90 kppm and 120 kppm.	50% 75% 100%	0% 30% 70% 100%
Different Oil Viscosities (cSt, at 40°C,)	100 EP 320 EP (baseline) 650 EP 1000 EP		
Different Oil Volumes (litre)	Baseline, 2.6 litres lubricant Lubricant loss 600 ml (2 litres lub.) Lubricant loss 1100 ml (1.5 litres lub.)		

4.6.3.1 *Water Contaminated Oil*

Any significant change detected in the measured oil viscosity could be indicative of severe degradation or cross-contamination in the oil. Water is one of the most destructive contaminants in lubricants. Water contamination causes rust and undesirable effects on the lubricating performance such as change in viscosity, decrease in lubricant film strength and load-carrying ability [177]. Furthermore, the water can cause a polarity shift in many lubricant formulations, which allow them to have some affinity with or attraction to water [178].

A wide range of water contamination, measured by parts per million (ppm), see Figure 4-16, was added to the oil lubricant of the test gearbox which was then run under various operating conditions. The gearbox vibration signal was recorded for each condition, in order to get valuable information regarding its response to changes in radial load, speed and lubricant viscosity.

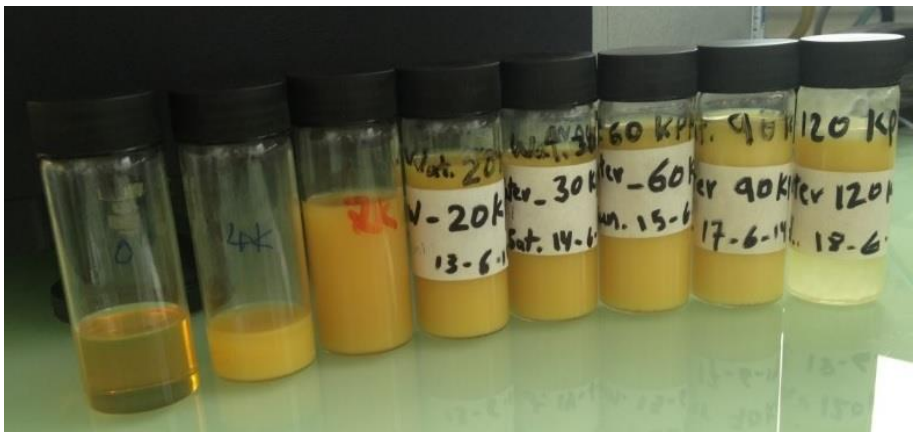

Figure 4-16 MILLGEAR 320 EP samples with different water contents

4.6.3.2 *Oil with Different Viscosities*

Viscosity is an important factor determining oil quality, a second test investigated whether change in viscosity only, had any effect on vibration signature and/or power supply parameters of the gearbox. Results of this test will help to confirm the conclusions reached from the previous stage of the study when different proportions of water contaminated the oil and increased oil viscosity. It also would be used for oil quality and lifetime detection technique that can be utilised for lubricating problems detection and diagnosis. Four different oil characteristics, see Table 4-5, were used to study the effect of different oil viscosities on the gearbox vibration signal.

Table 4-5 Characteristics of different Millgear oils [169]

EP Mineral Oil Characteristics	100 EP	320 EP	650 EP	1000 EP
Specific Gravity (at 15°C)	0.885	0.901	0.918	0.927
Kinematic Viscosity (at 100°C, cSt)	10.95	23.5	49.5	71.0
Kinematic Viscosity (at 40°C, cSt)	100	320	650	1000
Viscosity Index	93	92	126	140

4.6.3.3 *Different Oil Levels*

Low oil level or starvation of lubrication leads to more frequent metal-to-metal contact. Reduced oil film thickness can increase bulk temperatures and cause higher surface shear stress. Insufficient lubrication of a gearbox, can increase friction, temperature and material wear, and ultimately leads to failure of the component materials that are essential to the system functions [101]. Micropitting is also caused by poor lubrication and thus online health monitoring of oil levels should help prevent its occurrence. Here different oil volumes were tested: namely the recommended level (BL = 2.6 litres), 600ml less than the recommended volume (LL-600 = 77% of the recommended volume) and 1100ml less (LL-1100 = 57.7% of the recommended volume), see Table 4-4.

4.7 Experimental Procedure

Figure 4-2 show the positions of the transducers and the assembled mechanical/electrical components. The operator enters the required test scenario for the rig via the touch screen interface of the PLC controller. Based on the required operating profile, multiple combinations of speeds, loads and working duration times can be implemented. The controller sends the required settings to the AC-motor and the DC-generator to run under

different speeds and loads and the accelerometers, electric sensors, thermocouples and encoders measure the required sensor signals.

Different gearbox tests were simulated using the following procedures:

- To simulate a common industrial machine conditions, different operating conditions (loads and speeds) were applied to both the DC and the AC machines, via the touch screen.
- The data acquisition, accelerometers, cables and all sensors were correctly connected together and checked by YE7600 software on the computer.
- The controller setting was programmed for up to 12 cycles, which includes speed setpoints, load setpoints and time durations for each cycle.
- YE7600 software was used to interface the DAQ and to set the required parameters for the recorded signal, e.g. input range, number of samples to be taken and sampling frequency.
- Each data set was saved for a duration of 30 seconds to allow the slowest gear in the gearbox to be able to perform an adequate number of revolutions.
- The test data was saved at a high sampling frequency of 96 kHz.
- To get accurate and repeatable performance data, the operating condition was repeated five-times for each data set.
- A suitable graph was built in YE7600 to monitor and check the signals of the test rig and then save the required data for further analysis using MATLAB.
- A series of tests were conducted to simulate different gear defects under fully controlled operating conditions.

4.8 Key Findings

- An experimental study using a benchmark test rig system is commonly used to investigate the validity of using the vibration signal for the online CM of gearboxes.
- Piezo-electric accelerometers are the most commonly used transducer for vibration measurement, due to ease of use, low purchase price and low maintenance cost, large dynamic range, high quality measurement capability and reliability.
- Accelerometers have a wide frequency range and are available with different sensitivities, masses and shapes, which make them ideal for use with either portable data collectors/analysers or as part of online machine protection system.

- A versatile DAQ needs to be used for acquiring data reliably with efficient data storage and fast data conversion, along with the capability to set up various channel parameters.
- Fault seeding and a run-to-failure tests are the main two approaches used to simulate faults in a real situation, and to investigate the capability of gear vibration signatures to diagnose faults using various fault detection schemes.

Chapter 5

Dynamic Model of a Helical Gear Transmission System

To develop diagnostic features accurately for vibration based monitoring, this chapter is provided to study the dynamic model of a two-stage helical gearbox with an effective and convenient calculation of mesh stiffness variations. The model consists of an 18-DOF (degree-of-freedom) vibration system to describe the full dynamics of the test system and take into account the effect of supporting bearings, driving motor and loading system. Moreover, it couples with transverse and torsional motions resulted from time-varying friction forces based on EHL, time varying mesh stiffness excitations and different tooth fault severities.

5.1 Introduction

Helical gear drive system is one of the most important transmission forms for power transmission, speed variation and/or working direction when high transmission efficiency and strong load capacity are required. Dynamic analysis of geared systems is a major consideration in gear design, and essential for understanding, controlling and eliminating noise and vibration problems [87, 179-184].

To attain an accurate diagnostic for vibration based monitoring, a significant number of studies have been carried out on the modelling and simulation of gear dynamics. They have resulted in a wide variety of dynamic models available to predict the response of gear vibration in order to improve the current techniques of diagnosis and monitoring [143]. Simulation can be very valuable for getting a better understanding of the complex interaction between transmission components in a dynamic environment and hence improving machine diagnostics and prognostics. It helps to develop effective signal processing methods for characterizing complicated weak fault signatures contaminated by different noises [18].

5.2 Review of Helical Gear Simulation

A wide number of dynamic models for various gearbox systems have been presented in [185-188], in which both torsional and translational vibration responses of gears were studied as a tool for aiding gear fault diagnosis. A variety of models have been developed for the diagnostics of different faults, such as gear spalling or tooth breakage [56, 186, 189, 190], tooth crack [184, 191-193], shaft misalignment [194, 195], tooth surface pitting and wear [64, 196-201]. More models have been developed to analyse the time varying mesh stiffness in a helical gear [202-206] and to study the effect of parametrical design on the dynamic behaviour of helical gear system [179, 207-209].

Most of the earlier researches focused on spur gears than the helical gears due to the complexity with its time-varying characteristics and the existence of helix angle that increases the length of the contact line. Recently, several studies have been reported on the dynamic models of gear systems, Velex (2012) [74] offered a comprehensive review of these models. He presented a general equation of motion for single-stage of spur and helical gears by using three-dimensional lumped models and a thin-slice approach for mesh elasticity without dealing with multi-mesh gears, friction, bearing-shaft-gear interactions,

etc. His review concluded that comprehensive study of gear dynamics requires multi-scale, multi-disciplinary approaches for embracing non-linear vibrations, tribology, fluid dynamics etc.

He et al. (2007) [77] combined the sliding friction and realistic time-varying stiffness into analytical model of helical gear meshing. They used 12-dof dynamic model to include the rotational and translational motions along the line-of-action, off-line-of-action, and axial directions. Also, they developed different values of friction coefficient in their model belong with analytical formulations to derive the multidimensional mesh forces and moments.

Kar and Mohanty (2007) [210, 211] suggested an algorithm for determination of time-varying frictional force and torque at meshing teeth of helical gears. They investigated the torsional vibration characteristics of helical gear system using only 2-dof for rotation formulation. A uniform Load distribution and constant friction coefficient across the contact line were used with some limitations of the width of the contact zone. They observed that the fluctuation of frictional force and torque are the principal source of excitation of noise and vibration in gear models.

Han et al. (2013) [212] presented an improved approach to determine the friction force and torque in involute helical gears to reveal the differences between uniform and nonuniform load distributions along the variation of contact lines. Time-varying friction was included in their model with the assumption of constant friction coefficient. They detailed that the differences induced by friction are negligible and may result in different dynamic responses.

Jiang et al. (2014) [76] used a new analytical method to study frictional excitations and contact stiffness based on the time-varying length of contact line in helical gears. They determined the excitation characteristics in helical gears with tooth spalling defects. A 6-dof analytical helical gear pair model was developed by incorporating the time-varying sliding friction and mesh stiffness based on the changes of friction force and mesh stiffness which were calculated based on the length of the contact lines. A constant friction coefficient was used to simulate the frictional excitation of the helical gear system.

Jiang (2015) [213] presented time-varying friction coefficient based on EHL which was an extension of the model proposed in [76]. He regarded that time-varying sliding friction force and friction torque are non-negligible excitation sources of vibration and noise in

gears. Several gear design parameters such as coefficient, helix angle, and face width were analyzed to illustrate their effects on the time-varying contact line and friction excitations. The results demonstrated that the refined general formulation is effective for the calculation of the friction excitations in helical gears under different range of contact ratios, and the parametric analysis could supply some guidance for choosing gear parameters in the design of helical gears to reduce the frictional effects.

Wang et al. (2015) [203] introduced a dynamic model for analyzing the influence of tooth shape deviations and assembly errors on the different meshing parameters of helical gears. They simulated the helical gear meshing by a series of independent spur gear slices along the axial direction and used potential energy method to calculate the relative position relationships with tooth profile errors and the stiffness of the sliced tooth. They demonstrated that the model is effective for calculating the stiffness of helical gear pairs. The model was also analysed the effect of some design parameters such as tooth tip reliefs, lead crown reliefs and misalignments on the gear mesh stiffness, transmission error, tooth contact stress and tooth root stress.

Zhang et al. (2013) [214] studied the effect of geometric eccentricity on the dynamic characteristics of the helically geared rotor system using a three-dimensional (flexural-torsional-axial) model. They used 12-dof to simulate multi-shaft geared rotor system included bearing flexibility. Eigenvalue solution and the modal summation technique are used to predict the natural frequencies and forced responses of the system. They concluded that some modes can be excited by static transmission error in a low rotating speed range and leads to existence of resonances.

Li et al. (2014) [215] suggested that it is necessary to take into account the coupled lateral-torsional-axial vibration for nonlinear dynamic model of helical gear rotor- bearing system They studied the effects of rotational speed, eccentricity and bearing clearance on the vibration characteristics of the helical gear-rotor-bearing systems by considering nonlinear analytical model via lumped-parameter method. A 22-dof of second order nonlinear differential equations was used to simulate the helical gears meshing, support bearing and the coupled lateral-torsional-axial vibration. They concluded that the vibration amplitudes have obvious fluctuation and random frequency components become increasingly obvious with changing rotational speed and eccentricity at gear and bearing positions. However, there is no obvious effect of the bearing clearance on the vibration response.

As a consequence, a variety of dynamic models have been developed in the past decades to identify helical gear incipient faults. However, monitoring of gear surface defects based on vibration are not particularly well-established, and most of the models either ignore or assume constant frictional effects, which is likely to be very different from real applications where the load and hence the frictional forces vary during the meshing process. Therefore, more accurate models are needed to investigate the effect of tooth surface defects on helical gear dynamic performance for easier demonstrating and evaluating of CM perspective.

5.3 Analysis of Helical Gear Driving System

The power transmission by helical gears can produce radial, tangential and axial dynamic forces at the mesh point, which can cause lateral vibration, torsional vibration, and axial vibration [215, 216]. To examine these dynamic forces, a three-dimensional dynamic model is established in this study, whereby the helically geared rotor system is modelled as two rigid cylinders connected by mesh stiffness along the line-of-action (LOA) in the plane of action with oblique contact lines relating to helix angle β_b, as shown in Figure 5-1.

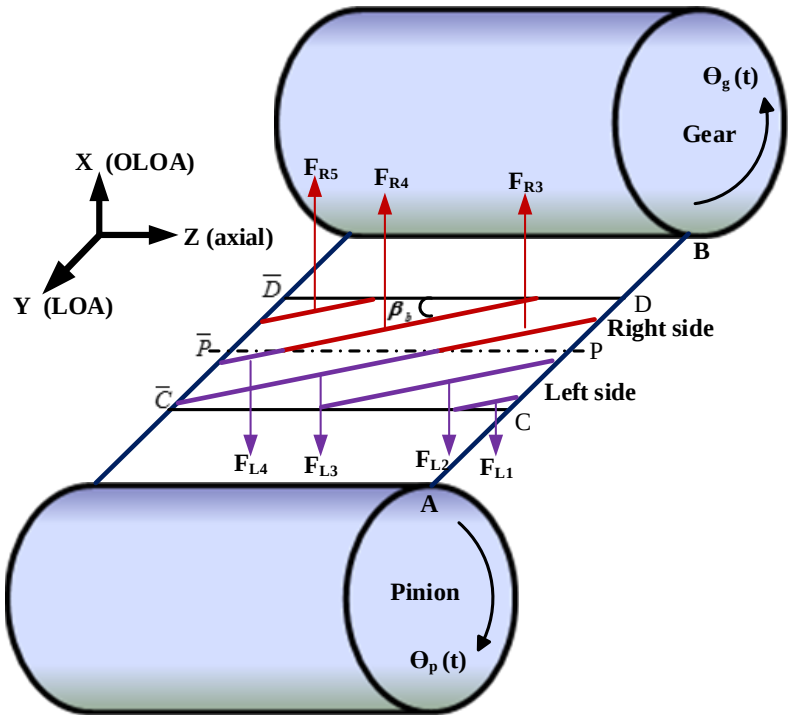

Figure 5-1 Equivalent dynamic model of a helical gear system

A coordinate system is arranged at the centre of the gears, in which x-axis is associated to the off-line of action (OLOA) and directed perpendicularly to the plane of action ($CD\overline{D}\overline{C}$), y-axis is referred to the LOA, which is perpendicular to both the shaft axis and x-axis,

and z-axis is aligned (axial) along the centre of shaft. As shown in Figure 5-1, a mesh cycle for five pair contacts start from point C and moves diagonally as the gears roll across the contact zone till point $\bar{D}$ for normal helical gears. Friction forces (F_{Li}, F_{Ri}) of each segment of the contact lines are also shown in the same figure. These forces influence the contact plane into two directions, depending on the left and right side of the inclined pitch line $P\bar{P}$, see Sec. 5.7.

5.4 Gear Meshing Stiffness

In gear pair systems, coupling between the torsional vibration and lateral vibration is mainly caused by mesh stiffness, thus it is very important to calculate the mesh stiffness conveniently and effectively. In the potential energy method [184, 205], the total potential energy stored in the mesh gear system can be decomposed into multi-components: axial compressive energy U_a, bending energy U_b, shear energy U_s, Hertzian energy U_h and fillet foundation energy U_f. The elastic deflection of the tooth along the direction of tooth load is contributed by axial deformation, bending deformation, and shear deformation, which can be used to calculate axial compressive stiffness k_a, bending mesh stiffness k_b and shear mesh stiffness k_s respectively.

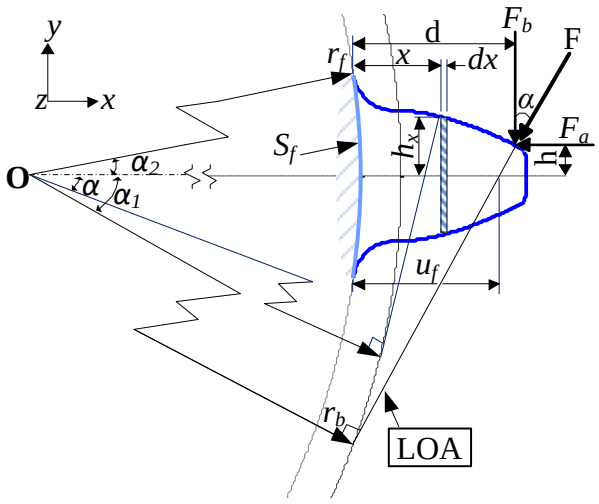

Figure 5-2 Elastic force on a tooth of gear

The gear tooth can be simplified as a cantilever beam on the root circle with a varying cross section (A_x) and an effective length (d) [217]. Based on the tooth geometry, the contact point of the load moves along the tooth surface pattern during the variation of the incident angle. The variations of tooth stiffness is caused by the changing tooth thickness and the

load position [218]. The applied load (F) is decomposed into two perpendicular components (F_a and F_b) relating to the pressure angle α, as illustrated in Figure 5-2, where:

$$F_a = F \sin\alpha$$
$$F_b = F \cos\alpha \tag{5.1}$$

5.4.1 Axial Compressive, Bending, and Shear Energies

The F_a component introduces both axial compressive and bending effects while F_b component causes bending and shear. According to material mechanics, the potential energies stored in beam due to axial compressive, bending and shear energies can be calculated as follows [60, 219]:

$$dU_a = \frac{F^2}{2\,dk_a} = \int_0^d \frac{F_a^{\,2}}{2E\,dA_x}\,dx \tag{5.2}$$

$$dU_b = \frac{F^2}{2\,dk_b} = \int_0^d \frac{[F_b(d-x) - F_a\,h]^2}{2E\,dI_x}\,dx \tag{5.3}$$

$$dU_s = \frac{F^2}{2dk_s} = \int_0^d \frac{1.2\,F_b^{\,2}}{2G\,dA_x}\,dx \tag{5.4}$$

where, A_x and I_x are the area and the moment of inertia of a slice segment $dL(t)$ with distance 'x' measured from the root circle (r_f).

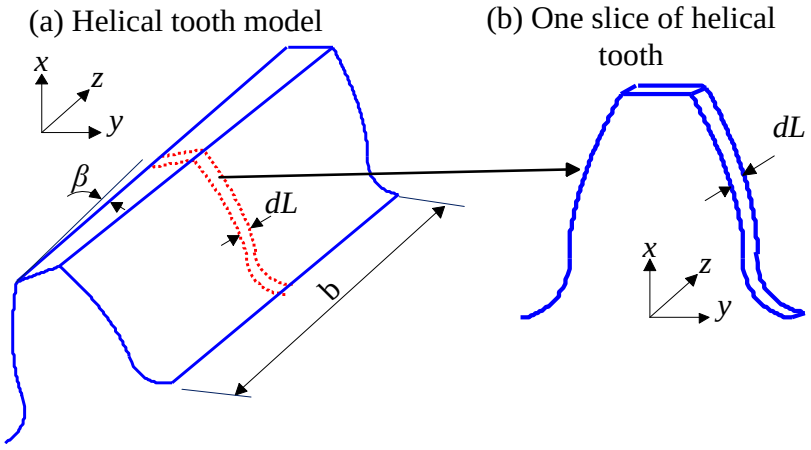

Figure 5-3 Helical tooth model with one slice segment of tooth width

For the slice segment of helical tooth depicted in Figure 5-3, the area and the moment of inertia can be determined respectively as:

$$dA_x = (2h_x)\,dL(t) \tag{5.5}$$

$$dI_x = \frac{1}{12}(2h_x)^3 dL(t) \tag{5.6}$$

where h, h_x, r_f, x, dx and d are illustrated in Figure 5-2. The material properties of the tooth are represented by: E is the Young modulus, G is the shear modulus and υ is the Poisson ratio. Based on the elastic mechanical of the tooth, the axial, bending, and shear stiffness can be expressed in the same direction of the acting force F as follows:

$$\frac{1}{dk_a} = \int_0^d \frac{\sin^2 \alpha_1}{E\, dA_x} dx \tag{5.7}$$

$$\frac{1}{dk_b} = \int_0^d \frac{\left(x\cos\alpha_1 - h\sin\alpha_1\right)^2}{E\, dI_x} dx \tag{5.8}$$

$$\frac{1}{dk_s} = \int_0^d \frac{1.2\cos^2 \alpha_1}{G\, dA_x} dx \tag{5.9}$$

Where, α_1 is the pressure angle. After simplifying the mesh stiffness formulae, the axial compressive stiffness k_a, bending mesh stiffness k_b and shear mesh stiffness k_s can be expressed as:

$$\frac{1}{dk_a} = \int_{-\alpha_1}^{\alpha_2} \frac{(\alpha_2 - \alpha)\cos\alpha \sin^2 \alpha_1}{2E\, dL(t)[\sin\alpha + (\alpha_2 - \alpha)\cos\alpha]} d\alpha \tag{5.10}$$

$$\frac{1}{dk_b} = \int_{-\alpha_1}^{\alpha_2} \frac{3(\alpha_2 - \alpha)\cos\alpha \left\{1 + \cos\alpha_1[(\alpha_2 - \alpha_1)\sin\alpha - \cos\alpha]\right\}^2}{2E\, dL(t)[\sin\alpha + (\alpha_2 - \alpha)\cos\alpha]^3} d\alpha \tag{5.11}$$

$$\frac{1}{dk_s} = \int_{-\alpha_1}^{\alpha_2} \frac{1.2(1+\upsilon)(\alpha_2 - \alpha)\cos\alpha \cos^2 \alpha_1}{E\, dL(t)[\sin\alpha + (\alpha_2 - \alpha)\cos\alpha]} d\alpha \tag{5.12}$$

Where, α is the pressure angle of the arbitrary point at the involute curve. The α_1 and α_2 are illustrated in Figure 5-2.

5.4.2 Hertzian Energy

The elastic compression of two isotropic material bodies is also considered to calculate the Hertzian mesh stiffness k_h, which is practically constant along the contact of two meshing teeth. The Hertzian potential energy and its corresponding stiffness can be expressed as:

$$dU_h = \frac{F^2}{2\, dk_h} \tag{5.13}$$

$$\frac{1}{dk_h} = \frac{\pi E\, dL(t)}{4(1-\upsilon^2)} \tag{5.14}$$

5.4.3 Fillet-Foundation Energy

In addition, besides the tooth deformation, the fillet-foundation deflection also influences the stiffness of gear tooth [220], which is represented by fillet foundation stiffness k_f. The gear foundation elasticity and fillet-foundation deflection can be calculated as follows [221]:

$$dU_f = \frac{F^2}{2\,dk_f}, \quad \frac{1}{dk_f} = \frac{\delta_f}{F} \tag{5.15}$$

$$\delta_f = \frac{F\cos^2\alpha_1}{E\,dL(t)}\left\{L^*\left(\frac{u_f}{S_f}\right)^2 + M^*\left(\frac{u_f}{S_f}\right) + P^*\left(1+Q^*\tan^2\alpha_1\right)\right\} \tag{5.16}$$

The coefficients L^*, M^*, P^**and* Q^* can be approximated using polynomial functions [221],

$$X_i^* = A_i/\theta_f^2 + B_i/h_{fi}^2 + C_i h_{fi}/\theta_f + E_i h_{fi} + F_i \tag{5.17}$$

where X_i^* represents the previous coefficients. The values of A_i, B_i, C_i, D_i, E_i and F_i are given in [221-224] with an explanation of the parameters θ_f, S_f, u_f and h_{fi}. The gear fillet geometry parameters r_f, θ_f, S_f and u_f are defined in Figure 5-2.

$$\frac{1}{dk_f} = \frac{\cos^2\alpha_1}{E\,dL(t)}\left\{L^*\left(\frac{u_f}{S_f}\right)^2 + M^*\left(\frac{u_f}{S_f}\right) + P^*\left(1+Q^*\tan^2\alpha_1\right)\right\} \tag{5.18}$$

5.4.4 Total Tooth Stiffness and Potential Energy

The total potential energy dU stored in a slice of single pair meshing teeth can be obtained by summing axial compressive energy dU_a, bending energy dU_b, shear energy dU_s, Hertzian energy dU_h and fillet foundation energy dU_f.:

$$\begin{aligned} dU &= \frac{F^2}{2\,dk} = dU_h + dU_{b1} + dU_{s1} + dU_{a1} + dU_{f1} + dU_{b2} + dU_{s2} + dU_{a2} + dU_{f2} \\ &= \frac{F^2}{2}\left(\frac{1}{dk_h} + \frac{1}{dk_{b1}} + \frac{1}{dk_{s1}} + \frac{1}{dk_{a1}} + \frac{1}{dk_{f1}} + \frac{1}{dk_{b2}} + \frac{1}{dk_{s2}} + \frac{1}{dk_{a2}} + \frac{1}{dk_{f2}}\right) \end{aligned} \tag{5.19}$$

The subscripts 1 and 2 denote the pinion and gear, respectively. The effective mesh stiffness of the contact section of meshing teeth can be expressed as:

$$dk = \frac{1}{\frac{1}{dk_h} + \frac{1}{dk_{b1}} + \frac{1}{dk_{s1}} + \frac{1}{dk_{a1}} + \frac{1}{dk_{f1}} + \frac{1}{dk_{b2}} + \frac{1}{dk_{s2}} + \frac{1}{dk_{a2}} + \frac{1}{dk_{f2}}} \tag{5.20}$$

Then, the total effective stiffness of one tooth pair can be obtained by integrating along the tooth face width b as:

$$k_t = \int_0^b dk \tag{5.21}$$

Due to the complex contact geometry of the helical gears, the time-varying mesh stiffness should be calculated at each instant of time. The total length of tooth width segment depends on the length of the contact lines, which can be determined from the kinematic compatibility between the contact surfaces.

5.5 Time-Varying Contact Lines

An accurate analysis must be performed to indicate the nonlinear characteristics of helical gear meshing process. The meshing process can be imagined as a series of oblique lines (the contact lines) passing through a stationary viewing frame (the plane of action), as explained in Figure 5-4. Several contact lines of mating pairs lay in the zone of contact with apart spacing equals to the transverse base pitch p_t.

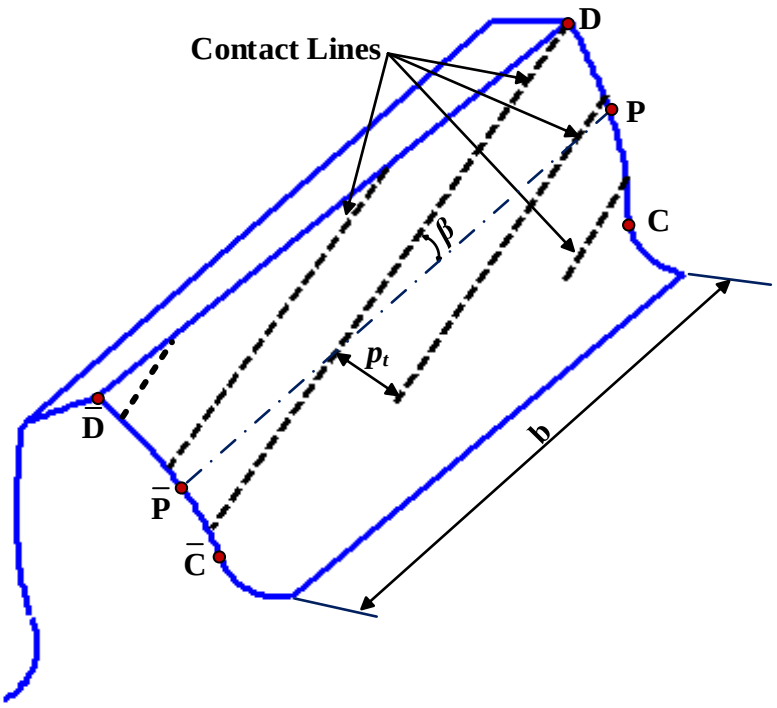

Figure 5-4 Equivalent dynamic model of a helical gear system

Dynamic measurements have verified that helical gear mesh stiffness is roughly proportional to the sum of lengths of the all contact lines in the plane of action [75]. To determine the length of contact lines between mating helical gears, an analytical surface

formula can be characterized by graphical or analytical methods at each instant of time. The region of contact is rectangle with two-sides equal to the tooth face width b and the length of the LOA (L_{CD}), which can generally be divided into different contact patterns as shown in Figure 5-5.

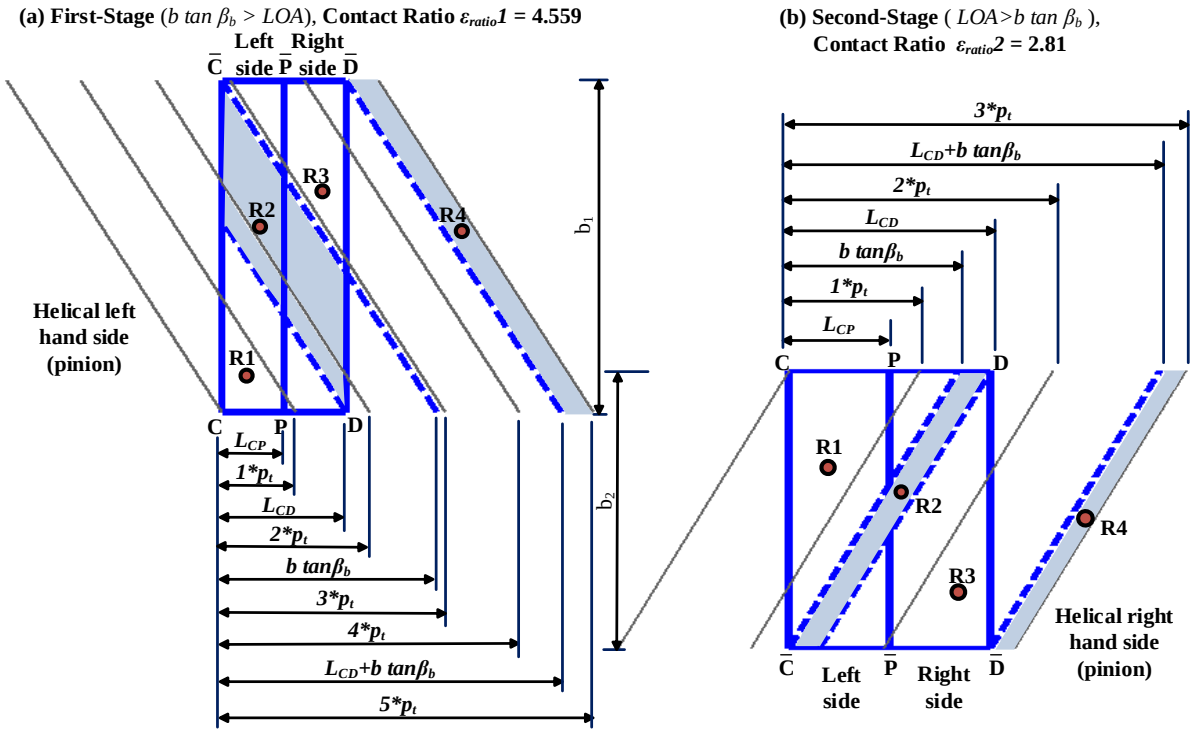

Figure 5-5 Zones of the contact lines in the plane of action for each stage

During the progression of the mesh, the length of a single tooth pair increases gradually in region R_1, commencing at the root of one end of the tooth face, and then remaining constant in region R_2, after that it decreases in region R_3 and remains zero for some distance in region R_4. In general, the number of contact lines present in the contact zone depends upon the geometric parameters of the engaged gears, in which helical gears are basically divided into two groups, depending on the tooth face width and the length of LOA as explained in [76, 210, 211, 225].

For simplification, two groups have been induced to reveal the meshing contact of each stage, based on the tooth face width and the length of LOA, whereby for $btan\beta_b > LOA$ this relates to the first stage and $LOA > btan\beta_b$ category relates to the second stage of the simulated gearbox. The contact and overlap ratios of the first-stage are ε_{a1}=1.669 and ε_{b1}=2.89, respectively. Since, the total contact ratio ε_{ratio1}=4.559, which clarifies that the number of mating tooth pairs is fluctuating between four and five during the mesh process. The second stage is meshing with a transverse contact ratio ε_{a2}=1.521 and overlap ratio

ε_{b2}=1.289, in which the number of mating tooth pairs is fluctuating frequently between two and three, based on the total contact ratio ε_{ratio2}=2.81.

The total number of the engaged tooth pairs is the upwards rounding of the number of contact pairs $n=ceil(\varepsilon_{ratio})$. The length of the contact lines of each stage can be calculated based on graphical and analytical algorithm as:

$$L_{i1}(t)=\begin{cases} DL_i(t)\csc\beta_b & 0\le DL_i(t)<L_{CD} \\ L_{CD}\csc\beta_b & L_{CD}\le DL_i(t)<b\tan\beta_b \\ (L_{CD}+b\tan\beta_b-DL_i(t))\csc\beta_b & b\tan\beta_b\le DL_i(t)<L_{CD}+b\tan\beta_b \\ 0 & L_{CD}+b\tan\beta_b\le DL_i(t)<n*P_t \end{cases} \quad (5.22)$$

$$L_{i2}(t)=\begin{cases} DL_i(t)\csc\beta_b & 0\le DL_i(t)<b\tan\beta_b \\ b\tan\beta_b\csc\beta_b & b\tan\beta_b\le DL_i(t)<b\tan\beta_b \\ (L_{CD}+b\tan\beta_b-DL_i(t))\csc\beta_b & b\tan\beta_b\le DL_i(t)<L_{CD}+b\tan\beta_b \\ 0 & L_{CD}+b\tan\beta_b\le DL_i(t)<n*P_t \end{cases} \quad (5.23)$$

Where

$$DL_i(t)=\mathrm{mod}(r_{bp}\times\theta_{pi}, n\times p_t) \quad (5.24)$$

‘‘mod’’ is the modulus function defined as [226],

$$\mathrm{mod}(x,y)=x-y\ floor(x/y) \quad , \quad y\neq 0 \quad (5.25)$$

$$\theta_{pi}=\theta_p+(i-1)\,P_{angle} \quad (5.26)$$

$$p_t=2\pi\, r_{bp}/z_p \quad (5.27)$$

$$P_{angle}=2\pi/z_p \quad (5.28)$$

$$L_{CD}=LOA=\sqrt{r_{ap}^2-r_{bp}^2}+\sqrt{r_{ag}^2-r_{bg}^2}-(r_p+r_g)\sin\alpha_t \quad (5.29)$$

Where, θ_p is the rotational angle of the pinion, Z_p is the pinion teeth number, P_{angle} and p_t denote the pitch duration angle and the circular transverse base pitch of the meshing gears respectively. The contact pairs is denoted by *i=1, 2, …, n*, whereas *n* represents the maximum number of contact teeth. Also, r_{ap} and r_{bp} are the addendum radius and base radius of the pinion, r_{ag} and r_{bg} are the addendum and base radius of the gear, r_p and r_g are the pitch circle radius of the pinion and gear respectively, whereas β_b and α_t are the base helical angle and transverse pressure angle respectively.

As previously mentioned, the length of each contact line increases gradually from the root of one end of the tooth face and then remains constant before decreasing to zero, and

because of this then the total of the contact lines is the summation of the instantaneous contact lines in the mesh cycle. The total length of the entire contact lines is calculated by:

$$L_{sum}(t) = \sum_{i=1}^{n} L_i\ (t) \tag{5.30}$$

Figure 5-6 shows the variation of the contact lines and the total length with the duration angle for each stage. It shows that the contact lines exhibit a periodic variation with the angular displacement of the pinion gear. Such variations will induce time-varying frictional excitations in meantime they cause the time variations in gear mesh stiffness and damping variations [211].

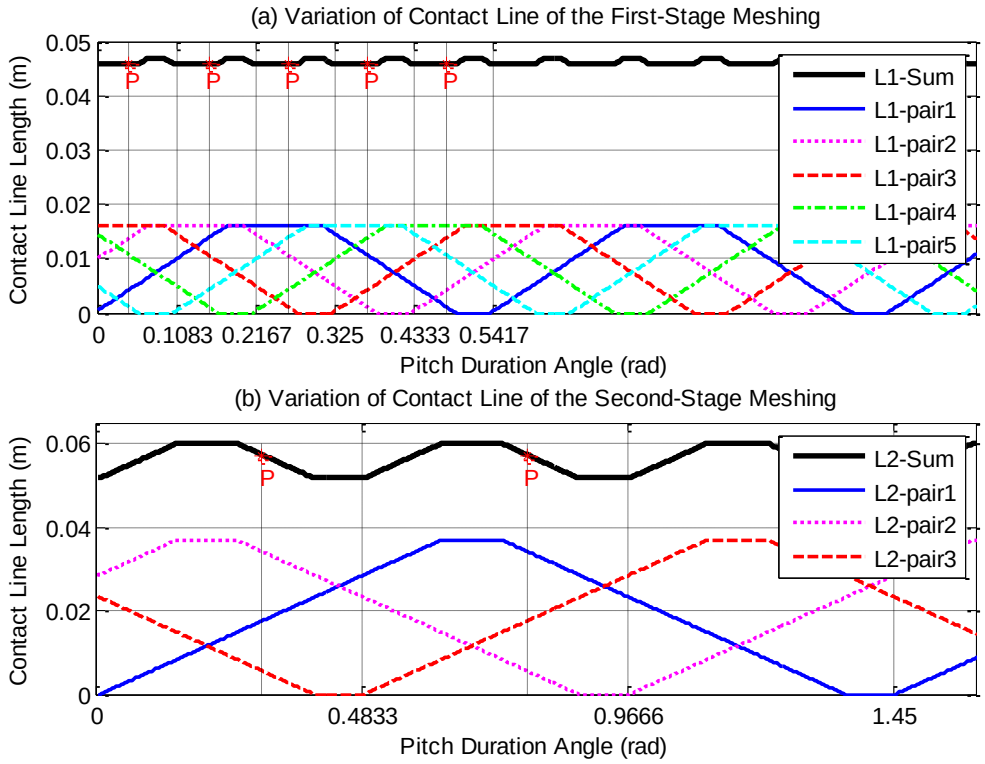

Figure 5-6 Length variations of the contact lines

5.6 Time Varying Mesh Stiffness

Dynamic measurements have verified that the mesh stiffness of a helical gear is roughly proportional to the sum of the lengths of the contact lines of all the tooth pairs in contact [75]. The contact line for a helical gear pair can be determined from the kinematic compatibility between the numerically generated surfaces of the teeth in contact, as expressed by Kar and Mohanty ([210, 211] and subsequently modified by Jiang [76, 225]. The number of contact lines present in the contact zone depends upon the basic parameters

of the gears, such as the normal module, the helix angle, the face width and the transmission ratio.

The summation of the lengths of the contact lines can be used as an alternative method to identify the varying mesh stiffness of helical gears [76, 210, 211, 225, 227], which is otherwise difficult to obtain due to the complexity of the contact geometry. The overall stiffness function is defined as a combination of the total length of the contact lines and a constant mesh stiffness density per unit length along the contact lines, as expressed in the ISO Standard Number 6336 [76, 77].

$$K_{mi}(t) = k_t \; L_i(t) \tag{5.31}$$

Where k_t is the mesh stiffness density per unit length, as defined in Eq. (5.21). The variation of the time-varying mesh stiffness during the meshing of each stage are shown in Figure 5-7 (a) and Figure 5-8 (a).

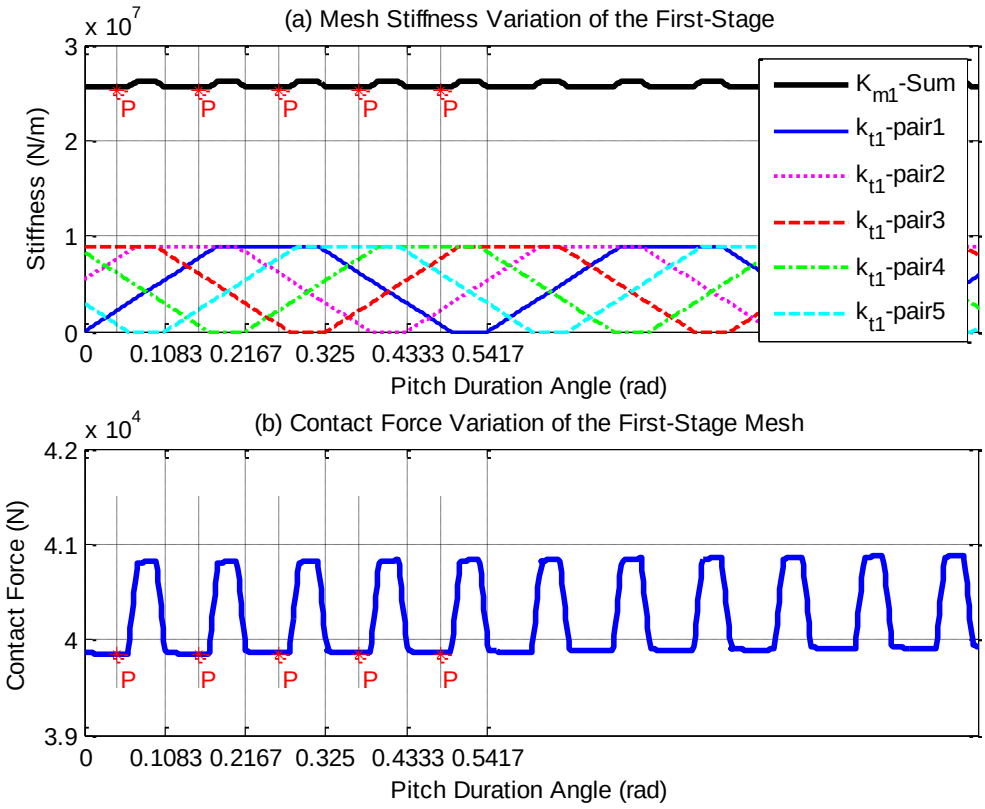

Figure 5-7 Time-varying mesh stiffness variations and contact force variations during the meshing of the first stage

As a result of stiffness and damping between the meshing gears, a fluctuating contact force will be provided to transmit the torque in terms of the given mesh position, as illustrated in Figure 5-7 (b) and Figure 5-8 (b). The contact force was determined by:

$$N_i(t) = K_{mi}(t)\,(r_{bp}\theta_p - r_{bg}\theta_g + y_p - y_g) + C_{mi}(t)\,(r_{bp}\dot{\theta}_p - r_{bg}\dot{\theta}_g + \dot{y}_p - \dot{y}_g) \tag{5.32}$$

The damping coefficient $C_{mi}(t)$, of the meshing gears can be calculated by [76, 77]:

$$C_{mi}(t) = 2\xi\sqrt{K_{mi}(t)\,I_e} \tag{5.33}$$

$$I_e = \frac{I_p I_g}{I_p r_{bg}^2 + I_g r_{bp}^2} \tag{5.34}$$

where $i = 1,\ldots,n$ and ξ is the damping ratio of the gear contact surfaces, I_e is the equivalent moment of inertia of the meshing gears and I_p, I_g are the inertia around the rotational axes of the pinion and the gear respectively.

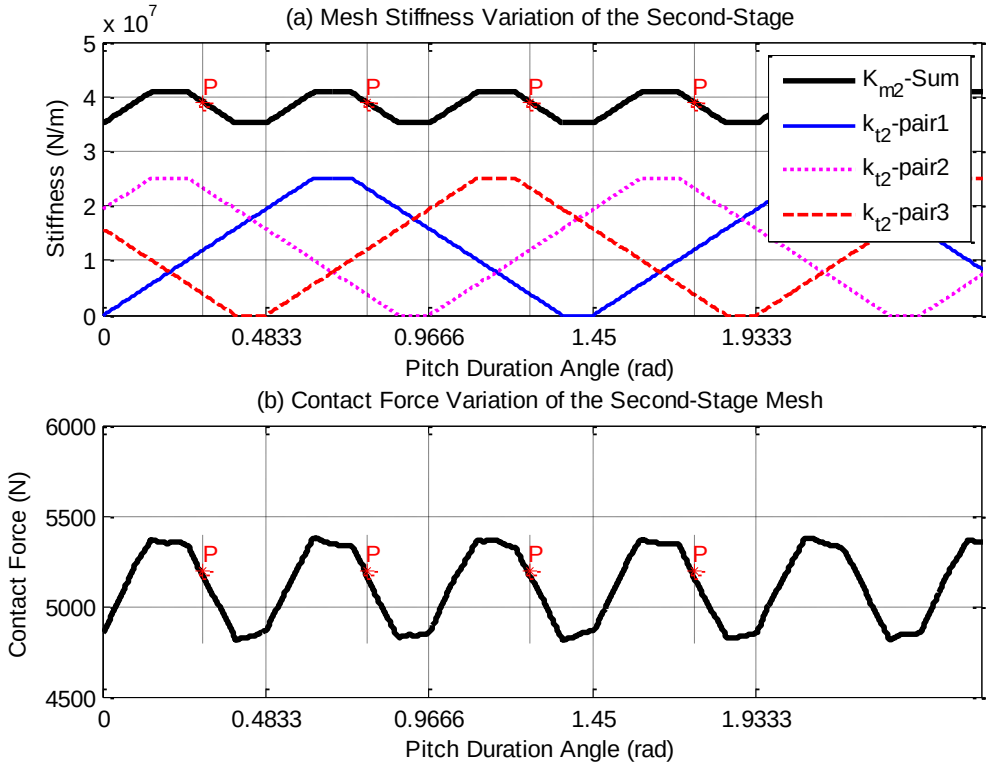

Figure 5-8 Time-varying mesh stiffness variations and contact force variations during the meshing of the first stage

5.7 Frictional Excitations

Friction force fluctuates considerably along the meshing line and as such it is a considerable source of helical gear system excitation [80, 228]. Its effect includes moments about the gear centre perpendicular to the line of action (affecting gear rotations), excitation gear translations in OLOA, nonlinearity excitation dependence on sliding velocity of the gears, and energy dissipation. This may reduce the system stability and generate undesired vibration and noise.

To investigate the influence of gear lubricant parameters on its dynamic response, a theoretical friction coefficient can be derived from EHL and tribological theory [38]. It was considered as the dominant mode of lubrication accumulated with the gears meshing surfaces [38]. The friction representation formula used in this study was derived by Xu and Kahraman [83] based on experimental study, and it was found to accurately model the instantaneous coefficient of friction along the path of contact during gears mesh process. This can be used in a numerical simulation as a means to study the EHL process. The friction coefficient (μ) can be written as:

$$\mu = e^{f(SR,P_h,\upsilon_o,S)} P_h^{b2} |SR|^{b3} V_e^{b6} v_0^{b7} R^{b8} \tag{5.35}$$

where:

$$f(SR,P_h,\upsilon_o,S) = b1 + b4|SR|P_h \log_{10}(\upsilon_o) + b5e^{-|SR|P_h \log_{10}(\upsilon_o)} + b9e^{S} \tag{5.36}$$

In Xu's expressions, v_k and v_o are the kinematic and dynamic viscosities respectively of the lubricant (EP320) that was used in the experimental test. P_h is the maximum Hertzian pressure, which determines based on an equivalent cylindrical contact as:

$$P_h = \sqrt{\frac{W'E'}{2\pi R}} \tag{5.37}$$

Where, W' is the applied normal load per unit width for each contact point along the contact lines. E' is the effective modulus of elasticity and R is the combined radius of curvature as:

$$E' = \frac{2E_1E_2}{E_1 + E_2} \tag{5.38}$$

$$R = \frac{R_1R_2}{R_1 + R_2} \tag{5.39}$$

Where E_1, E_2 are Young's modulus of elasticity of gears and R_1, R_2 are the radii of curvature of the contacting surfaces of the pinion and gear. S is the root mean-square surface roughness amplitude (set such that S=0.07μm), which is the mean value used in [83]. The constant parameters (b1 … b9) are also used with the values proposed in the same reference, which are based on the lubricant type to be as follows [83]: bi = -8.92, 1.03, 1.04, −0.35 , 2.81, -0.10, 0.75, -0.39 and 0.62 for i = 1 to 9.

The model includes the key parameters influencing friction at the contacting gear surfaces under various loads and entraining speed of pure rolling and sliding/rolling conditions. The

kinematic analysis of the rolling/sliding relative motion are based on the surface contact speed of the meshing teeth u_1 and u_2 respectively, where the sliding velocity V_s and rolling velocity V_r are defined by:

$$V_s = u_1 - u_2$$
$$V_r = u_1 + u_2 \tag{5.40}$$

The entrainment velocity V_e and the slide-to-roll ratio SR are determined by:

$$V_e = \frac{u_1 + u_2}{2}$$
$$SR = \frac{2(u_1 - u_2)}{u_1 + u_2} \tag{5.41}$$

Figure 5-9 demonstrates the variation of friction coefficient based on EHL model along the tooth profile of each contact pair during the mesh process. It fluctuates periodically with roll angle and it is zero at its pitch point and no contact regions. The friction force along the portion of contact line is reversed along the portion of contact line surpass the pitch point P, as a result of reversal sliding velocity.

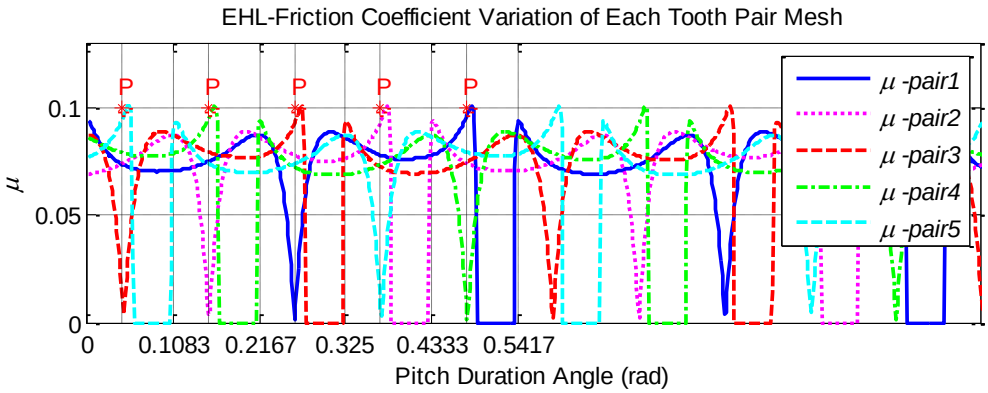

Figure 5-9 EHL friction coefficient of the first stage

The friction force has been assumed to be uniformly distributed along the contact lines, which splits into two components with opposite directions as shown by the arrows F_{Li}, F_{Ri}, see Figure 5-1. Hence, the friction force of the i^{th} segment of the contact line at the meshing instance is given by:

$$F_{fi}(t) = \mu_i(t) \frac{N_i(t)}{L_{sum}(t)} (L_{ri}(t) - L_{li}(t)) \tag{5.42}$$

Where $\mu_i(t)$ is the time varying friction coefficient based on the EHL model of each contact line and $N_i(t)$ is the normal resultant force of the stiffness and damping forces within the meshing contact. $L_{ri}(t)$ and $L_{li}(t)$ are the contact lines of the right and left side, respectively.

For a single tooth mesh, these lines can be determined as [76, 225]:

$$L_{ri}(t)=\begin{cases}0 & 0\le DL_i(t)<L_{CP}\\ (DL_i(t)-L_{CP})\csc\beta_b & L_{CP}\le DL_i(t)<L_{CD}\\ (L_{CD}-L_{CP})\csc\beta_b & L_{CD}\le DL_i(t)<L_{CP}+b\tan\beta_b\\ (L_{CD}+b\tan\beta_b-DL_i(t))\csc\beta_b & L_{CP}+b\tan\beta_b\le DL_i(t)<L_{CD}+b\tan\beta_b\\ 0 & L_{CD}+b\tan\beta_b\le DL_i(t)<nP_t\end{cases} \tag{5.43}$$

$$L_{li}(t)=\begin{cases}DL_i(t)\csc\beta_b & 0\le DL_i(t)<L_{CP}\\ L_{CP}\csc\beta_b & L_{CP}\le DL_i(t)<b\tan\beta_b\\ (L_{CP}+b\tan\beta_b-DL_i(t))\csc\beta_b & b\tan\beta_b\le DL_i(t)<L_{CP}+b\tan\beta_b\\ 0 & L_{CP}+b\tan\beta_b\le DL_i(t)<nP_t\end{cases} \tag{5.44}$$

where

$$L_{CP}=\sqrt{r_{ag}^2-r_{bg}^2}-r_{bg}\tan\alpha_t \tag{5.45}$$

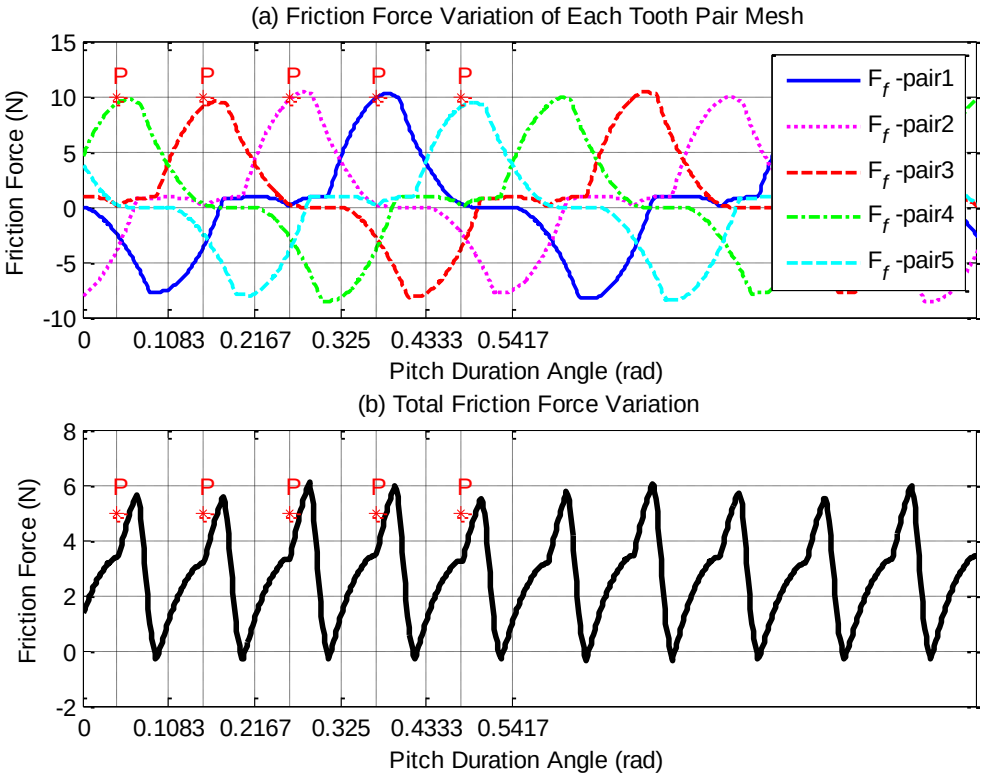

Figure 5-10 Frictional force variation of the first stage mesh

The total friction force of all meshing tooth pairs can be calculated by:

$$F_f(t)=\sum_{i=1}^{n}F_{fi}(t) \tag{5.46}$$

The resultant friction force is calculated by the summation of all forces of the contact teeth, which fluctuates during the meshing process, as shown in Figure 5-10.

Moreover, the frictional torque of each contact line is determined from the moment formed by the friction force and the radius of curvature of each segment ($X_{ri}(t)$ and $X_{li}(t)$) as:

$$T_{fi}(t) = \mu_i(t)\frac{N_i(t)}{L_{sum}(t)}\left(L_{ri}(t)\times X_{ri}(t) - L_{li}(t)\times X_{li}(t)\right) \tag{5.47}$$

Where, $X_{ri}(t)$ and $X_{li}(t)$ are the right and left arms of each friction force segment, which are obtained by taking the midpoint distance of each piece of the contact line length ($L_{ri}(t)$ and $L_{li}(t)$) as explained in [76, 225].

$$X_{pri}(t) = \begin{cases} 0 & 0 \le DL_i(t) < L_{CP} \\ L_{AP} + (DL_i(t) - L_{CP})/2 & L_{CP} \le DL_i(t) < L_{CD} \\ L_{AP} + (L_{PD})/2 & L_{CD} \le DL_i(t) < L_{CP} + b\tan\beta_b \\ L_{AP} + (L_{PD} + DL_i(t) - L_{CD} - b\tan\beta_b)/2 & L_{CP} + b\tan\beta_b \le DL_i(t) < L_{CD} + b\tan\beta_b \\ 0 & L_{CD} + b\tan\beta_b \le DL_i(t) < nP_t \end{cases} \tag{5.48}$$

$$X_{gri}(t) = \begin{cases} 0 & 0 \le DL_i(t) < L_{CP} \\ L_{PB} - (DL_i(t) - L_{CP})/2 & L_{CP} \le DL_i(t) < L_{CD} \\ L_{PB} - (L_{PD})/2 & L_{CD} \le DL_i(t) < L_{CP} + b\tan\beta_b \\ L_{PB} - (L_{PD} + DL_i(t) - L_{CD} - b\tan\beta_b)/2 & L_{CP} + b\tan\beta_b \le DL_i(t) < L_{CD} + b\tan\beta_b \\ 0 & L_{CD} + b\tan\beta_b \le DL_i(t) < nP_t \end{cases} \tag{5.49}$$

$$X_{Pli}(t) = \begin{cases} L_{AC} + DL_i(t)/2 & 0 \le DL_i(t) < L_{CP} \\ L_{AC} + (L_{CP})/2 & L_{CP} \le DL_i(t) < b\tan\beta_b \\ L_{AC} + (L_{CP} + DL_i(t) - b\tan\beta_b)/2 & b\tan\beta_b \le DL_i(t) < L_{CP} + b\tan\beta_b \\ 0 & L_{CP} + b\tan\beta_b \le DL_i(t) < nP_t \end{cases} \tag{5.50}$$

$$X_{gli}(t) = \begin{cases} L_{DB} + L_{CD} - DL_i(t)/2 & 0 \le DL_i(t) < L_{CP} \\ L_{DB} + L_{CD} - L_{CP}/2 & L_{CP} \le DL_i(t) < b\tan\beta_b \\ L_{DB} + L_{CD} - (L_{CP} + b\tan\beta_b - DL_i(t))/2 & b\tan\beta_b \le DL_i(t) < L_{CP} + b\tan\beta_b \\ 0 & L_{CP} + b\tan\beta_b \le DL_i(t) < nP_t \end{cases} \tag{5.51}$$

Where:

$$L_{AP} = r_{bp}\tan\alpha_t \tag{5.52}$$

$$L_{PB} = r_{bg}\tan\alpha_t \tag{5.53}$$

$$L_{AC} = (r_{bp} + r_{bg})\tan\alpha_t - \sqrt{r_{ag}^2 - r_{bg}^2} \tag{5.54}$$

$$L_{DB} = (r_{bp} + r_{bg})\tan\alpha_t - \sqrt{r_{ap}^2 - r_{bp}^2} \tag{5.55}$$

The contact points and the radius of curvature are changing over the time that forcing frictional torques acting on pinion and gear to be time varying during the mesh process. The total frictional torque of all engaged tooth pairs (n) can be calculated by

$$T_f(t) = \sum_{i=1}^{n} T_{fi}(t) \tag{5.56}$$

The frictional torque fluctuates periodically at every pitch duration angle of the contact lines as shown in Figure 5-11. A possible consequence of negative frictional torque due to opposite direction of the gear rotation, in which it has considerable effects and should not be ignored in the dynamic analysis of the gear mesh process.

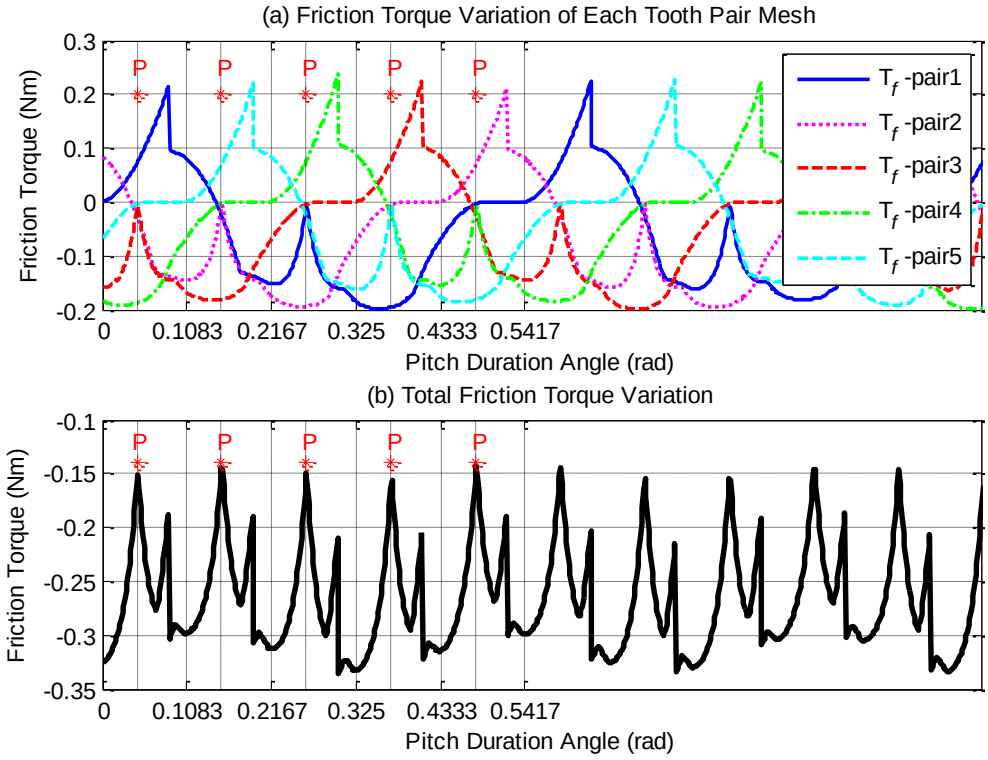

Figure 5-11 Frictional torque variation of the first stage mesh

5.8 Modelling and Simulation of a Two-Stage Helical Gearbox

An improved understanding of vibration signal is required to achieve high reliability for early detection of incipient gear failure. Gear faults under different operating conditions can be simulated easily by producing a numerical model in order to simplify the development of diagnostic and prognostic techniques in real systems. An 18-DOF nonlinear model is proposed to simulate the dynamics of a two-stage helical gearbox system that explained in Sec. 4.4.1.

Each gear is represented by rigid blocks with 4-dof (three translations and one rotation). The first and second stages of the gearbox are denoted by subscripts 1 and 2, and the pinion and gear are denoted by subscripts p and g, respectively. As explained in the geometric specification, see Table 5-1, the chosen gear train system is a speed decreaser, typical of that used in many industrial applications. The model includes six inertias, one each for the load motor, drive motor, two pinions and two gears, the latter four are denoted for the two stages of the gearbox using subscripts p1, g1, p2 and g2.

Table 5-1 Geometric property of the meshing gears

Description	**First Stage**		**Second Stage**	
	Pinion	**Gear**	**Pinion**	**Gear**
Number of teeth	Z_1=58	Z_2=47	Z_3=13	Z_4=59
Ref. circle diameter (mm)	81.369	65.937	26.684	121.1
Pitch radius (mm)	r_{p1}=37.6	r_{g1}=30.5	r_{p2}=12.5	r_{g2}=56.7
Mass (kg)	m_{p1}=0.9	m_{g1}=0.58	m_{p2}=0.4	m_{g2}=3.62
Direction	LH	RH	RH	LH
Shaft diameter (mm)	28	24	25 (gear shaft)	39.5
Rotation speed (Hz)	f_{r1}	f_{r2}	f_{r2}	f_{r3}
Meshing frequency	f_{m1}		f_{m2}	
Reduction ratio	1.234		0.2203	
Overall reduction ratio	0.2719 (as speed reducer)			
Working face width	b_1=25 mm		b_2=36 mm	
Module	M_1=1.25mm		M_2=2.0mm	
Helix angle (°)	27		13	
Pressure angle (°)	α=20		α=20	
Contact ratio	ε_{a1}=1.669		ε_{a2}=1.521	
Overlap ratio	ε_{b1}=2.89		ε_{b2}=1.289	

To represent an accurate gear transmission system, the model takes into account the effects of the speed-torque characteristics of both the driving and loading motor systems. The torsional compliances (stiffness and damping) of the shafts and the transverse compliances of supporting bearings are included in the model. The resilient elements of the supports are described by stiffness and damping coefficients as $K_{b\text{-}ij}$ and $C_{b\text{-}ij}$, the four bearings (i =1, 2, 3, 4) that in the j= x, y and z directions (i.e. LOA, OLOA and axial or shaft direction). The shafts between the system components are represented by torsional stiffness and torsional damping components k_1, k_2, k_3, c_1, c_2 and c_3. Furthermore, the model takes into account the influence of the driving torque and load torque T_m and T_L, respectively.

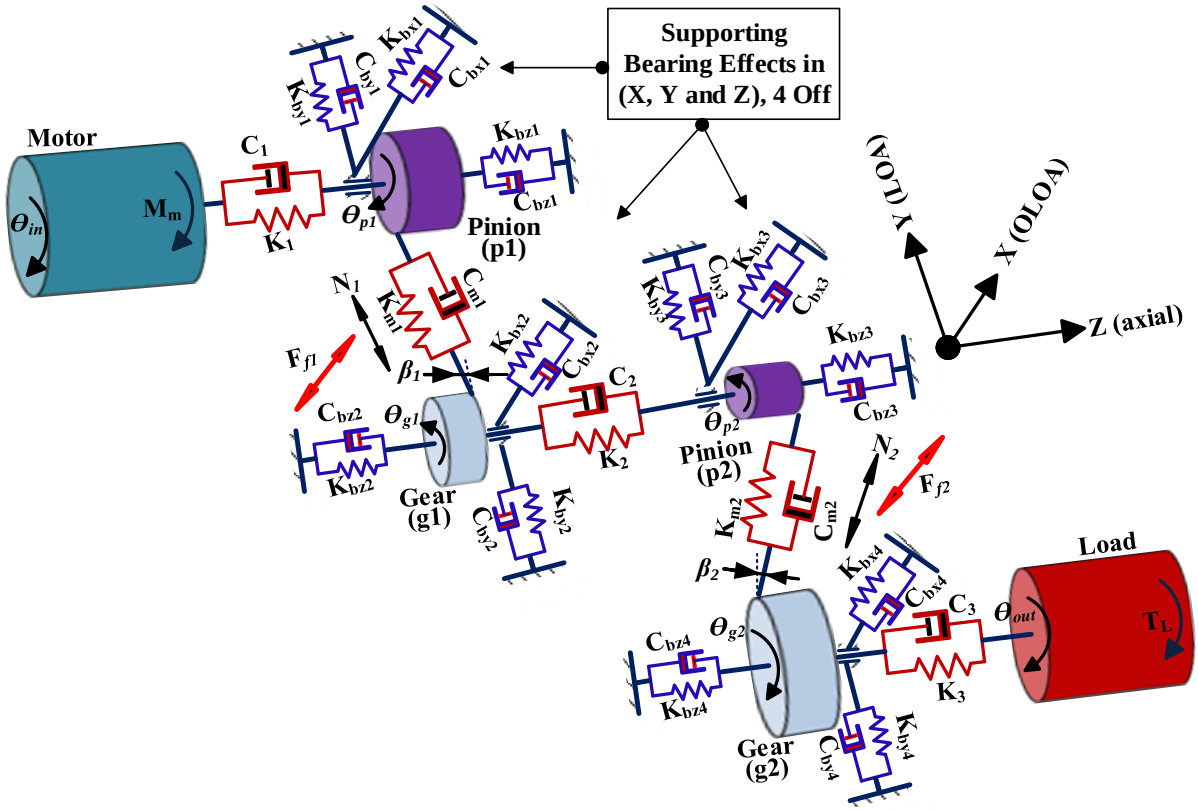

Figure 5-12 Two-stage gearbox system model

The equations of motion were represented in the state space form and then solved using the MATLAB ODE solver. The governing equations of motion for the model, depicted in Figure 5-12, were derived with the following assumptions:

- The pinion and gear are modelled as rigid disks with radius equal to the base circle radius and flexibility at the gear teeth;
- Input torque and load torque are applied to the system;
- Shaft mass and inertia are lumped with the gears;
- The effects of static transmission error are much smaller than the dynamic transmission error so it can be neglected.
- An EHL model is used to simulate the time variation of the friction coefficient μ;
- The helical gear teeth are assumed to be perfectly involute, manufacturing and assembly errors are ignored;
- Backlash is not considered in the model as gears are undertaking static loads.

According to Newton's laws of motion, the governing equations have been derived for the rotation of the motor rotor, the rotations of the pinions and gears of the two transmission

stages, the rotation of the load rotor, and the translations for all rotors in the Y-direction (LOA), the Z-direction (axial) and the X-direction (OLOA), as presented in Equations from Eq. (5.57) to Eq. (5.74):

$$I_m\ddot{\theta}_{in} + c_1\left(\dot{\theta}_{in} - \dot{\theta}_{p1}\right) + k_1\left(\theta_{in} - \theta_{p1}\right) = M_m \tag{5.57}$$

$$\begin{aligned} &I_{p1}\ddot{\theta}_{p1} - c_1\left(\dot{\theta}_{in} - \dot{\theta}_{p1}\right) - k_1\left(\theta_{in} - \theta_{p1}\right) + r_{bp}C_{m1}(t)\left(r_{bp1}\dot{\theta}_{p1} - r_{bg1}\dot{\theta}_{g1} + \dot{y}_{p1} - \dot{y}_{g1}\right) \\ &\quad + r_{bp1}K_{m1}(t)\left(r_{bp1}\theta_{p1} - r_{bg1}\theta_{g1} + y_{p1} - y_{g1}\right) + T_{fp1} = 0 \end{aligned} \tag{5.58}$$

$$\begin{aligned} &I_{g1}\ddot{\theta}_{g1} + c_2\left(\dot{\theta}_{g1} - \dot{\theta}_{p2}\right) + k_2\left(\theta_{g1} - \theta_{p2}\right) - r_{bg1}C_{m1}(t)\left(r_{bp1}\dot{\theta}_{p1} - r_{bg1}\dot{\theta}_{g1} + \dot{y}_{p1} - \dot{y}_{g1}\right) \\ &\quad - r_{bg1}K_{m1}(t)\left(r_{bp1}\theta_{p1} - r_{bg1}\theta_{g1} + y_{p1} - y_{g1}\right) - T_{fg1}(t) = 0 \end{aligned} \tag{5.59}$$

$$\begin{aligned} &I_{p2}\ddot{\theta}_{p2} - c_2\left(\dot{\theta}_{g1} - \dot{\theta}_{p2}\right) - k_2\left(\theta_{g1} - \theta_{p2}\right) + r_{bp2}C_{m2}(t)\left(r_{bp2}\dot{\theta}_{p2} - r_{bg2}\dot{\theta}_{g2} + \dot{y}_{p2} - \dot{y}_{g2}\right) \\ &\quad + r_{bp2}K_{m2}(t)\left(r_{bp2}\theta_{p2} - r_{bg2}\theta_{g2} + y_{p2} - y_{g2}\right) + T_{fp2} = 0 \end{aligned} \tag{5.60}$$

$$\begin{aligned} &I_{g2}\ddot{\theta}_{g2} + c_3\left(\dot{\theta}_{g2} - \dot{\theta}_{out}\right) + k_3\left(\theta_{g2} - \theta_{out}\right) - r_{bg2}C_{m2}(t)\left(r_{bp2}\dot{\theta}_{p2} - r_{bg2}\dot{\theta}_{g2} + \dot{y}_{p2} - \dot{y}_{g2}\right) \\ &\quad - r_{bg2}K_{m2}(t)\left(r_{bp2}\theta_{p2} - r_{bg2}\theta_{g2} + y_{p2} - y_{g2}\right) - T_{fg2}(t) = 0 \end{aligned} \tag{5.61}$$

$$I_L\ddot{\theta}_{out} - c_2\left(\dot{\theta}_{g2} - \dot{\theta}_{out}\right) - k_1\left(\theta_{g2} - \theta_{out}\right) = -T_L \tag{5.62}$$

$$\begin{aligned} &m_{p1}\ddot{y}_{p1} + C_{m1}(t)\cos\beta_{b1}\left(r_{bp1}\dot{\theta}_{p1} - r_{bg1}\dot{\theta}_{g1} + \dot{y}_{p1} - \dot{y}_{g1}\right) + K_{m1}(t)\cos\beta_{b1}(r_{bp1}\theta_{p1} - r_{bg1}\theta_{g1} \\ &\quad + y_{p1} - y_{g1}) + C_{by1}\dot{y}_{p1} + K_{by1}y_{p1} = 0 \end{aligned} \tag{5.63}$$

$$\begin{aligned} &m_{g1}\ddot{y}_{g1} - C_{m1}(t)\cos\beta_{b1}\left(r_{bp1}\dot{\theta}_{p1} - r_{bg1}\dot{\theta}_{g1} + \dot{y}_{p1} - \dot{y}_{g1}\right) - K_{m1}(t)\cos\beta_{b1}(r_{bp1}\theta_{p1} - r_{bg1}\theta_{g1} \\ &\quad + y_{p1} - y_{g1}) + C_{by2}\dot{y}_{g1} + K_{by2}y_{g1} = 0 \end{aligned} \tag{5.64}$$

$$\begin{aligned} &m_{p2}\ddot{y}_{p2} + C_{m2}(t)\cos\beta_{b2}\left(r_{bp2}\dot{\theta}_{p2} - r_{bg2}\dot{\theta}_{g2} + \dot{y}_{p2} - \dot{y}_{g2}\right) + K_{m2}(t)\cos\beta_{b2}(r_{bp2}\theta_{p2} \\ &\quad - r_{bg2}\theta_{g2} + y_{p2} - y_{g2}) + C_{by3}\dot{y}_{p2} + K_{by3}y_{p2} = 0 \end{aligned} \tag{5.65}$$

$$\begin{aligned} &m_{g2}\ddot{y}_{g2} - C_{m2}(t)\cos\beta_{b2}\left(r_{bp2}\dot{\theta}_{p2} - r_{bg2}\dot{\theta}_{g2} + \dot{y}_{p2} - \dot{y}_{g2}\right) - K_{m2}(t)\cos\beta_{b2}(r_{bp2}\theta_{p2} \\ &\quad - r_{bg2}\theta_{g2} + y_{p2} - y_{g2}) + C_{by4}\dot{y}_{g2} + K_{by4}y_{g2} = 0 \end{aligned} \tag{5.66}$$

$$\begin{aligned} &m_{p1}\ddot{z}_{p1} + C_{m1}(t)\sin\beta_{b1}[\dot{z}_{p1} - \dot{z}_{p1} + \tan\beta_{b1}(r_{bp1}\dot{\theta}_{p1} - r_{bg1}\dot{\theta}_{g1} + \dot{y}_{p1} - \dot{y}_{g1})] + K_{m1}(t). \\ &\sin\beta_{b1}[z_{p1} - z_{g1} + \tan\beta_{b1}(r_{bp1}\theta_{p1} - r_{bg1}\theta_{g1} + y_{p1} - y_{g1})] + C_{bz1}\dot{z}_{p1} + K_{bz1}z_{p1} = 0 \end{aligned} \tag{5.67}$$

$$m_{g1}\ddot{z}_{g1} - C_{m1}(t)\sin\beta_{b1}[\dot{z}_{p1} - \dot{z}_{p1} + \tan\beta_{b1}(r_{bp1}\dot{\theta}_{p1} - r_{bg1}\dot{\theta}_{g1} + \dot{y}_{p1} - \dot{y}_{g1})] - K_{m1}(t).$$
$$\sin\beta_{b1}[z_{p1} - z_{g1} + \tan\beta_{b1}(r_{bp1}\theta_{p1} - r_{bg1}\theta_{g1} + y_{p1} - y_{g1})] + C_{bz2}\dot{z}_{g1} + K_{bz2}z_{g1} = 0 \quad (5.68)$$

$$m_{p2}\ddot{z}_{p2} + C_{m2}(t)\sin\beta_{b2}[\dot{z}_{p2} - \dot{z}_{p2} + \tan\beta_{b2}(r_{bp2}\dot{\theta}_{p2} - r_{bg2}\dot{\theta}_{g2} + \dot{y}_{p2} - \dot{y}_{g2})] + K_{m2}(t).$$
$$\sin\beta_{b2}[z_{p2} - z_{g2} + \tan\beta_{b2}(r_{bp2}\theta_{p2} - r_{bg2}\theta_{g2} + y_{p2} - y_{g2})] + C_{bz3}\dot{z}_{p2} + K_{bz3}z_{p2} = 0 \quad (5.69)$$

$$m_{g2}\ddot{z}_{g2} - C_{m2}(t)\sin\beta_{b2}[\dot{z}_{p2} - \dot{z}_{p2} + \tan\beta_{b2}(r_{bp2}\dot{\theta}_{p2} - r_{bg2}\dot{\theta}_{g2} + \dot{y}_{p2} - \dot{y}_{g2})] - K_{m2}(t).$$
$$\sin\beta_{b2}[z_{p2} - z_{g2} + \tan\beta_{b2}(r_{bp2}\theta_{p2} - r_{bg2}\theta_{g2} + y_{p2} - y_{g2})] + C_{bz4}\dot{z}_{g2} + K_{bz4}z_{g2} = 0 \quad (5.70)$$

$$m_{p1}\ddot{x}_{p1} + C_{bx1}\dot{x}_{p1} + K_{bx1}x_{p1} - F_{f1} = 0 \quad (5.71)$$

$$m_{g1}\ddot{x}_{g1} + C_{bx2}\dot{x}_{g1} + K_{bx2}x_{g1} + F_{f1} = 0 \quad (5.72)$$

$$m_{p2}\ddot{x}_{p2} + C_{bx3}\dot{x}_{p2} + K_{bx3}x_{p2} - F_{f2} = 0 \quad (5.73)$$

$$m_{g2}\ddot{x}_{g2} + C_{bx4}\dot{x}_{g2} + K_{bx4}x_{g2} + F_{f2} = 0 \quad (5.74)$$

$$M_m = M_m + 10(\omega_{p1} - \dot{\theta}_1) \quad (5.75)$$

As these coupled equations are nonlinear, a numerical solution was derived to study the vibration responses of the gear system under different conditions. A Runge–Kutta algorithm, with a fixed time step, was used to integrate the governing differential equations to produce the time domain responses of the system, in line with the time varying mesh stiffness and the EHL frictional excitations. Eq. (5.75) was used in the model to adjust the motor input torque to maintain its speed as constant as possible. Especially, additional static torque is needed in order to balance the torque due to friction effects. This torque adaptation is to simulate the speed-torque characteristics for a common induction motor.

5.9 Simulation Procedure

A numerical simulation study was performed to obtain the solution of the nonlinear equations. However, to ensure the correctness of parameters used and model structures, linear solutions was obtained whereas an average meshing stiffness value is used in the model without friction influences, which allows the adjustment of the model parameters so that major resonances agree with the real system as close as possible. Subsequently, the non-linear effects of EHL friction and mesh stiffness variation have been applied to the model and numerical integration method is used to solve the model within appropriate set

of initial conditions. More details of the simulation procedure used in this study are summarized in a flowchart shown in Fig. 5-12.

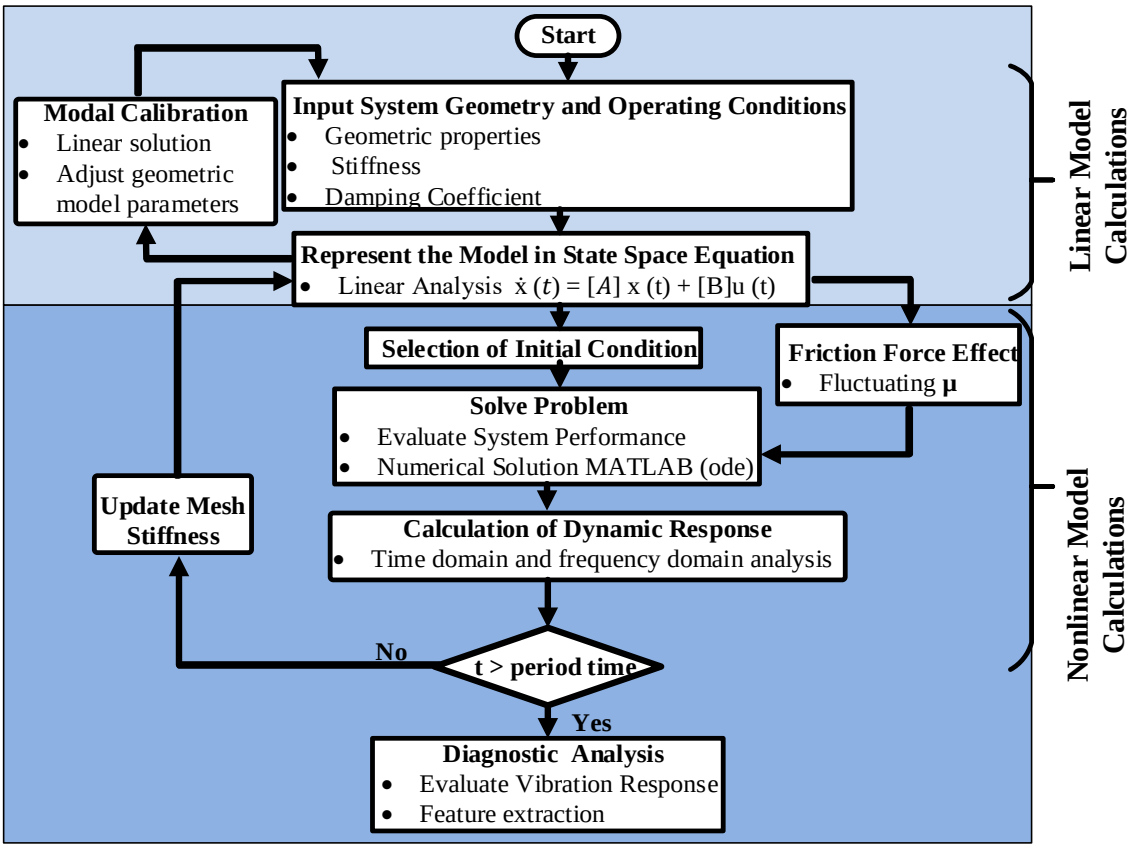

Figure 5-13 Simulation procedure used in this study

5.10 Model Calibration

5.10.1 Liner Solution

In order to obtain an estimation of the eigen frequencies of the full model, a simplified linear version of this model is developed to monitor and identify vibration frequencies associated with the meshing gears. A simplified linear version of this model is developed by using the average mesh stiffness value in Eqs. (5.57)-(5.74). It allows modal parameters including resonance frequencies and damping ratios to be found conveniently with the gearbox modal analysis, explained in **Appendix A** and **Appendix B**. The mode shapes and natural frequencies were adjusted using the standard eigen method. By considering linear factors of the system, the vibration differential equations were expressed by:

$$[M]\{\ddot{q}\}+[C]\{\dot{q}\}+[K]\{q\}=f(t) \tag{5.76}$$

$$\{\dot{\mathbf{V}}\}=[\mathbf{A}]\{\mathbf{q}\} \tag{5.77}$$

Where, [*M*] is mass matrix, [*C*] is damping matrix, [*K*] is stiffness matrix and q is vibration response vector consisting of displacements and velocity of the system.

Using standard method for linear system analysis, the frequency response can be obtained conveniently under different parameters settings. Figure 5-14 shows the system responses with refined parameters. It can be seen that the 1st mode is at 84.6Hz which is 3-times away from the shaft frequency at about 25Hz. The eighth, ninth and tenth modes are close to the 2nd harmonic of $2xf_m = 2xf_r$ Z=2*1435.5Hz.

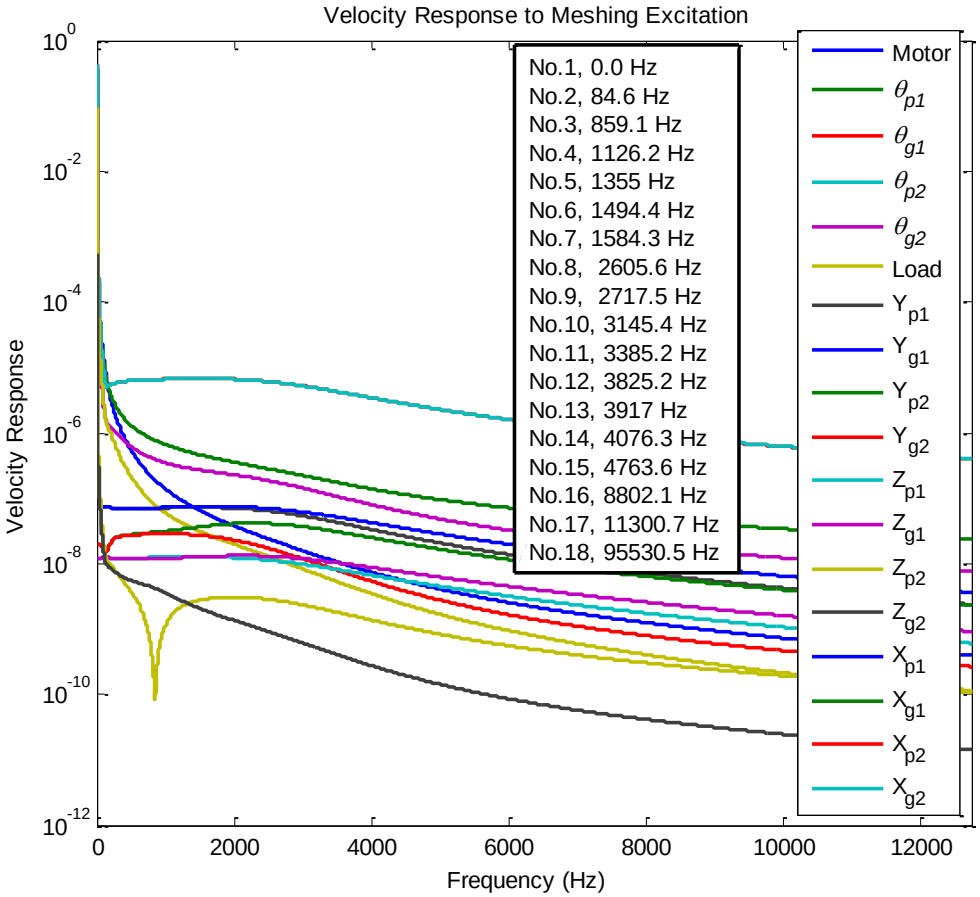

Figure 5-14 Velocity responses of gear system excited with impulsive inputs at the pinion and gear

To maintain the solution stability in the case of solving the nonlinear equations, these modes are applied with high damping ratios so that the frequency responses around these frequency ranges are relatively flat. Also, note that there is no response in X-directions as there is no friction effect included in the linear mode. Moreover, the frequency responses are similar to that of measurements from the gearbox installed in the laboratory, see **Appendix A**. It shows that the key parameters such as tooth stiffness values and damping

ratios are used appropriately and the numerical solutions can be proceeded to obtain the nonlinear responses.

5.10.2 Nonlinear Solution

The time domain behaviour of the nonlinear system is obtained by integrating the set of governing differential equations numerically using an ode15s Runge–Kutta algorithm with a fixed time step size. This solver is suitable for solving differential algebraic stiff problems with a mass matrix, whereas high fluctuations and large noises are in the solution with ode45. Moreover, ode45 is not be able to find an accurate solution of a stiff differential equations, or may need excessive computation times for taking very small time steps.

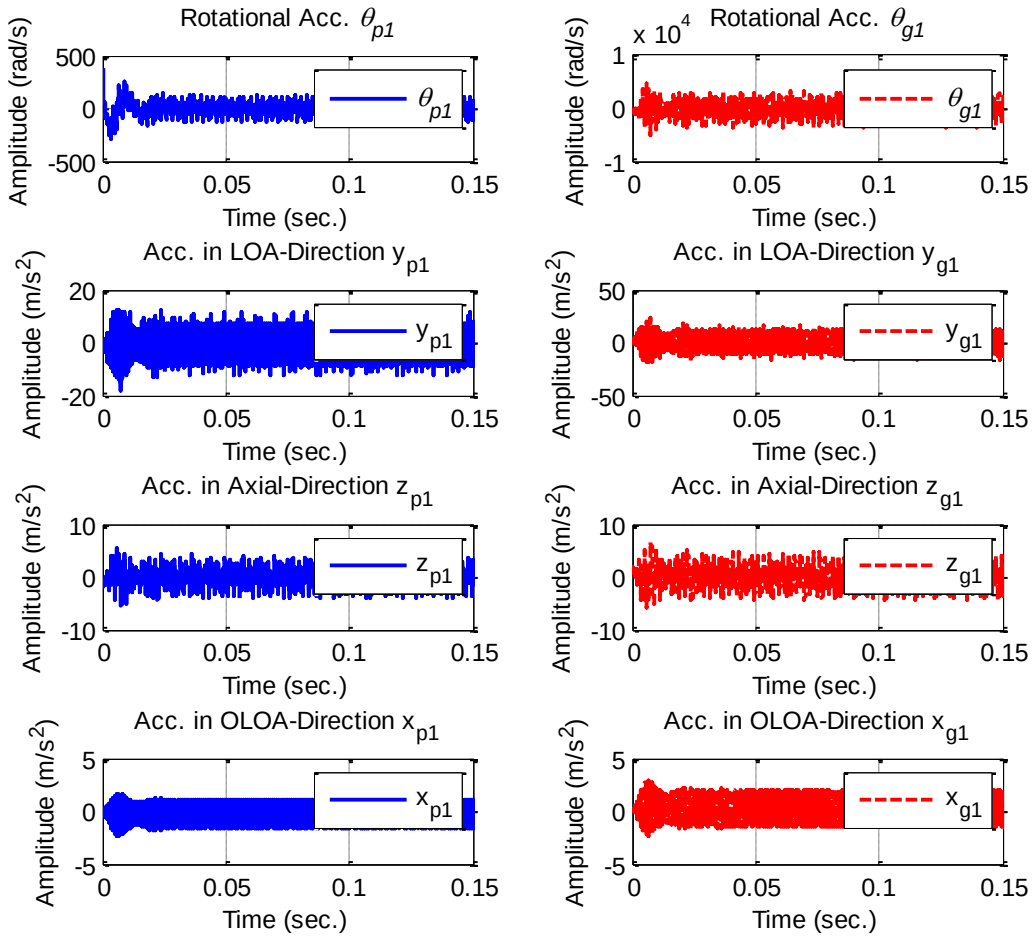

Figure 5-15 Acceleration response of the 1st stage motions

The ode15s is a better choice and can be applied to integrate the problem with appropriate set of initial conditions. The operating conditions of the system observed convergent responses corresponding to the constant speed of interest.

Figures 5-15 and Figures 5-16 present acceleration responses of the raw data for each motion in the first and second stage, respectively. In the time domain, all the responses including pinion and gear in the rotation (Θ_{p1}, Θ_{g1}, Θ_{p2}, Θ_{g2}), translation in the LOA (y_{p1}, y_{g1}, y_{p2}, y_{g2}), translation in the axial (shaft) direction (z_{p1}, z_{g1}, z_{p2}, z_{g2}) and OLOA (x_{p1}, x_{g1}, x_{p2}, x_{g2}) directions exhibit periodic profiles follows the time-varying mesh stiffness and time-varying frictional effects.

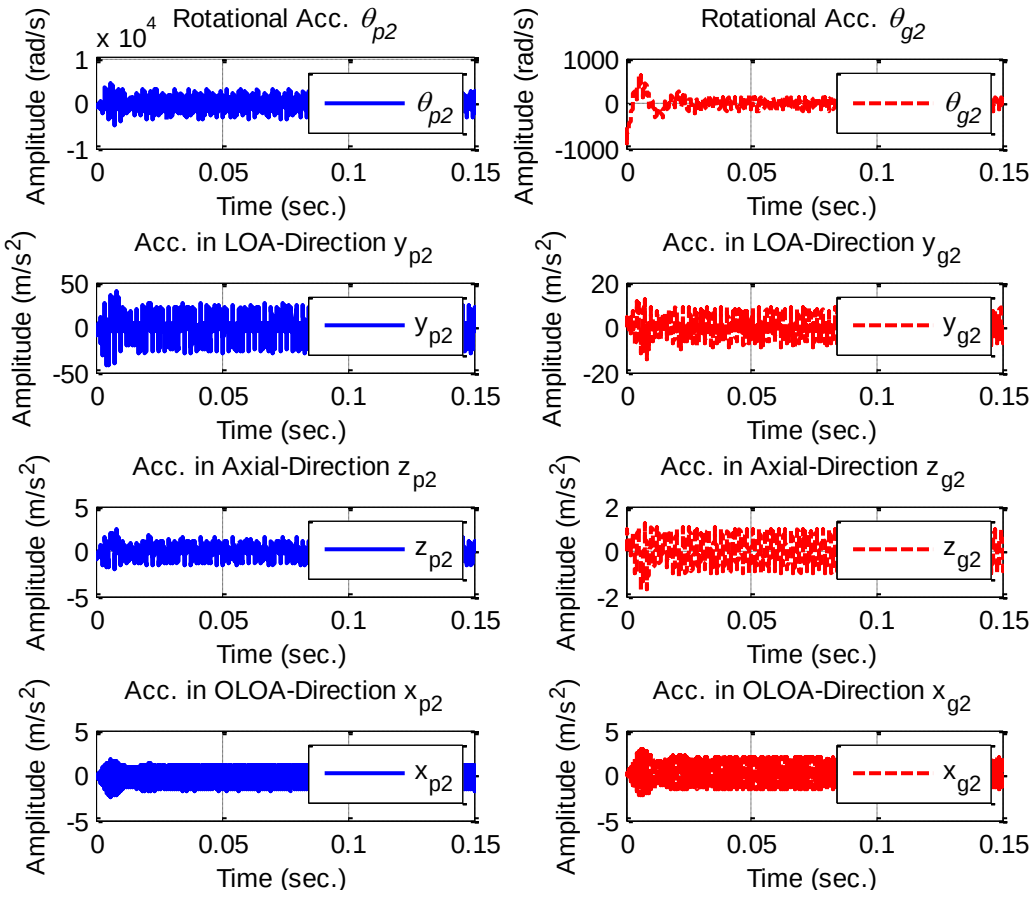

Figure 5-16 Acceleration response of the 2nd stage motions

5.11 Model Evaluation

As tooth breakage (TB) is a common gear failure mode, understanding the dynamic characteristics of its effect is considerably helpful for the detection and diagnosis schemes. TB can be loss of total or part of the tooth and mainly occurs in gears due to impact or static overloads. Identifying breakage in helical gears is a big diagnostic challenge due to high contact ratio, in which accurate dynamic model of helical gear system is essential to obtain reliable dynamic characteristics for detecting a small damage severity.

This section explores the performance of using vibration analysis for monitoring and diagnosing of TB in a two-stage helical gearbox using experimental test and numerical model. In which, vibration analysis is applied for diagnostics of different missing parties of tooth width. Different degrees of TB severities (20% TB and 40% TB, see Sec. 4.6.1) have been simulated to obtain reliable features for fault diagnosis in an early stage of its development.

5.11.1 Mode Shapes of TB

Due to the high contact ratio of the helical gears, partial breakage is more likely to happen during the high transmission loads [227]. Three mode of TB have been simulated within the first stage, as depicted in Figure 5-17, in which a variety of gear faults can be simulated in the numerical model by altering the time-varying mesh stiffness to reflect the reduction caused by the defect.

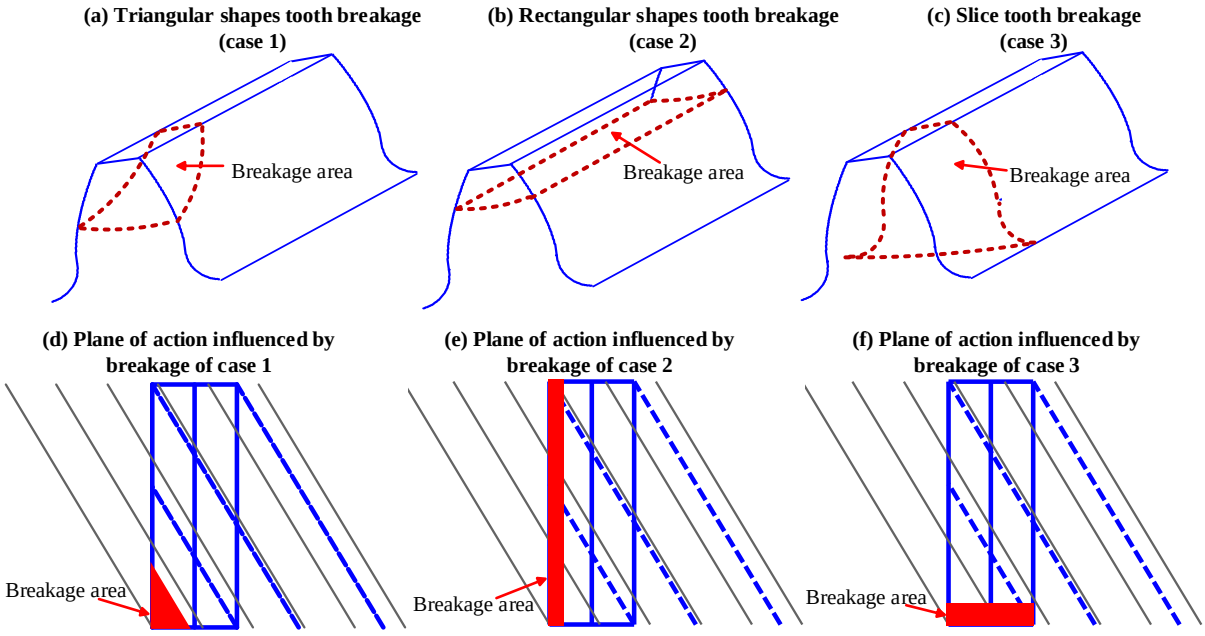

Figure 5-17 Schematic of tooth breakage modes in helical gears

The mesh stiffness pattern is reduced based on the gear failure modes, whereas the stiffness variations of the different TB-modes are illustrated in Figure5-18 to Figure 5-20. It can be seen that the distinctive pattern of the fault reduces the contact stiffness based on its shape and severity.

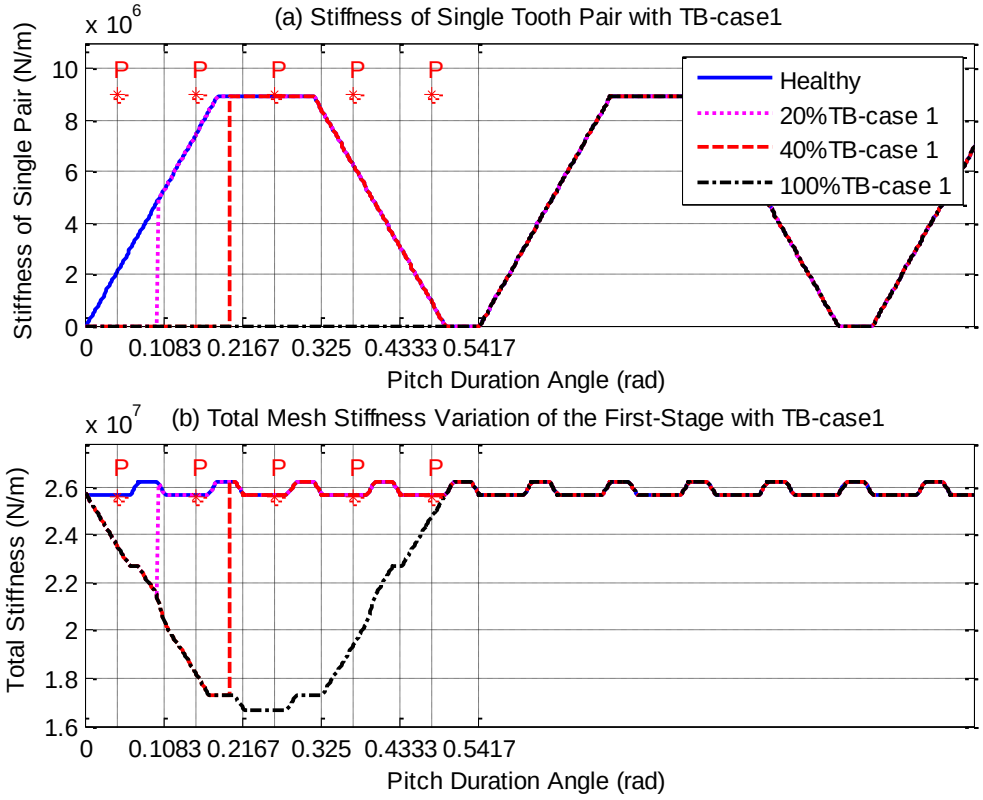

Figure 5-18 Single pair and total stiffness variations with different triangular tooth breakages

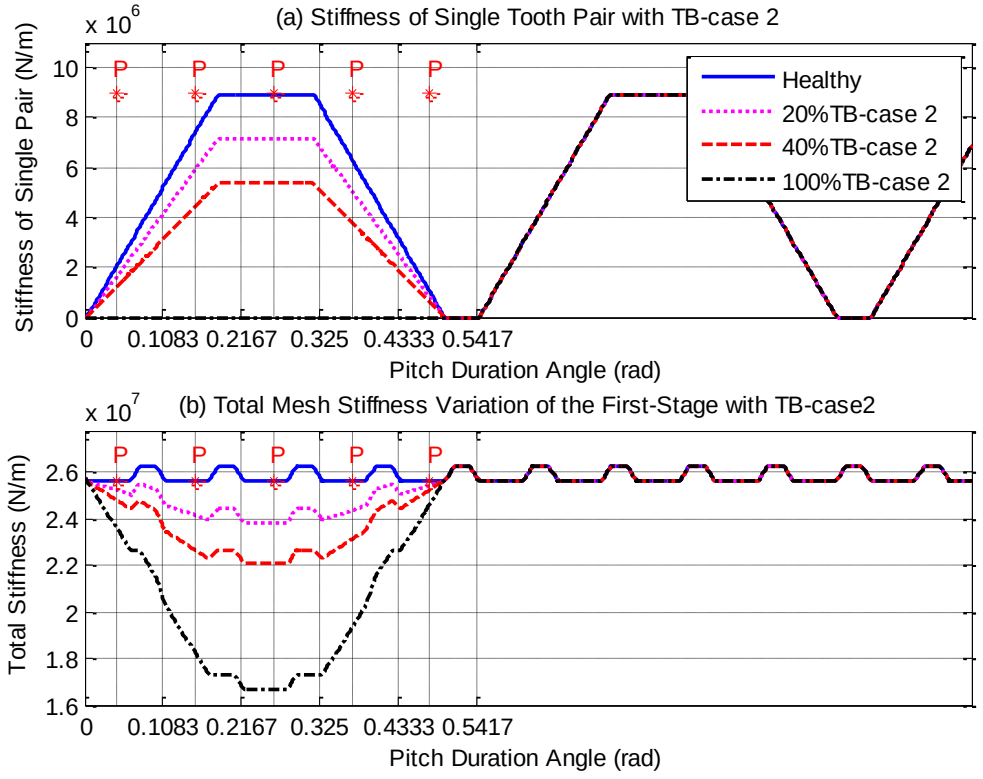

Figure 5-19 Single pair and total stiffness variations with different rectangular tooth breakages

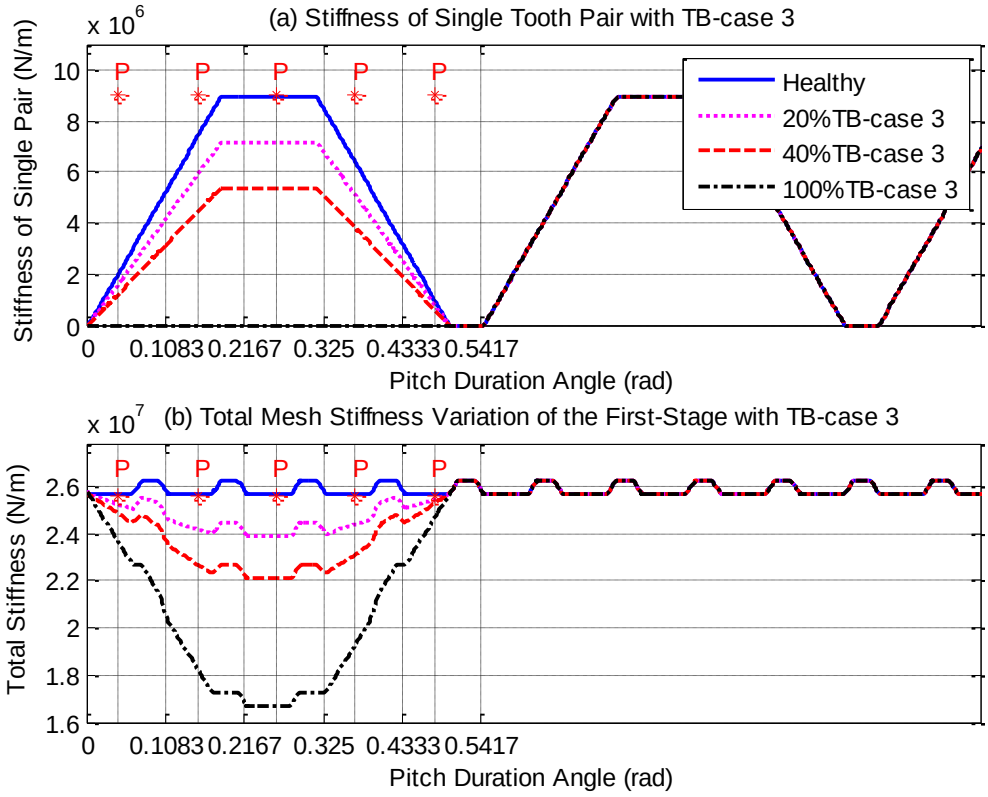

Figure 5-20 Single pair and total stiffness variations with different slice tooth breakages

5.11.2 Friction Models

The numerical model was developed with the inclusion of different time varying frictional models such as friction-free, Coulomb friction and EHL models, as depicts in Figure 5-21.

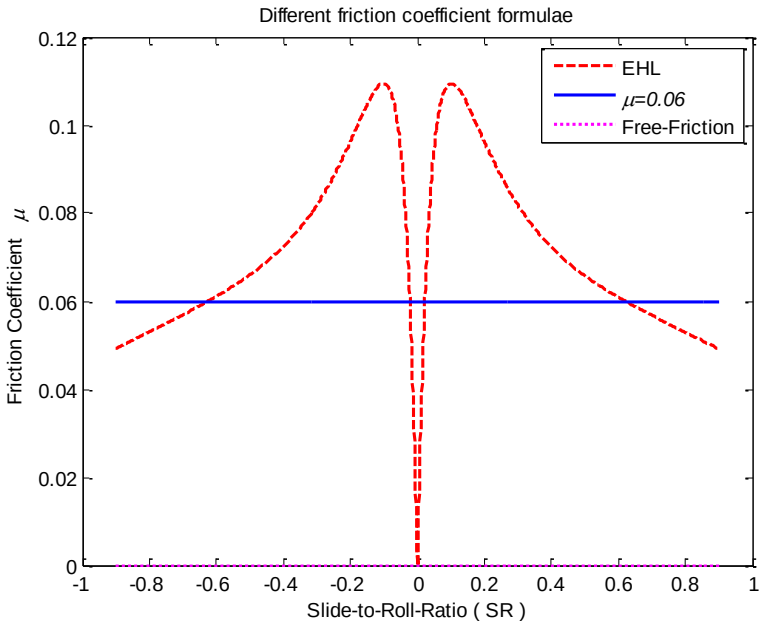

Figure 5-21 Different models of friction coefficient

For the purpose of explanation, the coefficient of friction is represented as an idealized mathematical entity. The constant friction coefficient is defined as the mean value of EHL. The gear vibration signatures due to different TB severities have been obtained to evaluate the model performance under different frictional excitations. This could increase the capability of conventional modelling of helical gear systems for providing accurate diagnostic determinations.

5.11.3 Time and Frequency Responses

Time and frequency domain analyses are commonly used to highlight the impulsive vibration of tooth breakage [56]. Figure 5-22 and Figure 5-23 show the vibration response after applying TSA to the experimental raw data and the translational raw data of the dynamic model, respectively. The influence of TB gives higher amplitudes in both experimental and numerical model signals during the rotation of the gear. Useful information can be extracted from the analysis of time domain and frequency domain, to provide an accurate diagnostics of TB.

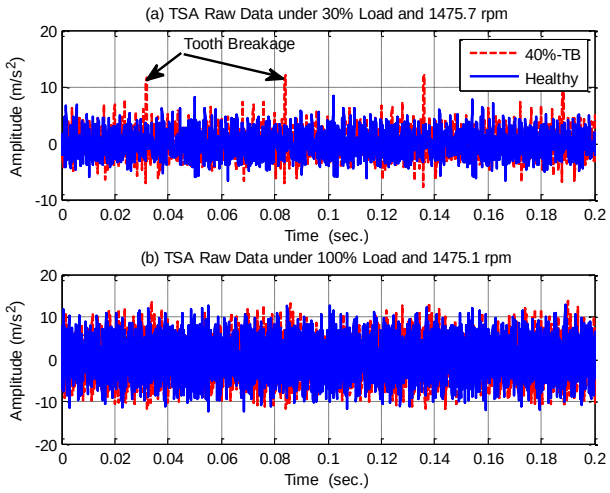

Figure 5-22 Experimental raw data (TSA) for healthy and 40%TB under full speed and different loads

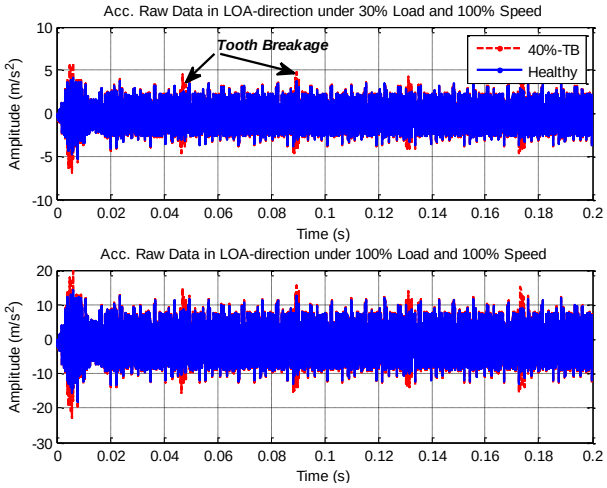

Figure 5-23 Numerical raw data for healthy and 40%TB under full speed and different loads

Significant local pulses in the time domain can be identified from the experimental and model responses, which can give an early indication to diagnose the impulsive vibration due to TB. However, spectrum analysis is the most efficient method used for the diagnostics. A general behaviour of the gearbox vibration spectra are represented in Figure 5-24 with a comparison between the model and experimental responses.

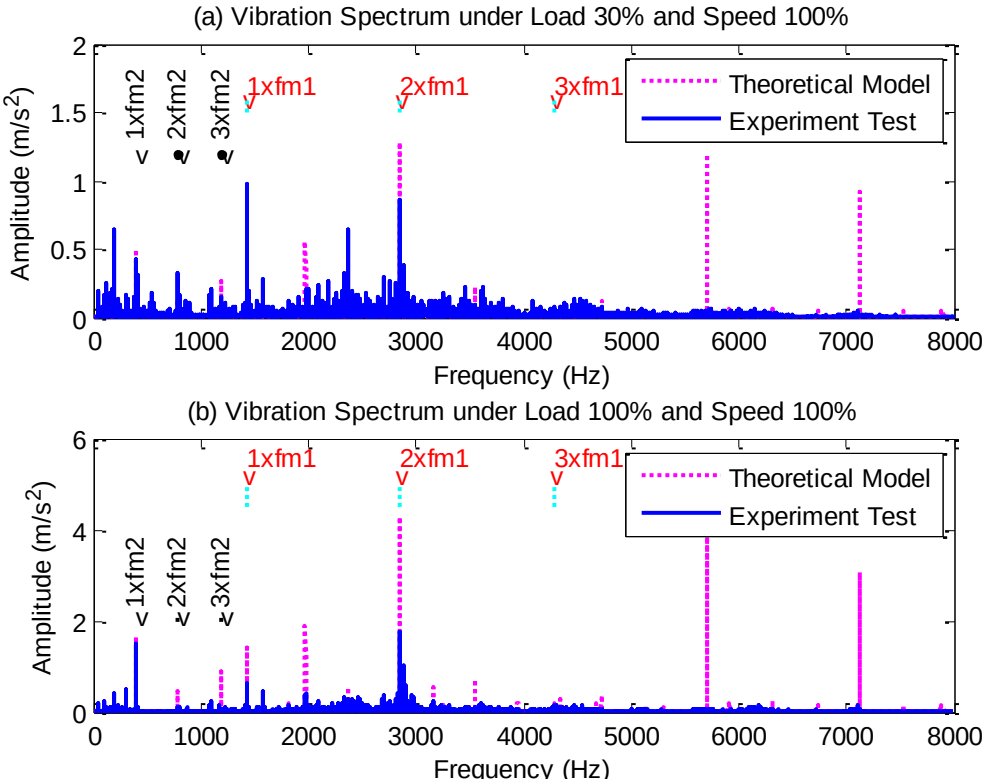

Figure 5-24 Theoretical and experimental vibration spectrum under full speed and different loads

The gear meshing frequencies and their components (up to 3rd harmonics) are also shown. The exhibition of the meshing frequency components shows a good correlation trend especially at low frequency range, in which the amplitudes at the meshing frequencies and their harmonics show a good agreement in the response behaviour. However, the difference at high frequency is possibly arisen due to the resonance effect, in which all modes must be included to develop an accurate simulation model.

Figure 5-25 shows the acceleration transverse response in the LOA-direction from the model, which is considered as the major vibration response. The effect of TB shows the richness of frequency components; of which many can be correlated with the mesh components in the form of sidebands even though there are several distinctive local spectral clusters due to system resonances.

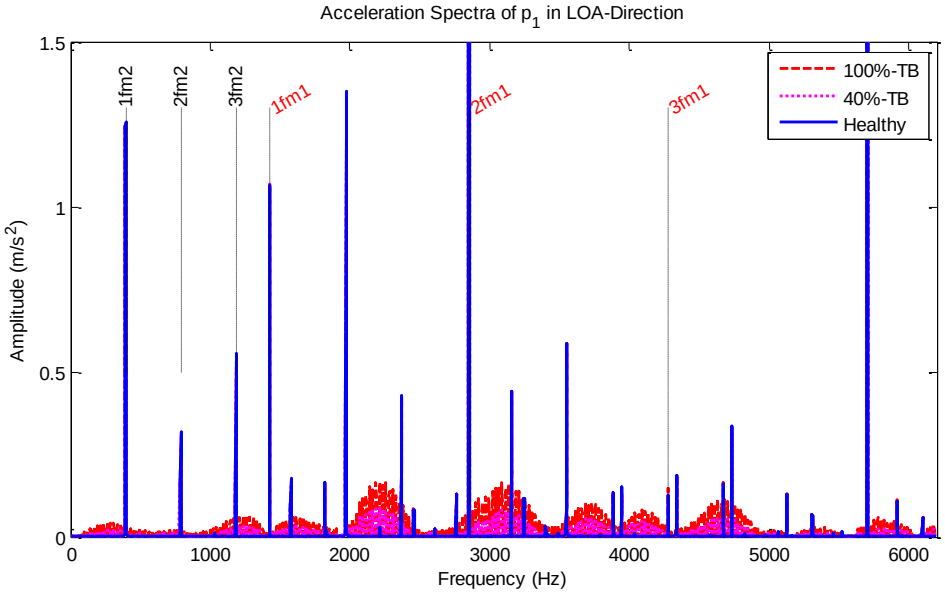

Figure 5-25 Vibration spectra of the model with different tooth breakages

5.11.4 Vibration Amplitude at Mesh Frequency Components

To diagnose gear condition, the examination of frequency spectrum characteristics is necessitated to analysis the vibration signature. The change in spectral amplitudes is usually based on to indicate the gear condition. The spectral peaks up to the three harmonics of the 1st and 2nd meshing frequency for the experimental and model signals are depicted in Figure 5-26 and Figure 5-27. It can be seen that the 1st harmonic (*1xfm1*) shows a quite decrease in the amplitudes, which could be due to lack of tooth's stiffness that is proportional to its damage, while the other harmonics are generally increased with the TB severity.

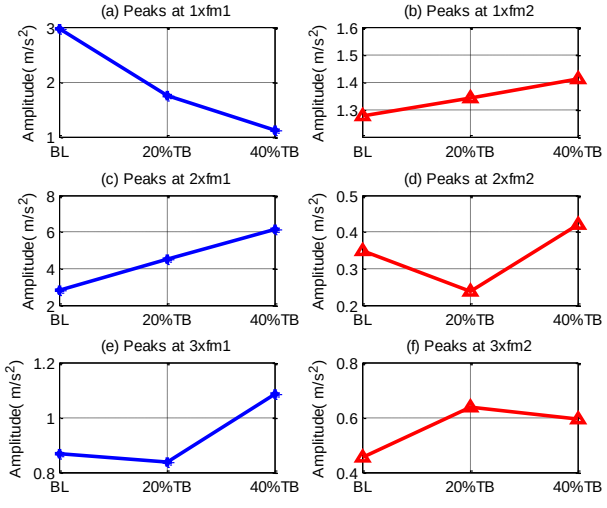

Figure 5-26 Experimental spectral peaks at the meshing frequencies

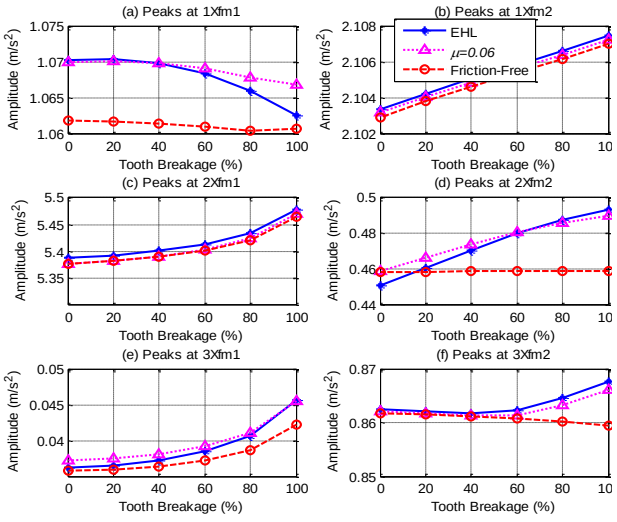

Figure 5-27 Numerical spectral peaks at the meshing frequencies

In addition, the EHL friction model shows the most consist behaviour with the experimental results. Therefore, friction should be considered effectively in the dynamic model when the spectral at meshing components are used for detection and diagnostics gear surface faults.

5.11.5 Vibration Amplitude at Sideband Frequency Components

While a local defect such as TB and cracks etc. occurred, the gear vibration responses exhibit with additional impulsive components, which results in more amplitude and phase modulations to the gear meshing components. The presence of sidebands around the gear mesh frequency and its harmonics are mainly caused by a local stiffness reduction [189], in which TB is one of the damages that reduce the tooth contact stiffness and rise richness of sideband frequency components.

The spectral peaks of the lower and upper sideband frequencies ($f_{sb}=f_m \pm f_r$) of the meshing frequency components are shown in Figure 5-28 to Figure 5-31. It can be seen that all sideband peaks of the experiment and the model are generally increased with the TB severity. However, the most influential increase can be identified with the EHL friction model. Therefore, based on the sideband changes, the TB can be diagnosed and based on the difference of change rate, and lubrication conditions could be evaluated. Thereby, to increase the capability of conventional modelling of helical gear systems, effective friction model should be implemented for providing accurate diagnostic determinations.

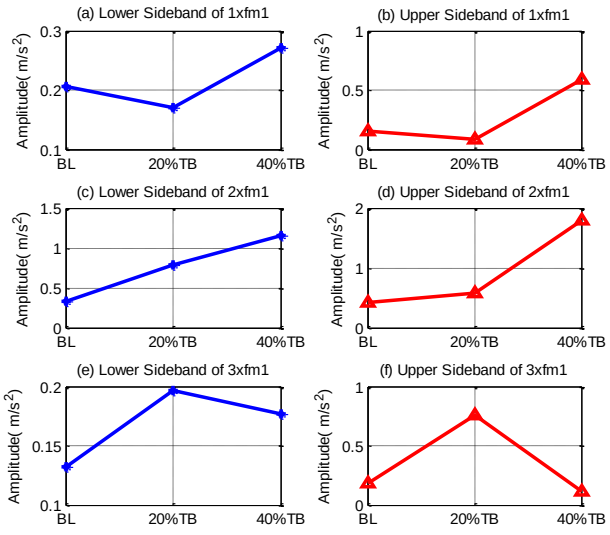

Figure 5-28 Experimental spectral peaks at the sideband of the 1st meshing frequency

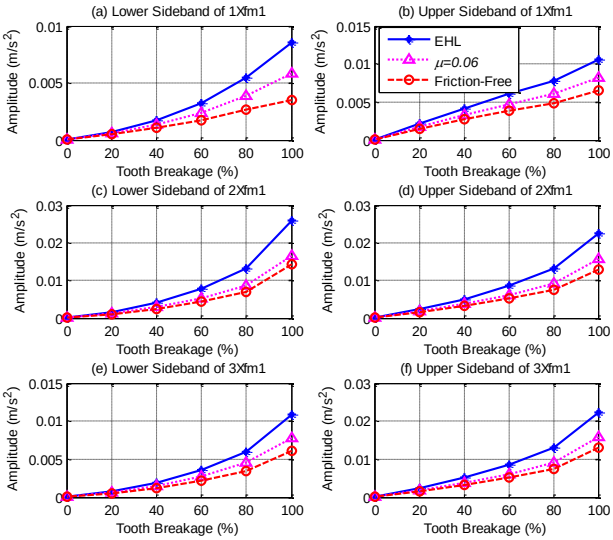

Figure 5-29 Numerical spectral peaks at the sideband of the 1st meshing frequency

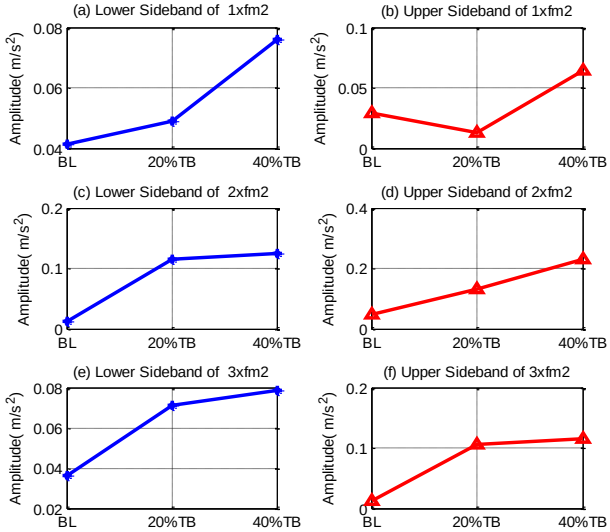

Figure 5-30 Experimental spectral peaks at the sideband of the 2nd meshing frequency

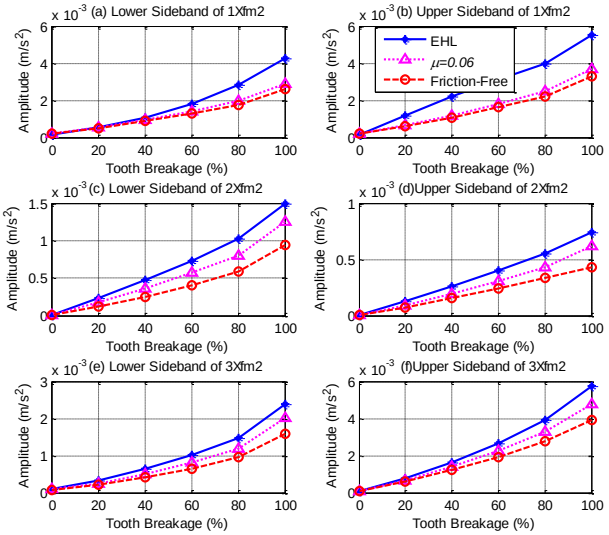

Figure 5-31 Numerical spectral peaks at the sideband of the 2nd meshing frequency

5.12 Key Findings

- Numerical models can be valuable for getting an in-depth understanding of the complex interaction between the transmission components, whereby effective methods can be developed to process the vibration signals for implementing accurate and reliable diagnostics.
- Few models have been presented for fault detection and diagnosis in helical gear systems, likely due to the increased complexity of time-varying contact lines during the meshing process.
- Numerous models have indicated that friction appears as a non-negligible excitation source, which can generate significant time-varying excitations and enhance the amplitudes of the lower and higher harmonics of the translational responses, which in turn can enhance conventional diagnostic features.
- Most of the developed models either ignore or assume constant frictional effects, which is likely to be very different from real applications where the load and hence the frictional forces vary during the meshing process.
- Helical gears produce radial, tangential and axial dynamic forces at the mesh point, so that lateral vibration, torsional vibration, and axial vibration are needed to be included in the numerical model.

- An accumulated integral potential energy method can be implemented with the changing processes of the effective contact line length, for the convenient and effective calculation of helical gear mesh stiffness.
- The mesh stiffness of helical gears is roughly proportional to the sum of the lengths of the contact lines, which can be determined based on the kinematic compatibility between the numerically generated surfaces in the plain of action.
- EHL was considered as the dominant mode of lubrication accumulated between the gear meshing surfaces, so that time-varying friction along the path of contact can be derived from EHL and tribological theory for relatively stable indicating of gear lubrication conditions.
- Linear solution is important to allow the modal parameters including resonance frequencies and damping ratios to be found conveniently, in which major resonances should be agree with the real system as close as possible to develop a stable analysis of simulating model for the purpose of vibration based monitoring.
- ODE15s Runge–Kutta algorithm is a suitable solver for solving stiff differential algebraic problems with a mass matrix and strong state dependence, whereas its solution takes a small amount of time and low fluctuations and noises are excited.
- Gear mesh stiffness pattern are generally changed to reflect the failure mode of tooth surface defects.
- Vibration at 2^{nd} and 3^{rd} harmonics are the most influence with the severity of TB, in the meantime vibration at associated sidebands are also increased significantly, which can be effective features for detecting different TB severities.
- EHL model shows the most consist behaviour with the experimental results and can significantly enhance the diagnostic features.
- Friction contributions should be considered effectively in the gear dynamic model to increase the capability of the conventional models in developing accurate diagnostic features for detecting tooth surface defects.

Chapter 6

Modelling and Experimental Validation of Gear Wear

This chapter is provided to examine the gear dynamic responses from both experimental and numerical studies when increasing extents of wear on tooth contact surfaces. A representative vibration datasets obtained from a run-to-failure gear test are used to validate the numerical models reflecting the dynamic effect of light tooth wear. Then, an explanation of the loading process to allow the gear wear fault to progress naturally is constructed properly. Finally, a correlation behaviour is acquired for the identification and validation of the model with the experimental results, and demonstrates that the surface vibrations are sufficiently sensitive to monitor the light progression of wear.

6.1 Introduction

Gears are important mechanical components for power transmissions in a wide range of industrial applications. Gear wear is one of the most common failure modes that affects the service lifetime of the gears. It is an inevitable phenomenon and this can lead to a progressive removal material from contacting tooth surfaces. Thus, monitoring the progression of gear wear is important for the timely predictive maintenances. The diagnosis of wears as early as possible can avoid catastrophic failures and improve system availability [15, 229, 230]. To date, few studies have focused on the diagnostics of tooth surface wear with the inclusion of frictional effects and most of the presented helical gear models have not been validated with the experimental work.

To increase the capability of conventional modelling of helical gear systems for providing accurate diagnostic determinations, this study examines gear dynamic responses from both experimental and numerical studies with the developing of wear degree between tooth contact surfaces. An efficient and stable analysis computation of the dynamic response of a two-stage helical gearbox influenced by tooth surface wear using an EHL frictional model, and validated by experimental test. The numerical model is developed to simulate time-varying mesh stiffness, coupled with EHL characteristics, as a basis for increasing the accuracy of gear diagnostics by examining the changes in the dynamic forces and the corresponding vibration responses under different degrees of tooth surface wear [231].

6.2 Review

Numerical models can be very valuable for gaining in-depth understanding of the complex interaction between transmission components, whereby effective methods to process vibration signals for implementing accurate and reliable diagnostics can be developed. However, few models have been presented to study helical gear systems, likely due to the increased complexity of time-varying contact lines during the meshing process.

Numerous dynamic models of gear systems were incorporated with a generalized wear formulation to predict the interactions between the dynamic behaviour and tooth surface wear [197]. A family of dynamic models of spur and helical gear systems incorporated with a wear formulation based on Archard's wear model [64, 232-238] due to its simplicity, however it requires an experimental wear coefficient which is difficult to be determined as

it depends on many aspects such as material properties, lubricants, surface quality, operating conditions [64].

In dynamic respect, the wear effect is mainly characterized by loss of tooth profile that represented by modulated mesh excitations [201, 239, 240], to investigate the effects of surface wear on system's dynamic characteristics. They indicated that tooth surface wear and gear dynamics are highly interacted, whereas tooth wear may cause unfavourable changes in the tooth surface topography and have a significant adverse effect on gear life and performance. However, limited number of contributions have been reported to include the combined influence of wear evolutions and vibrations for helical gears with respective to accuracy and easiness of implementation for condition monitoring and diagnostics for the early stages of wear. In addition, monitoring of gear wear based on vibration is not particularly well-established [241] and most of the models either ignore or assume constant frictional effects, which is likely to be very different from real applications where the load and hence the frictional forces vary during the meshing process.

Various models have been produced to evaluate the effect of sliding friction on spur and helical gear dynamic responses [242], based on the finite element method [243] and numerical modelling [77], using different values of the coefficient of friction. These have indicated that friction appears as a non-negligible excitation source, which can generate significant time-varying excitations and enhance the amplitudes of the lower and higher harmonics of the translational responses, which in turn can enhance conventional diagnostic features [244]. To date, few studies have focused on the diagnostics of tooth surface wear with the inclusion of frictional effects and most of the presented helical gear models have not been validated with the experimental work. Therefore, to increase the accuracy of helical gear diagnostics, it is necessary to develop and validate an accurate dynamic model of the gear transmission system under various possible failure conditions.

6.3 Modelling Tooth Wear in Helical Gears

Gear wear results in deviation from gear tooth profile and thickness as well as altering load distributions and contact stresses, which can accelerate the occurrence of other failure modes such as pitting and scoring [109, 110]. Stiffness reduction is commonly used in dynamic gear mesh models to represent tooth surface defects [196, 245, 246]. Tooth surface wear can cause sliding and the normal load amplitudes to vary with the position of the

contact on the tooth surfaces, in turn this can cause difficulties with the computation of load distributions for the gears [247].

Wear tends to accumulate gradually under dynamic loading and may cause progressive change in the contact regions due to the tooth profile alterations [248]. As a result, the shape of the tooth is varying continuously due to the progressive effect of wear, which influences the vibration behaviour and gear meshing parameters such as backlash, centre distance, tooth thickness, pressure angle etc. [249].

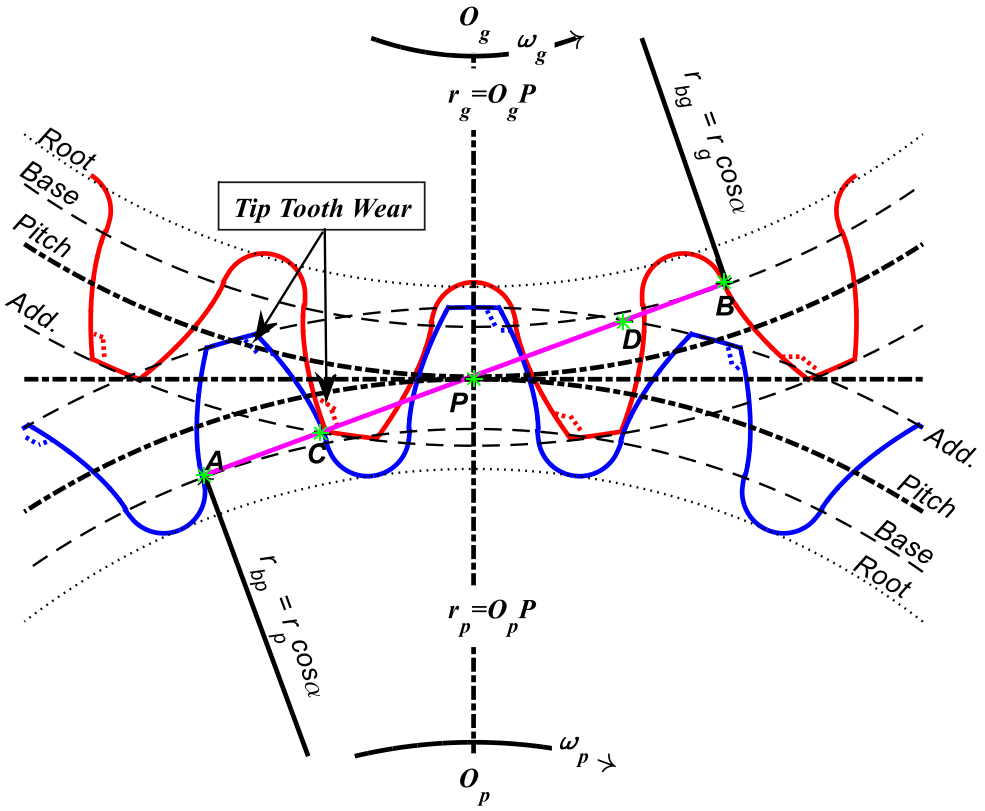

Figure 6-1 Gear meshing process of a single cross-sectional plane of helical gears with tooth wear

Figure 6-1 shows a single cross-sectional plane of a helical gear mesh with involute teeth whereby the contact points passing through the LOA moves from point C to point D. A uniform tooth surface wear is also shown, which gives an approximate explanation to the effect of wear on tooth pattern geometry. An increase in wear severity on tooth surface will enlarge the gear centre distance and the pressure angle, while the length of the LOA will be decreased [113]. This implies that gear stiffness is also varying and acts as a parametric excitation in a gear dynamic system. As a consequence of wear, higher dynamic forces along with higher frictional effects will be induced during the meshing process.

6.4 Time-Varying Contact Length for Modelling Wear

The power transmission of helical gears produces radial, tangential and axial dynamic forces on the mesh points, which excite vibrations in these directions [215, 216]. To examine these dynamic forces, a coordinate system is arranged as shown in Figure 6-2 (a), in which the x-axis is aligned with the OLOA and directed perpendicularly to the plane of action ($CD\bar{D}\bar{C}$), the y-axis is aligned to the line-of-action LOA, which is perpendicular to both the shaft axis and x-axis, and finally the z-axis is aligned (axial) along the centreline of the shafts.

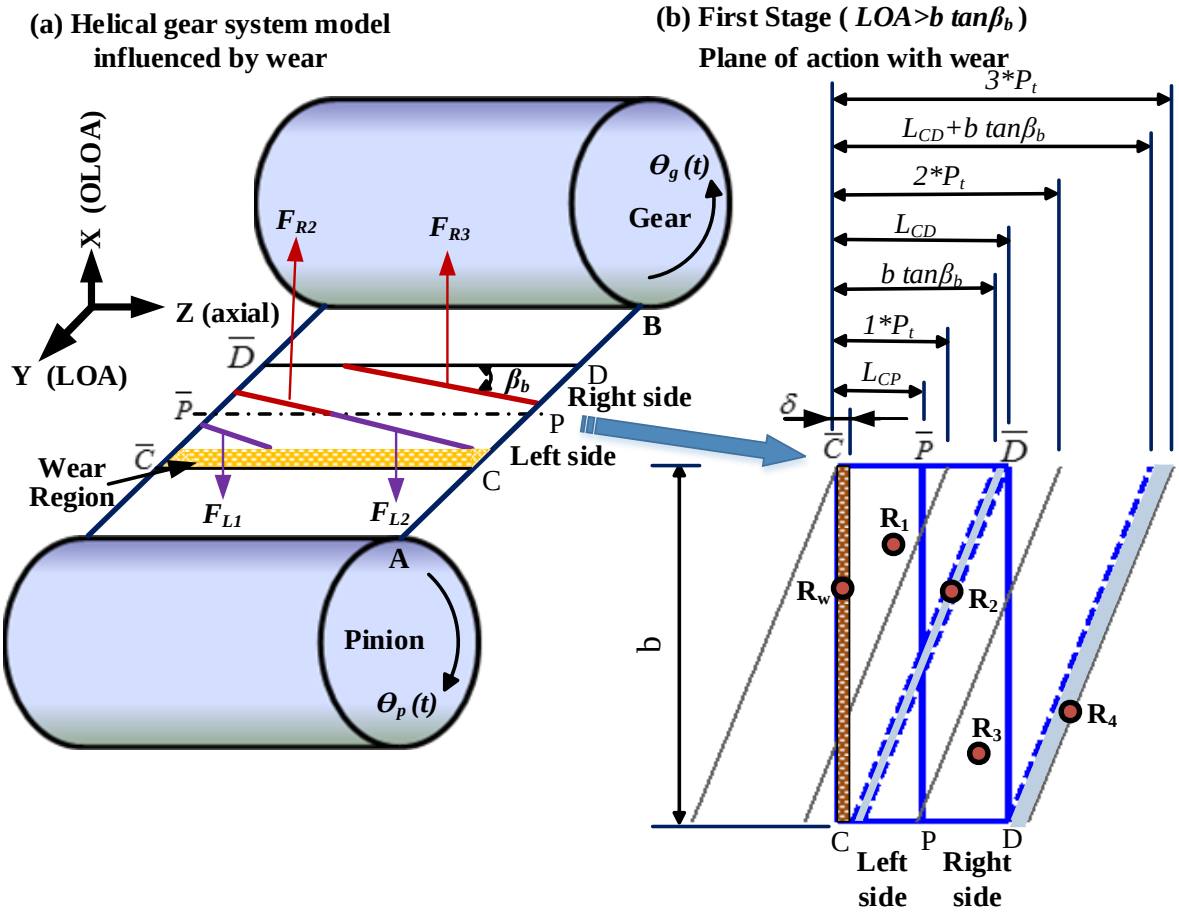

Figure 6-2 Equivalent plane of action of a helical gear system influenced by uniform wear

For healthy gears, the mesh cycle of three contacting pairs starts from point C and moves diagonally as the gears roll across the contact zone until point $\bar{D}$. However, uniform tooth wear will shift the starting point C and shorten the plane of action in proportion to the wear severity δ. This will affect the gear meshing stiffness, the contact surface friction and hence the gear vibration. The equivalent frictional forces of each segment of the contact lines are

also shown in Figure 6-2 (a). These forces influence the contact plane in two directions, on either side of the inclined pitch line ($P\bar{P}$).

Moreover, the length of L_{CD} will be reduced by wear severity by an amount δ, which shortens the left side length (as defined in Figure 6-2(a)) of the plane of action by an amount R_w, which is equal to the removal of material due to wear. The percentage of tooth wear was simulated as a ratio of the wear width δ to the length of the LOA (L_{CD}):

$$r_\delta = \frac{\delta}{L_{CD}} \tag{6.1}$$

The contact line is a function of gear geometric parameters and also depends on tooth face width and the length of LOA, as explained in [76, 210, 211, 225]. For the case of $b\tan\beta_b > L_{CD}$ (first stage), the time-varying contact length of each pair of meshing teeth can be calculated by taking into account the effect of tooth wear δ through a reduction of contact line in different mesh phases.

$$L_i(t) = \begin{cases} 0 & 0 \le DL_i(t) < \delta \\ (DL_i(t) - \delta)\csc\beta_b & \delta \le DL_i(t) < b\tan\beta_b + \delta \\ b\tan\beta_b \csc\beta_b & b\tan\beta_b + \delta \le DL_i(t) < L_{CD} \\ (L_{CD} + b\tan\beta_b - DL_i(t))\csc\beta_b & L_{CD} \le DL_i(t) < L_{CD} + b\tan\beta_b \\ 0 & L_{CD} + b\tan\beta_b \le DL_i(t) < n * P_t \end{cases} \tag{6.2}$$

where the variables are defined in Sec. 5.5.

6.5 Effect of Wear on Time Varying Mesh Stiffness

To investigate the effects of surface wear on system's dynamic characteristics, the wear effect is modelled by the loss of tooth profile as that of [201, 239, 240], which is much easier to be implemented. Moreover, the material loss on the tooth surface is more uniformly in the early or mild wear phases. The uniform tooth wear adopted for the helical gears is considered to be more realistic for early operations as the gear operating conditions are under a relatively wide range in which the stress distribution spread more widely across tooth surfaces and hence uniform material removes, provided that gear meshes under adequate lubrication, high quality surface finishing and high quality of surface contact [199, 232, 234, 236].

In addition, tooth wear also reduces slightly the thickness of the tooth and increases the roughness of the surfaces, which can all induce a reduction in stiffness. Based on the

fluctuations of the contact line, the gear mesh stiffness is changed accordingly. The summation of the lengths of the contact lines can be used as an alternative method to identify the varying mesh stiffness of helical gears [76, 210, 211, 225, 227], which is otherwise difficult to obtain due to the complexity of the contact geometry.

The gear mesh stiffness is influenced by worn tooth surfaces, as reflected in the reduction in tooth stiffness. Due to this decrease, the gear mesh stiffness is itself decreased and it is also shifted angularly. The extent of subsequent tooth deflection depends upon the extent of tooth wear as shown in Figure 6-3(a). As a consequence of mesh stiffness changes, a higher contact force will be produced for the same torque delivered at any given mesh position as shown in Figure 6-3(b).

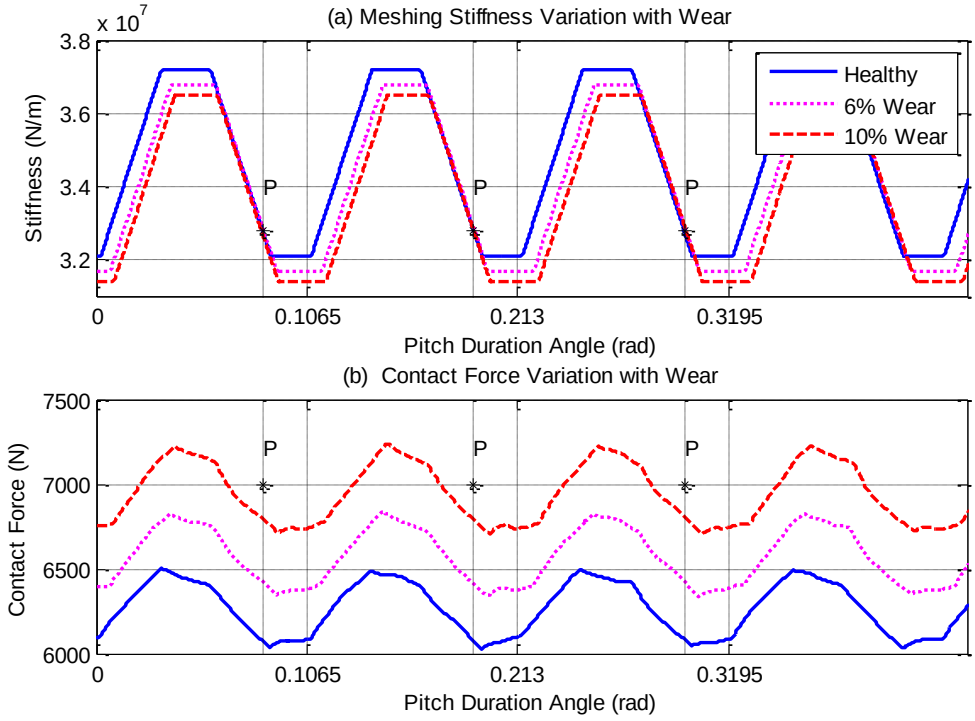

Figure 6-3 Time-varying mesh stiffness variations with different wear severities

6.6 Frictional Excitation

As the EHL friction model was considered to be the dominant mode of lubrication associated with the gear meshing surfaces, a theoretical friction coefficient representation has been used in this study based on the derived formula in [83]. Figure 6-4(a) demonstrates the variation of friction coefficient based on an EHL model along the tooth profile of each contacting pair during the meshing process. It can be seen to fluctuate periodically with the roll angle and it is zero at its pitch point and in the no-contact region R_4. Tooth surface

wear causes increases in tooth surface roughness and hence an increase in friction between meshing teeth. For this reason, the EHL friction coefficient increases with increasing wear as illustrated in Figure 6-4 (b).

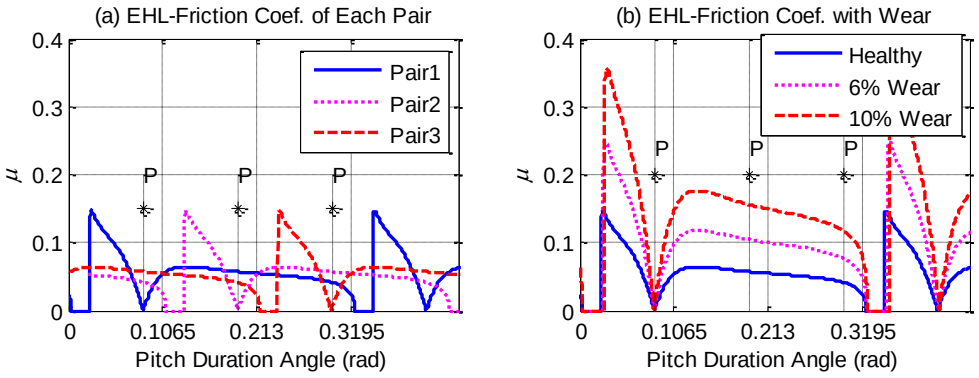

Figure 6-4 EHL friction coefficient of the first stage with wear

6.7 Validation Tests

To validate the model, a number of vibration datasets were obtained from a run-to-failure gear test. The test was based on a representative two-stage helical gearbox test system as depicted in Figure 6-5. The system consists of two industrial gearboxes installed back-to-back in series. The first gearbox (GB1) is driven by an AC drive motor, and acts as a speed reducer, whilst the second gearbox (GB2) is a speed increaser connected to a DC loading motor, in which the gear ratios of the two gearboxes are 5.094 and 3.678 respectively.

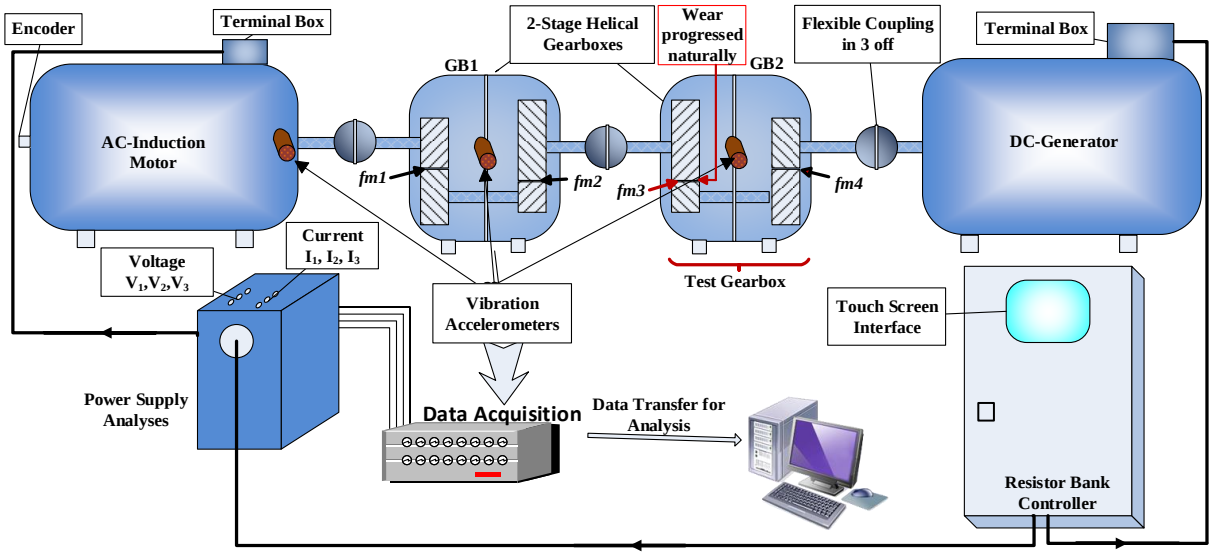

Figure 6-5 A schematic diagram of the test rig system (*fm1* and *fm2* are the mesh frequencies of each stage in GB1; *fm3* and *fm4* are the mesh frequencies of each stage in the test gearbox GB2)

A closed loop control system was used for setting up the required operating conditions of the test rig via a touch screen interface, which enabled the control of overall test duration, speed, load and number of operating cycles within a load setting. The test rig was driven by 15 kW AC motor at 1460 rpm while a DC motor/generator used to apply different loads.

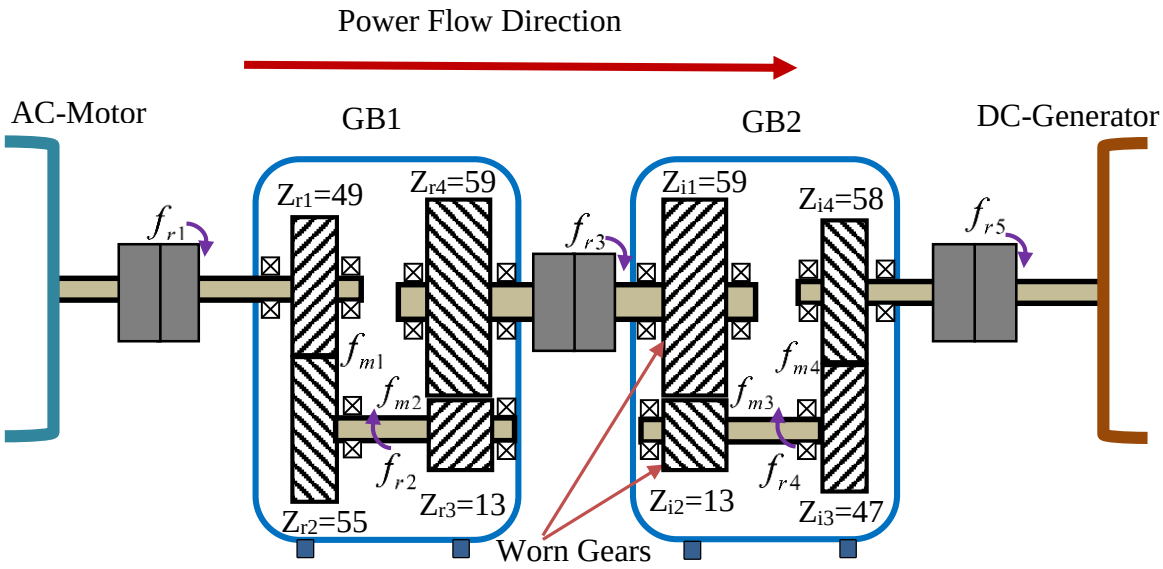

Figure 6-6 Schematic diagram of the two gearboxes

Figure 6-6 illustrates a geometric representation of the two gearboxes transmission system, whereas the fundamental frequencies of the gearbox transmission system are slightly different from that explained in Sec. 4.4.1. The simultaneous shaft rotational frequencies via the two gearboxes can be determined as follows:

$$
\begin{aligned}
f_{r1} &= \frac{Motor\ Speed}{60} = \frac{1060\,rpm}{60} \approx 17.67\,Hz \\
f_{r2} &= \left(\frac{Z_{r1}}{Z_{r2}}\right) f_{r1} = \left(\frac{49}{55}\right) \times 17.6 = 15.12\,Hz \\
f_{r3} &= \left(\frac{Z_{r1}}{Z_{r2}}\right)\left(\frac{Z_{r3}}{Z_{r4}}\right) f_{r1} = \left(\frac{49}{55}\right)\left(\frac{13}{59}\right) \times 17.67 = 3.47\,Hz \\
f_{r4} &= f_{r3}\left(\frac{Z_{i1}}{Z_{i2}}\right) = 3.47 \times \frac{59}{13} = 15.75\,Hz \\
f_{r5} &= f_{r4}\left(\frac{Z_{i3}}{Z_{i4}}\right) = 15.75 \times \frac{47}{58} = 12.75\,Hz
\end{aligned}
\tag{6.3}
$$

Moreover, the meshing frequencies of each stage are:

$$
\begin{aligned}
f_{m1} &= f_{r1}Z_{r1} = 17.67 \times 49 = 865.68Hz \\
f_{m2} &= f_{r2}Z_{r3} = 15.7 \times 13 = 204.61Hz \\
f_{m3} &= f_{r3}Z_{i1} = 3.47 \times 59 = 204.61Hz \\
f_{m4} &= f_{r4}Z_{i3} = 15.75 \times 47 = 739.75Hz
\end{aligned}
\tag{6.4}
$$

The main challenge of the test is to identify fatigue signatures at an early stage, in which run to failure test scenario was performed on this specially designed test rig under natural progression of damage condition. To simulate variable load operating scenarios experienced by wind turbine and helicopter gearboxes [250, 251], different operating loads and speeds were applied to the system, whereby the test rig operated for more than 800 hours under two different loading regimes: sinusoidal variable load which fluctuates at a frequency of 0.077 Hz, from 0 up to 12.5 kW with 1038 rpm speed (70% of rated speed) followed by an increasing 25% stepped load at 70% and 50% rated speed, the total test time being 60 minutes, as illustrated in Figure 6-7.

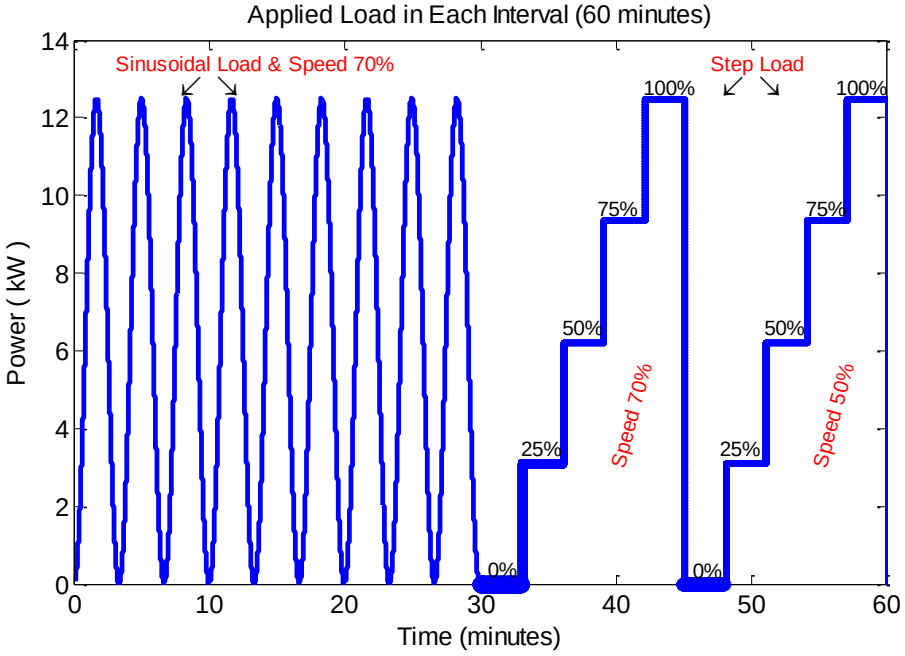

Figure 6-7 Sinusoidal and stepped load regimes of the experiment test

During the test, the online monitoring system was recorded the change in the first three mesh harmonics and associated sidebands for each stage, obtained from the amplitude spectrum of the time synchronous averaged (TSA) vibration signals. The test was terminated when vibration sideband features exhibited a significant increase (higher than twice their baselines), showing an existence of a considerable fault in the test gearboxes.

After the test was terminated, significant surface scuffing due to wear effects that progressed naturally in the first stage of the second gearbox, as illustrated in Figure 4-15. It can be seen that both the pinion and gear tooth surfaces worn by almost the same size severity, showing the gears are considerably faulty. The worn regimes are in the late stage of tooth surface wear, whereas the photos have been taken at the end of the test that show the surface wear is not uniform anymore.

As the worn regimes (shown in Figure 4-15) indicate the late stage of tooth surface wear, the uniform tooth wear adopted for the helical gears is considered to be more realistic for early operations as the test operating conditions change in a wide range, see Figure 6-7. In general, surface wear and mild wear are more realistic for very early stages of wear that commonly happen due to metallurgical defects in gear material, improper heat treatment, improper surface finish and manufacturing error. To diagnose the tooth surface wear in its early stages, a uniform wear model was simulated in the dynamic model, whereas the small amount of wear and uniform material removes can be demonstrated and assessed effectively for the condition monitoring scheme.

6.8 Model Validation and Discussion

Different degrees of wear (from 0% to 10% of the tooth thickness, see Figure 6-2) were simulated in the model in steps of 2% to obtain features for wear fault diagnosis at an early stage in its development. The dynamic responses of the model were obtained in terms of the displacement, velocity and acceleration of the gear system under healthy and faulty conditions. Seven data sets (each of duration 1hour) were selected from across the final five hundred operating hours, as illustrated in Figure 6-8.

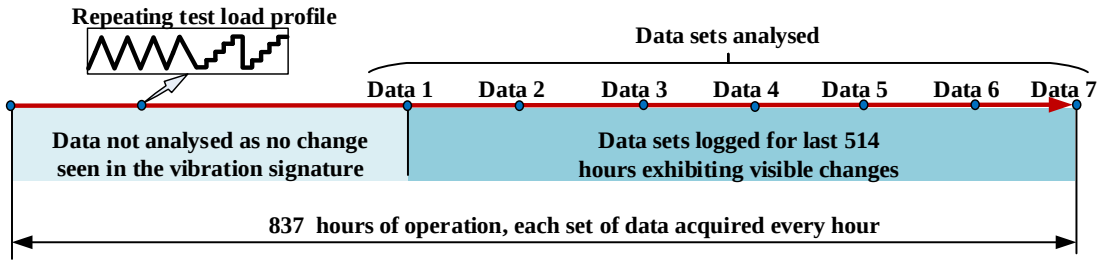

Figure 6-8 A schematic diagram of the experimental scenario illustrates the selected tests

6.9 Signals in the Time and Frequency Domains

The tooth surface wear was found to affect the dynamic signals of the gearbox, resulting in higher vibration and noise. Time-domain analysis can be used as an effective indicator of the impulsive vibration of gear faults [56], but the spectrum is also commonly used for monitoring machine vibration characteristics. So, the numerical solutions were converted into accelerations by differentiating the velocity responses, which themselves had been derived from time data using the FFT.

In addition, to implement an effective means of detecting wear, TSA was applied to the experimental test data, which can suppress the influences of noise that asynchronous to those features of interest [126]. Figure 6-9(a) shows the time domain vibration responses after applying TSA to the experimental raw data, whereas Figure 6-9(b) demonstrates the translational responses in the LOA direction acquired from the model when influenced by different wear severities. It can be seen that, depending on the extent of wear, higher impulsive vibration responses and higher amplitudes feature in both the experimental and model predicted signals of the gear meshing process.

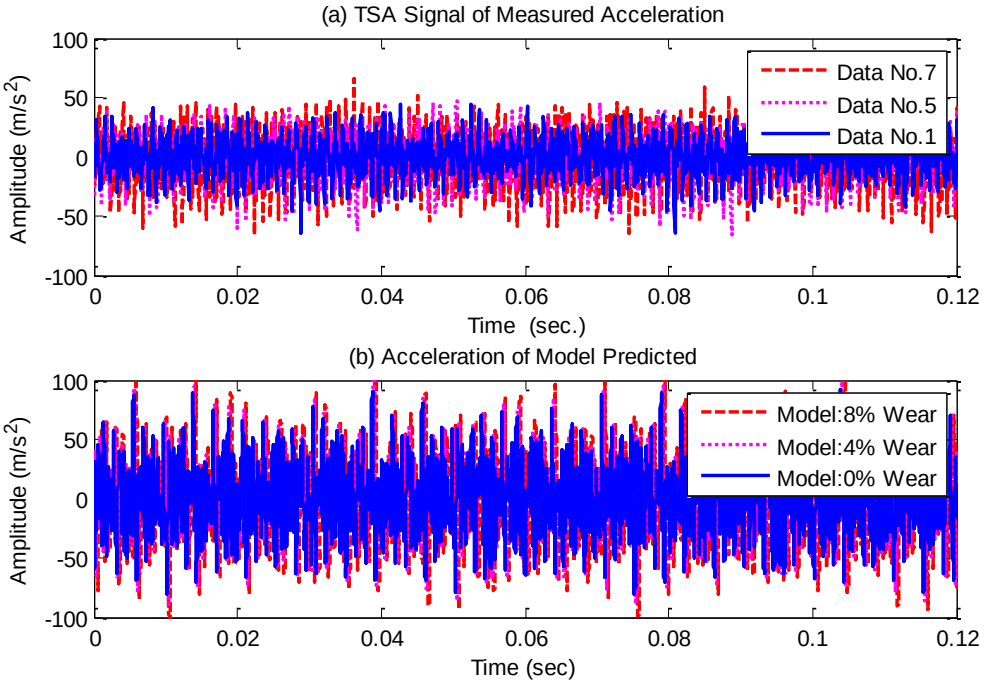

Figure 6-9 Experimental and numerical raw data of the gearbox under different wear severities

However, limited excitations can be identified in the numerical data with increasing the wear degree because the model was developed to focus on the effect of the tooth surface wear at its early stage. It does not take into account other potential excitations such as

backlash, eccentricity, unbalance, run-out errors that can become severer as with the progression of wear and induce more vibrations. Those effect of gear imperfection with gear determinations still remains opening although many studies have been carried out.

Spectrum analysis is commonly used for monitoring and interpreting the information contained in machine vibration characteristics, and the general behaviour of the vibration spectrum is illustrated in Figure 6-10. for the experimental and numerical data. To enhance the vibration signal features, TSA was used to extract a deterministic signal for vibration components related to the rotational frequency of the target gear, and to reduce non-synchronous components and noise. The gear meshing frequencies and their components (up to 3rd harmonics) are shown. It can be seen that the meshing frequencies and their harmonics exhibit the similar trends between the experimental and model-predicted data, underlining that, the model response is simulated effectively.

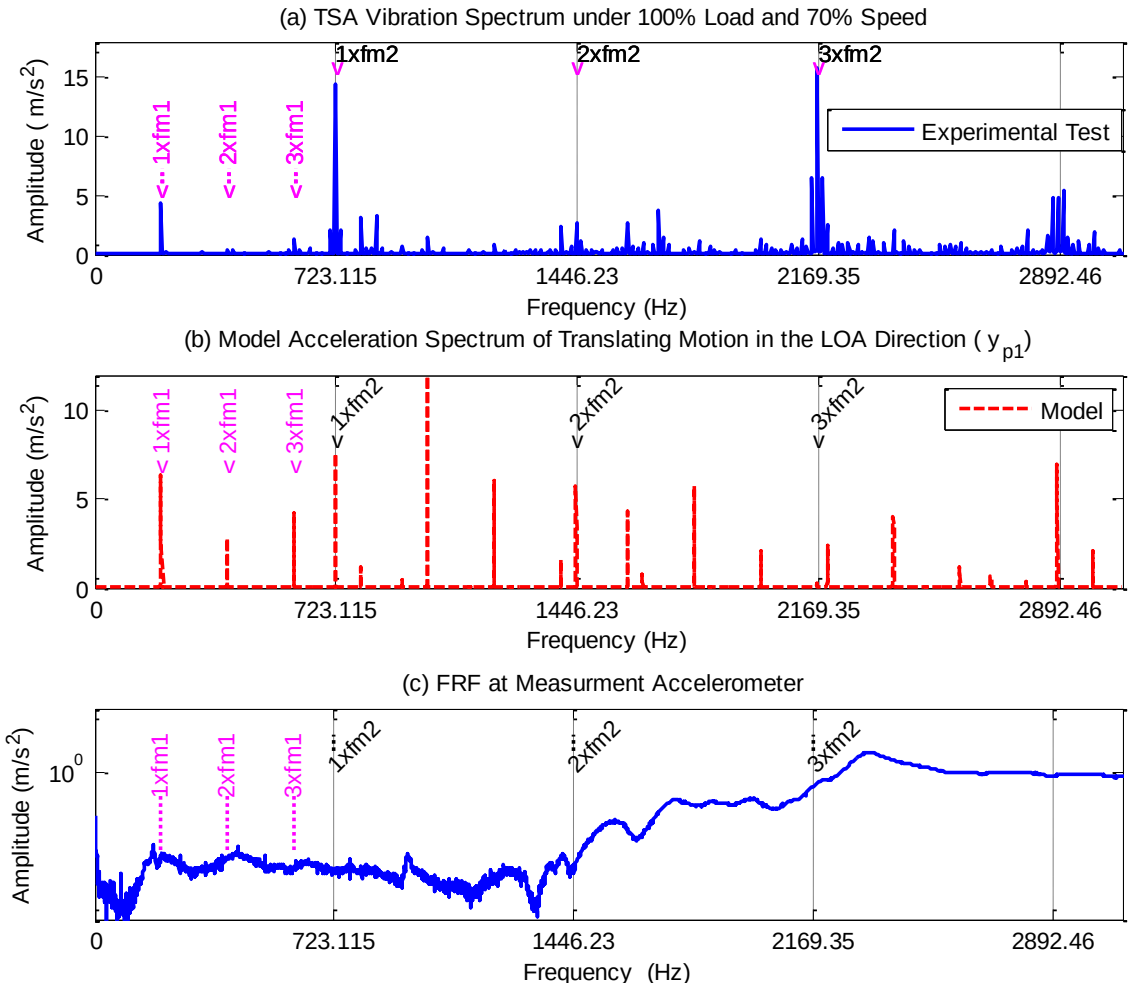

Figure 6-10 Experimental and numerical vibration spectra with FRF signal of the test gearbox (components at 70% speed)

The amplitudes at the meshing harmonics are not predicted as closely as would have been liked, possibly because of signal attenuation and noise in the experimental data and resonance effects in the vibration transmission paths. Especially, the transmission path alters more to the amplitudes at the high frequency range. As shown Figure 6-10(c), the frequency response function (FRF), see **Appendix A**, exhibit higher magnitudes around 2,200Hz due to housing resonances. This makes the spectral peaks at and around $3\times f_{m2}$ particularly higher, as shown in Figure 6-10(a). The FRF was measured using impact hammer testing to conclude the modes and natural frequencies of the gearbox components, in which all modes must be included to develop an accurate simulation model. In addition, it would have been possible to include the gear housing flexibility, backlash and all potential excitation errors in the numerical model for more enhancing the correlation with the experimental results.

6.9.1 Vibration at Meshing Frequencies

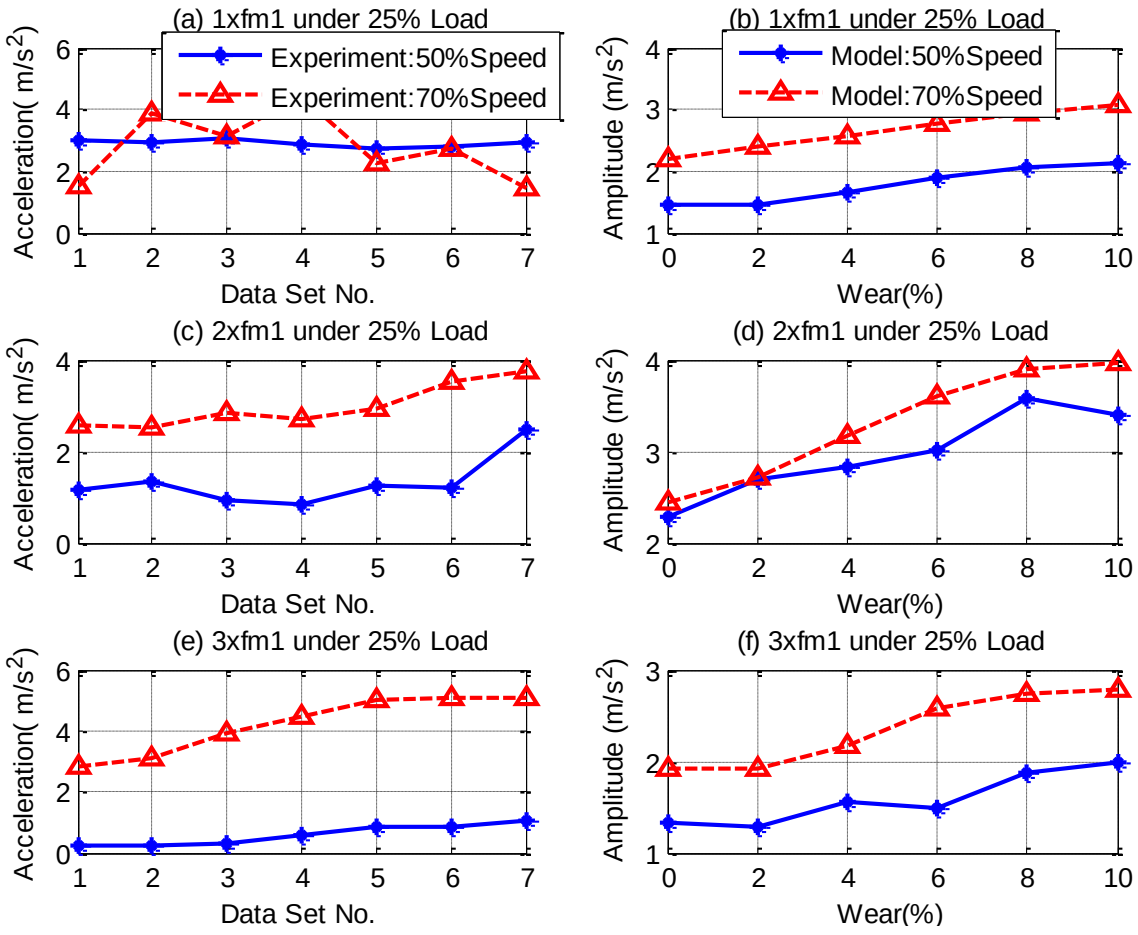

Fig.6-11. Spectral amplitudes of the first stage meshing components of the test gearbox under 25% load

To diagnose gear condition, the spectral peaks up to the third tooth mesh harmonics of the 1st and 2nd stage meshing frequencies for the experimental results and the combined translational responses of the numerical model are represented in Figure 6-11 and Figure 6-12. It can be seen that the 2nd and 3rd harmonics of the mesh component ($f_{m1}=f_{r1}\times Z_{p1}$) associated with the first stage show a clear and consistent increase in spectral amplitude with developing of wear severity, under different operating load conditions, and for both the experimental and EHL model results. The selected experimental data sets show that the amplitudes at the 2nd and 3rd harmonics of the meshing frequency increase by more than 50%.

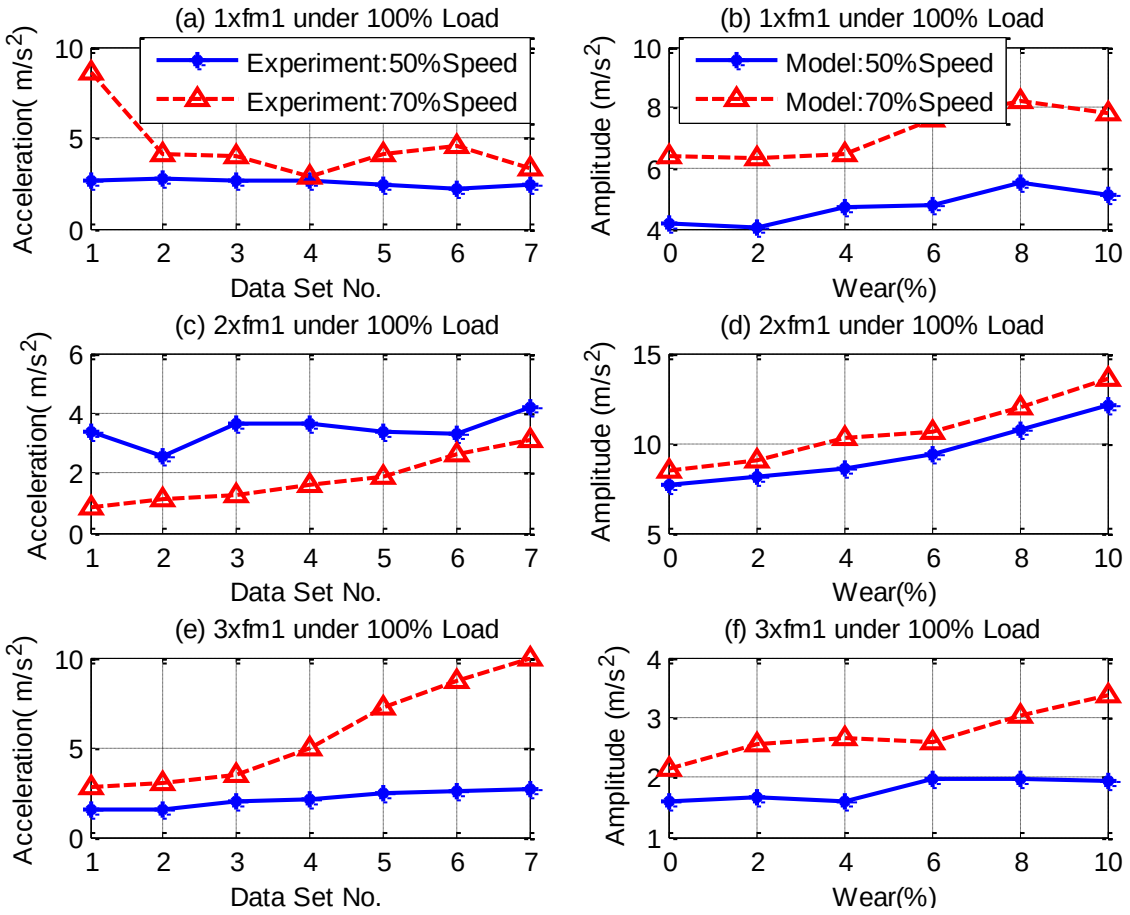

Figure 6-12 Spectral amplitudes at the first stage meshing components of the test gearbox under 100% load

The 2nd harmonic peaks show that under 100% load, the vibration level at 70% speed is lower than that at 50% speed, see Figure 6-12 (c), this can be possibly because of the nonlinearity effect of the contact process. In which the high load can change the hertz

contact deformation and the contact stiffness that implemented between the meshing teeth, and also due to the resonance that result induced within a particular frequency range.

Similarly, the predicted spectral peaks of the 2nd and 3rd harmonic components from the EHL model also clearly increase, but not generally by as much as 50% at 10% wear, which suggests that more tooth surface wear was happened between the gears. This could be due to the reversed friction force at the pitch point and/or to the fluctuating nature of the meshing process between two and three contact pairs.

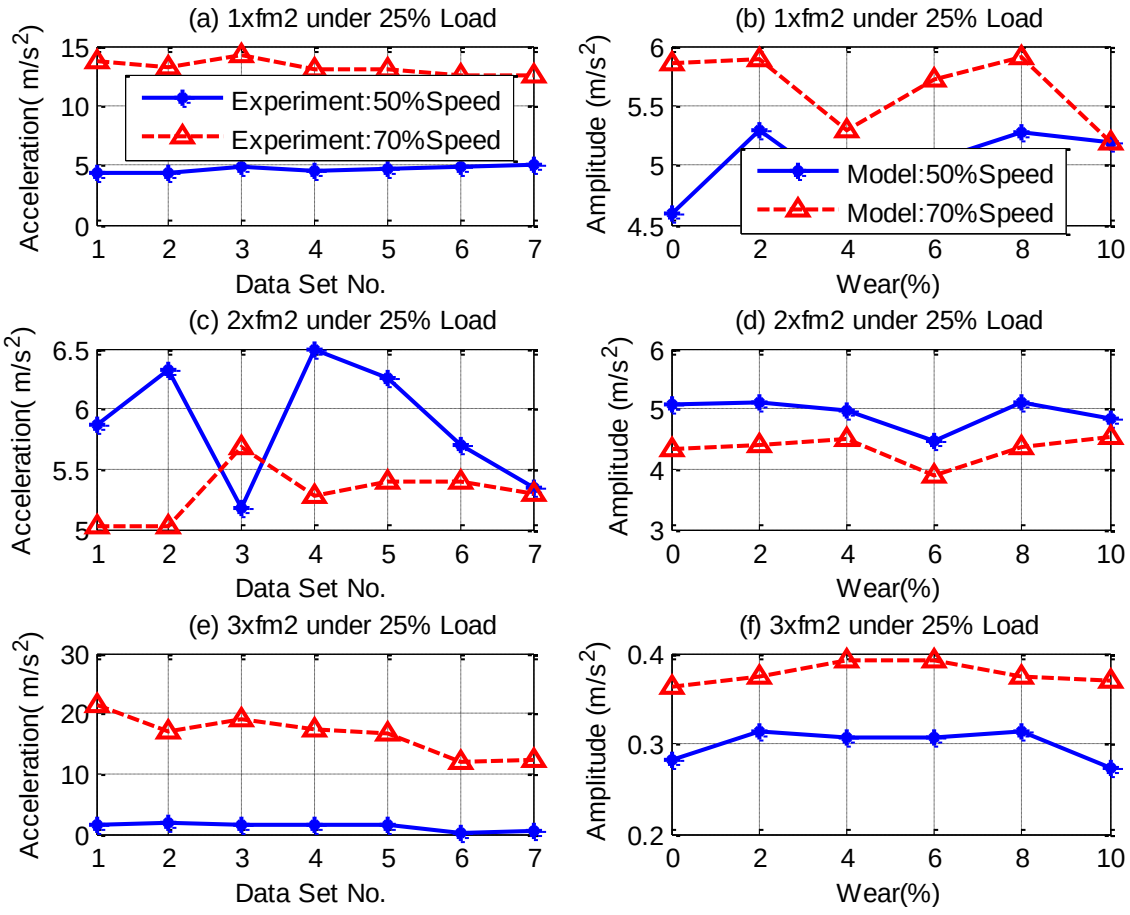

Figure 6-13 Spectral amplitudes of the second stage (healthy) meshing components of the test gearbox under 25% load

Evidently, these features can be considered as an effective indicator to diagnose wear severity between meshing gears. Hence, to identify tooth surface faults, the higher harmonics of the meshing frequency should be examined. By means of contrast, the amplitude of the vibration for the second stage meshing frequency components are illustrated in Figure 6-13 and Figure 6-14, for these un-worn gears there is no evident trend in either the experimental or model-predicted results.

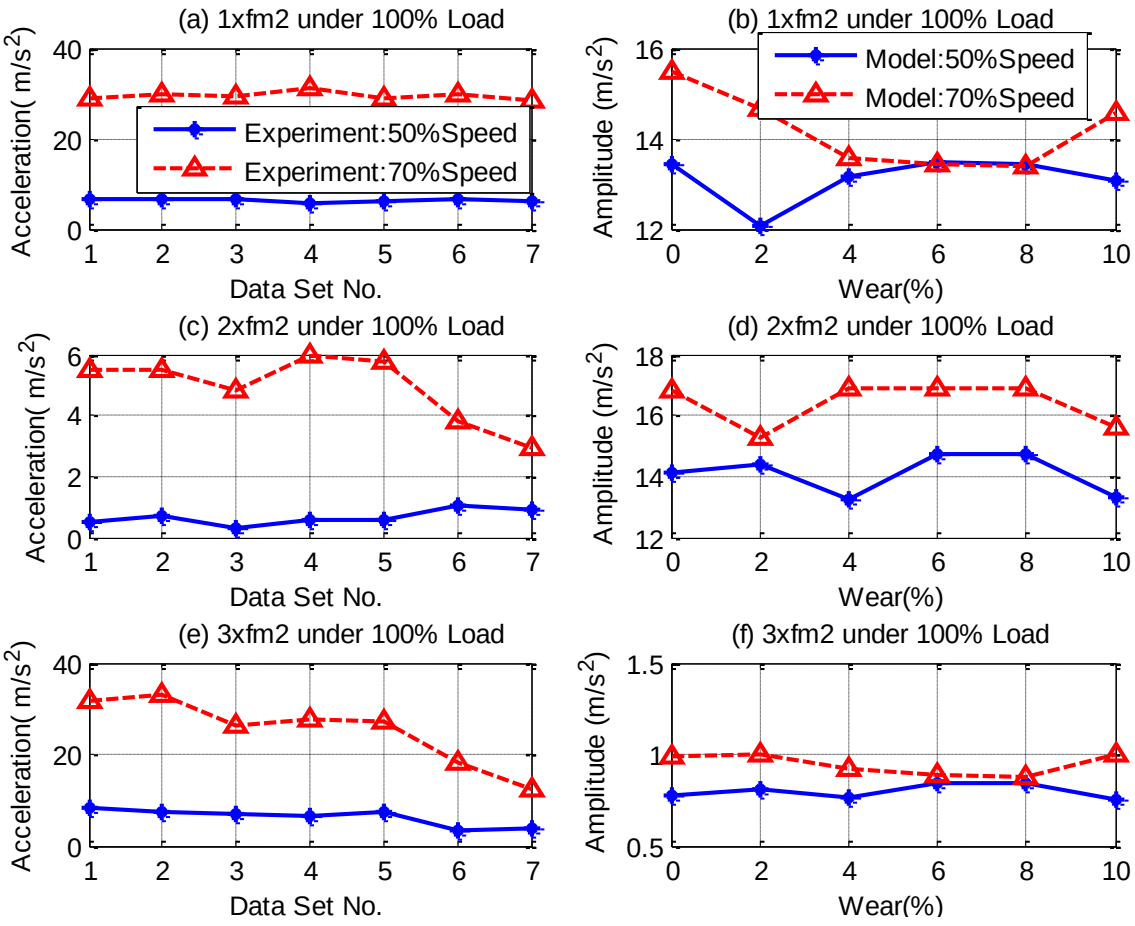

Figure 6-14 Spectral amplitudes of the second stage (healthy) meshing components of the test gearbox under 100% load

6.9.2 Vibration at Sideband Frequency

The difference in the vibration responses between healthy and faulty gears also causes changes in the sideband presence around the fundamental and harmonics of the gearbox meshing frequencies. The dynamic response computed with the analytical stiffness shows that the presence of sidebands arises from the amplitude modulation caused by the fall in stiffness [189].

The spectral amplitudes of the lower and upper sidebands ($f_{sb} \pm f_r$) around the first three harmonics of the first stage meshing frequency are shown in Figure 6-15 and Figure 6-16. It can be seen that the sideband peaks generally increase with wear for both experiment and model responses, with the most significant increase demonstrated by the higher sideband components. This is likely due to the non-linearity of the wear and friction between the tooth contact surfaces. The maximum difference increase between the selected experiment tests at the sideband components is about 100% for all harmonics.

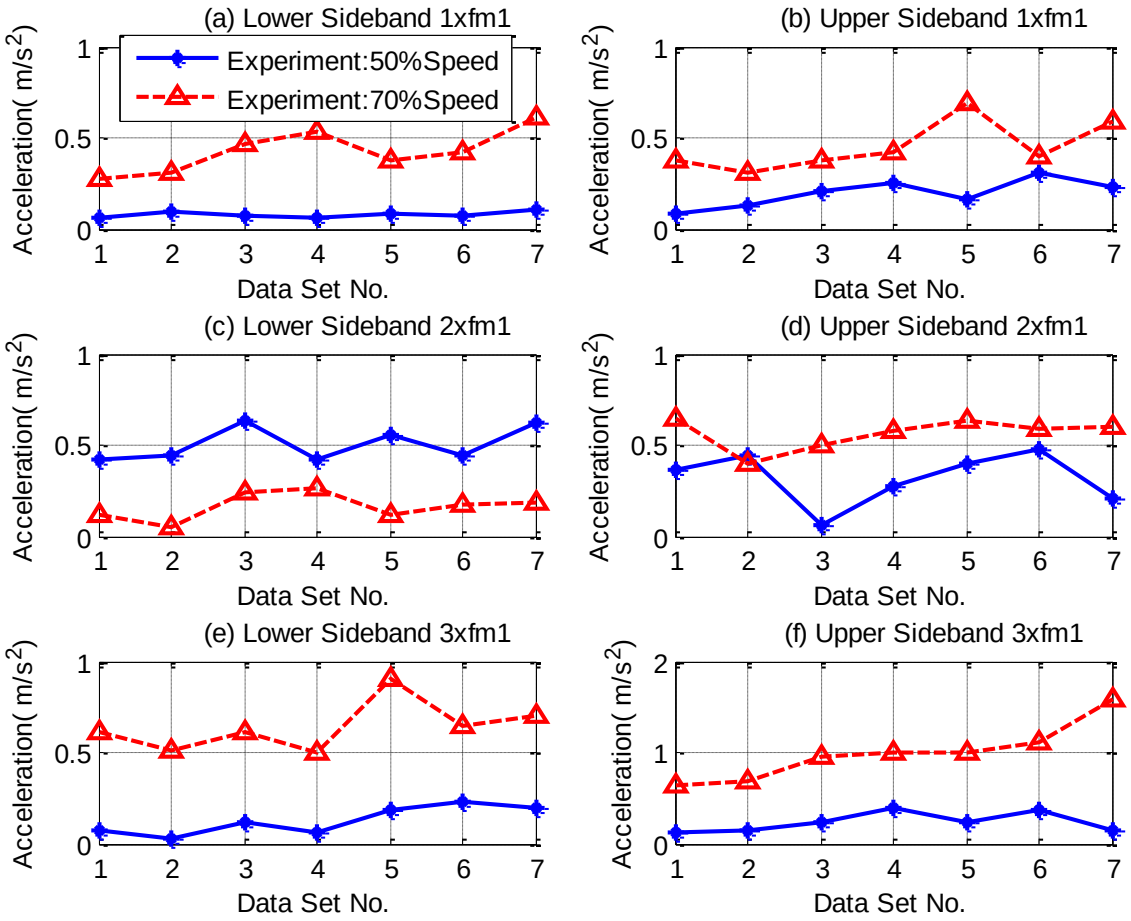

Figure 6-15 Experimental spectral amplitudes of the sidebands of the first stage meshing frequency components

The spectral peaks for 10% tooth wear from the predictive model increase by approximately 50%, which also give a clear indication to the presence of wear. Sideband features can hence also provide useful information on the diagnostics of gear surface faults. However, same nonlinearity effect can be illustrated in Figure 6-15(c), which is consistent with the behaviour of the 2nd harmonic peaks, Figure 6-12(c). This could be due to the large inducing effect of resonance around this frequency range.

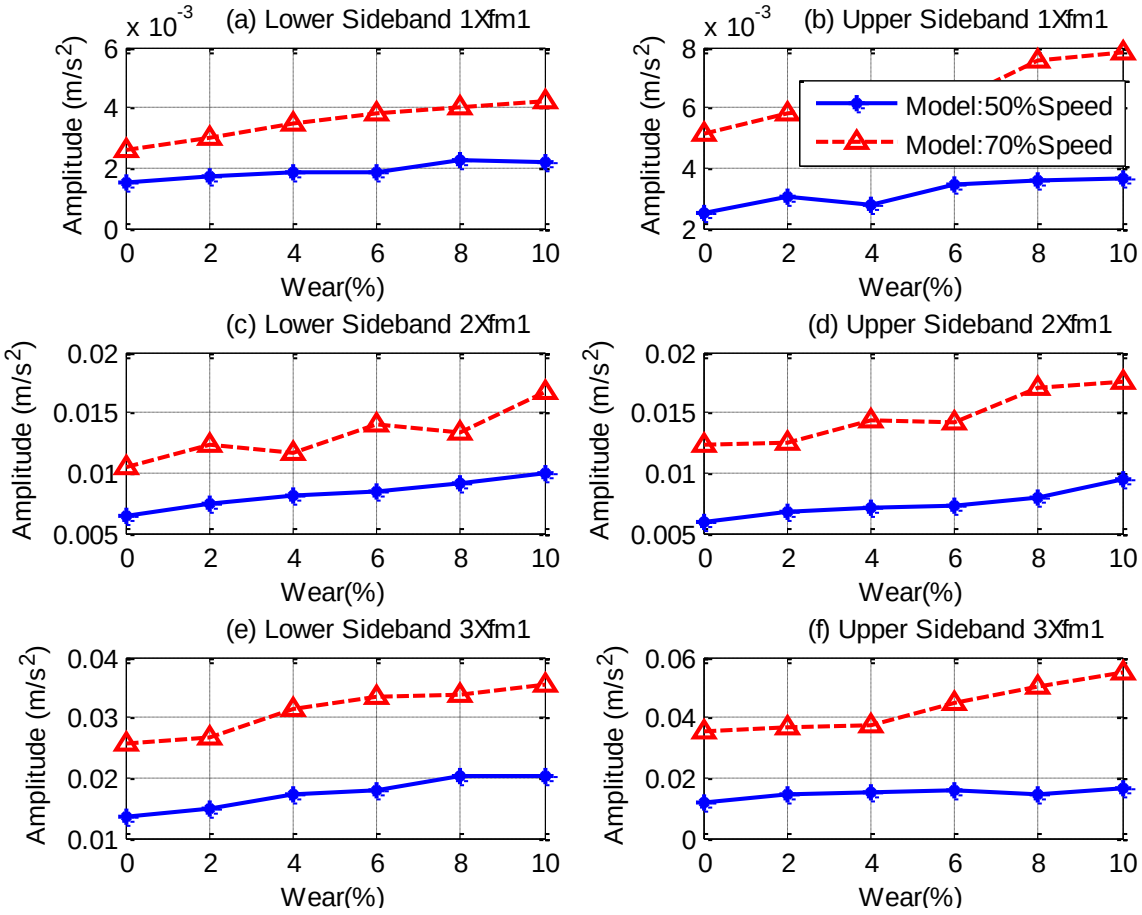

Figure 6-16 Predicted spectral amplitudes of the sidebands of the first stage meshing frequency components

6.9.3 Response to Wear with Different Gear Parameters

For further validation of the numerical model, different gear geometries were examined to explore the effect of tooth surface wear on meshing frequency components.

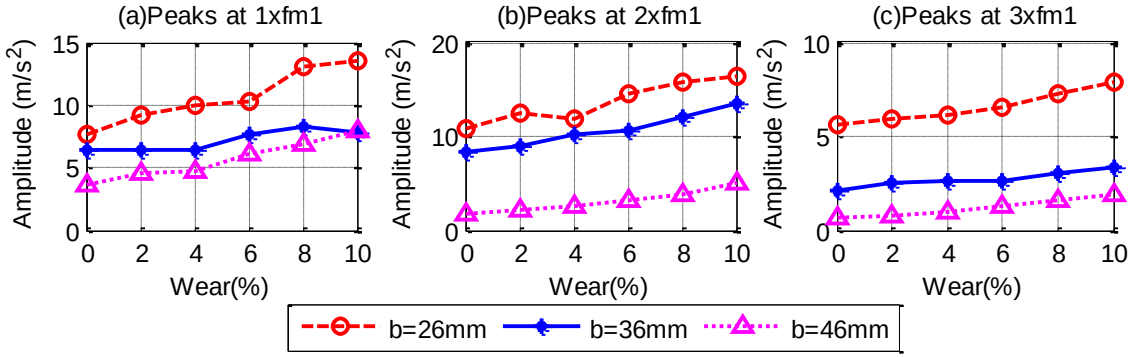

Figure 6-17 Spectral amplitudes of the first stage mesh frequency components with different tooth face widths (b)

Different tooth face widths and helix angles were simulated in the model with consideration of the effect that these changes have on the gear geometry parameters which affect the calculation of contact line length. Figure 6-17 shows the effect of wear on the meshing gear components for different tooth face widths.

From Figure 6-17, it can be seen that the 2nd and 3rd harmonics increase by more than 50% with 10% wear severity for a range of different tooth widths. A lower vibration level can be observed with decreasing tooth width, as a result of reduced frictional effects. The same trend behaviour with wear degree for low and high helix angles is identified at the 1st and 2nd harmonics of the mesh frequency as illustrated in Figure 6-18. However, the 3rd harmonic exhibits quadratic behaviour potentially because of reducing gear vibration with increasing helix angle.

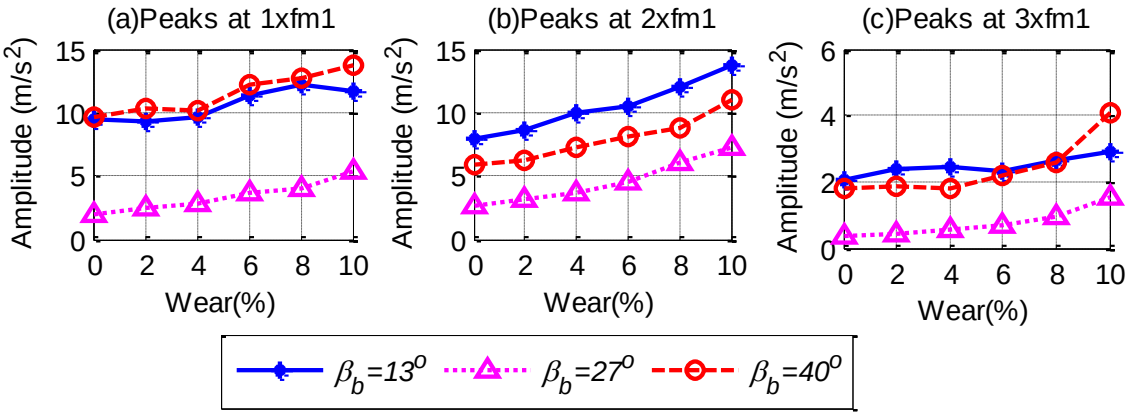

Figure 6-18 Spectral amplitudes of the first stage mesh frequency components with different base helix angles (β_b)

6.10 Key Findings

- Due to the complexity in gear wearing process, limited number of contributions have been reported to include the combined influence of wear evolutions and vibration modelling for helical gears with respect to accuracy and ease of implementation for CM and diagnostics for the early stages of wear.
- Tooth wear can be modelled by reduced mesh stiffness and increased fictional effects, because wear reduces the thickness of the tooth and increases the roughness of the contact surfaces.
- An increase in wear severity enlarges the centre distance between the meshing gears while the contact mesh stiffness decreases and retards angularly, in which higher

dynamic forces along with higher frictional effects will be induced during the meshing process.

- A run-to-failure test is more comprehensive and more realistic approach for simulating defects in gears
- Validation by dataset from a run-to-failure test with a natural progress of wear, can be more reliable wand data as compared with manually induced wear by lowering the grade of lubrication oils.
- Sinusoidal variable loads and different stepped loads are more convenient to match the load variations in different industrial applications such as wind turbines, automotive transmissions, centrifugal pumps, etc.
- A uniform tooth wear adopted for the helical gears can be considered to be more realistic for early operations as the test operating conditions change in a wide range.
- TSA analysis has the inherent capability to extract a deterministic signal for vibration components related to the rotational frequency of the target gear as well as reduce noise and enhance signal.
- Spectral peaks at the 2^{nd} and 3^{rd} harmonics of the meshing frequency (and associated sideband frequencies) are influenced more significantly by increasing wear degree, which can be used as effective wear indicators for the detection and diagnosis of tooth surface deterioration.
- Including the effect of gear potential excitations such as backlash, eccentricity, unbalance and run-out errors become more severe with the progression of wear to induce more vibrations, in which those effect of gear imperfection with gear determinations still remains opening and a challenging task.

Chapter 7
Condition Monitoring of Gearbox Lubrication Based on Vibration Analysis

This chapter is provided to develop an online CM technique of gearbox lubrication based on vibration signal analysis. Three different oil conditions: oil volume, water contamination and oil viscosity have been simulated within the two-stage helical gearbox, in which vibration signal was recorded via an accelerometer mounting on the gearbox housing. To get realistic results, different operating conditions were applied and each condition was repeated several times. Moreover, TSA and MSB analysis methods have been used to characterise any measurable changes that correlates the variation of gearbox with oil conditions and thereby is based for online and real time lubrication monitoring.

7.1 Introduction

The reliability, life time and availability of the most rotating machines such as gearbox depend largely on the lubrication condition. In modern industries, lubrication oil plays a critical role in condition maintenance of the rotating machineries. Recently, CM and prognostics of lubrication have become a significant topic among academia and industry [252, 253]. The purpose of most research is to provide early warning of machine failure and also extend the operating duration of lubricant life.

The efficiency, life time and availability of gearboxes and rotary systems are subjected to the quality of lubricating services, hence in many cases, lubricant failure is due to oil degradation by external contamination with water, dust particles, etc. [254]. For instance, water is one of the most significant destructive contaminations to lubricants, which causes a degradation on its characteristics and excessive water contaminant leads to insufficient lubrication and subsequently to abrasive wear and corrosion [255]. Therefore, monitoring external contamination of lubrication is an important issue in a proactive maintenance program.

Vibration analysis is an effective technique that widely used for monitoring and diagnosis of various industrial applications. Despite the fact that many problems are caused by lubrication failure, very few works examine the possibility of employing vibration analysis for detecting lubrication statues [256-259]. This study develop online CM of gearbox lubrication based on vibration signal analysis using an effective denoising method, as an approach to characterise any measurable changes that correlates the variation of gearbox with oil conditions

7.2 Gearbox Oil Tests

As gearbox is important and widely used in industry, failure in its lubrication may lead to a catastrophic and huge cost. Therefore, it is important to monitor the condition of lubrication to ascertain any degradation can be progressed within the oil. Different conditions of gearbox lubrication have been done in this research as follows:

7.2.1 Monitoring of Gearbox Lubricant Starvation

Different gear failure modes are strongly correlated with lubricant status, for example low oil level or starved lubrication leads to significant gear damages. Insufficient lubrication can increase friction, temperature and material wear, which ultimately leads to material

failure [101]. The limitation of oil dip lubrication availability in the contact of gears and bearings with respect to their scuffing failure performance and flank load carrying capacity was investigated by Höhn B.-R. et al. (2011) in [102, 103]. They indicated that lack of cooling oil leads to high gear bulk temperatures and therefore increases risk of gear failures such as scuffing, pitting, micropitting and low-speed wear.

Gear vibration characteristics are the key indicators in the diagnosis of machine faults, which was used to detect lubrication level of gearboxes with some limitations, as in Refs. [101, 256], [257] and [260]. Smith, J. [260] confirmed that, loss of lubricant could produce severe metal-to-metal contact, which should generate high levels of stress pulses and would be detected immediately by accelerometer(s) on the rotor to give an early indication of problems.

The references indicated that there is a strong relationship between gearbox lubricant volume and its vibration signatures, however, a few works emphasis this relationship for the purpose of condition monitoring and diagnosis. To fill this gap, this study will examine the vibration characteristics to normalise the condition indicator and investigate any measurable changes correlated with the variation of gearbox oil capacity for future preventive maintenance [261].

7.2.1.1 *Test Procedure*

A schematic structure of the tested gearbox (two stage helical gear box manufactured by David Brown Radicon Limited) is shown in Figure7.1. The recommended oil lubrication of the gearbox is mineral oil of 320 EP with volume capacity of 2.6 Litres. The simulated quantities (BL 2.6 L, 600ml less and 1100ml less) and the gearbox components are also depicted in the figure, in which the meshing teeth of the first stage is splashed while the second stage is fully submerged in the oil.

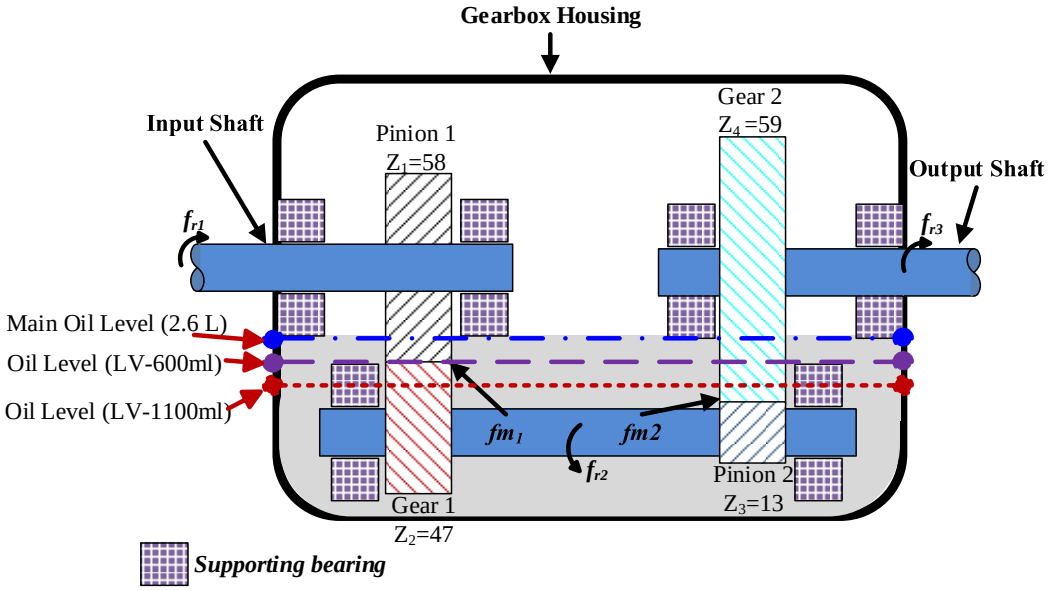

Figure 7-1 A schematic description of two-stage helical gearbox with different oil levels

7.2.1.2 Oil Starvation Methodology

The main change of decreasing gearbox oil level, is decreasing in the required power to circulate the oil belong with decreasing in potential power losses, which are dominated by the oil drag losses and the churning losses of the gears [103]. Furthermore, power losses such as squeezing, splashing and ventilation losses can be reduced by lowering the oil volume [102]. Recently, different works have been done in terms of oil churning losses and sliding friction losses. As a result of these studies, the drag torque acting on a gear C_{ch} and the oil churning losses P_{ch} can be estimated as follows [181, 262-265]:

$$C_{ch} = \frac{1}{2}\rho\omega^2 R_p^3 S_m C_m$$
$$P_{ch} = C_{ch}\omega \qquad (7.1)$$

Where ρ is the lubricant density, ω is the rotational speed, R_p is the gear pitch radius, S_m is the gear submerged surface area and C_m is non-dimensional torque parameter.

Several analytical expressions of C_m were deduced from dimensional analysis, which depend on the flow regime, immersion depth and submerged volume of lubricant. Equation (7.1) shows a vast correlation between lubrication capacity (wetted surface area of the gear) and the churning losses. In which, less drag torque and less churning losses are required with the decreasing of gear submerged surface S_m.

In contrary to the beneficial effect of reducing immersion depth, higher contact friction and lower load carrying capacity are expected along with damaging effect of reduced cooling of the gear mesh must to be considered. As a result, more vibration and noise due to increase the risk of gear failures such as scuffing, pitting, micropitting and low-speed wear [102]. The lubrication starvation has significant effects on the friction coefficient and the frictional power losses due to decrease in the inlet oil film thickness [266]. The reversed friction moment T_{fr}, and the sliding friction losses P_{fr} can be calculated by:

$$T_{fr} = \rho_f F_f$$
$$P_{fr} = T_{fr}\,\omega \tag{7.2}$$

Where, ρ_f is the meshing friction arm and F_f is the sliding friction force between meshing teeth. The friction torque opposes the transmission torque in which low oil service result in more friction and more nonlinear vibrations. The change in vibration signature due to oil shortfall could be used in the detection and diagnostic of gearbox lubrication conditions.

7.2.1.3 *Measurement Validation*

To show direct perceive of various lubrication volumes, TSA of the gearbox vibration signals are used to diagnose its oil volume.

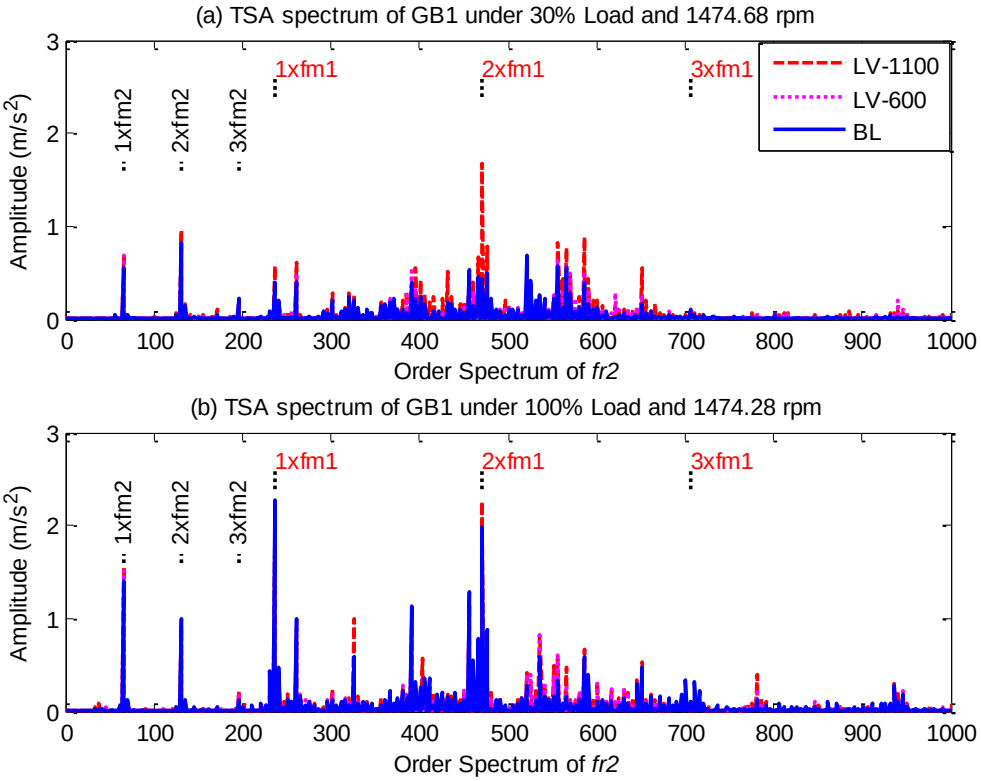

Figure 7-2 TSA vibration spectrum of the tested gearbox (GB1)

The general behaviour of the vibration spectrum with different oil volumes under various operating conditions are represented in Figure 7-2. Gear mesh frequency components (up to 3th harmonics) are also shown, which is verified that the TSA vibration signal is synchronised with the second shaft (f_{r2}).

7.2.1.4 *Effect of Oil Starvation on Vibration Level*

RMS is the most reliable parameter in CM to measure the power content in the signal [267]. To represent the overall level of vibration signature under different oil volumes, Figure 7-3 shows the RMS values of the TSA vibration signals of GB1 and GB2 under full speed and different load conditions, whereas each dataset was repeated five times for gaining more reliable results.

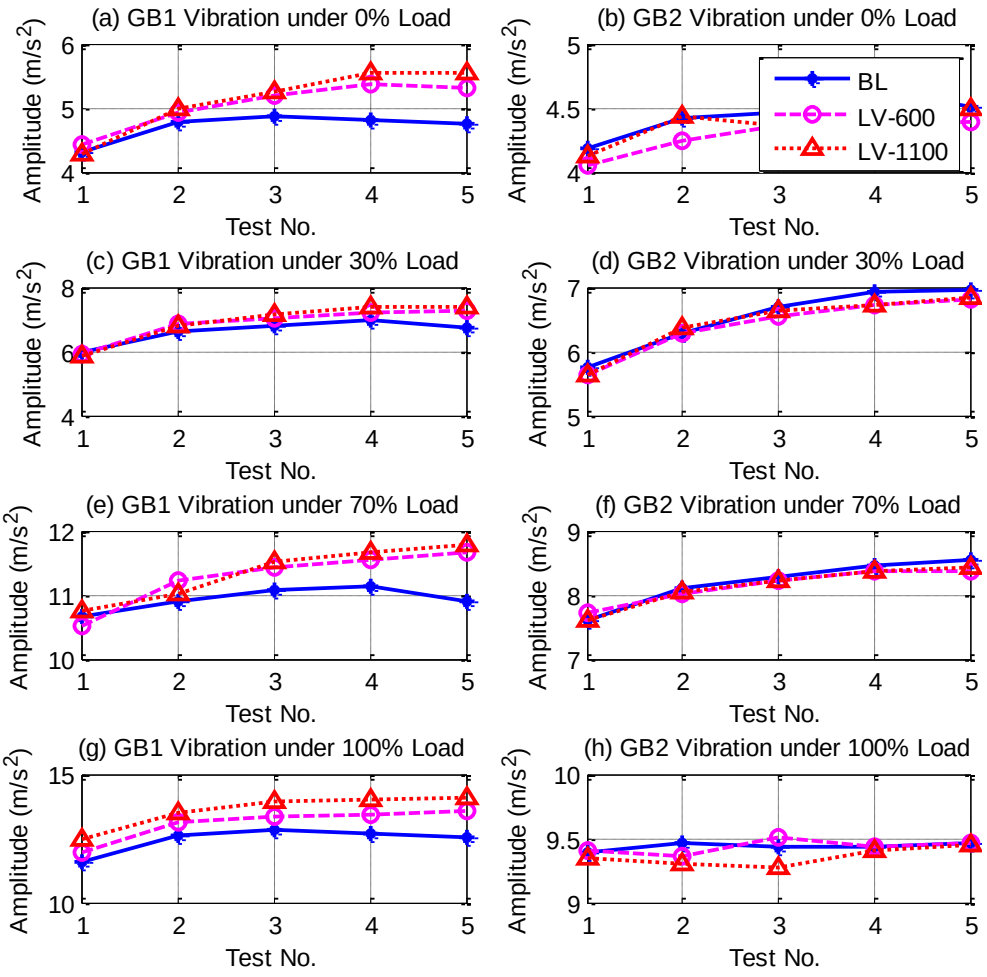

Figure 7-3 RMS vibration signals of the two gearboxes

It can be seen that the vibration levels of the GB1 are generally increased with the reduction of oil quantity as compared with the normal gearbox (GB2), which shows approximately unchanged in the vibration level. The vibration changes are consistent with the results that

presented in [101], which is owing to more friction between the contact surfaces of the meshing teeth. Moreover, there is also slight increase in the vibration level of the repeated tests, which is correlated with the increasing of gearbox oil temperature, as explained in Figure 7-4. The oil temperature is decreased with the decreasing of oil level, due to less contact between the oil and the submerged gear surfaces. However, the gear bulk temperature is increased with reducing immersion depth, as explained in [103].

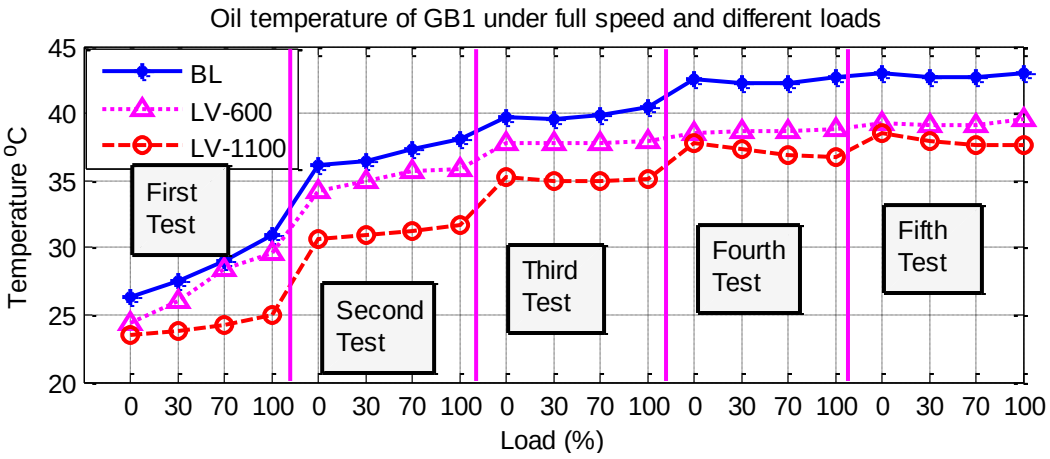

Figure 7-4 GB1 oil temperature of the test scenario

For more explanation, Figure 7-5 shows the average RMS results of the last three tests under different operating conditions, which are approximately at more consistent temperature. The average results show an increase in the RMS under different load conditions with oil shortfalls, especially at full speed (1474.1 rpm).

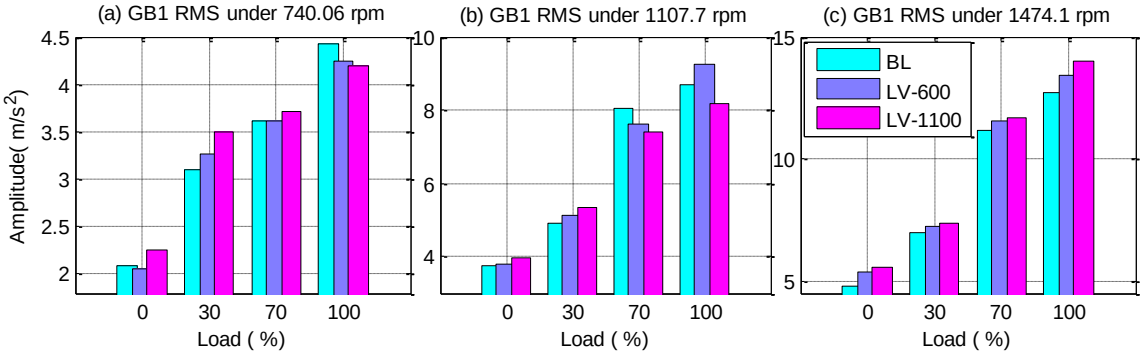

Figure 7-5 Average of the RMS vibration signals under different loads and speeds

In which, after extended running, removing oil supply from a gearbox leads to breakdown the oil film between the meshing teeth, so that the vibration levels provide reliable information in the technical diagnostics [260]. However, RMS is often not sensitive enough in detecting faults in particular.

7.2.1.5 *Effect of Oil Starvation on Power Supply*

To examine the data quality and test reliability, signals including data from the electric signals (current and voltage) of the driving motor are processed to demonstrate its consumption power. The decreased lubricity affects the oil churning and the friction between the contact surfaces during the mesh process. As a consequence, the submerge depth will be affected, which may affect the operational attitude.

Figure 7-6 presents the averaging of the consumption power of the driving motor under various operating conditions for different gearbox lubrication volumes. The results show consistent decrease with the lubrication capacity, especially under low and high speed. However, the change in power is less than 0.4%.

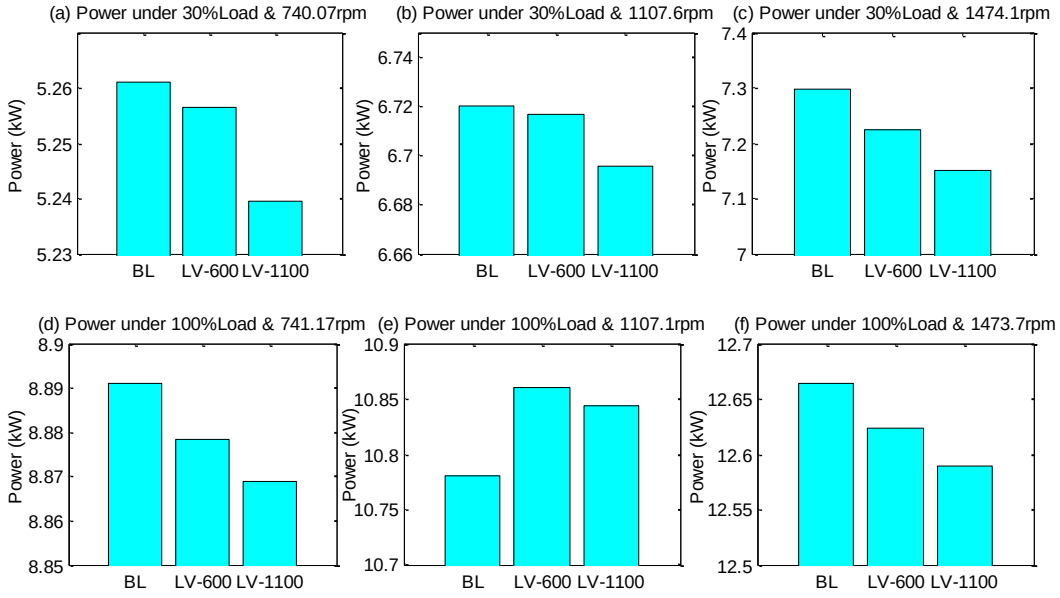

Figure 7-6 Power supply under different speeds and loads

7.2.1.6 *Vibration Response at Mesh Frequency*

The change in spectral amplitudes is usually based on a measure of the vibration variations [268]. Decreasing of oil service level has significant influence on the gearbox consumption power as a result of reducing oil churning losses and increasing frictional contact between the meshing teeth, which affect the gear dynamic responses. For further understanding of vibration change and hence to obtain a more detailed and accurate diagnosis of oil capacity variations, the change of spectral amplitudes at meshing frequency components are investigated, which usually indicate the gearbox conditions.

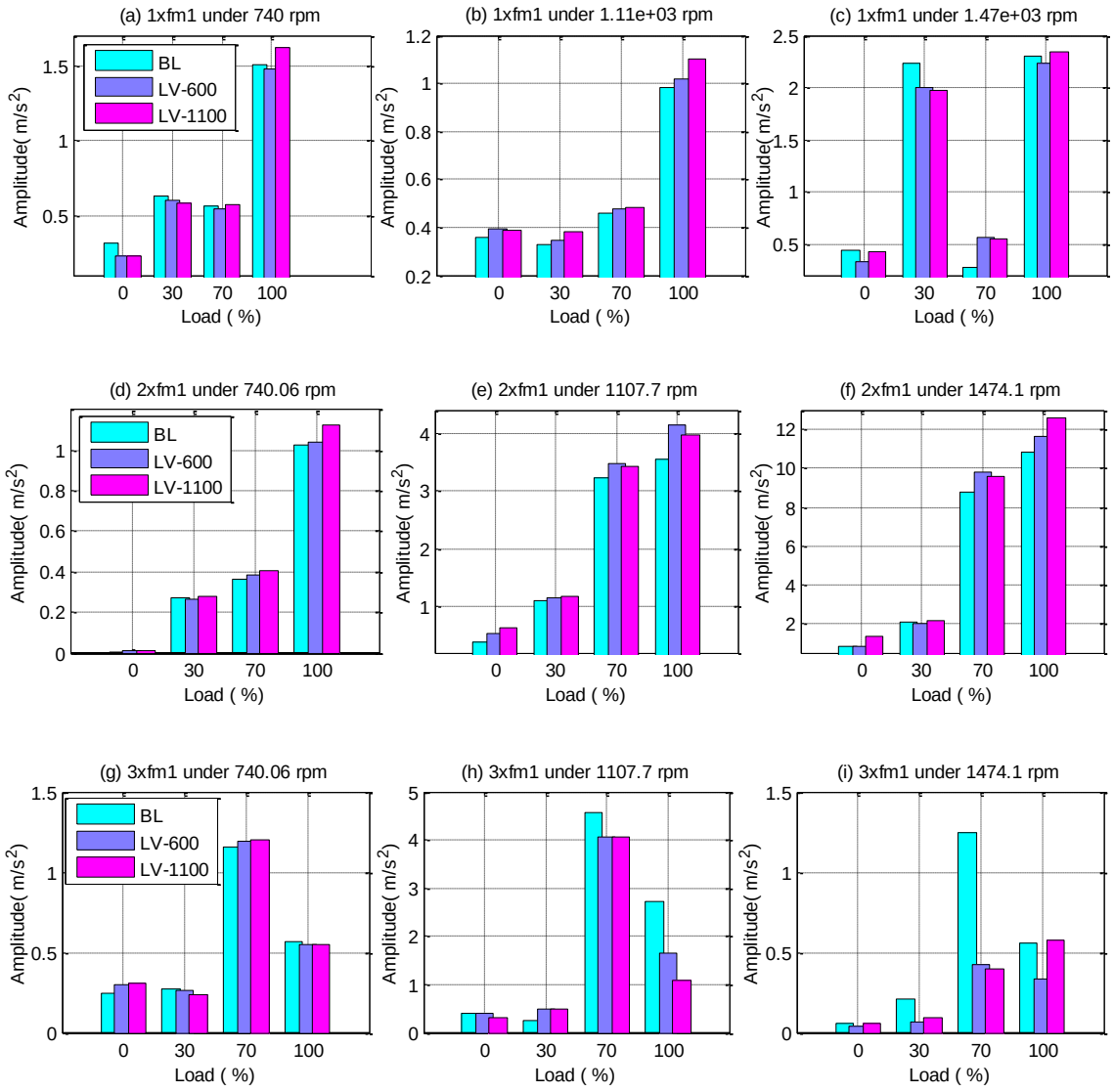

Figure 7-7 Spectral peaks of the first meshing frequency components under different operating conditions

Figure 7-7 shows the average amplitudes of vibration response at the first three harmonics of the first meshing frequency (*fm1*). It can be seen that the second harmonic (2x*fm1*) shows a very clear increase in the amplitude with oil shortages by more than 8% for the most operating conditions (Figure 7-7(d-f)), which give a good indication to diagnose lubricant starvations. This could be due to the double change in the reversal friction force at the pitch point or/and due to the dual fluctuations of sliding velocity during the gear meshing cycle. In which, an approximate of friction model that extensively used in the study of friction-induced vibration can be indicated by [78, 81, 269]:

$$F_f = \mu(V_s)\, N\, \mathrm{sgn}(V_s) \tag{7.3}$$

$$\mu(V_s)\,\mathrm{sgn}(V_s) = \begin{cases} \mu & V_s > 0 \\ -\mu & V_s < 0 \end{cases} \tag{7.4}$$

Where V_s is the relative sliding velocity between the contact teeth, $\mu(v)$ is the velocity-dependent coefficient of friction, and N is the normal force pressing the two sliding surfaces together.

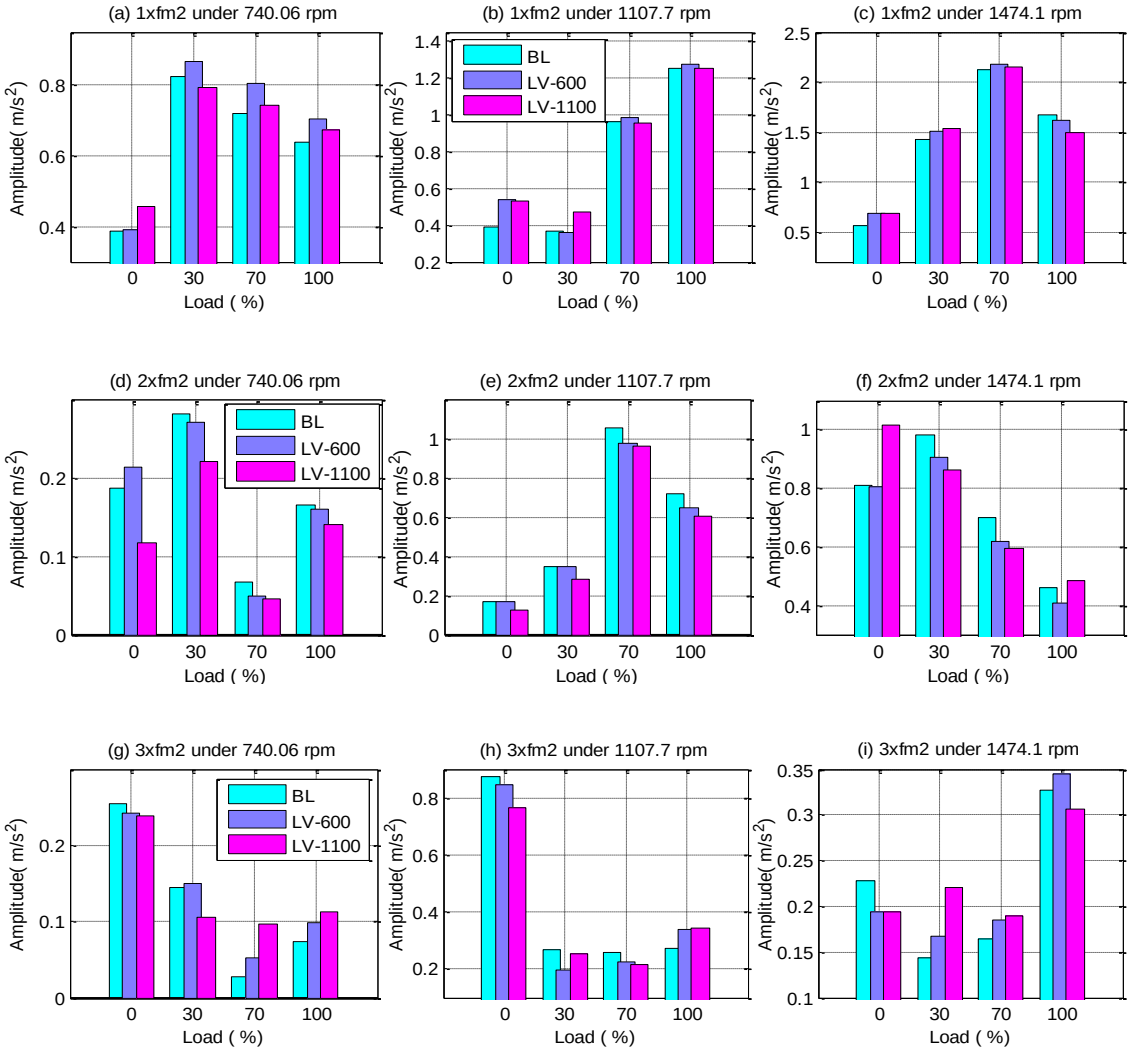

Figure 7-8 Spectral peaks of the second meshing frequency components under different operating conditions

In the same way, Figure 7-8 shows the average spectral amplitudes of the second meshing frequency (f_{m2}) components, which is the low speed stage with high transmission load. The results show inconsistent behaviour with the change of lubricant capacity. This possibly because of the gearbox geometry, that taking-off oil makes the oil level lower than the

contact region of the first stage, whereas the second stage is still fully submerged within the oil.

The average amplitudes of vibration up to the tenth high order harmonics of the two meshing frequencies are shown in Figure 7-9. The average vibration at the first mesh frequency, which is the high speed stage with low load shows higher amplitude changes relating to the oil level variations. It is enhanced by more than 8% with the change of oil capacity, especially at low and high speeds, which can be also considered as an effective feature to perform the instant diagnosis of gearbox lubrication levels. However, the vibration at the second mesh frequency shows unclear behaviour, this is possibly because its meshing teeth are still fully submerged in oil.

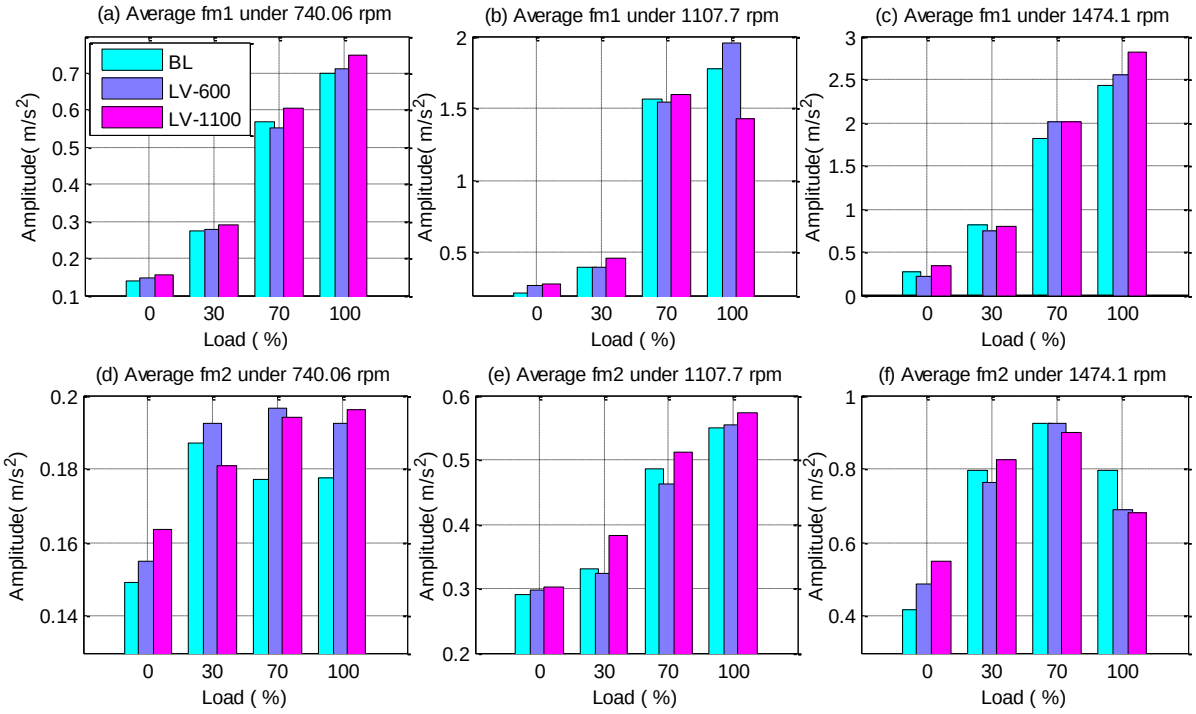

Figure 7-9 Average vibrations at mesh frequency components

7.2.1.7 *Vibration Response at Sideband Frequency*

The analysis of sideband around meshing frequency is also often based for the detection and diagnosis of gear surface statues, as it relates more to gear asymmetric faults such as broken tooth and investable manufacturing errors. Any differences on the gear dynamics may cause changes in the sidebands across the fundamental and harmonics of the mesh frequency. As the second harmonic of the first mesh frequency (2x*fm1*) is the most

influential component, the average spectral peaks of the last three tests at the lower and upper sidebands (f_{sb}= f_{m1}± f_{r2}) around this harmonic are shown in Figure 7-10.

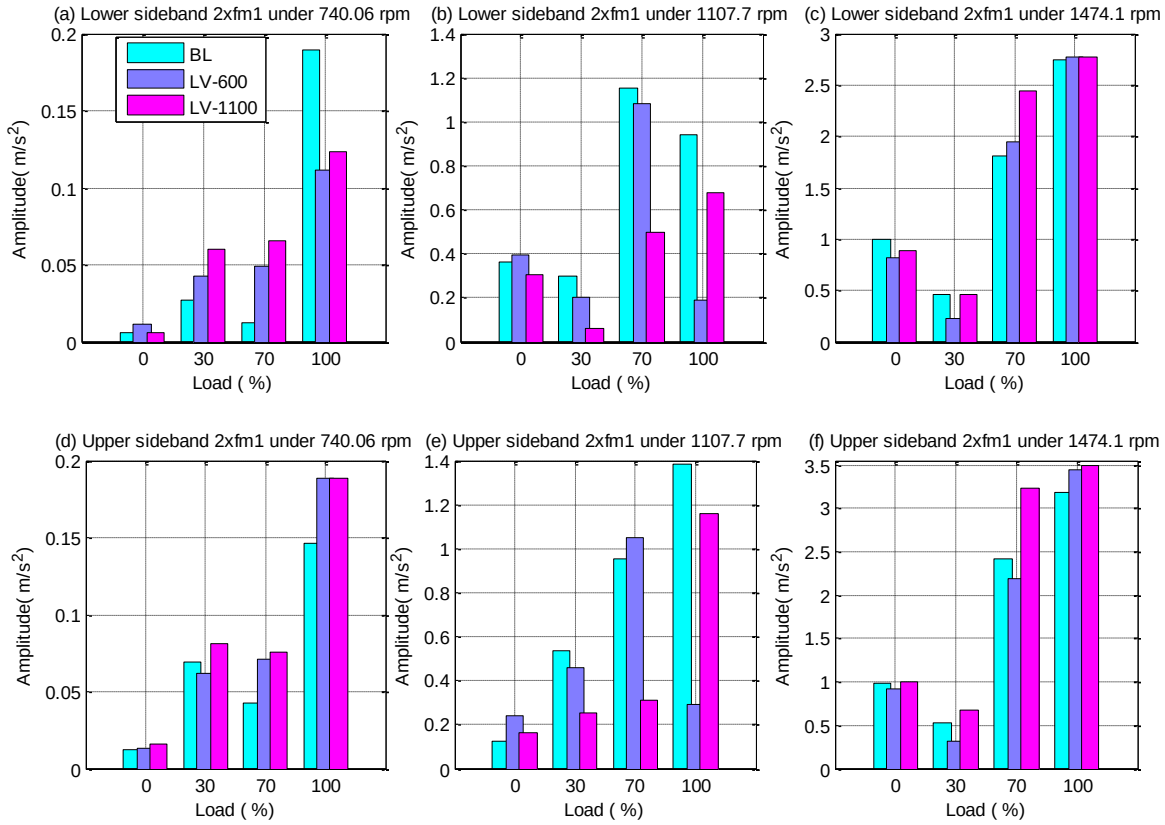

Figure 7-10 Spectral peaks of the lower and upper sideband components around the 2x f_{m1} under different operating conditions

It can be seen that the sideband amplitudes are generally increased with the reduction of oil capacity, especially at low and high speed. For more explanation, the average amplitude of the lower and upper sideband components (up to 3-components) are shown in Figure 7-11. The results show that there is a significant increase in the average amplitude of the sidebands especially under high transmission load, which are enhanced by more than 6%. As a result, these features can be also considered as effective indictors to poor lubrications. In conjunction with the change patterns of meshing components and TSA kurtosis, it is possible to make difference between tooth breakages and oil shortfall.

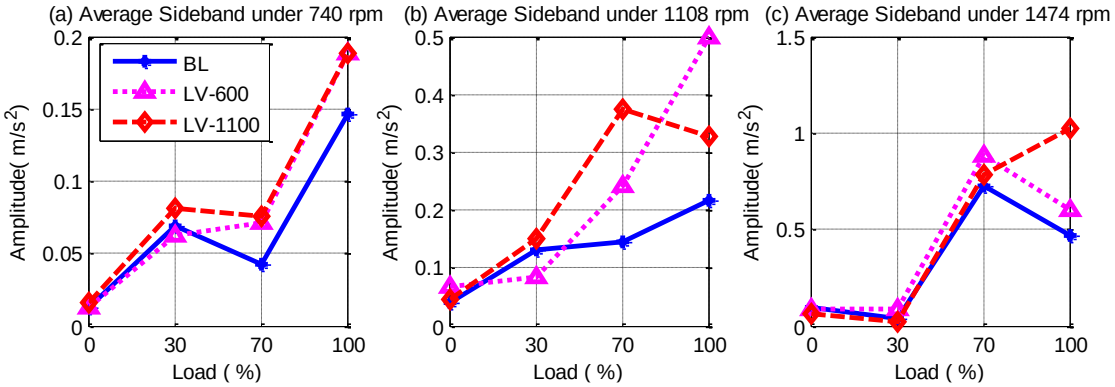

Figure 7-11 Average sideband of 2xf_{m1} components

7.2.2 Monitoring of Water Contamination

CM of lubrication is mainly applied to ensure that lubricant has retained its physical characteristics, and it has not degraded by external contaminants. Water is one of the most significant destructive contaminations to lubricants that cause degradation on its characteristics and leads to undesirable mechanical effects such as change in viscosity and chemical reactions with anti-wear additives and oxidation inhibitors to generate solid precipitates [99]. Hence, oil degradations influence the dynamic behaviour of the gears and make significant changes on the vibration levels and load carrying capacity of the transmission system. Therefore, online CM of gear lube oil is crucial to prevent the machines failures.

Vibration analysis can be effective for performing the instant diagnosis of water contamination so as to prevent further damages to gearboxes running with water contents, as stated by Abusaad et al. [270]. However, vibration signal needs an effective signal processing method to extract transient signals and suppress random noise. MSB was developed based on the demodulation characteristics, which has the capability to suppress the noise background and extract useful features from the mechanical vibration signals [156, 157].

This study develops online CM of gearbox lubrication based on vibration signal analysis using an effective denoising method, as an approach to extract effective diagnostic information based on the utilization of the modulation characteristics [271].

7.2.2.1 *Test Facility*

Water undermines the lubricant performance from forming an effective lubrication film between the contact components. Hence, detection of water contamination has received significant attention to avoid catastrophic failures and increase the life cycle of equipment [270]. The typical acceptable water content for transmission oils are in the range of 1 to 2% (10 to 20 kppm) [272, 273]. To ascertain the root causes contributed to the degradation characteristics, different contaminations below and above this range were simulated, which allows a variety of different underlying measurements to be examined in a wide range for defining their corresponding detection performances.

(a) Kinexus pro+ rheometer device (b) Gearbox oil samples

Figure 7-12 Kinexus pro+ rheometer and oil samples with different water contaminations

As oil viscosity is the most important parameter of lubrication; a Kinexus pro+ rheometer, shown in Figure 7-12(a), was used to measure the oil viscosity and taken as references to represent the deterioration progress due to water contamination. Different MILLGEAR 320 EP (320 cSt at 40°C) samples were taken from gearbox housing just when the test was stopped, as shown in Figure 7-12(b). It can be seen that the oil colour was changed due to water content and there is free water in the sample content of 120 kppm. This confirms that the water content was added effectively according to the test design.

Figure 7-13 represents the viscosity values of the oil samples at the correlated stable operating temperature of the gearbox. It can be seen that the viscosity is generally increased

with the interaction extend of the water droplets. The water can cause a polarity shift in many lubricant formulations, which allow them to have some affinity with or attraction to water [178]. The effect of water in oil is changing both physical and chemical properties. This could be due to polarity shift in lubricant formulations and the presence of rigid boundary when oil and water meet each other head-on [178, 274], Fernando Bresme (2008) referred that when oil and water meet each other head-on, they form a strong and rigid boundary between them [274], and as a result of this boundary converging, the viscosity is increased with the solubility of dissolved water.

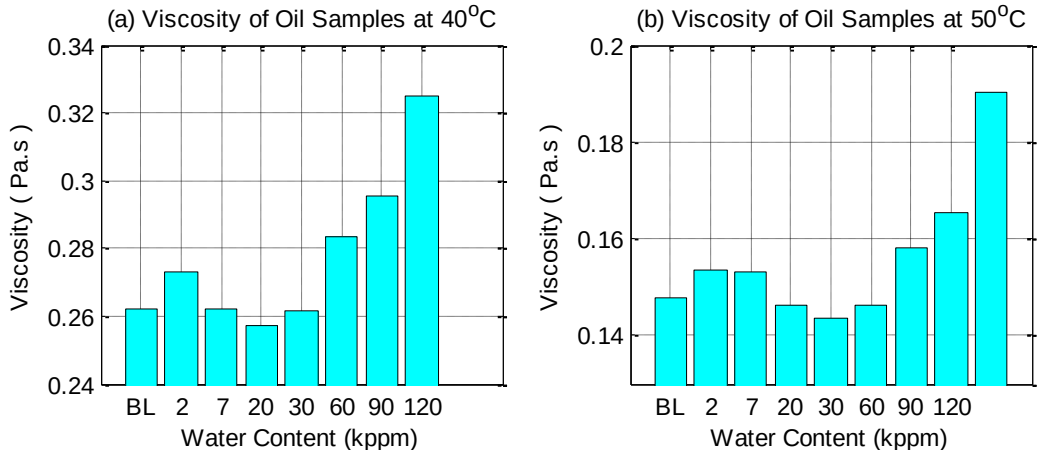

Figure 7-13 Viscosity of lube oil with different water contents at selected temperatures

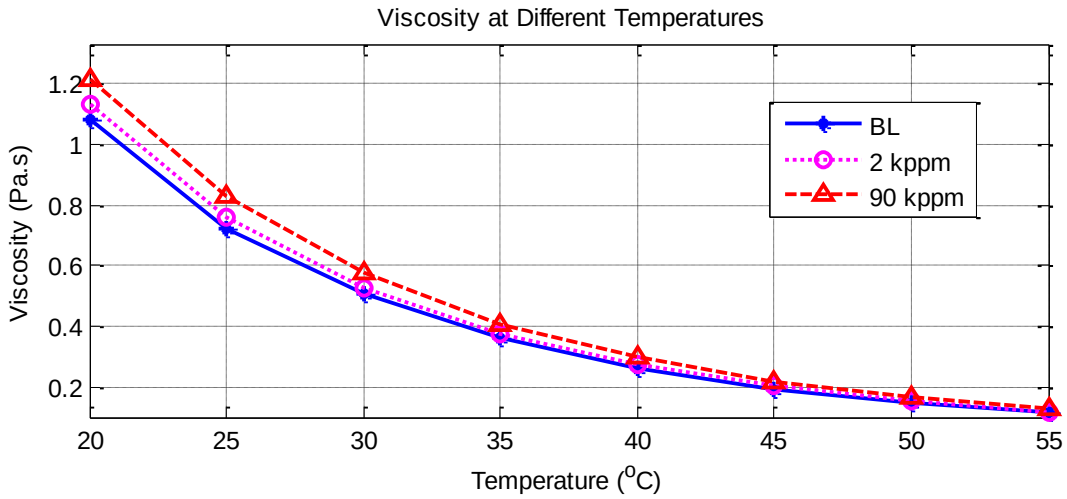

Figure 7-14 Viscosity of lube oil under different temperatures

Moreover, temperature has a significant influence on the viscosity, i.e. the higher temperature corresponds to lower viscosity. Figure 7-14 shows the performance of different oil lube contaminations with temperature, in which less differences in viscosity with water

contents can be identified at high temperature. This can be a result of increasing the solubility of dissolved water with temperature [177].

The average oil temperature of the test scenario is illustrated in Figure 7-15, whereas the oil temperatures with different water contents were kept in the same range. The slight different in the oil temperature between the cases due to the fact that the operating temperature is partially dependent on the factors beyond control, e.g. ambient temperature. It can be seen that the oil temperature is increased up to around 40-45^{o}C, whereas they stabilise of all cases follow the same trend during different operating conditions.

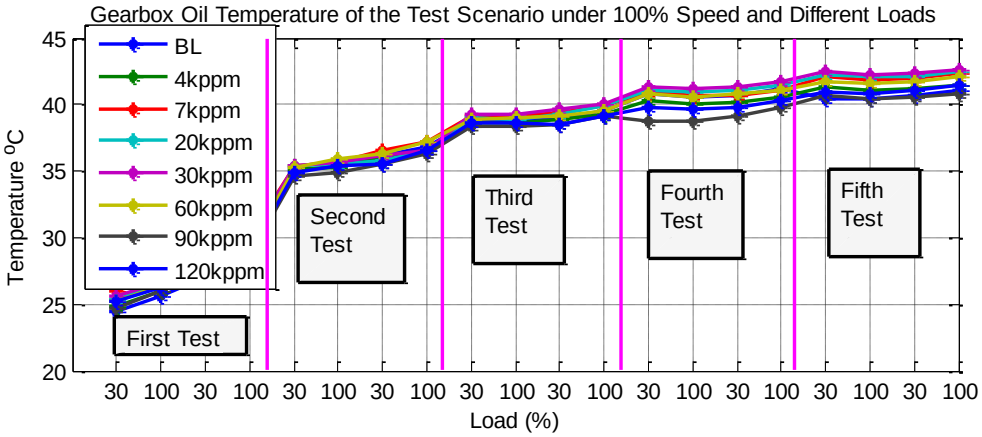

Figure 7-15 Gearbox oil temperature with different water contaminations

7.2.2.2 Vibration Responses

The general behaviour of the gearbox vibration spectrum with different water contents under various operating conditions are shown in Figure 7-16. For a reliable operating condition of machinery, various methods for fault detection and diagnosis have been developed. Vibration analysis is widely used in condition monitoring and diagnostics, however it needs effective signal processing methods to extract the transient signals and suppress the random noise.

Water contaminations can lead to significant mechanical effects and complicated nonlinear vibration, which resulting in a modulation phenomenon in vibration signals. Therefore, an effective demodulation methods are required to decompose the nonlinear modulation components and suppress the noise background. MSB was developed based on the demodulation characteristics (see Sec. 3.2.4.2.2), which has the capability to decompose the nonlinear modulation components and suppress the noise background hence, extract useful features from the mechanical vibration signals [156, 157].

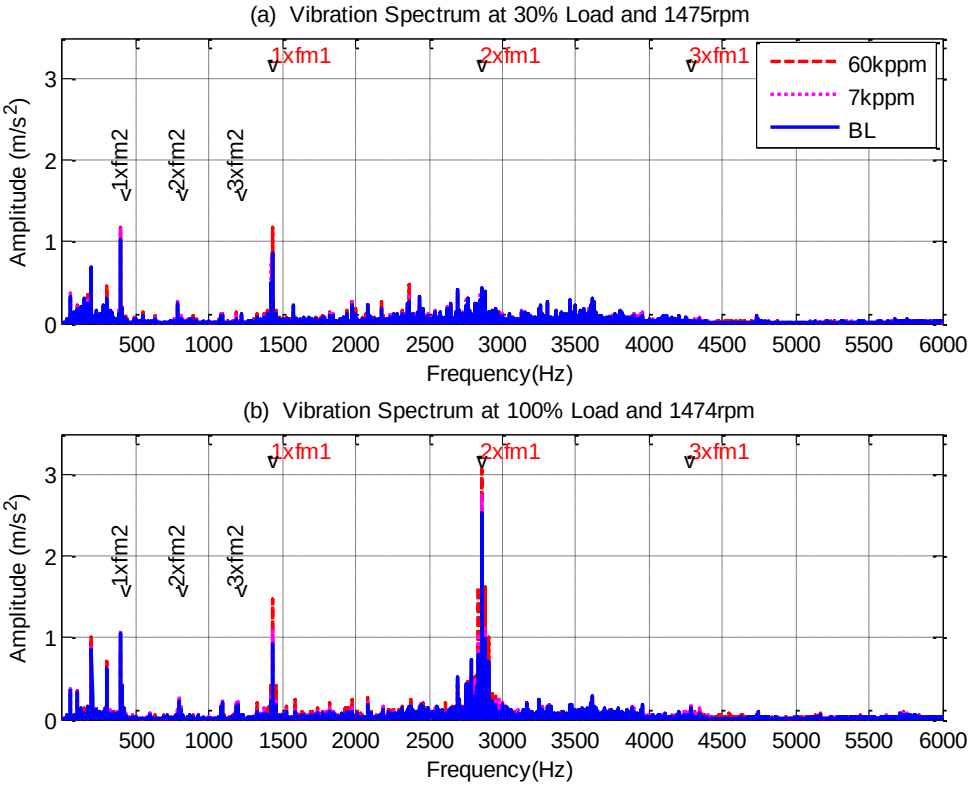

Figure 7-16 Vibration spectrum of the tested gearbox

7.2.2.3 MSB Characteristics at Mesh Frequency

In order to evaluate the performance of the MSB approach in monitoring the progression of water contaminations, the recorded vibration data were processed using MSB method, in which 90 averages were implemented based on the data length and 70% overlap ratio between successive data frame. In addition, a Henning window was applied to the vibration data during the calculation of FFT to suppress any leakages in the spectral signal.

As mesh frequency is the most feature associated with the gear dynamics, Figure 7-17 shows the averaged amplitudes of the five repeated runs at the first mesh frequency components under different operating conditions. It can be seen that the MSB at the f_{m1} harmonics are almost the same with no clear indication for the water contaminations. This could be because this stage is functioned to a high speed with low load, and the mesh region is not fully submerged in the oil lube (see Figure 7-1).

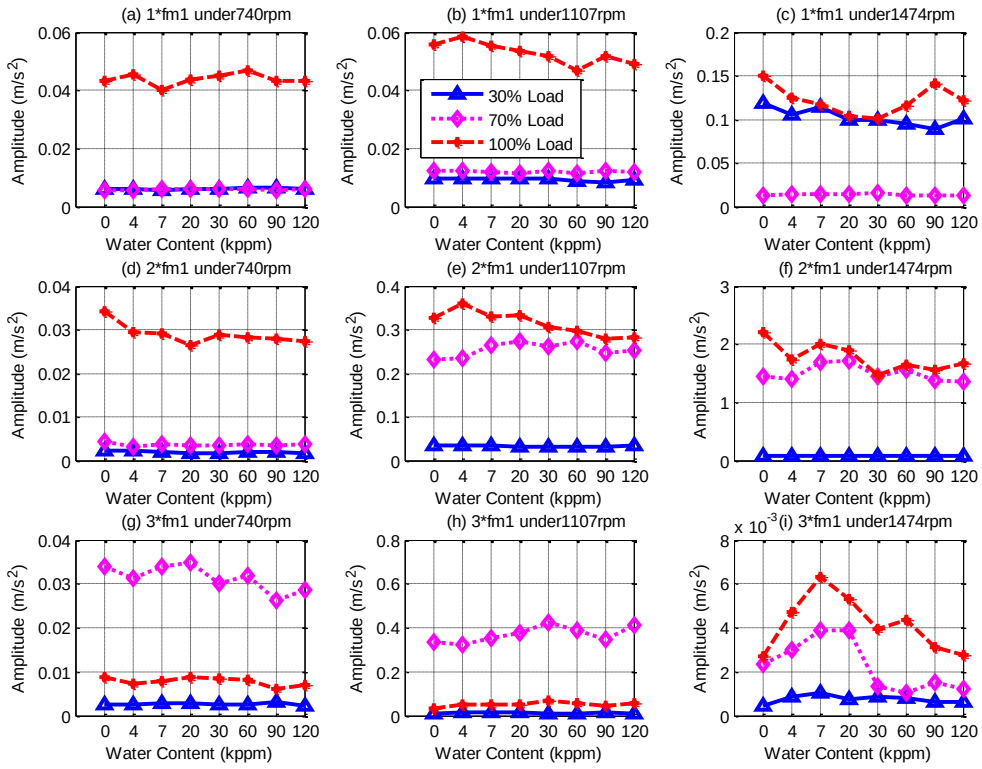

Figure 7-17 Average amplitudes of the *fm1* components under different operating conditions

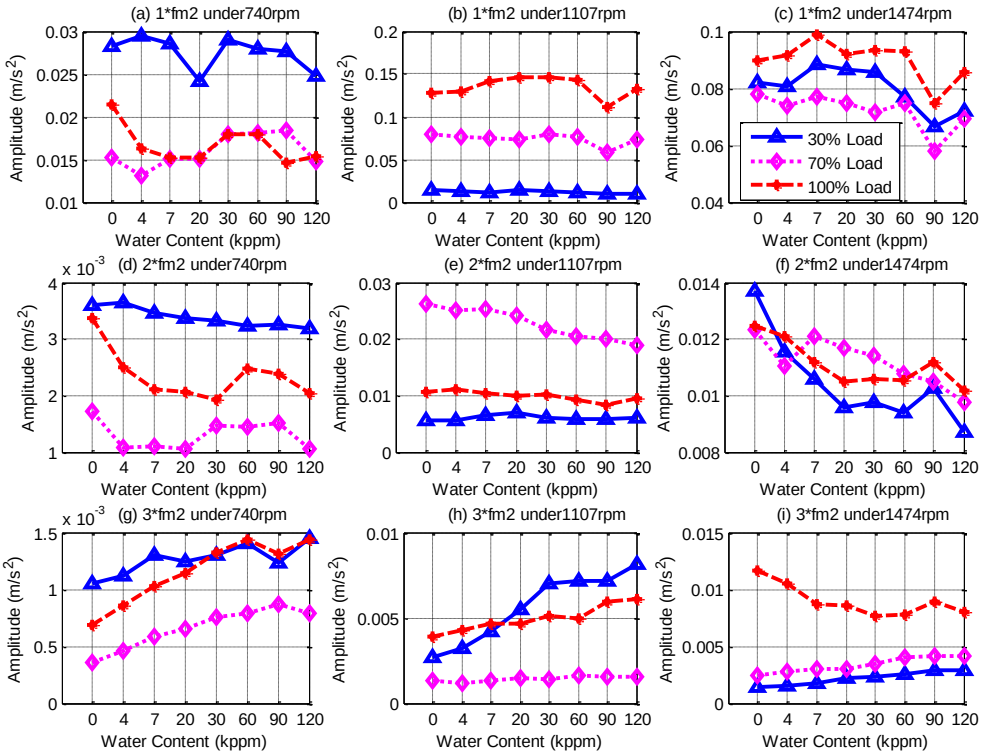

Figure 7-18 Average amplitudes of the *fm2* components under different operating conditions

The MSB response at the harmonics of f_{m2}, which is the fully submerged stage and influenced by low speed stage with high load transmission, exhibit with more consistent

behaviours with water contaminations. In which the third harmonic (3*f_{m2}) is significantly increased with increasing of water contents and can be a good indicator to lubricant deterioration. However, there is a slight decrease in the amplitude of this harmonic under high speed and full load, a higher nonlinear effects of gear mesh stiffness and the higher nonlinear influence of dynamic friction between the contact tooth surfaces. Moreover, under these conditions, the nonlinear effect of frictional forces belong with the oil splashing and squeezing lead to more bending in the contact teeth, in which the higher nonlinear interactions are based on the oil specification condition and the operating condition of the transmission gears, such as speed, load and temperature.

7.2.2.4 *MSB Characteristics at Sideband Components*

Based on the gearbox geometry, the mesh frequency harmonics could be modulated with the components of shaft frequency at $nf_{m2} \pm nf_{ri}$. Figure 7-19 depicts the MSB result of the f_{m2} components with their modulated sidebands and the coherence of each signal.

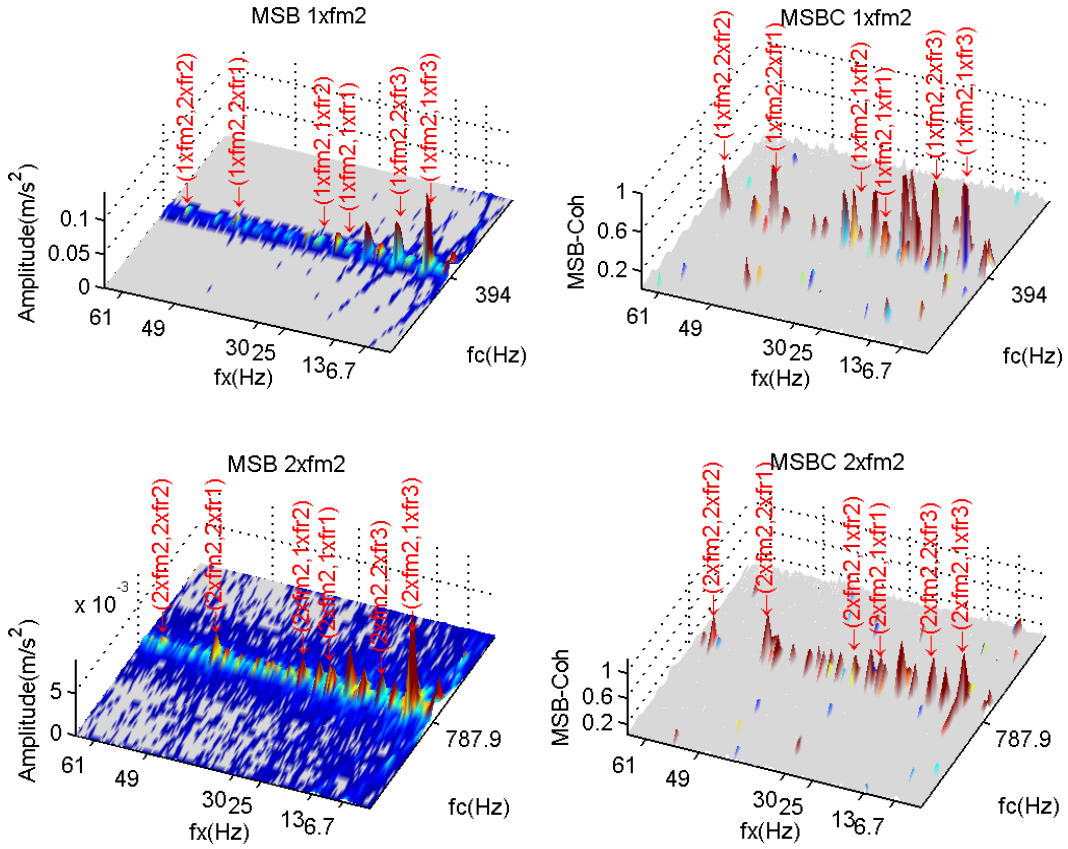

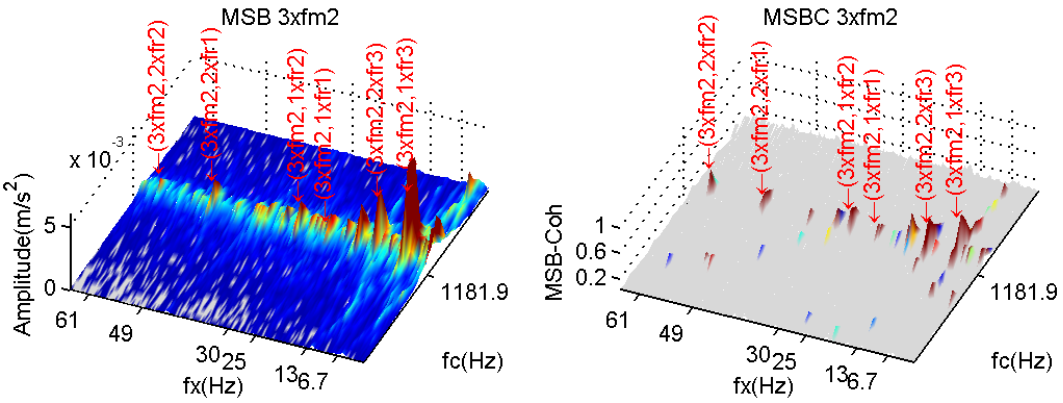

Figure 7-19 MSB results around *fm2* components with their sidebands at high speed

Due to fully submerged meshing teeth, the second stage (f_{m2}) is more influenced by the water contaminations than the first stage, thus the sideband frequencies around f_{m2} components have been examined. For clearness and further analysis, the bifrequency axis is labelled with only the first two harmonics (i=1, 2) of the characteristic frequencies: i$x f_{r1}$, i$x f_{r2}$, i$x f_{r3}$. The MSB-magnitude and its corresponding MSBC results are presented in the region f_r < 70 Hz to include the sidebands up to $2f_{r2}$ (61 Hz) and f_m < 1240 Hz to include the carrier frequency up to $3f_{m2}$ (1182 Hz).

As the third harmonic ($3*f_{m2}$) shows the most beneficial trends than the other harmonics, the sideband frequencies around this component have been examined to extract the usefulness of these sidebands in diagnosing the water contaminations with the help of MSB demodulations. Therefore, the amplitudes of all the repeated runs have been averaged to extract the MSB results with different water contents.

Figure 7-20 presents the average amplitudes at the first two components of the input shaft ($1x f_{r1}$, $2x f_{r1}$) under different operating conditions. It can be seen that the amplitudes are generally increased with water content for the most working conditions. The MSB results at the components of the intermediate shaft ($1x f_{r2}$, $2x f_{r2}$), which is the highest transmission shaft speed, are shown in Figure 7-21. The amplitudes are also increased with water content, however for the high speed the trends are fluctuating. This may be because the effect of sliding friction between the engaged gears is decreased with increasing the running speed.

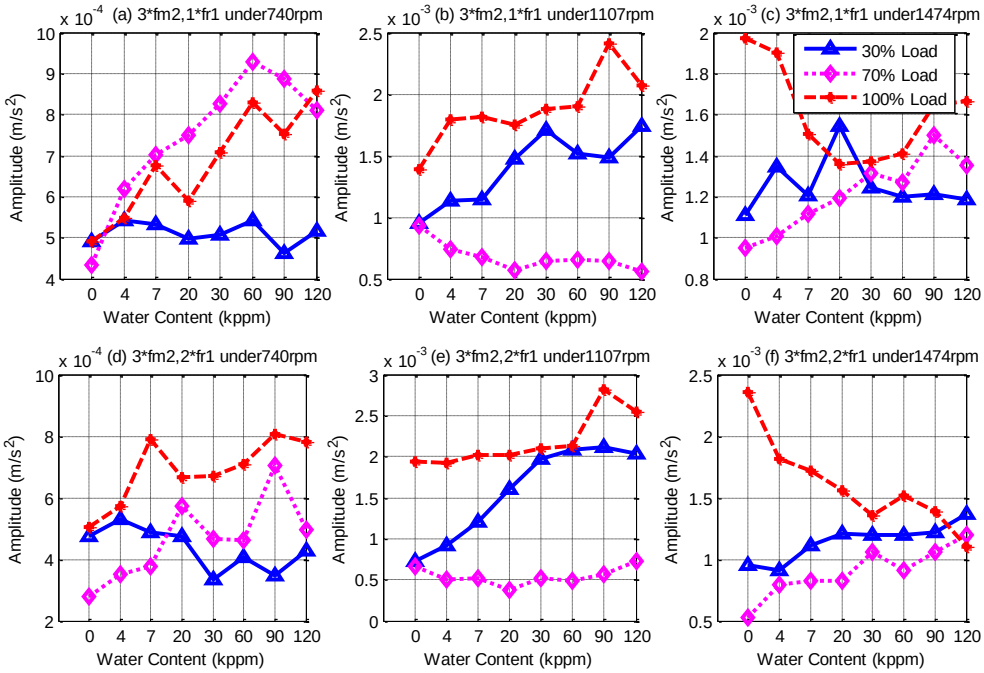

Figure 7-20 Average amplitudes of the input shaft components under different operating conditions

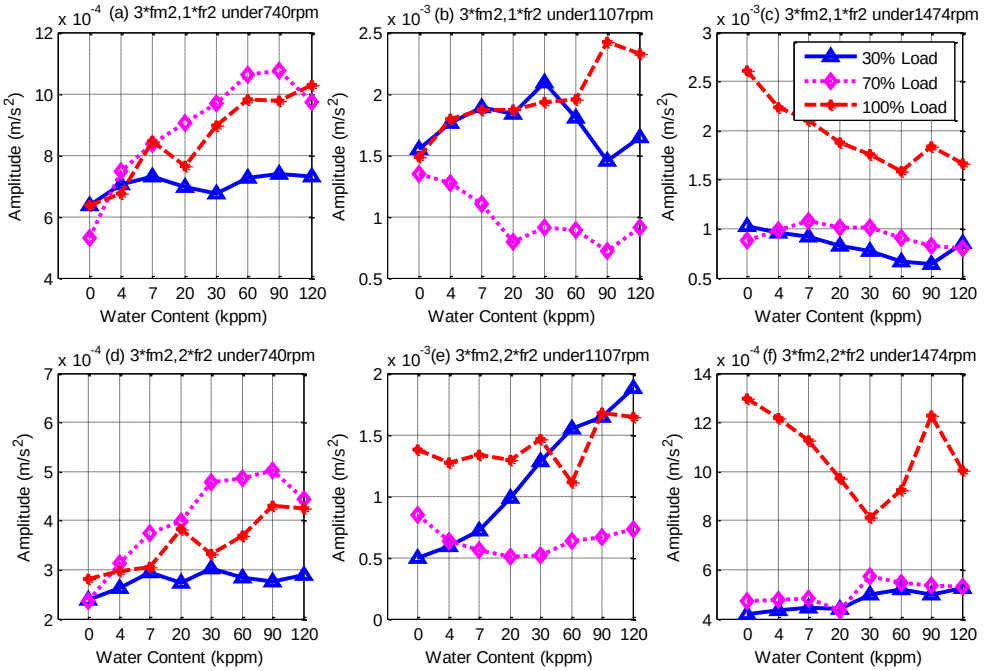

Figure 7-21 Average amplitudes of the second shaft components under different operating conditions

Similarly, the average MSB results at the components of the third shaft (1xf_{r3}, 2xf_{r3}), which is the lowest transmission shaft speed, are shown in Figure 7-22. It can be seen that the trend behaviours of the amplitudes are very close to the trends of 3xf_{m2}, which are generally

increased with water content and high influence of modulation at these components under different operating conditions. In which this feature can be also considered as effective indictors to the degradation of gear lubricant. However, under high load and high speed it is difficult to use these features for stable diagnostics of lubricant contaminations.

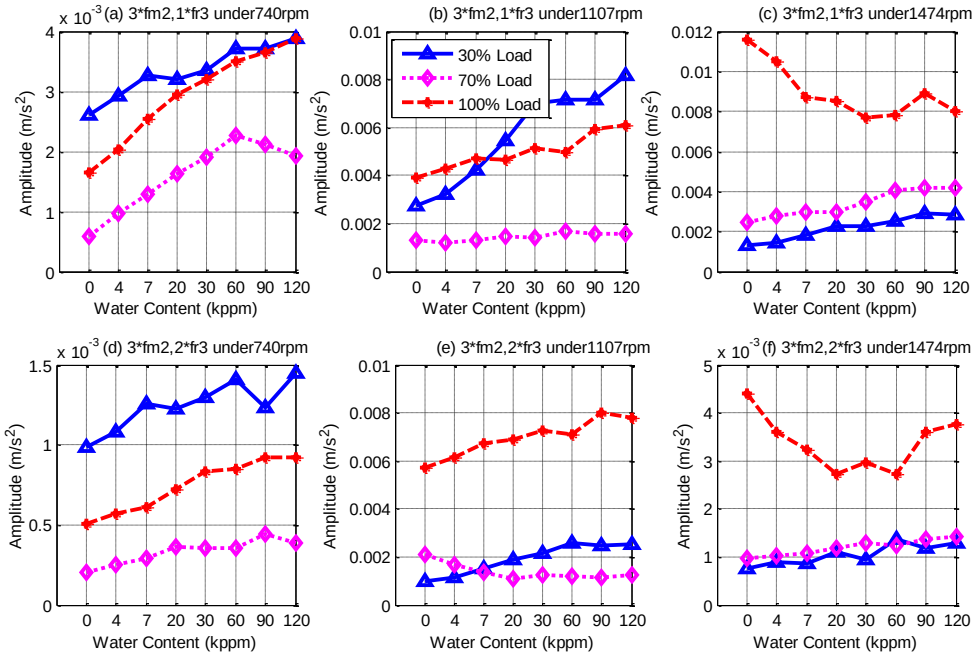

Figure 7-22 Average amplitudes of the third shaft components under different operating conditions

7.2.3 Monitoring of Oil Viscosity

Since, viscosity is an important performance parameter of lubrication that commonly used as the mean factor for oil quality. It can generally increase due to lubricant oxidation and degradation or contamination with water, dust etc. Therefore, this study emphasises lubricant viscosity to get an effective relationship between lubricant problems and other aspects. The aims of this test is to investigate whether the viscosity has any effects on both power supply parameters and vibration signals of the gearboxes; this will help confirming the pervious stage of this study, whereby different oil contaminations with water show significant increase in viscosity.

Different pure oils with significant viscosity change, as illustrated in Table (4.1), have been used to investigate the effect of viscosity on gearbox dynamic behaviour. The viscosity was measured using a rotary viscometer test method to get the absolute dynamic viscosity of

each type of oil. The dynamic viscosity was measured at a wide range of temperature, as shown in Figure 7-23, whereas the viscosity is generally decreased with the temperature.

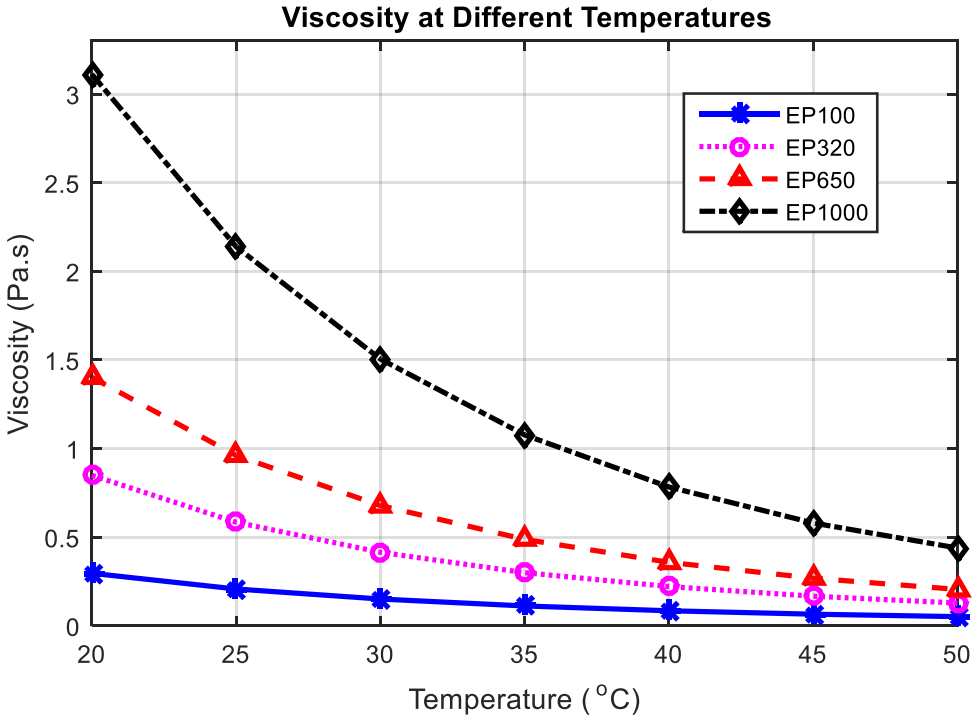

Figure 7-23 Dynamic viscosity at different temperatures

7.2.3.1 *Effect of Oil Viscosity on Vibration Level*

RMS can be used to measure the vibration level of each gearbox, as shown in Figure 7-24. It can be seen that the vibration levels of both gearboxes are generally increased with increasing oil temperature (repeated runs). The most interesting point is that the RMS results of the recommended oil (EP320) shows the lowest vibration level for all the datasets and the vibration levels of the GB2 are almost the same.

Several studies show that oil properties considerably affect the gearbox performance due to the change of oil film thickness, oil churning and splashing [275]. The proper industrial gear lubricant is important for long-term and efficient operation. According to AGMA 9005-E02, the choice of the appropriate lubricant depends on matching its properties to the particular application. In which, the viscosity grade must be selected based on the lowest and highest operating and/or ambient temperature experienced [168].

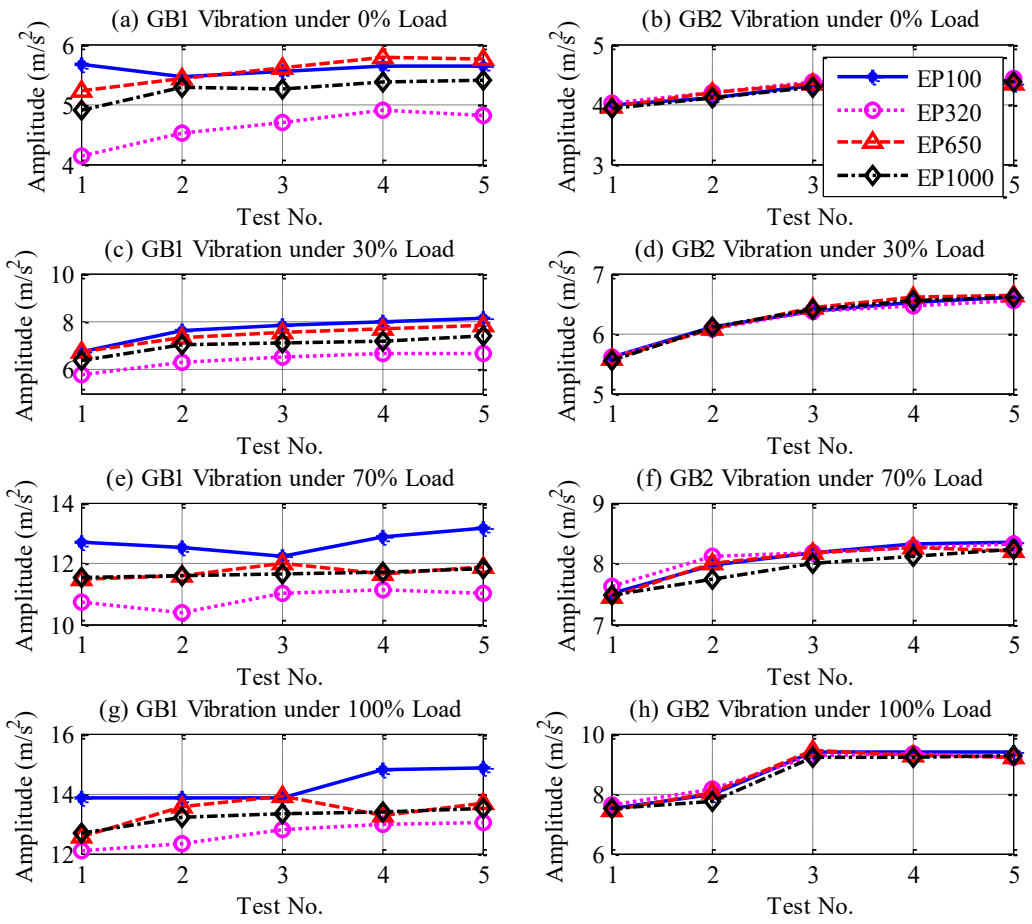

Figure 7-24 RMS vibration signals of the two gearboxes

The viscosity grade selection is based upon the industrial gear drive's horsepower rating, reduction ratio, the speed of the gear drive and the type of lubrication method used to lubricate the gears. An empirical formula for determining the required viscosity have been detailed by J.R. Davis (2005) [170]:

$$v_{40} = \frac{7000}{V^{0.5}} \tag{7.5}$$

Where, υ_{40} is the lubricant kinematic viscosity at 40 °C (105 °F) (in cSt) and V is the operating pitch line velocity (in ft/min) given by:

$$V = 0.262\, d.N \tag{7.6}$$

Where d is the operating pitch diameter of pinion (in inches) and N is the pinion speed (rev/min). According to the previous equations, the required kinematic-viscosity levels in gearboxes application could be designed and selected, which gives kinematic viscosity about v_{40}=322 cst and the ISO the recommended viscosity grade for this value is ISO VG 320 as established by BS 4231:1992 and ISO 3448:1992 [171].

7.2.3.2 *Effect of Oil Viscosity*

The selection of oil viscosity is also based upon the type of lubrication method, the lowest and highest operating and/or ambient temperature. In which, the higher the speed of the gear drive, the lighter the viscosities need to be [168]. Lubricating oil has a great role in reducing friction at the contact surfaces. Hence, studying oil viscosity change can assess the quality and life time of the lubricant.

Figure 7-25 shows the gearbox oil temperature during five repeated tests under full speed and different loads, which refers to an increase in oil temperature with increasing oil viscosity. In which, high viscous lubricant generates more heat from the internal fluid friction, and may also consume more power to turn the gears. The oil temperature increase significantly with the change of viscosity. This could be due to higher kinetic friction energy between the oil and wetted surface area of the gears as well as the thicker gear lubes have greater internal resistance (intra-fluid friction), which causes them to run hotter [276, 277].

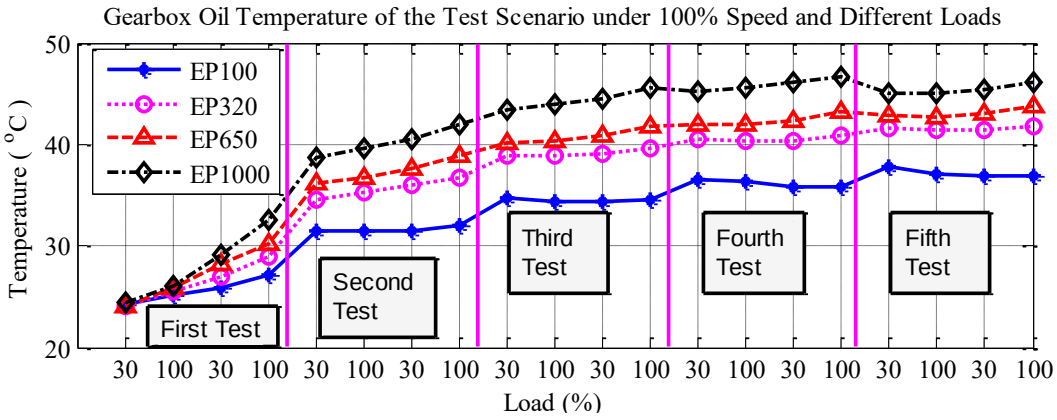

Figure 7-25 Gearbox oil temperature for different oil viscosities

Figure 7-26 shows the effects of different oil viscosity on the consuming power of the driving motor under different operating conditions. It can be seen that generally thicker lubricant needs more input power to run at the interest speed.

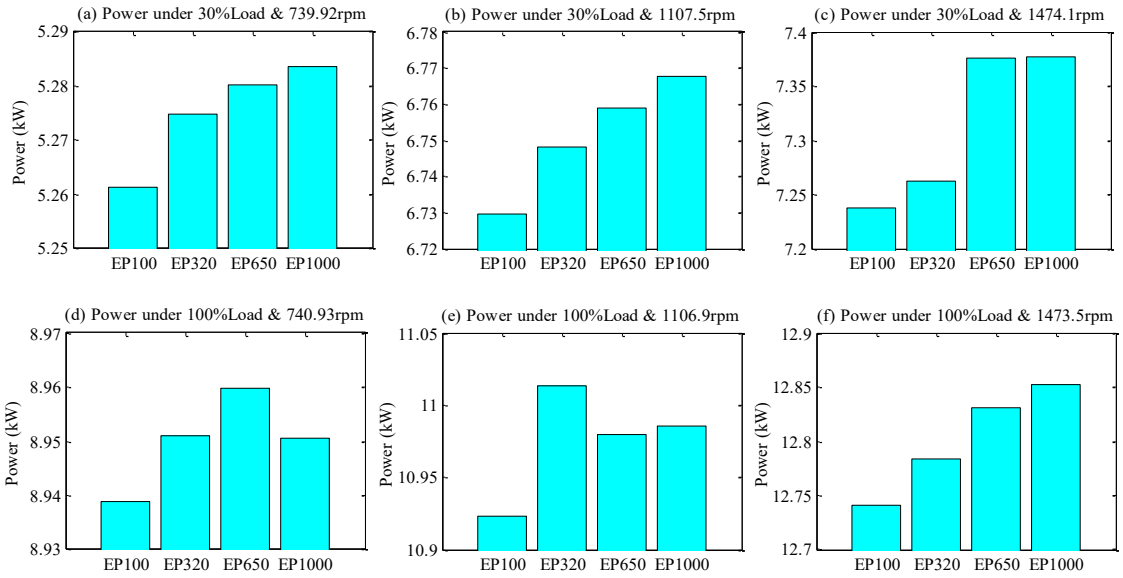

Figure 7-26 Power supply under different speeds and loads

7.2.3.3 MSB Characteristics at Mesh Frequency

Figure 7-27 and Figure 7-28 show the MSB results with its bifrequency of f_{m1} and f_{m2} components, respectively. For clearness and further analysis, the bifrequency axis is labelled the characteristic frequencies: 1xf_{r1}=25Hz, 1xf_{r2}=30Hz, 1xf_{r3}=6.7Hz. The MSB-magnitude and its corresponding MSBC results are presented in the region f_r < 70 Hz to include the sidebands up to 2f_{r2} (61 Hz) and f_m < 4400 Hz to include the carrier frequency up to 3f_{m1} (4275.1 Hz).

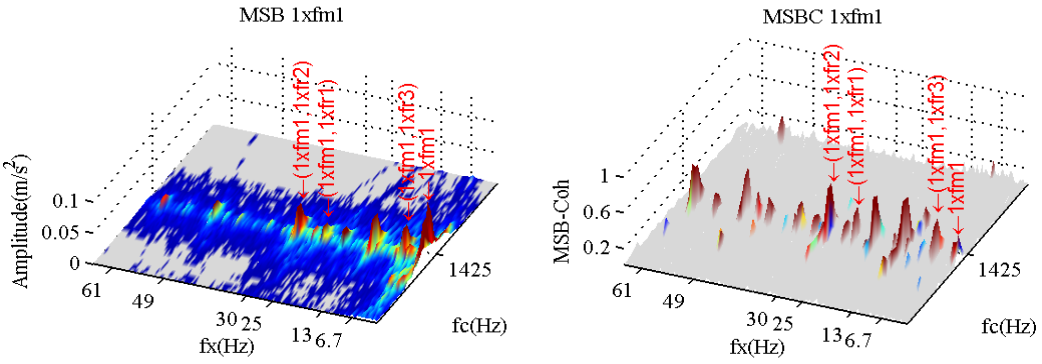

Figure 7-27 The components of f_{m1} at high speed

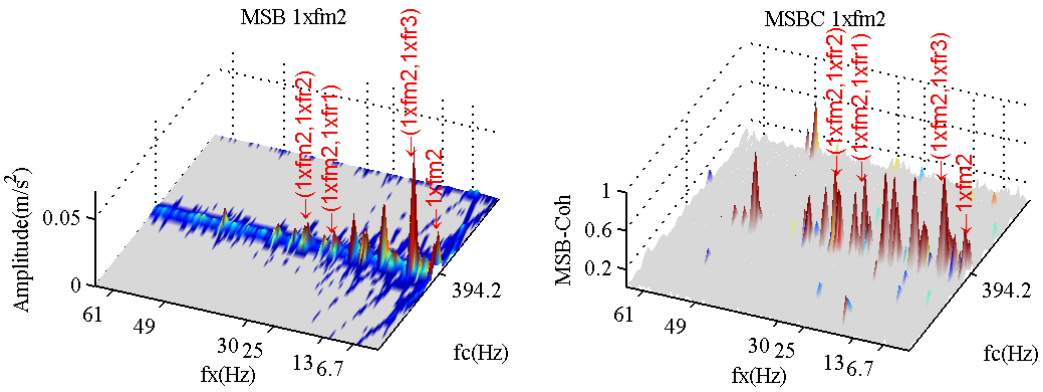

Figure 7-28 The components of f_{m2} at high speed

The MSB magnitudes of the mesh frequency components are significant as confirmed by the sufficiently high amplitudes of MSB coherence at corresponding frequencies. Figure 7-29 shows the averaged amplitudes of the last three runs at the f_{m1} components under different operating conditions. The MSB results are almost the same, however there are some increase in the amplitude of f_{m1} at 1107rpm (75% of full speed), especially under high load. As a consequence, the gear vibration characteristics are mainly changed based on the oil viscosity and the operating conditions.

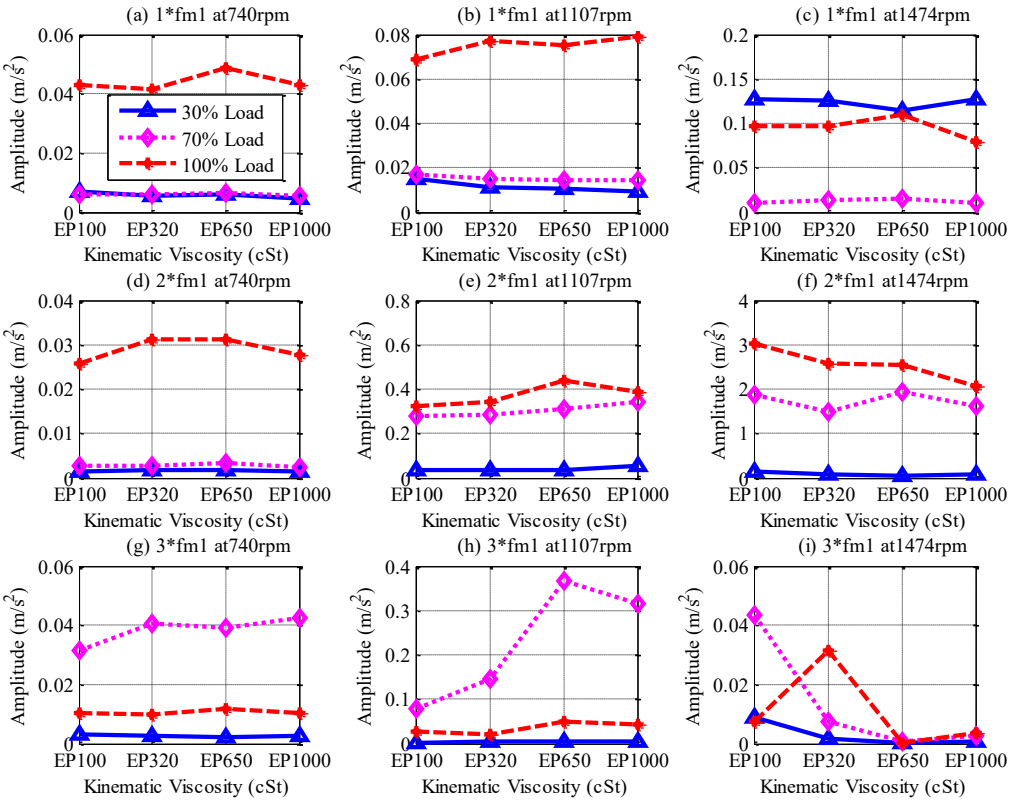

Figure 7-29 Average amplitudes of the f_{m1} components

Similarly, the MSB magnitude at the harmonics of f_{m2} are illustrated in Figure 7-30. As this stage is fully submerged in oil, the first harmonic 1x f_{m2} shows significant change with the oil viscosity at high speed rotation, and its components could be good indicators to lubricant viscosity. This change may be because of thicker lubricant increases the oil film thickness and internal fluid friction [278], whereby the influence is clear within the fully submerged stage.

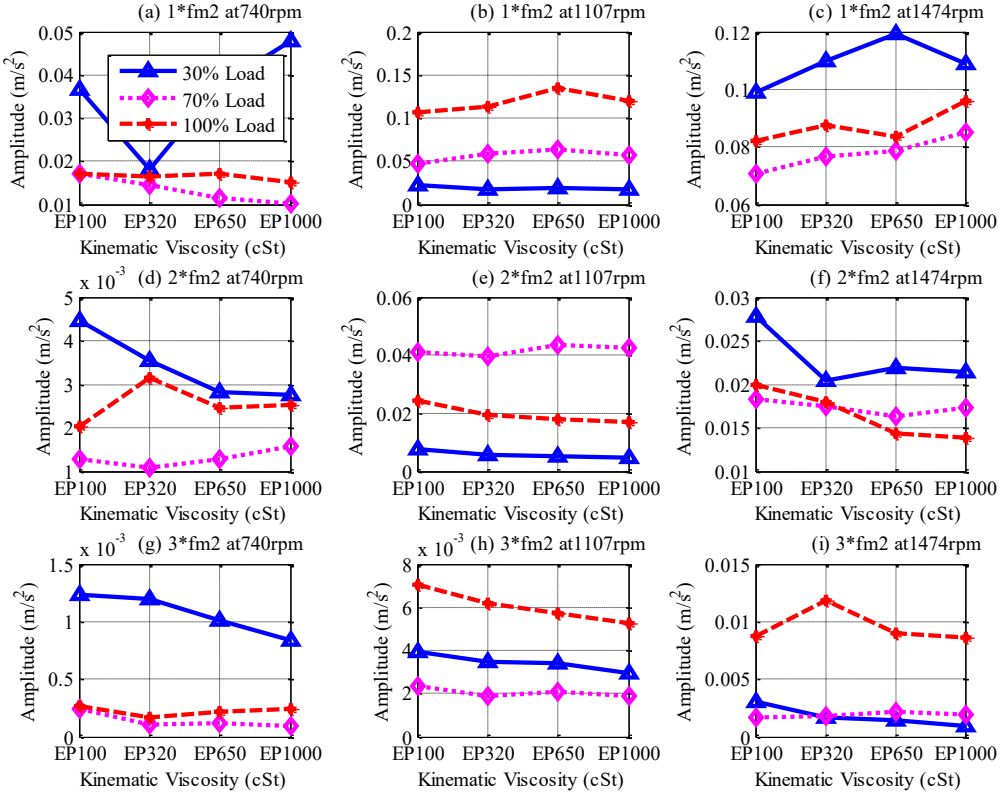

Figure 7-30 Average amplitudes of the f_{m2} components

7.2.3.4 MSB Characteristics of Mesh Components

The magnitude of each mesh component slice can be extracted by a simple search of the peak value around the corresponding mesh frequencies in the MSB results. To identify the associated components of gear mesh frequency, Figure 7-31 to Figure 7-33 depict the averaged slice magnitude of the last three tests at each component around the first mesh frequency. The most consistent results can be identified at (1xf_{m1}, 1xf_{r1}) under high speed condition. However, Figure 7-32 shows that the second shaft slices (1xf_{m1}, 1xf_{r2}) are generally decrease with increasing oil viscosity, due to increase of damping effects between the meshing gears.

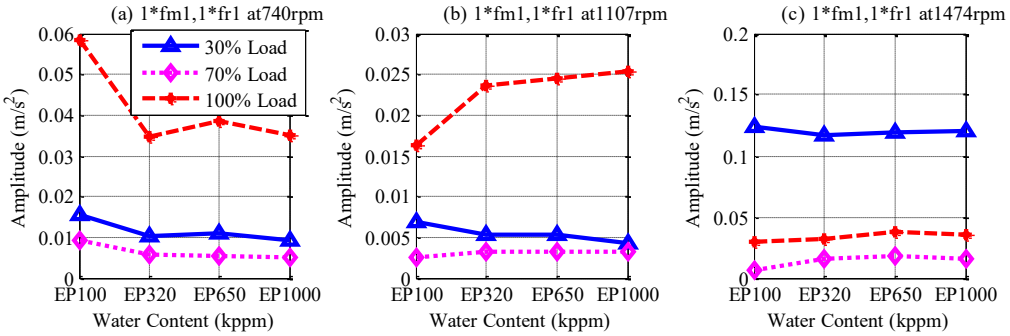

Figure 7-31 MSB peaks at f_{r1} of f_{m1} slice

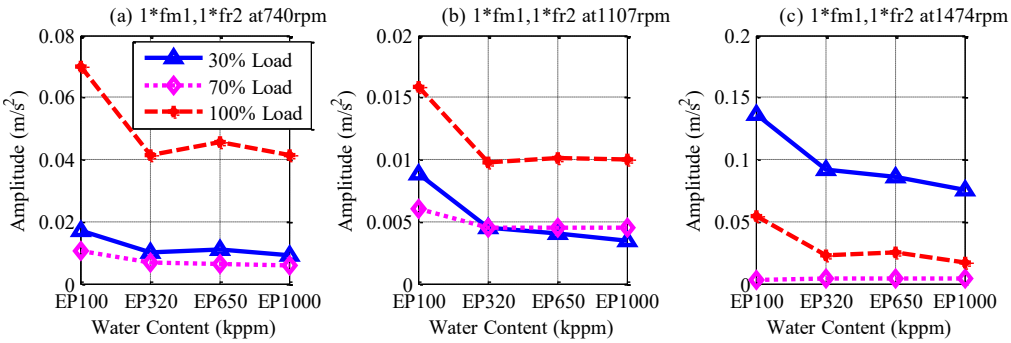

Figure 7-32 MSB peaks at f_{r2} of f_{m1} slice

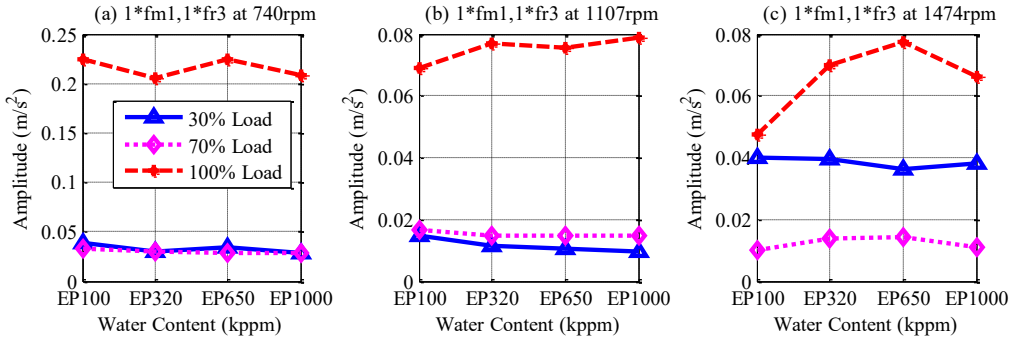

Figure 7-33 MSB peaks at f_{r3} of f_{m1} slice

In the same way, as the first harmonic of the fully submerged stage (1*f_{m2}) shows more beneficial trends than the other harmonics, the slice peaks have been examined to extract the usefulness of these sidebands in diagnosing. Figure 7-34 depicts the average magnitude of the last three runs at the slice (1xf_{m2}, 1xf_{r1}), in which the higher load show more consist increase patterns under different operating conditions.

Figure 7-35 illustrates the average magnitude at the slice (1xf_{m2}, 1xf_{r2}), whereas the second shaft (f_{r2}) is the highest shaft speed inside the gearbox and it fully submerged with oil. The

MSB magnitudes at this slice show some increase with the oil viscosity change but not in constant trends.

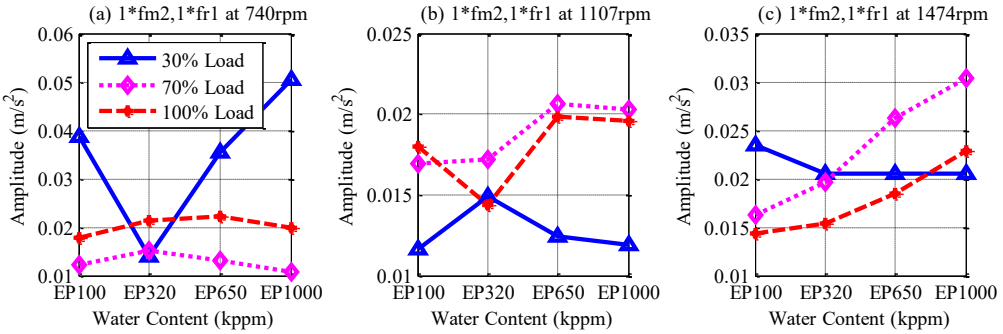

Figure 7-34 MSB peaks at f_{r3} of f_{m2} slice

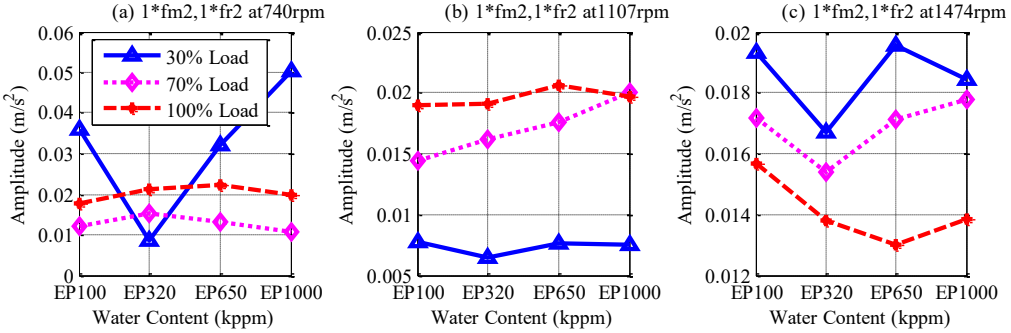

Figure 7-35 MSB peaks at f_{r2} of f_{m2} slice

Figure 7-36 depicts that the most useful information for diagnosing the change of oil viscosity is at slice (1xf_{m2}, 1xf_{r3}), whereas the third shaft (f_{r3}) is the lowest shaft speed in the gearbox. It can be seen that the trend behaviours of this slice magnitudes are generally increased with increasing oil viscosity, which can be considered as an effective indictor to the gear lubricant viscosity.

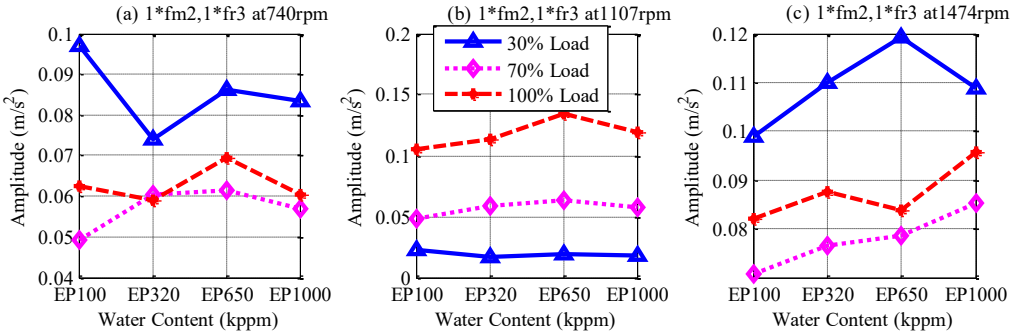

Figure 7-36 MSB peaks at f_{r3} of f_{m2} slice

7.3 Key Findings

- Very few works examine the possibility of employing vibration analysis for monitoring the health condition of lubrication in machinery.
- Lubricant failure causes equipment failure and vice-versa, in which different gear failure modes are strongly correlated with lubricant condition.
- Insufficient lubrication or loss of lubricant could produce severe metal-to-metal contact, which should generate high levels of stress pulses and would be detected immediately by accelerometer.
- Power losses such as squeezing, splashing and ventilation losses can be reduced by lowering the oil volume, however higher contact friction, higher gear bulk temperature and lower load carrying capacity are intensely expected.
- After extended running, low oil service result in more friction and more nonlinear vibrations due to breakdown the oil film, which raise the vibration level and can produce reliable information in the technical diagnostics.
- TSA has the inherent capability for pre-noise reduction, which can be implemented reliably to detect and diagnose the oil service level based on vibration signal analysis.
- Gearbox vibration signature changes significantly with lubricant starvation, in which under high transmission load, both meshing frequency and sideband components can be considered as effective measurements to recognize and perform the instant diagnosis of gearbox lubrication capacity.
- The second harmonic of the mesh frequency and its sideband components provide good indication to diagnose lubricant starvations due to the double change in the reversal friction force at the pitch point or/and the dual fluctuation of sliding velocity during the gear mesh process.
- Effective condition monitoring of lubrication can also be implemented to ensure that lubricant has retained its physical characteristics, and it has not degraded by external contaminants.

- Water is one of the most significant destructive contaminations to lubricants, which causes a degradation on its characteristics and leads to undesirable mechanical effects.
- Oil viscosity is generally increased with the interaction extend of the water droplets, whereby the physical characteristics of the oil are changed.
- The higher temperature corresponds to lower viscosity and increased the solubility of dissolved water in oil.
- Water contaminations can lead to significant mechanical effects and complicated nonlinear vibrations, which resulting in a modulation phenomenon in vibration signals, therefore an effective demodulation method such as MSB, is required to decompose the nonlinear modulation components and suppress the noise background.
- Based on effective demodulation of the mesh frequency components, the third harmonic and its sidebands can produce useful information for assisting and diagnosing water contamination.
- Water contamination and the oil viscosity change have significant effect on the fully submerged gear mesh stage, while the splashed stage is the most affected by oil starvation.
- Studying oil viscosity change can utilise for oil quality and life time detection technique, in which higher viscous lubricant generates more heat from the internal resistance fluid friction and higher kinetic friction energy between the oil and the wetted surface area of the gears, which also consumes more power to turn the gears.
- The recommended oil for the general specification of gearbox transmission system typically displays the lowest vibration level under different operating conditions.
- The gear vibration characteristics are typically changed based on the variation of oil viscosity and the operating conditions, whereas MSB can extract useful diagnostic information from the slice peaks of the meshing frequency components.
- MSB results can extract a useful information for diagnosing the oil viscosity change based on the amplitudes of the first harmonic of the meshing frequency and its sidebands.

- The first mesh harmonic of the fully submerged gear mesh stage belong with their slice components, shows consistent trends with oil viscosity change and can be considered to be effective indictors to the gear lubricant viscosity.
- Higher nonlinear influences of gear dynamics are resulting from the complex nonlinear interactions of dynamic forces, friction forces and the nonlinearity of oil splashing and squeezing, which mainly change based on and the lubrication statues and the operating conditions.
- Vibration signal needs an effective signal processing method to suppress the noise background and extract effective diagnostic information for monitoring gearbox lubrication condition.

Chapter 8

Diagnosis of Increased Bearing Clearances based on MSB Analysis

This chapter examines the process of detecting and diagnosing excessive bearing clearance which is due to inevitable wear as a result of long term gear operation and abnormal lubricating. The MSB analysis is applied to the vibration signals acquired at three bearings with different clearance values to suppress noise and enhance the modulation effects at the first few mesh components to find consistent changes of vibrations with increasing bearing clearances and thereby to achieve early detecting and diagnosing the gear mesh conditions.

8.1 Introduction

As gears and bearings are used in almost every industrial right, and often work under very severe environments, vibration and noise remain the main source of intense annoyance and have strong influence of instabilities on the overall dynamic systems. Thus, monitoring these components has received significant attentions in recent years. Bearing is important element in rotating machine that support the rotating components such as gear shafts. Abnormal radial clearance in bearing are inevitable phenomena that occur due to assemblage and manufacturing errors [279]. Especially gradual wear that is from the unavoidable light material removals due to fatigue wear and contaminated lubricant, as a result the dynamics of the gears vary with its lifetime.

Therefore, it is important to have an appreciation for understanding the dynamic effect of different clearances on the characteristic vibration features, thereby achieving an early and accurate fault-detection and diagnosis. The objective of this chapter is to study the effect of bearing wear based on its clearance variations on the characteristics of helical gear vibration. This will assess the performance of vibration features in diagnosing wear instabilities, in which there was no experimental result to verify the analytical result of this research.

8.2 Test Procedure

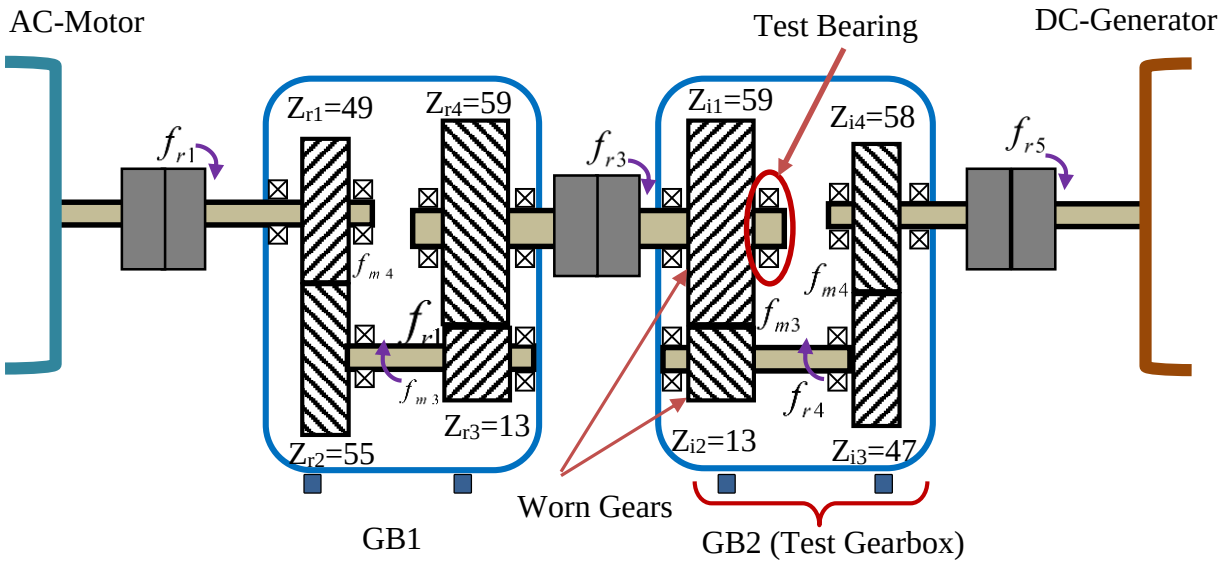

Figure 8-1 Schematic diagram of gear wear test

To benchmark the performance of gear vibration based on the run-to-failure gear wear test (explained in Sec. 6.7), three bearing with different standard clearances have been used under the same conditions. The vibration signal was collected using one accelerometer mounted on the gearbox casing close to the worn gears to reduce the vibration influences of the other parts and the attenuation of the transition paths. Figure 8-1 depicts the tested bearing and the parameter scheme of the test rig, which are detailed in Sec. 6.7.

In general, clearance between contact surfaces become gradually larger due to inevitable wear, in which the contact gapping is expected. Because of the lack of information on the effect of bearing clearance on the gear dynamic response, different bearing clearances have been used to verify the effect of clearance on the performance of gear wear. A tested ball bearing 6207 mounted to the first stage shaft of the GB2 was changed with different clearance sizes as illustrated in Table 8-1.

Table 8-1 Bearing types

Bearing 6207	**Clearance**
C2	0.006 mm
C3 (Recommended/Healthy)	0.028 mm
C5	0.051 mm

The test rig was run under different operating conditions, in which each bearing test was repeated three-times and saved the data in the same sequence. Figure 8-2 shows the clearance (C) between the inner race, ball and outer race of the bearing.

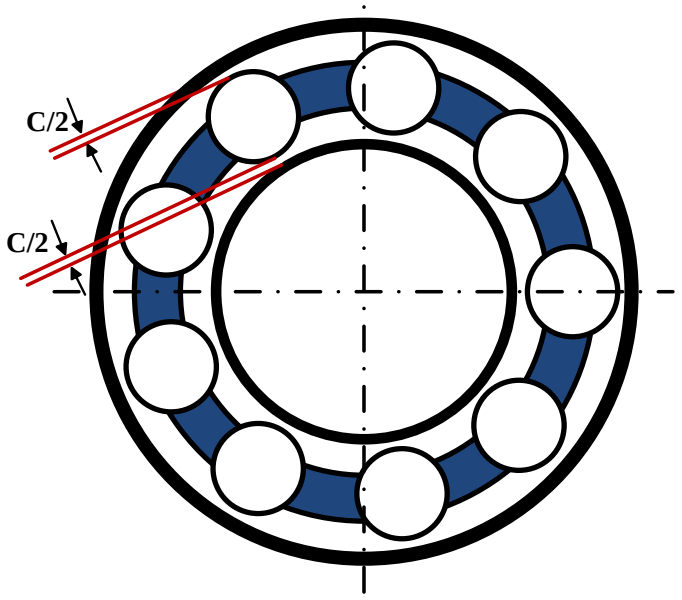

Figure 8-2 Rolling bearing scheme

8.3 Effect of Bearing Clearance

Bearing clearance has a significant effect on the thermal, vibration, noise and fatigue life of the bearing [280]. The internal clearance must be as close to zero as possible during its operating in order to extend the bearing's lifetime and improve the machine's reliability [281]. However, clearances in the shaft-bearing system may be either designed to provide better lubrication and eliminate interferences or due to manufacturing errors and/or inevitable wear [282]. An increase in the clearance size result in severe vibrations of rotating machinery, and consequently degrade the system performance.

Excessive clearance introduces very strong nonlinearity and could be a source of high impact forces that result in wear and tear of the contact surfaces. Moreover, clearances induced transverse and torsional vibration may cause tooth separation, which could deteriorate the reliability and durability of the geared system [282].

8.4 MSB Implementation

For the motivation of MSB analysis to make a concise representation of the complicated modulation, it has been applied for detecting and diagnosing the nonlinearity effect of different bearing clearances. The properties of the bearing clearance vary due to wear of the contact surfaces over a long period of service time, which introduces strong nonlinearity effect and has a negative influence on the dynamic behaviour of the gear train system [112, 114]. The MSB representations are able to characterise the complicated modulation in signals, suppress noises and allow easy analysis to manipulate of characteristic features.

8.4.1 MSB Characteristics at Mesh Frequency

Existing studies have stated that the first three gear meshing harmonics and their sidebands provide sufficient information for the successful identification of gear faults [143]. In addition, the amplitude of higher order gear mesh harmonics introduce useful and reliable information in detecting wear at its early stage [283, 284]. In order to evaluate the performance of the MSB approach in monitoring excessive bearing clearances and the gear wear progression, the recorded vibration data were processed using MSB method with effective averaging data length and 70% overlap ratio between successive data frame.

The MSB analysis was performed on the gearbox vibration signals to extract the characteristic information of the gear meshing harmonics and their sideband components. Figure (8-3) shows the MSB amplitudes at the first mesh frequency (f_{m3}) components, of

the GB2. It can be seen that excessive bearing clearance has significant effects on the first and third harmonics of the gear mesh frequency, especially under higher load conditions. This could be because excessive clearance result in large impact forces between the rolling elements, which can cause severe vibration at the fundamental mesh frequency. Moreover, the second stage meshing components behave almost consistently with the clearance variations because the tested bearing is used to support the gear shaft of the first stage, as illustrated in Figure (8-1).

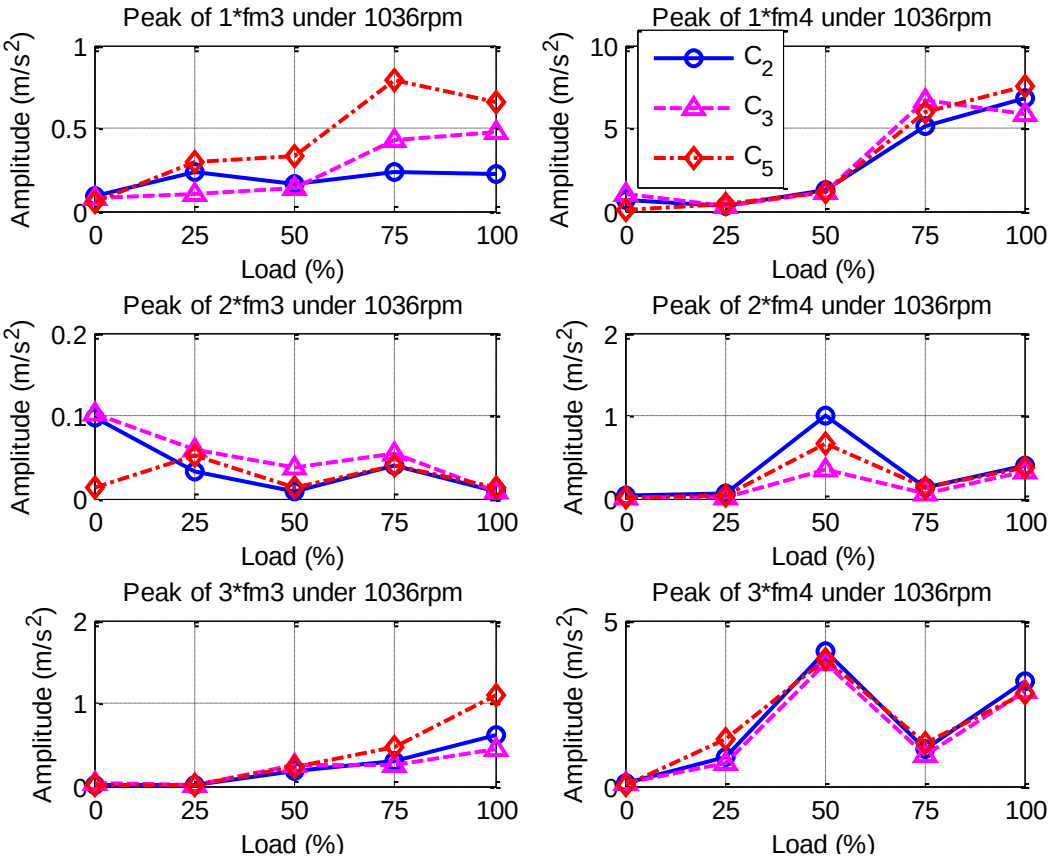

Figure 8-3 Average amplitudes of the mesh frequency components

As the f_{m3} harmonics are the most influential feature due to the bearing clearance changes, the MSB analysis was performed to reveal the modulated components with the rotational frequencies. Figure 8-4 depicts the MSB result of the f_{m3} components with their modulated sidebands and the related coherence signals. In the graphs, the significant peaks can be identified at the harmonics of the shaft frequencies, in which the bifrequency axis is labelled with the first two harmonics (i=1, 2) of the characteristic shaft frequencies: ixf_{r3}, ixf_{r4}, ixf_{r5}. The MSB-magnitude and its corresponding MSBC results are presented in the region f_r < 40 Hz to include the sidebands up to 2xf_{r4} (31 Hz) and f_m< 6100 Hz to include the carrier frequency up to 3xf_m (599.1 Hz).

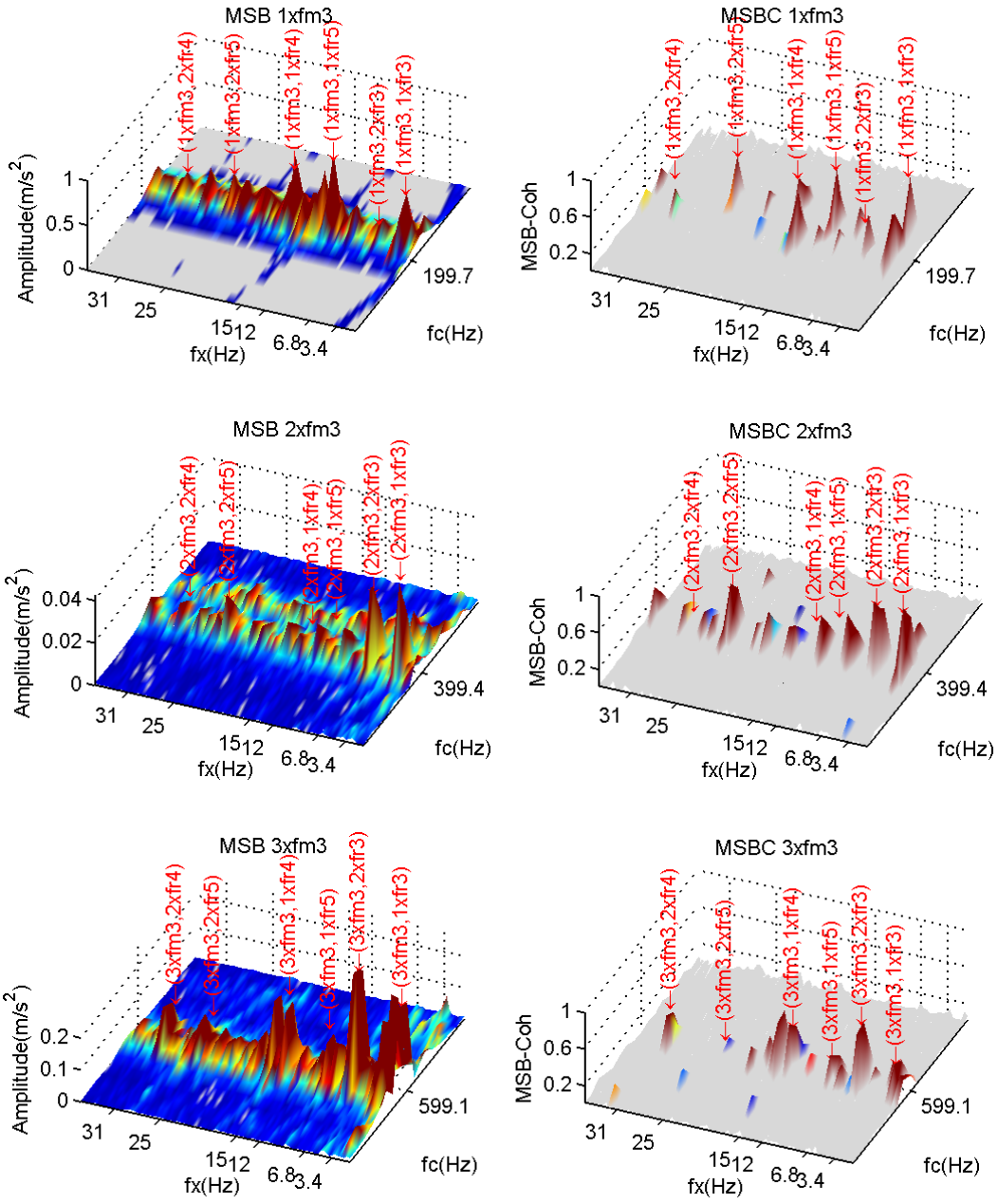

Figure 8-4 MSB results of the first 3-harmonics of *fm3* at 1037 rpm

8.4.2 MSB Characteristics of Mesh Components

For a concise representation of the complicated modulation spectrum, the sideband frequencies around the f_{m3} components have been examined to monitor the change in bearing clearance. The peaks of MSB at the bifrequency sidebands have been proposed to assess the effect of clearance changes on the characteristics of the gear vibration signature. To identify the associated peaks of the three shaft frequency components with f_{m3}, Figure 8-5 to Figure 8.7 depicts the averaged slice magnitude of the three repeated tests.

As the components of first shaft frequency ($1xf_{r3}$, $2xf_{r3}$) have significant bifrequency peaks, Figure 8-5 shows the peak magnitudes of various bearing clearances under different operating loads. It can be seen that the bifrequency peaks of f_{r3} components with $1xf_{m3}$ and $3xf_{m3}$ show a good indication for the clearance variations, in which the C5-bearing exhibits as the highest amplitudes under different loaded conditions.

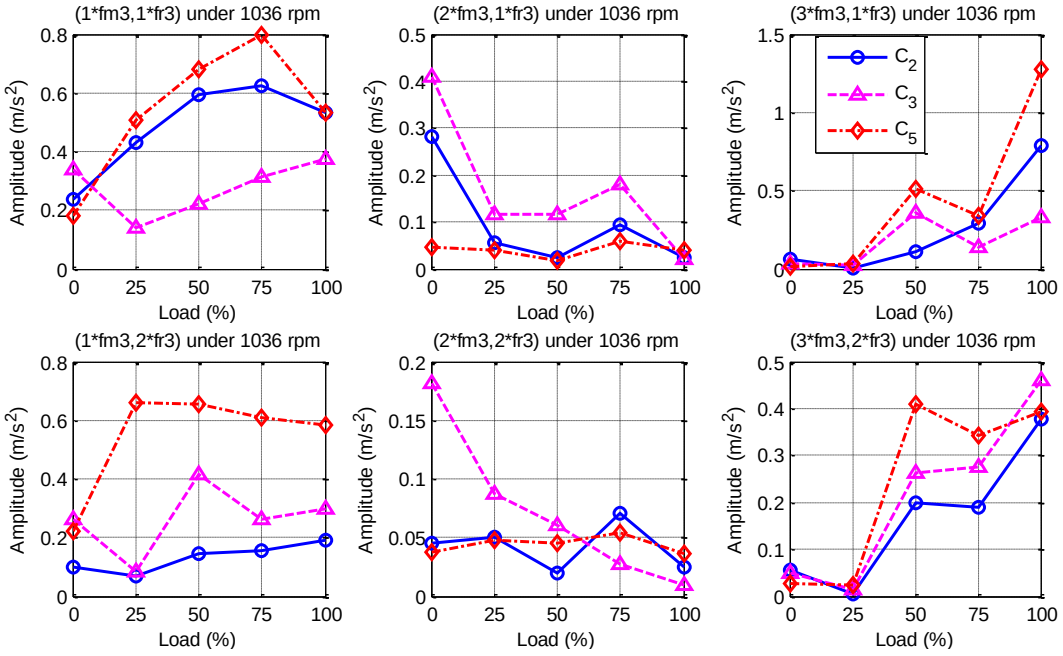

Figure 8-5 MSB peaks at f_{r3} components of f_{m3} slice

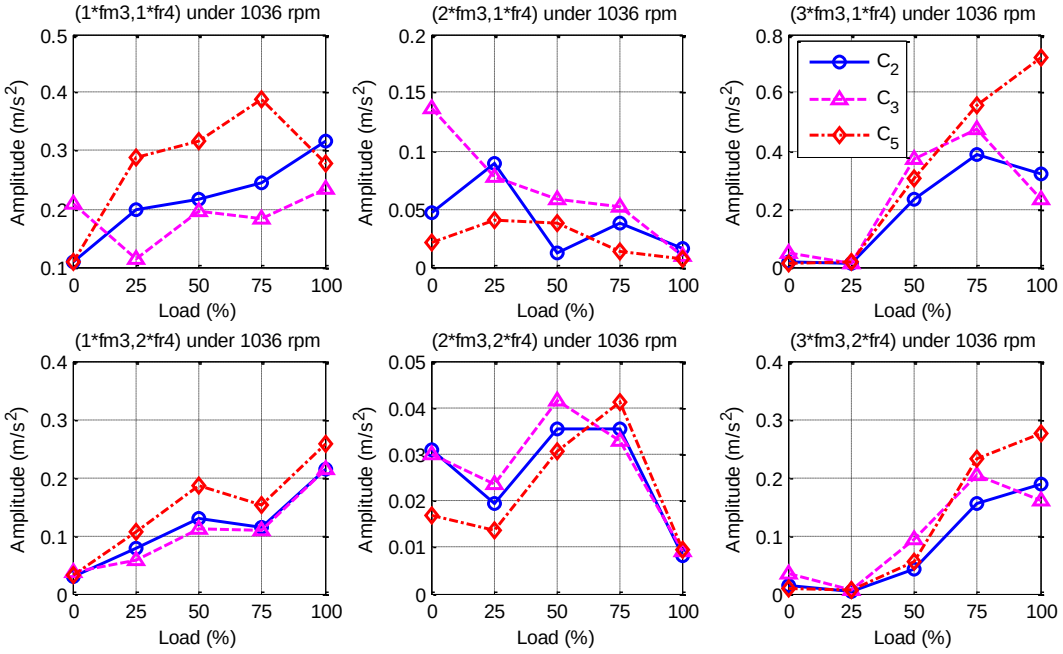

Figure 8-6 MSB peaks at f_{r4} components of f_{m3} slice

In addition, Figure 8-6 depicts the peaks of the magnitude at the bifrequency of f_{r4} components with the first three f_{m3} harmonics. Generally, the bifrequency peaks around the 1xf_{m3} and 3xf_{m3} give a good indication to the bearing clearance and can be considered as an effective indicator to the excessive clearance.

The excessive bearing clearance has strong nonlinearity effect in the dynamic behaviour of the gear system. Figure 8-7 shows the bifrequency of the f_{r5} components, which have the most influential peaks with the bearing clearances, especially around the 1xf_{m3} and 3xf_{m3}, whereas the peaks of the recommended bearing (C3) are almost the lowest under high loads. In general, these bispectral peaks show that MSB analysis of gearbox vibration signal can reveal the nonlinear interaction between the gear mesh frequency and the modulated components of the shaft frequencies. These can be used to monitor and diagnose the inevitable wear that leads to excessive clearances in the ball bearing.

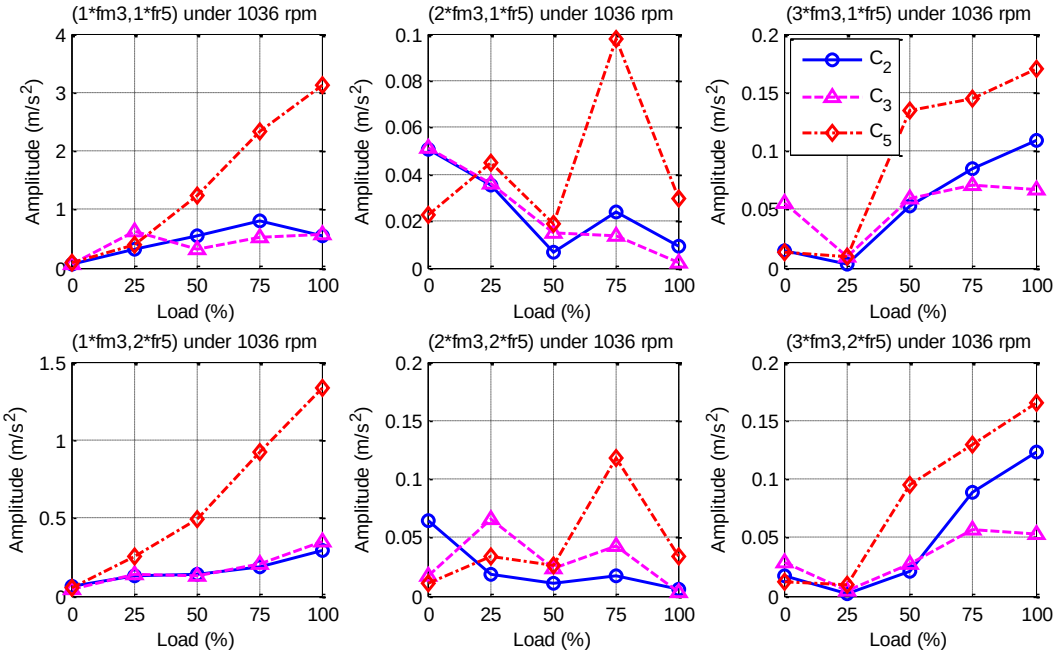

Figure 8-7 MSB peaks at f_{r5} components of f_{m3} slice

8.5 Key Findings

- Because of the lack of information on the effect of bearing clearance on the gear dynamic response, study the combination of gear wear with excessive bearing clearances is important to assess the performance of gear dynamics in diagnosing the wear instabilities in gears.

- Bearing clearance is varied and become gradually larger based on its life time, which leads to higher contact gapping and introduces strong nonlinearity effect in the dynamic behaviour of the system.
- Excessive clearance due to wear can be a source of impact forces, which induce more transverse and torsional vibration, and consequently degrade the system performance.
- The bearing clearance variation influence the dynamic characteristics of the supported meshing gears and cause strong nonlinearity effects on their dynamic behaviour.
- The MSB representations are able to characterise the complicated modulation due to bearing clearance change and allow easy analysis to manipulate of characteristic features.
- Excessive bearing clearance has significant influences on the 1^{st} and 3^{rd} harmonics of the gear mesh frequency, especially under high load conditions.
- Most of the bifrequency peaks around the 1^{st} and 3^{rd} mesh frequency could give a good indication to the change of bearing clearance and can be considered as an effective detectors of excessive clearance.

Chapter 9

Conclusions and Future Work

This chapter summarises the main conclusions of this research. It explains the key achievements in the light of the original objectives stated in Chapter 1. Next there is a summary of the author's contributions to knowledge and the novel aspects of the research. Finally, future research avenues in online condition monitoring of gear transmission systems are recommended for further improvement of the schemes developed in this thesis.

9.1 Objectives and Achievements

The purpose of this study was to investigate dynamic interactions within a gearbox and develop an improved numerical model to assist the reliable condition monitoring and fault diagnostics of helical gearboxes. A comprehensive dynamic model was developed with the inclusion of time-varying stiffness and tooth friction based on the elastohydrodynamic lubrication model, for validation with the experimental results, in which, successful diagnostic features of different gear faults can be identified under different operating conditions. The research has focused on using vibration signal monitoring to detect gearbox lubricant deterioration using effective signal processing techniques.

All the proposed objectives of this research have been fulfilled, and the key achievements corresponding to the objectives detailed in Sec. 1.7.2, are as follows:

Objective 1. To review existing condition monitoring techniques and assess the performance of the most common techniques used for online CM and early fault detection of gearboxes.

Achievement 1: An extensive concept review was conducted to assess the performance of the most common techniques used for online CM in terms of early gear fault detection and diagnosis, these were defined and discussed in Chapter 1. It was found that vibration analysis is the most reliable method for machine condition monitoring, detection and diagnosis, and is widely used in different industrial applications. It was decided to implement vibration signal monitoring in this study as an effective and reliable method for online health monitoring of gearbox mechanical components and to detect gearbox lubricant deterioration.

Objective 2. To review the main sources of gear vibration to obtain an in-depth understanding of the dynamic interactions between transmission components.

Achievement 2: Chapter 2 identifies the sources of gear vibration and noise, which provided an understanding of how to control the excessive vibration in gears and the need for intensive monitoring and diagnosis of gear faults in their early stages to improve working conditions and enhance the capability of the transmission system.

Objective 3. To design and construct a mechanical transmission test rig for the evaluation of a multistage gearbox transmission systems under different operating conditions, which allow different faults to be introduced into the gearbox components, enabling subsequent system behaviour to be characterised.

Achievement 3: Two test rigs have been developed to investigate different gear fault conditions. Chapter 4 describes in detail two industrial gearboxes installed back-to-back with piezoelectric accelerometers used to measure vibration signals, via a high-performance data acquisition system. The test rig could vary load and speed conditions imposed on the test gearbox. A run-to-failure test rig was designed and built for a more realistic approach so that the measured signals are closer to practical conditions, this is described in Chapter 6. It is similar to the previous test rig (back-to-back gearbox arrangement) with different design and control implications. Different operating conditions such as sinusoidal variable loads and different stepped loads were imposed on the system via a control system panel to better match the load variations likely to be found in different industrial applications, see Sec. 6.7.

Objective 4. To develop an accurate dynamic model using numerical simulation, and compute the periodic mesh stiffness variation of helical gears as a function of the contact position of the meshing teeth. Also, to characterise the vibration signature changes, enabling more reliable diagnostics under different operating conditions.

Achievement 4: A comprehensive dynamic model was developed in Chapter 5, to study the interaction of helical gear dynamic responses, with the inclusion of time-varying stiffness and tooth friction based on the EHL model. For the time-varying mesh stiffness of helical gears, a convenient and effective calculation was implemented, which included the total potential energy stored in the meshing teeth with the kinematic compatibility variation of the contact lines in the plane of action.

The model consists of an 18-DOF vibration system which incorporates the effects of the supporting bearings, driving motor and loading system. Moreover, it couples the transverse and torsional motions resulting from time-varying friction forces, time varying mesh stiffness excitations and different tooth surface defects. The model investigates the effect of different tooth surface defects on kinematic performance of the helical gears providing a demonstration and evaluation which assists condition monitoring assessment.

Objective 5. To calibrate the linear and nonlinear responses of the dynamic model and evaluate the model for different frictional modes with progressive tooth breakages.

Achievement 5: The linear and nonlinear responses of the dynamic model have been achieved numerically using MATLAB. The linear solution is based on the average variation of gear mesh stiffness, as described in Sec. 5.10.1. This allowed the modal

parameters to be determined such that the major resonances agreed with the real system, in which the resonance frequencies and damping ratios were found conveniently using the standard eigenvalue method. Subsequently, the non-linear effect of time-varying friction and mesh stiffness were introduced into the model and a numerical integration method based on the ordinary differential equation solver (ODE15s) was used to solve the model, as described in Sec. 5.10.2.

The accurate dynamic modelling of helical gear system is crucial to acquire reliable diagnostic features. Different tooth breakage severities were simulated numerically and experimentally, see Sec. 5.11, so that the model performance could be evaluated realistically. To increase the ability of conventional modelling of helical gear systems to provide more accurate diagnostic determinations, the model was developed to include different time-varying frictional models: friction-free, Coulomb friction and EHL. The results demonstrated that any analysis of vibration must take into account friction effects if it is to be an accurate method for the detection and diagnosis of different tooth defects. The vibration responses of the model were closest to the experimental test results when the EHL friction model was used, i.e. the influences of lubrication and surface roughness were included in the numerical model.

Objective 6. To develop an efficient computation and stable analysis of the dynamic responses of a tooth surface worn in a two-stage helical gearbox using a run-to failure experimental test and a comprehensive dynamic model including EHL friction effects.

Achievement 6: The experimental run-to-failure test applied variable sinusoidal and step increment loads combined with variable speeds, and gear wear was allowed to progress naturally, as explained in Sec. 6.7. A numerical model was developed to include the time-varying mesh stiffness and EHL friction model, with the tooth wear modelled by reduced mesh stiffness and increased frictional excitation, see Sec. 6.3 to Sec. 6.6. The comparison of the experimental and model-predicted results shows a high degree of correlation in trend behaviour.

The vibration response of both the experimental test and the numerical model showed that the 2^{nd} and 3^{rd} harmonics of the meshing frequency (and associated sideband frequencies) are influenced more significantly by increasing wear, and hence these components can be used as effective wear indicators for the detection and diagnosis of tooth surface deterioration.

Objective 7. To investigate nonlinearities in vibration transmission and viscoelastic properties of gearbox lubrication, and hence develop effective signal processing methods for online monitoring and diagnosis of different gearbox oil deterioration conditions under different gear operating conditions, and any constraints on its usage that should be considered.

Achievement 7: Effective signal processing methods based on vibration signal analysis, have been implemented to suppress background noise and identify stable diagnostic features from the complicated modulation components of the gearbox frequencies. Time Synchronous Averaging was used to detect and diagnose the oil service level because of its capability for noise reduction, as explained in Sec. 7.2.1. However, the diagnostics of water contamination and oil viscosity needed a more advanced and more effective method; MSB analysis has the capability to decompose the nonlinear components and suppress the noise background effectively, as detailed in Sec. 7.2.2 and Sec. 7.2.3.

Both TSA and MSB results show that the gearbox vibration signature changes significantly with lubricant deterioration, with a consistent increase in the amplitudes of vibration responses at meshing frequency harmonics and their associated sideband components. These changes demonstrate that the vibration signal can be considered a reliable condition indicator of gearbox lubrication. However, the vibration signal needs effective signal processing to suppress the noise background and to extract useful diagnostic information for monitoring the gearbox's lubrication condition.

Objective 8. To develop guidelines for future research activity relating to this field.

Achievement 8: Several suggestions for future research in the CM of helical gearboxes are presented in Sec. 9.5. A number of useful paths on condition monitoring of gear system are recommended for future work.

9.2 Conclusions

Based on the investigation described in the former chapters, the main conclusions of this thesis can be summarised to be:

1. A comprehensive dynamic model of the helical gear system is crucial for developing reliable diagnostics. It allows a detailed characterisation of vibrations corresponding to any small changes such as inadequate lubrication and light surface

wear and thereby provide a reliable basis for signal processing and diagnostic information retrieval.

2. The gear vibration model must take into account friction effects if it is to be an accurate method for the detection and diagnosis of tooth surface defects. As shown in this study, the frictional dynamics contribute significantly to the measured vibration response, especially the second harmonic of mesh components.
3. It is sufficiently accurate that a light wear prediction model for a helical gear has been developed by combining a translational-rotational nonlinear dynamic model with time-varying stiffness and tooth friction based on EHL principles. The tooth surface wear was represented by modulated mesh excitations and introduced into the dynamic model to reveal the effects of wear on the dynamic characteristics of a two-stage helical gearbox.
4. Based on vibration signals analysed by TSA analysis methods, the extracted mesh frequency components and the associated sidebands can provide useful information for detecting and diagnosing tooth surface wear. However, MSB analysis is more efficient in decomposing the complicated nonlinear components and suppressing the noise background more, though no additional equipment such as angular references for TSA is required.
5. The results presented in Chapter 7 have demonstrated the capability of vibration signatures for monitoring gearbox oil conditions. It is concluded that vibration analysis with advanced signal processing methods can be used to reliably reveal the subtle changes of the lubricants (with different viscosities, water in oil and oil starvation) and hence to detect gearbox lubricant deteriorations.
6. Vibration signal analysis with the help of MSB shows the ability to detect oil deterioration accurately, online and continuously, enabling optimum timely preventative maintenance. The MSB analysis can provide an accurate characterisation of the mesh frequency components and the associated shaft modulating components and consequently produce consistent diagnosis of lubricant status.
7. The MSB analysis of gearbox vibration signal has good detection capability to indicate the nonlinear behaviour of excessive bearing clearance due to inevitable wear, and enhances the modulation effects of the first few mesh components.

9.3 Novel Feature Summary

This research project presents a set of novel aspects that have not been considered by previous researchers. The following provides a summary of these novel aspects:

Novelty One: A dynamic model is developed to predict friction and wear influences on vibration response and thus to characterise diagnostic features. The author of the thesis found no research describing in any detail the vibration responses of a multistage helical gearbox transmission system with the inclusion of the friction and wear, for the identification and validation with the experimental results.

Novelty Two: This study, for the first time, bridges the gap between experimental tooth wear induced by a run-to failure test with nonlinear dynamic behaviour for a multistage helical gear system. Studying the gearbox vibration response from realistic validation data to accurately detect and diagnose gear wear in its early stage, has not been presented in previous research.

Novelty Three: The model responses at the meshing frequencies and their harmonics are shown to exhibit differences when friction is considered, enabling the theoretical investigation of the influences of lubrication and surface roughness. The vibration responses were closest to the experimental test results when the EHL friction model was included.

Novelty Four: This was one of the first studies to use vibration monitoring to detect gearbox lubricant deteriorations, and has shown vibration monitoring can be a cost-effective and reliable method for online health monitoring of gearbox lubricant condition.

Novelty Five: The detection and diagnosis of different gearbox oil deterioration conditions using the vibration signal in conjunction with MSB analysis method is entirely novel. The MSB results with coherence allow more reliable diagnostic results to be obtained, see Chapter 7.

Novelty Six: The author believes that, the implementation of MSB to evaluate the effect of unavoidable light material removals (excessive bearing clearance) on the gear dynamic behaviour has not been undertaken previously.

9.4 Contributions to Knowledge

This study has generated a number of new developments in the dynamic modelling of helical gear systems and the use of effective analysis of vibration signals to diagnose lubricant deteriorations in gearboxes.

The key contributions of this thesis are outlined below:

- **Contribution One:** Including friction effects increased the capability of conventional modelling of helical gear systems to provide a more reliable and accurate diagnostic tool.
- **Contribution Two:** The use of frequency, demodulation, and bispectrum analyses of gearbox vibration signal has proved to be adequate to provide useful information for condition monitoring of different gear lubricant deteriorations.
- **Contribution Three:** TSA has the inherent capability for pre-noise reduction, and can be implemented reliably to detect and diagnose gear lubricant starvation, in which the second harmonic of mesh frequency or/and its sideband components can be good indicator for lubricant shortfall.
- **Contribution Four:** Water contaminations change the physical characteristics of the oil and lead to complicated nonlinear interactions in gear dynamics, which resulting in angular modulations of multiple transmission stages. By decomposing the nonlinear modulation components, MSB results show that the third harmonic and its sidebands can produce useful information for assisting and diagnosing water contamination.
- **Contribution Five:** The lowest vibration level revealed from the recommended gearbox oil, and the first mesh harmonic with its modulated components shows consistent trends with oil viscosity change and can be considered to be effective indictors to the changes of gear lubricant viscosity.
- **Contribution Six:** Higher nonlinear influences in gear dynamics are mainly resulting from the complex nonlinear interactions of dynamic forces, friction forces and the nonlinearity of oil splashing and squeezing, which mainly change based on and the lubrication statues and the operating conditions.

9.5 Recommendations for Future Work

To develop early detection and accurate diagnosis of gearbox serving conditions based on online vibration measurements, further development study is needed for the detection of different types of faults with different levels of severity. Future studies should include three

categories: experimental investigations, signal processing and simulation models. The author suggests a number of recommendations for future research to enhance the condition monitoring and diagnostics of gear system components.

- **Recommendation One:** More experimental work with a test rig with additional load sensors to further investigate and evaluate the sensitivity and reliability of the proposed detection method. Different gear types with different degrees of fault severities need to be studied experimentally to assess the developed method.
- **Recommendation Two:** Online monitoring of various types of oil degradation needs to be investigated, and it is recommended to develop an algorithm for the detection of oil degradation scheme based on vibration signal analysis.
- **Recommendation Three:** To develop more advanced signal processing techniques for more robust and reliable feature development for monitoring gearbox components.
- **Recommendation Four:** For more realistic simulation, churning and windage effects in gear lubrication need to be included in the dynamic model. This can help to depict more accurately frictional effects on the diagnosis of incipient gear faults.
- **Recommendation Five:** Enhance the dynamic model to include different characteristics such as gear housing, backlash, manufacturing and other excitation errors, so that the input may include the tooth patterns, and different wear profiles can be simulated effectively.
- **Recommendation Five:** Develop the dynamic model to simulate the gearbox casting and the accelerometer components that may affect the transmission path of the gear meshing vibration signal. This can enhance the numerical model signal to extract more realistic vibration signal and be closer to the monitoring vibration that measured by accelerometer.
- **Recommendation Six:** Improve the dynamic model to include the characteristic of bearing components, so that a more realistic response can be acquired to diagnose the combined state of gears and bearings simultaneously.
- **Recommendation Seven:** Develop more accurate empirical formula to estimate the frictional variations on the numerical modelling of different gear types. In which, different operating conditions need to be included within the tribological theory of lubricating mechanisms in gearing.

Reference

1. Barron, D.R., *Engineering condition monitoring: practice, methods and applications*. 1996: Longman.

2. Dalpiaz, G., A. Rivola, and R. Rubini. *Gear fault monitoring: comparison of vibration analysis techniques*. in *Proc. of the 3rd Int. Conf. on Acoustical and Vibratory Surveillance Methods and Diagnostic Techniques*. 1998.

3. Davies, A., *Handbook of condition monitoring: techniques and methodology*. 2012: Springer Science & Business Media.

4. De Silva, C.W., *Vibration monitoring, testing, and instrumentation*. 2007, USA: CRC Press, Taylor & Francis Group.

5. Girdhar, P. and c. Scheffer, *Practical machinery vibration analysis and predictive maintenance*. 2004, Oxford: Newnes.

6. Nie, M. and L. Wang, *Review of condition monitoring and fault diagnosis technologies for wind turbine gearbox.* Procedia Cirp, 2013. **11**: p. 287-290.

7. Sait, A.S. and Y.I. Sharaf-Eldeen, *A review of gearbox condition monitoring based on vibration analysis techniques diagnostics and prognostics*, in *Rotating Machinery, Structural Health Monitoring, Shock and Vibration, Volume 5*. 2011, Springer. p. 307-324.

8. Shah, H. and H. Hirani, *Online condition monitoring of spur gears.* International Journal of Condition Monitoring, 2014. **4**(1): p. 15-22.

9. Devendiran, S. and K. Manivannan, *Vibration Based Condition Monitoring and Fault Diagnosis Technologies For Bearing and Gear Components-A Review.* International Journal of Applied Engineering Research, 2016. **11**(6): p. 3966-3975.

10. Lu, B.L., Yaoyu Wu, Xin Yang, Zhongzhou. *A review of recent advances in wind turbine condition monitoring and fault diagnosis*. in *Power Electronics and Machines in Wind Applications, 2009. PEMWA 2009. IEEE*. 2009. IEEE.

11. Lei, Y.L., Jing Zuo, Ming J He, Zhengjia, *Condition monitoring and fault diagnosis of planetary gearboxes: a review.* Measurement, 2014. **48**: p. 292-305.

12. Dalpiaz, G., A. Rivola, and R. Rubini, *Effectiveness and sensitivity of vibration processing techniques for local fault detection in gears.* Mechanical Systems and Signal Processing, 2000. **14**(3): p. 387-412.

13. Randall, R.B. and I. Books24x, *Vibration-based condition monitoring: industrial, aerospace, and automotive applications*. Vol. 1. Aufl.;1;. 2011, Chichester: Wiley.

14. Jian, J. and B. Zhang, *Rolling element bearing vibration modeling with applications to health monitoring.* Journal of Vibration and Control, 2011: p. 1077546311422241.

15. Aherwar, A., *An Investigation on Gearbox Fault Detection Using Vibration Analysis Techniques a Review.* Australian Journal of Mechanical Engineering, 2012. **10**(2).

16. Pan, M.-C., P.-C. Li, and Y.-R. Cheng, *Remote online machine condition monitoring system.* Measurement, 2008. **41**(8): p. 912-921.

17. Mehala, N., *Condition monitoring and fault diagnosis of induction motor using motor current signature analysis*. 2010, NATIONAL INSTITUTE OF TECHNOLOGY KURUKSHETRA, INDIA.

18. Jardine, A.K., D. Lin, and D. Banjevic, *A review on machinery diagnostics and prognostics implementing condition-based maintenance.* Mechanical systems and signal processing, 2006. **20**(7): p. 1483-1510.

19. Crabtree, C., Y. Feng, and P. Tavner. *Detecting incipient wind turbine gearbox failure: a signal analysis method for on-line condition monitoring*. in *Proceedings of European Wind Energy Conference (EWEC 2010), Warsaw, Poland*. 2010.

20. Faulstich, S., et al., *Windenergie Report Deutschland 2008.* Institut für solare Energieversorgungstechnik (Hrsg.), Kassel, 2008.

21. CRABTREE, C., *Condition monitoring techniques for wind turbines*. 2011, Durham University.

22. Higgs, P.A., Parkin, Rob, Jackson, Mike, Al-Habaibeh Amin, Zorriassatine Farbod, Coy Jo. *A survey on condition monitoring systems in industry*. in *ASME 7th Biennial Conference on Engineering Systems Design and Analysis*. 2004. American Society of Mechanical Engineers.

23. *Plant Maintenance Resource Center, 2002 Condition Monitoring Survey Results.* http://www.plant-maintenance.com/articles/condition-monitoring-survey-02.shtml, 2002.

24. Mobley, R.K., *An introduction to predictive maintenance*. 2002: Butterworth-Heinemann.

25. Barron, R., *Engineering condition monitoring: practice, methods and applications*. 1996, Harlow, Essex: Longman.

26. García Márquez, F.P.T., Andrew Mark Pinar Pérez, Jesús María Papaelias, Mayorkinos, *Condition monitoring of wind turbines: Techniques and methods.* Renewable Energy, 2012. **46**: p. 169-178.

27. Mohanty, A.R., *Machinery condition monitoring: principles and practices*. 2015, Boca Raton, Florida: CRC Press.

28. Yang, W., P.J. Tavner, and R. Court, *An online technique for condition monitoring the induction generators used in wind and marine turbines.* Mechanical Systems and Signal Processing, 2013. **38**(1): p. 103.

29. Yang, W.T., P. J. Crabtree, C. J. Wilkinson, M., *Cost-Effective Condition Monitoring for Wind Turbines.* IEEE Transactions on Industrial Electronics, 2010. **57**(1): p. 263-271.

30. Zhu, J.H., David Qu, Yongzhi Bechhoefer, Eric. *Lubrication oil condition monitoring and remaining useful life prediction with particle filtering*. in *IEEE, Int. Conf. on Prognostics and Health Management.* 2013.

31. Tchakoua, P.W., René Ouhrouche, Mohand Slaoui-Hasnaoui, Fouad Tameghe, Tommy Andy Ekemb, Gabriel, *Wind Turbine Condition Monitoring: State-of-the-Art Review, New Trends, and Future Challenges.* Energies, 2014. **7**(4): p. 2595-2630.

32. Hameed, Z.H., YS Cho, YM Ahn, SH Song, CK, *Condition monitoring and fault detection of wind turbines and related algorithms: A review.* Renewable and Sustainable energy reviews, 2009. **13**(1): p. 1-39.

33. Večeř, P., M. Kreidl, and R. Šmíd, *Condition indicators for gearbox condition monitoring systems.* Acta Polytechnica, 2005. **45**(6).

34. Elforjani, M.A., *Condition monitoring of slow speed rotating machinery using acoustic emission technology*. 2010, Cranfield University.

35. Loutas, T.H.R., D. Pauly, E. Kostopoulos, V., *The combined use of vibration, acoustic emission and oil debris on-line monitoring towards a more effective condition monitoring of rotating machinery.* Mechanical Systems and Signal Processing, 2011. **25**(4): p. 1339-1352.

36. Gu, D.k., JaeGu An, YoungSu Choi, ByeongKeun, *Detection of faults in gearboxes using acoustic emission signal.* Journal of Mechanical Science and Technology, 2011. **25**(5): p. 1279-1286.

37. Tan, C.K., P. Irving, and D. Mba, *A comparative experimental study on the diagnostic and prognostic capabilities of acoustics emission, vibration and spectrometric oil analysis for spur gears.* Mechanical Systems and Signal Processing, 2007. **21**(1): p. 208-233.

38. Hamel, M.A., *Condition monitoring of helical gears using acoustic emission (AE) technology*. PhD Thesis, Cranfield University, 2013.

39. Qu, Y.Z., Junda He, David Qiu, Bin Bechhoefer, Eric. *Development of a new acoustic emission based fault diagnosis tool for gearbox*. in *Prognostics and Health Management (PHM), 2013 IEEE Conference* Gaithersburg, MD: IEEE.

40. Kia, S.H., H. Henao, and G.-A. Capolino, *Gear Tooth Surface Damage Fault Detection Using Induction Machine Stator Current Space Vector Analysis.* IEEE Transactions on Industrial Electronics, 2015. **62**(3): p. 1866-1878.

41. Haram, M., et al. *Electrical Motor Current Signal Analysis using a Modulation Signal Bispectrum for the Fault Diagnosis of a Gearbox Downstream*. in *Journal of Physics: Conference Series*. 2012. IOP Publishing.

42. Kar, C. and A.R. Mohanty, *Monitoring gear vibrations through motor current signature analysis and wavelet transform.* Mechanical Systems and Signal Processing, 2006. **20**(1): p. 158-187.

43. Huda, A.S.N. and S. Taib, *Suitable features selection for monitoring thermal condition of electrical equipment using infrared thermography.* Infrared Physics and Technology, 2013. **61**: p. 184-191.

44. Cardillo, E. and K. Feser, *New approach in thermal monitoring of large power transformers applied on a 350 MVA odaf-cooled unit.* Prace Naukowe Instytutu Podstaw Elektrotechniki i Elektrotechnologii Politechniki Wrocławskiej. Konferencje, 2004. **40**(15): p. 77-81.

45. International Atomic Energy, A., *Implementation strategies and tools for condition based maintenance at nuclear power plants*. 2007: IAEA-TECDOC-1551.

46. Hiroaki, E. and S. Nader, *Gearbox simulation models with gear and bearing faults*, in *Mechanical engineering*. 2012, InTech.

47. Ibrahim, G.R. and A. Albarbar, *Gearbox Fault Features Extraction Using Vibration Measurements and Novel Adaptive Filtering Scheme.* Advances in Acoustics and Vibration, 2012. **2012**.

48. Lebold, M., et al. *Review of vibration analysis methods for gearbox diagnostics and prognostics*. in *Proceedings of the 54th meeting of the society for machinery failure prevention technology*. 2000.

49. Tuma, J., *Gearbox noise and vibration prediction and control.* International Journal of Acoustics and Vibration, 2009. **14**(2): p. 99-108.

50. Kuemmlee, H., T. Gross, and J. Kolerus. *Machine vibrations and diagnostics the world of ISO*. in *Petroleum and Chemical Industry Technical Conference (PCIC), 2013 Record of Conference Papers Industry Applications Society 60th Annual IEEE*. Chicago, IL: IEEE.

51. Daw, O., *Dynamic Modelling and Vibration Analysis for Gear Tooth Crack Detection*. 2015, Luleå University of Technology.

52. Saeed, A., *Online condition monitoring system for wind turbine*. 2008, MSc Thesis, Blekinge Institute of Technology.

53. Carter, D.L., *A new method of processing rolling element bearing signals.* Proceeding 20th Annual Meeting of the Vibration Institute, 1996.

54. Shreve, D.H., *Introduction to vibration technology.* IRD Mechanalysis, Inc. Columbus, Ohio, 1994. **43229**.

55. Khwaja, H.A., S. Gupta, and V. Kumar, *A statistical approach for fault diagnosis in electrical machines.* IETE Journal of Research, 2010. **56**(3): p. 146-155.

56. Jia, S. and I. Howard, *Comparison of localised spalling and crack damage from dynamic modelling of spur gear vibrations.* Mechanical Systems and Signal Processing, 2006. **20**(2): p. 332-349.

57. Shigley, J.E., R.G. Budynas, and C.R. Mischke, *Mechanical engineering design.* 2004.

58. Gope, P., *Machine Design: Fundamentals and Applications*. 2012: PHI Learning Pvt. Ltd.

59. A. Bhatia, B.E., *Basic Fundamentals of Gear Drives.* PDHonline Course M229 (4 PDH), http://www.pdhonline.com/courses/m229/m229content.pdf 2012.

60. Shigley, J.E., C.R. Mischke, and T.H. Brown, *Standard handbook of machine design*. 2004, New York; London: McGraw-Hill.

61. Eftekharnejad, B., *Condition monitoring of gearboxes using acoustic emission.* 2010.

62. Qu, Y., et al., *Gearbox tooth cut fault diagnostics using acoustic emission and vibration sensors—A comparative study.* Sensors, 2014. **14**(1): p. 1372-1393.

63. Dalpiaz, G., et al. *Advances in Condition Monitoring of Machinery in Non-Stationary Operations*. in *Proceedings of the third International Conference on Condition Monitoring of Machinery in Non-Stationary Operations CMMNO*. 2013. Springer.

64. Ding, H. and A. Kahraman, *Interactions between nonlinear spur gear dynamics and surface wear*. Journal of Sound and Vibration, 2007. **307**(3): p. 662-679.

65. Liu, G., *Nonlinear dynamics of multi-mesh gear systems*. 2007, The Ohio State University.

66. Parker, R.G., et al., *Vibration Propagation of Gear Dynamics in a Gear-Bearing-Housing System Using Mathematical Modeling and Finite Element Analysis*. NASA report, NASA/CR-2012-217664, 2012.

67. Lin, J. and R.G. Parker, *Mesh stiffness variation instabilities in two-stage gear systems*. Journal of vibration and acoustics, 2002. **124**(1): p. 68-76.

68. LIN, J. and R. Parker, *Parametric Resonance in Two-Stage Gears from Fluctuating Mesh Stiffness.* IFToMM International Journal of Gearing and Transmissions, 2001. **3**: p. 127-134.

69. Shing, T.-K., *Dynamics and control of geared servomechanisms with backlash and friction consideration.* 1994.

70. Radzevich, S.P. and D.W. Dudley, *Handbook of practical gear design*. 1994: CRC press.

71. Kokare, D. and S. Patil, *Numerical Analysis of variation in mesh stiffness for Spur Gear Pair with Method of Phasing.* 2014.

72. Cheng-zhong, G. and C. Lie. *Effects of teeth surface friction on the vibration of gear transmission*. in *Mechanical and Electronics Engineering (ICMEE), 2010 2nd International Conference on*. 2010. IEEE.

73. Andersson, A., et al., *A dynamic model to determine vibrations in involute helical gears.* Journal of Sound and Vibration, 2003. **260**(2): p. 195-212.

74. Velex, P., *On the modelling of spur and helical gear dynamic behaviour*. arXiv preprint arXiv:1204.2636, 2012.

75. Kang, J.S. and Y.-S. Choi, *Optimization of helix angle for helical gear system.* Journal of mechanical science and technology, 2008. **22**(12): p. 2393-2402.

76. Jiang, H., Y. Shao, and C.K. Mechefske, *Dynamic characteristics of helical gears under sliding friction with spalling defect.* Engineering Failure Analysis, 2014. **39**: p. 92-107.

77. He, S., R. Gunda, and R. Singh, *Inclusion of sliding friction in contact dynamics model for helical gears.* Journal of mechanical design, 2007. **129**(1): p. 48-57.

78. Kahraman, A., J. Lim, and H. Ding. *A dynamic model of a spur gear pair with friction*. in *Proceedings of the 12th IFToMM World Congress*. 2007.

79. Liu, G. and R.G. Parker, *Impact of tooth friction and its bending effect on gear dynamics.* Journal of Sound and Vibration, 2009. **320**(4): p. 1039-1063.

80. Brethee, K.F.G., Fengshou Ball, Andrew D, *Frictional effects on the dynamic responses of gear systems and the diagnostics of tooth breakages.* Systems Science & Control Engineering, 2016. **4**(1): p. 270-284.

81. Vaishya, M. and R. Singh, *Sliding friction-induced non-linearity and parametric effects in gear dynamics.* Journal of sound and vibration, 2001. **248**(4): p. 671-694.

82. Vaishya, M. and R. Singh, *Analysis of periodically varying gear mesh systems with Coulomb friction using Floquet theory.* Journal of Sound and Vibration, 2001. **243**(3): p. 525-545.

83. Xu, H., *Development of a generalized mechanical efficiency prediction methodology for gear pairs*. 2005, PhD Thesis, The Ohio State University.

84. Mizutani, H., Y. Isikawa, and D.P. Townsend, *Effects of lubrication on the performance of high speed spur gears.* 1989.

85. Tharmakulasingam, R., *Transmission error in spur gears: Static and dynamic finite-element modeling and design optimization*. 2010, Brunel University School of Engineering and Design PhD Theses.

86. Åkerblom, M., *Gear Noise and Vibration: A Literature Survey*. TRITA-MMK 2001:11 /ISSN 1400-1179 /ISRN/KTH/MMK/R-01/11-SE, Stockholm, 2001.

87. He, S., et al., *Modeling and Dynamic Analysis of Planetary Gear Transmission Joints With Backlash.* Int. J. Control Autom, 2015. **8**(2): p. 153-162.

88. Zhou, S., et al., *Nonlinear dynamic response analysis on gear-rotor-bearing transmission system.* Journal of Vibration and Control, 2016: p. 1077546316667178.

89. Walha, L., T. Fakhfakh, and M. Haddar, *Backlash effect on dynamic analysis of a two-stage spur gear system.* Journal of Failure Analysis and Prevention, 2006. **6**(3): p. 60-68.

90. De Silva, C.W., *Vibration and shock handbook*. 2005: CRC Press.

91. Errichello, R., *Find the root cause of gear failure - part II.* Plant Services, 2006(http://www.plantservices.com/articles/2006/100/?show=all, Tuesday 07November 2016 at 14:40).

92. *BS 7848:1996, ISO 10825:1995: Gears. Wear and damage to gear teeth. Terminology*. 1996, British Standards Institute.

93. Chaari, F., et al., *Modelling of local damages in spur gears and effects on dynamics response in presence of varying load conditions.* Proceedings of Surveillance, 2011. **6**: p. 1-19.

94. Stokes, A., *Manual gearbox design*. 1992, Linacre House, Jordan Hill, Oxford OX2 8DP: Butterworth-Heinemann Ltd.

95. Rakić, R., *The influence of tribological properties of lubricating oils on the reliability of gears.* Industrial Lubrication and Tribology, 1999. **51**(4): p. 170-179.

96. Pirro, D.M., M. Webster, and E. Daschner, *Lubrication Fundamentals, Revised and Expanded*. 2016: CRC Press.

97. Stachowiak, G.W.B., Andrew W., *Engineering tribology*, ed. F. Edition. 2013: Butterworth-Heinemann.

98. Stachowiak, G.W. and A.W. Batchelor, *Engineering tribology*. 2001, Oxford; Boston: Butterworth-Heinemann.

99. Li, Y. and J. Schnable, *Solving water contamination problems in lubrication oil*. 2000, Elsevier B.V. p. 18-21.

100. Lauer, D.A., *29 Industrial Gear Lubricants.* Synthetics, Mineral Oils, and Bio-Based Lubricants: Chemistry and Technology, 2013: p. 473.

101. Banks, J.C., K.M. Reichard, and M.S. Brought. *Lubrication level diagnostics using vibration analysis*. in *Aerospace Conference, 2004. Proceedings. 2004 IEEE*. 2004. IEEE.

102. Höhn, B., K. Michaelis, and H. Otto, *Flank load carrying capacity and power loss reduction by minimized lubrication.* Journal of Gear manufacturing, 2011: p. 53-62.

103. Höhn, B.-R., K. Michaelis, and H.-P. Otto, *Influence of immersion depth of dip lubricated gears on power loss, bulk temperature and scuffing load carrying capacity.* International Journal of Mechanics and Materials in Design, 2008. **4**(2): p. 145-156.

104. Liu, Y., et al., *Experimental research on reasonable lubricant quantity for transmission gears used in high-speed train.* Science China Technological Sciences, 2012. **55**(12): p. 3455-3461.

105. Radzevich, S.P., *Dudley's handbook of practical gear design and manufacture*. S e c o n d E d i t i o n ed. 2012: CRC Press.

106. Fernandes, P. and C. McDuling, *Surface contact fatigue failures in gears.* Engineering Failure Analysis, 1997. **4**(2): p. 99-107.

107. Walton, D. and A. Goodwin, *The wear of unlubricated metallic spur gears.* Wear, 1998. **222**(2): p. 103-113.

108. Wulpi, D.J., *Understanding how components fail*. 2013, Materials Park, Ohio 44073-0002: ASM international.

109. Ding, H., *Dynamic wear models for gear systems*. 2007, PhD Thesis, The Ohio State University.

110. Osman, T. and P. Velex, *A model for the simulation of the interactions between dynamic tooth loads and contact fatigue in spur gears.* Tribology International, 2012. **46**(1): p. 84-96.

111. Muthuveerappan, G. and R. Thirumurugan. *Prediction of Theoretical Wear in High Contact Ratio Spur Gear Drive*. in *15th National Conference on Machines and Mechanisms, NaCoMM2011-117*.

112. Kuang, J. and A. Lin, *The effect of tooth wear on the vibration spectrum of a spur gear pair.* Journal of Vibration and Acoustics, 2001. **123**(3): p. 311-317.

113. Kumar, A., P. Jain, and P. Pathak. *Study of Tooth Wear on Spur Gear Performance Parameters Using Reverse Engineering*. in *International Conference on Production and Mechanical Engineering (ICPME-2014), Bangkok, Thailand*. 2014.

114. Wojnarowski, J. and V. Onishchenko, *Tooth wear effects on spur gear dynamics.* Mechanism and Machine Theory, 2003. **38**(2): p. 161-178.

115. Stachowiak, G. and A.W. Batchelor, *Engineering tribology*. Fourth Edition ed. 2013: Butterworth-Heinemann.

116. Janakiraman, V., S. Li, and A. Kahraman, *An investigation of the impacts of contact parameters on wear coefficient.* Journal of Tribology, 2014. **136**(3): p. 031602.

117. Wang, W.Q., F. Ismail, and M.F. Golnaraghi, *Assessment of gear damage monitoring techniques using vibration measurements.* Mechanical Systems and Signal Processing, 2001. **15**(5): p. 905-922.

118. Peng, Z., N.J. Kessissoglou, and M. Cox, *A study of the effect of contaminant particles in lubricants using wear debris and vibration condition monitoring techniques.* Wear, 2005. **258**(11): p. 1651-1662.

119. Yang, H., J. Mathew, and L. Ma, *Vibration feature extraction techniques for fault diagnosis of rotating machinery: a literature survey.* (in Asia-Pacific Vibration Conf., Australia, Nov. 12–14, 2003): p. 12–14.

120. Amit Aherwar and M.S. Khalid, *VIBRATION ANALYSIS TECHNIQUES FOR GEARBOX DIAGNOSTIC: A REVIEW.* International Journal of Advanced Engineering Technology, E-ISSN 0976-3945, 2012. **Vol. III**(Issue II): p. 04-12.

121. Tandon, N. and A. Choudhury, *A review of vibration and acoustic measurement methods for the detection of defects in rolling element bearings.* Tribology international, 1999. **32**(8): p. 469-480.

122. Forrester, B.D., *Advanced vibration analysis techniques for fault detection and diagnosis in geared transmission systems*. 1996, Swinburne University of Technology.

123. Cuc, A.I., *Vibration-based techniques for damage detection and health monitoring of mechanical systems*. 2002, University of South Carolina.

124. Jayaswal, P. and A. Aherwar, *Fault Detection and Diagnosis of Gear Transmission System via Vibration Analysis.* The IUP Journal of Mechanical Engineering, 2011. **4**(3): p. 26-43.

125. Bechhoefer, E. and M. Kingsley. *A review of time synchronous average algorithms*. in *Annual conference of the prognostics and health management society*. 2009.

126. Zhen, D., et al., *Acoustic measurements for the combustion diagnosis of diesel engines fuelled with biodiesels.* Measurement Science and Technology, 2013. **24**(5): p. 055005.

127. McFadden, P., *Detection of gear faults by decomposition of matched differences of vibration signals.* Mechanical Systems and Signal Processing, 2000. **14**(5): p. 805-817.

128. McFadden, P. and M. Toozhy, *Application of synchronous averaging to vibration monitoring of rolling element bearings.* Mechanical Systems and Signal Processing, 2000. **14**(6): p. 891-906.

129. Wang, W. and P. McFadden, *Decomposition of gear motion signals and its application to gearbox diagnostics.* Journal of vibration and Acoustics, 1995. **117**(3A): p. 363-369.

130. Forrester, B.D., *Advanced vibration analysis techniques for fault detection and diagnosis in geared transmission systems*. 1996: PhD Thesis, Swinburne University of Technology.

131. Wu, W., et al., *Time domain averaging based on fractional delay filter.* Mechanical Systems and Signal Processing, 2009. **23**(5): p. 1447-1457.

132. Houjoh, H., C. Ratanasumawong, and S. Matsumura, *Utilization of synchronous averaging for inspection of tooth surface undulations on gears (localization of nonmesh harmonic components to individual gear).* Journal of applied mechanics, 2007. **74**(2): p. 269-278.

133. Lebold, M., et al. *Review of vibration analysis methods for gearbox diagnostics and prognostics*. in *Proceedings of the 54th Meeting of the Society for Machinery Failure Prevention Technology*. 2000. Virginia Beach, VA, May 1-4.

134. Rao, S.S., *Mechanical vibrations*. 2004, Upper Saddle River, N.J: Prentice Hall.

135. Braun, S., *Mechanical signature analysis: theory and applications*. 1986: Academic Press Inc., London, UK.

136. Zhang, X., et al., *Features for fault diagnosis and prognosis of gearbox.* Chemical Engineering Transactions, 2013. **33**: p. 1027-1032.

137. Paez, T.L. and A.G. Piersol, *Harris' Shock and Vibration Handbook*. 2010, McGraw-Hill, New York, USA.

138. Peng, Z. and F. Chu, *Application of the wavelet transform in machine condition monitoring and fault diagnostics: a review with bibliography.* Mechanical systems and signal processing, 2004. **18**(2): p. 199-221.

139. Chaari, F., et al., *Gearbox vibration signal amplitude and frequency modulation.* Shock and Vibration, 2012. **19**(4): p. 635-652.

140. Mohammed, O.D., et al., *Vibration signal analysis for gear fault diagnosis with various crack progression scenarios.* Mechanical systems and signal processing, 2013. **41**(1): p. 176-195.

141. Smith, J.D., *Gear noise and vibration*. 2003: CRC Press.

142. Mobley, R.K., *An introduction to predictive maintenance*. 2002, Elsevier Science (USA): Butterworth-Heinemann.

143. Randall, R., *A new method of modeling gear faults.* Journal of Mechanical Design, 1982. **104**(2): p. 259-267.

144. Edwards, S., A. Lees, and M. Friswell, *Fault diagnosis of rotating machinery.* Shock and Vibration Digest, 1998. **30**(1): p. 4-13.

145. Lees, A., J.K. Sinha, and M. Friswell, *The identification of the unbalance of a flexible rotating machine from a single rundown.* Transactions of the ASME-A-Engineering for Gas Turbines and Power, 2004. **126**(2): p. 416-421.

146. Harris, C.M. and A.G. Piersol, *Harris' shock and vibration handbook*. Vol. 5. 2002: McGraw-Hill New York.

147. Gu, F.S., Yimin Hu, N Naid, A Ball, AD, *Electrical motor current signal analysis using a modified bispectrum for fault diagnosis of downstream mechanical equipment.* Mechanical Systems and Signal Processing, 2011. **25**(1): p. 360-372.

148. Stack, J.R., R.G. Harley, and T.G. Habetler, *An amplitude modulation detector for fault diagnosis in rolling element bearings.* IEEE Transactions on Industrial Electronics, 2004. **51**(5): p. 1097-1102.

149. Antoni, J. and R. Randall, *Differential diagnosis of gear and bearing faults.* Journal of Vibration and Acoustics, 2002. **124**(2): p. 165-171.

150. McFadden, P., J. Cook, and L. Forster, *Decomposition of gear vibration signals by the generalised S transform.* Mechanical systems and signal processing, 1999. **13**(5): p. 691-707.

151. Fan, X. and M.J. Zuo, *Gearbox fault detection using Hilbert and wavelet packet transform.* Mechanical Systems and Signal Processing, 2006. **20**(4): p. 966-982.

152. Dale, A., *Gear noise and the sideband phenomenon.* ASME, Gear Research Instltute, 1987. **84-SET-174.**

153. Krishnappa, G. *Gear fault detection parameter development based on modulation techniques*. in *Proceedings of the Fifth International Congress on Sound and Vibration*. 1997.

154. Guoji, S., et al., *Theoretical and experimental analysis of bispectrum of vibration signals for fault diagnosis of gears.* Mechanical Systems and Signal Processing, 2014. **43**(1): p. 76-89.

155. Zhiyuan, Z.H.C.X.L., *Bispectrum Based Gear Fault Feature Extraction and Diagnosis [J]*. Journal of Vibration Engineering, 2002. **3**: p. 022.

156. Rehab, I.T., Xiange Gu, Fengshou Ball, Andrew, *The fault detection and severity diagnosis of rolling element bearings using modulation signal bispectrum*, in *In: Eleventh International Conference on Condition Monitoring and Machinery Failure Prevention Technologies*. 2014: 10th 12th June 2014, Manchester, UK.

157. Tian, X.G., Fengshou Rehab, Ibrahim Abdalla, Gaballa M Ball, Andrew D, *An MSB based robust detector for bearing condition monitoring*, in *28th International Congress of Condition Monitoring and Diagnostic Engineering Management (COMADEM 2015)*. 2015: Buenos Aires, Argentina.

158. Nikias, C.L. and M.R. Raghuveer, *Bispectrum estimation: A digital signal processing framework.* Proceedings of the IEEE, 1987. **75**(7): p. 869-891.

159. Nikias, C.L. and J.M. Mendel, *Signal processing with higher-order spectra.* IEEE signal processing magazine, 1993. **10**(3): p. 10-37.

160. Brillinger, D.R., *Time series: data analysis and theory*. Vol. 36. 2001, USA: Siam.

161. Petropulu, A., *Higher-order spectral analysis.* Digital Signal Processing Handbook, VK Madisetti and DB Williams, editors, Chapman & Hall/CRCnetBASE, 1999.

162. Sundaramoorthy, G., M. Raghuveer, and S. Dianat, *Bispectral reconstruction of signals in noise: Amplitude reconstruction issues.* Institute of Electrical and Electronics Engineers (IEEE), 1990. **38**(7).

163. Peng, Y., et al. *Study on the feature extraction and classification of underwater target radiated noise based on bispectrum*. in *Sixth International Conference on Electronics and Information Engineering*. 2015. International Society for Optics and Photonics.

164. Collis, W., P. White, and J. Hammond, *Higher-order spectra: the bispectrum and trispectrum.* Mechanical systems and signal processing, 1998. **12**(3): p. 375-394.

165. Stack, J.R., R.G. Harley, and T.G. Habetler, *An amplitude modulation detector for fault diagnosis in rolling element bearings.* Industrial Electronics, IEEE Transactions on, 2004. **51**(5): p. 1097-1102.

166. Gu, F., et al. *Motor current signal analysis using a modified bispectrum for machine fault diagnosis*. in *ICCAS-SICE, 2009*. 2009. IEEE.

167. Naid, A., et al. *Bispectrum Analysis of Motor Current Signals for Fault Diagnosis of Reciprocating Compressors*. in *Key Engineering Materials*. 2009. Trans Tech Publ.

168. LuDWIG, L., *Lubrication Selection for Enclosed Gear Drives.* Machinery Lubrication, 2008.

169. *Millers Oils Ltd, Industrial > Machine Oil & Lubricants > Industrial Gear Oil > EP Mineral Oil,* *http://www.millersoils.co.uk/industrial/results-tds-ind.asp?SegmentID=119&market=Industrial*.

170. Davis, J.R., *Gear materials, properties, and manufacture*. 2005: ASM International.

171. *BS 4231:1992, ISO 3448:1992: Classification for viscosity grades of industrial liquid lubricants*. 1992, British Standards Institute.

172. *Brook Crompton, 20 hp, 380-415 V Electric Motor. Available from: http://www.brookcrompton.com/products*.

173. *Vibration Transducer Product Catalogue.* http://www.sensonics.co.uk/products/vibration_transducers/accelerometers.html, 2016.

174. SKF, *SKF Condition Monitoring / Vibration Sensors.* http://www.exvalos.cz/soubory/File/SKF/SNIMACE_VIBRACI.pdf, 1999.

175. Bruce Lent, E.C., *Acceleration/Vibration, Simple Steps to Selecting the Right Accelerometer.* http://www.sensorsmag.com/sensors/acceleration-vibration/simple-steps-selecting-right-accelerometer-1557, 2009.

176. Inman, D.J. and R.C. Singh, *Engineering vibration*. Vol. 3. 2001: Prentice Hall Upper Saddle River.

177. Bauer, C. and M. Day, *Water contamination in hydraulic and lube systems.* Practicing Oil Analysis Magazine, 2007. **9**(9-10).

178. Sander, J., *Water Contamina on: Management of Water During The Lubricant Life Cycle.*

179. Andersson, A. and L. Vedmar, *A dynamic model to determine vibrations in involute helical gears.* Journal of Sound and Vibration, 2003. **260**(2): p. 195-212.

180. Bartelmus, W., et al., *Modelling of gearbox dynamics under time-varying nonstationary load for distributed fault detection and diagnosis.* European Journal of Mechanics-A/Solids, 2010. **29**(4): p. 637-646.

181. He, S., S. Cho, and R. Singh, *Prediction of dynamic friction forces in spur gears using alternate sliding friction formulations.* Journal of Sound and Vibration, 2008. **309**(3): p. 843-851.

182. Omar, F.K., K.A.F. Moustafa, and S. Emam, *Mathematical modeling of gearbox including defects with experimental verification.* Journal of Vibration and Control, 2012. **18**(9): p. 1310-1321.

183. Parey, A., et al., *Dynamic modelling of spur gear pair and application of empirical mode decomposition-based statistical analysis for early detection of localized tooth defect.* Journal of sound and vibration, 2006. **294**(3): p. 547-561.

184. Wu, S., M.J. Zuo, and A. Parey, *Simulation of spur gear dynamics and estimation of fault growth.* Journal of Sound and Vibration, 2008. **317**(3): p. 608-624.

185. Bartelmus, W., *Mathematical modelling and computer simulations as an aid to gearbox diagnostics.* Mechanical Systems and Signal Processing, 2001. **15**(5): p. 855-871.

186. Begg, C.D., C.S. Byington, and K.P. Maynard. *Dynamic simulation of mechanical fault transition*. in *Proceedings of the 54th Meeting of the Society for Machinery Failure Prevention Technology, Virginia Beach, VA*. 2000.

187. Begg, C.D., et al. *Dynamics modeling for mechanical fault diagnostics and prognostics*. in *Maintenance and Reliability Conference (MARCON 99)*. 1999. Gatlinburg, Tennessee, May 10-12, 1999.

188. Van Khang, N., T.M. Cau, and N.P. Dien, *Modelling parametric vibration of gear-pair systems as a tool for aiding gear fault diagnosis*. technische mechanik, 2004. **24**: p. 3-4.

189. Chaari, F., et al., *Effect of spalling or tooth breakage on gearmesh stiffness and dynamic response of a one-stage spur gear transmission.* European Journal of Mechanics-A/Solids, 2008. **27**(4): p. 691-705.

190. Lu, D., X. Gong, and W. Qiao. *Current-based diagnosis for gear tooth breaks in wind turbine gearboxes*. in *Energy Conversion Congress and Exposition (ECCE), 2012 IEEE*. 2012. IEEE.

191. Tian, Z., M.J. Zuo, and S. Wu, *Crack propagation assessment for spur gears using model-based analysis and simulation.* Journal of Intelligent Manufacturing, 2012. **23**(2): p. 239-253.

192. Chen, Z. and Y. Shao, *Dynamic simulation of spur gear with tooth root crack propagating along tooth width and crack depth.* Engineering Failure Analysis, 2011. **18**(8): p. 2149-2164.

193. Mohammed, O.D., M. Rantatalo, and J.-O. Aidanpää, *Dynamic modelling of a one-stage spur gear system and vibration-based tooth crack detection analysis.* Mechanical Systems and Signal Processing, 2015. **54**: p. 293-305.

194. Jammal, A., et al. *An experimental study on high speed helical gears misalignments and dynamic behavior under random loading*. in *Mechanical and Aerospace Engineering (ICMAE), 2016 7th International Conference on*. 2016. IEEE.

195. Jiang, H., et al., *The influence of mesh misalignment on the dynamic characteristics of helical gears including sliding friction.* Journal of Mechanical Science and Technology, 2015. **29**(11): p. 4563-4573.

196. Choy, F., et al., *Analysis of the Effects of Surface Pitting and Wear on the Vibrations of a Gear Transmission System*. 1994, DTIC Document.

197. Ding, H., *Dynamic wear models for gear systems, PhD DISSERTATION*. 2007, The Ohio State University.

198. Ding, H., *A study of interactions between dynamic behavior of gear systems and surface wear*. 2007, The Ohio State University.

199. Flodin, A., *Wear of spur and helical gears.* Royal Institute of Technology, Stockholm, Doctoral Thesis, 2000.

200. Hu, C., et al., *Development of a gear vibration indicator and its application in gear wear monitoring.* Mechanical Systems and Signal Processing, 2016. **76**: p. 319-336.

201. Liu, X., Y. Yang, and J. Zhang, *Investigation on coupling effects between surface wear and dynamics in a spur gear system.* Tribology International, 2016. **101**: p. 383-394.

202. Wang, Q., et al., *Effects of different coupling models of a helical gear system on vibration characteristics.* Journal of Mechanical Science and Technology, 2017. **31**(5): p. 2143-2154.

203. Wang, Q. and Y. Zhang, *A model for analyzing stiffness and stress in a helical gear pair with tooth profile errors.* Journal of Vibration and Control, 2015: p. 1077546315576828.

204. Hedlund, J. and A. Lehtovaara, *A parameterized numerical model for the evaluation of gear mesh stiffness variation of a helical gear pair.* Proceedings of the Institution of Mechanical Engineers, Part C: Journal of Mechanical Engineering Science, 2008. **222**(7): p. 1321-1327.

205. Wan, Z., et al., *Mesh stiffness calculation using an accumulated integral potential energy method and dynamic analysis of helical gears.* Mechanism and Machine Theory, 2015. **92**: p. 447-463.

206. Abbes, M.S., et al., *Dynamic analysis of helical gears supported by rolling elements bearings.* Journal of Theoretical and Applied Mechanics, 2011. **41**(1): p. 33-50.

207. Gu, X., et al., *Analytical investigations on the mesh stiffness function of solid spur and helical gears.* Journal of Mechanical Design, 2015. **137**(6): p. 063301.

208. Walha, L., et al., *Effect of manufacturing defects on the dynamic behaviour for an helical two-stage gear system.* Mécanique & Industries, 2009. **10**(5): p. 365-376.

209. Zeyin, H., et al., *Parametric modeling and contact analysis of helical gears with modifications.* Journal of Mechanical Science and Technology, 2016. **30**(11): p. 4859-4867.

210. Kar, C. and A. Mohanty, *An algorithm for determination of time-varying frictional force and torque in a helical gear system.* Mechanism and machine theory, 2007. **42**(4): p. 482-496.

211. Kar, C. and A. Mohanty, *Determination of time-varying contact length, friction force, torque and forces at the bearings in a helical gear system.* Journal of Sound and Vibration, 2008. **309**(1): p. 307-319.

212. Han, L., et al., *An Improved Algorithm for Calculating Friction Force and Torque in Involute Helical Gears.* Mathematical Problems in Engineering, 2013. **2013**.

213. Jiang, H., *Analysis of time-varying friction excitations in helical gears with refined general formulation.* Proceedings of the Institution of Mechanical Engineers, Part C: Journal of Mechanical Engineering Science, 2015: p. 0954406215583886.

214. Zhang, Y., et al., *Dynamic analysis of three-dimensional helical geared rotor system with geometric eccentricity.* Journal of Mechanical Science and Technology, 2013. **27**(11): p. 3231-3242.

215. Li, C.-F., et al., *Coupled lateral-torsional-axial vibrations of a helical gear-rotor-bearing system.* Acta Mechanica Sinica, 2014. **30**(5): p. 746-761.

216. Wei, J., et al., *Effects of dynamic transmission errors and vibration stability in helical gears.* Journal of Mechanical Science and Technology, 2014. **28**(6): p. 2253-2262.

217. Ma, H., et al., *Time-varying mesh stiffness calculation of cracked spur gears.* Engineering Failure Analysis, 2014. **44**: p. 179-194.

218. Greczyn, W.G. and M.J. Pechersky, *Prediction of Gear Tooth Separation in Single-Stage Gear Systems, Using Numerical Techniques*. 1990, DTIC Document, Technical Report No. TR 90-005: APPLIED RESEARCH LABORATORY.

219. Hearn, E., *Mechanics of Materials, Vol. 2-The Mechanics of Elastic and Plastic Deformation of Solids and Structural Materials*. 1997, Butterworth-Heinemann.

220. Chaari, F., T. Fakhfakh, and M. Haddar, *Analytical modelling of spur gear tooth crack and influence on gearmesh stiffness.* European Journal of Mechanics-A/Solids, 2009. **28**(3): p. 461-468.

221. Sainsot, P., P. Velex, and O. Duverger, *Contribution of gear body to tooth deflections—a new bidimensional analytical formula.* Journal of mechanical design, 2004. **126**(4): p. 748-752.

222. Wan, Z., et al., *An improved time-varying mesh stiffness algorithm and dynamic modeling of gear-rotor system with tooth root crack.* Engineering Failure Analysis, 2014. **42**: p. 157-177.

223. Wang, Q., et al., *A model to determine mesh characteristics in a gear pair with tooth profile error.* Advances in Mechanical Engineering, 2014. **6**: p. 751476.

224. Mohammed, O.D., M. Rantatalo, and U. Kumar. *Analytical crack propagation scenario for gear teeth and time-varying gear mesh stiffness*. in *Proceedings of the International Conference on Applied Mechanics ICAM, Paris, France*. 2012.

225. Jiang, H., *Analysis of time-varying friction excitations in helical gears with refined general formulation.* Proceedings of the Institution of Mechanical Engineers, Part C: Journal of Mechanical Engineering Science, 2015. **229**(13): p. 2467-2483.

226. He, S., R. Gunda, and R. Singh, *Effect of sliding friction on the dynamics of spur gear pair with realistic time-varying stiffness.* Journal of Sound and Vibration, 2007. **301**(3): p. 927-949.

227. Jiang, H. and F. Liu, *Dynamic features of three-dimensional helical gears under sliding friction with tooth breakage.* Engineering Failure Analysis, 2016. **70**: p. 305-322.

228. Chang, Q., et al., *Nonlinear Modeling of Helical Gear Pair with Friction Force and Frictional Torque.* WSEAS Transactions on Applied and Theoretical Mechanics, 2014. **9**: p. 264-274.

229. Jayaswal, P., A. Wadhwani, and K. Mulchandani, *Machine fault signature analysis.* International Journal of Rotating Machinery, 2008. **(2008)**: p. 10.

230. Arunyanart, P., *Fault identification in drivetrain components using vibration signature analysis*. 2015, The University of Akron.

231. Brethee, K.F., et al., *Helical gear wear monitoring: Modelling and experimental validation.* Mechanism and Machine Theory, 2017. **117**: p. 210-229.

232. Osman, T. and P. Velex, *Static and dynamic simulations of mild abrasive wear in wide-faced solid spur and helical gears.* Mechanism and Machine Theory, 2010. **45**(6): p. 911-924.

233. Kahraman, A., P. Bajpai, and N. Anderson, *Influence of tooth profile deviations on helical gear wear.* Journal of Mechanical Design, 2005. **127**(4): p. 656-663.

234. Flodin, A. and S. Andersson, *A simplified model for wear prediction in helical gears.* Wear, 2001. **249**(3): p. 285-292.

235. Flodin, A., *Wear of spur and helical gears, Ph.D. Thesis, KTH Stockholm*, in *Royal Institute of Technology, Stockholm*. 2000.

236. Flodin, A. and S. Andersson, *Simulation of mild wear in helical gears.* Wear, 2000. **241**(2): p. 123-128.

237. Kahraman, A.A., NE Bajpai, P, *A surface wear prediction methodology for parallel-axis gear pairs.* Journal of Tribology, ASME, 2004.

238. Kahraman, A.B., P Anderson, NE, *Influence of tooth profile deviations on helical gear wear.* Journal of Mechanical Design, 2005. **127**(4): p. 656-663.

239. Wink, C.H. *Correlation of Tooth Surface Wear Prediction With Experimental Results of Spur and Helical Gears in Commercial Vehicle Transmissions*. in *in 25th International Conference on Design Theory and Methodology; ASME 2013, Power Transmission and Gearing Conference. 2013. Portland, Oregon, USA: American Society of Mechanical Engineers*. 2013. American Society of Mechanical Engineers.

240. Ding, H., *A study of interactions between dynamic behavior of gear systems and surface wear, PhD Thesis*, in *Mechanical Engineering*. 2007, The Ohio State University.

241. Hu, C., Smith, Wade A, Randall, Robert B, Peng, Zhongxiao, *Development of a gear vibration indicator and its application in gear wear monitoring.* Mechanical Systems and Signal Processing, 2016. **76**: p. 319-336.

242. Velex, P. and P. Sainsot, *An analytical study of tooth friction excitations in errorless spur and helical gears.* Mechanism and Machine Theory, 2002. **37**(7): p. 641-658.

243. Velex, P. and V. Cahouet, *Experimental and numerical investigations on the influence of tooth friction in spur and helical gear dynamics.* Journal of Mechanical Design, 2000. **122**(4): p. 515-522.

244. Brethee, K.F., et al. *Analysis of frictional effects on the dynamic response of gear systems and the implications for diagnostics*. in *21st International Conference on Automation and Computing (ICAC), 2015, University of Strathclyde, Glasgow, UK*. 2015. IEEE. ISBN 978-0-9926801-0-7

245. Yesilyurt, I., F. Gu, and A.D. Ball, *Gear tooth stiffness reduction measurement using modal analysis and its use in wear fault severity assessment of spur gears.* NDT and E International, 2003. **36**(5): p. 357-372.

246. Amarnath, M., S. Chandramohan, and S. Seetharaman, *Experimental investigations of surface wear assessment of spur gear teeth.* Journal of Vibration and Control, 2012. **18**(7): p. 1009-1024.

247. Park, D., *Development of surface wear and lapping simulation models for hypoid gears*. 2009, PhD Thesis, The Ohio State University.

248. Park, D., M. Kolivand, and A. Kahraman, *Prediction of surface wear of hypoid gears using a semi-analytical contact model.* Mechanism and Machine Theory, 2012. **52**: p. 180-194.

249. Bajpai, P., A. Kahraman, and N. Anderson, *A surface wear prediction methodology for parallel-axis gear pairs.* Journal of tribology, 2004. **126**(3): p. 597-605.

250. Chaari, F., et al., *Modelling of local damages in spur gears and effects on dynamics response in presence of varying load conditions.* Proceedings of Surveillance 6, UTC Complegne, 2011: p. 1-19.

251. Manwell, J.F., J.G. McGowan, and A.L. Rogers, *Wind energy explained: theory, design and application*. 2010: John Wiley & Sons.

252. Zhu, J., *Online Industrial Lubrication Oil Health Condition Monitoring, Diagnosis and Prognostics*. 2013, PhD Thesis, University of Illinois at Chicago.

253. Zhu, J., D. He, and E. Bechhoefer, *Survey of lubrication oil condition monitoring, diagnostics, and prognostics techniques and systems.* Journal of Chemical Science and Technology, 2013. **2**(3): p. 100-115.

254. Graça, B. and J. Seabra, *IMPROVING REALIBILITY OF WIND TURBINE GEARBOXES THROUGHT OIL ANALISIS.* 15th International Conference on Experimental Mechanics, ICEM15, 22-27 July 2012, Porto/Portugal, .

255. Kuntner, J., R. Chabicovsky, and B. Jakoby. *Oil condition monitoring using a thermal conductivity sensor*. in *Proc. GMe Forum (Vienna, USA)*. 2005.

256. Boškoski, P., et al., *Detection of lubrication starved bearings in electrical motors by means of vibration analysis.* Tribology international, 2010. **43**(9): p. 1683-1692.

257. Mokšin, V., A. Kilikevičius, and I. Tetsman, *7. Investigation of vibrational behavior of friction pair under starved lubrication conditions.* 2013.

258. Jamšek, J., Đ. Juričić, and P. Boškoski, *Lubrication starved bearings detection in electrical motors vibration signals by means of wavelet bispectral analysis.*

259. de Almeida, R.G. and L.R. Padovese. *Characterization of oil viscosity alterations in a gearbox through vibration signal analysis*. in *17th International Congress of Mechanical Engineering (COBEM2003)*. 2003. November 10-14, Sao Paulo, SP.

260. Smith, J., *Generation of Smith shocks in gears during oil starvation.* Proceedings of the Institution of Mechanical Engineers, Part C: Journal of Mechanical Engineering Science, 1993. **207**(4): p. 279-285.

261. Brethee, K.F., et al., *Influence of Lubricant Starvation on Gearbox Vibration Signatures for Condition Monitoring.* 2016.

262. Changenet, C. and P. Velex, *A model for the prediction of churning losses in geared transmissions—preliminary results.* Journal of Mechanical Design, 2007. **129**(1): p. 128-133.

263. Seetharaman, S. and A. Kahraman, *Load-independent spin power losses of a spur gear pair: model formulation.* Journal of Tribology, 2009. **131**(2): p. 022201.

264. Seetharaman, S., et al., *Oil churning power losses of a gear pair: experiments and model validation.* Journal of Tribology, 2009. **131**(2): p. 022202.

265. Diab, Y., F. Ville, and P. Velex, *Investigations on power losses in high-speed gears.* Proceedings of the Institution of Mechanical Engineers, Part J: Journal of Engineering Tribology, 2006. **220**(3): p. 191-198.

266. Liu, H., et al., *Starved lubrication of a spur gear pair.* Tribology International, 2016. **94**: p. 52-60.

267. Yang, H., J. Mathew, and L. Ma, *Vibration feature extraction techniques for fault diagnosis of rotating machinery: a literature survey.* 2003.

268. Wang, K., *Intelligent condition monitoring and diagnosis systems: a computational intelligence approach*. Vol. 93. 2003: IOS press.

269. Araghi, O.V., *Friction-induced Vibration in Lead Screw Systems*. 2009, University of Waterloo.

270. Abusaad, S.B., Ahmed Brethee, Khaldoon F Gu, Fengshou Ball, Andrew, *Investigating the Effect of Water Contamination on Gearbox Lubrication based upon Motor Control Data from a Sensorless Drive.* In: Proceedings of the 3rd international workshop and congress on eMaintenance: June 1718 Luleå, Sweden : eMaintenance, Luleå tekniska universite, Luleå, pp. 61-67,, 2014.

271. Brethee, K., F. Gu, and A. Ball, *Monitoring of Water Contamination in Gearbox Lubricant Based on Vibration Analysis.* 2017.

272. Jakoby, B. and M.J. Vellekoop, *Physical sensors for water-in-oil emulsions.* Sensors and Actuators A: Physical, 2004. **110**(1): p. 28-32.

273. Johnsen, E.E. and H.P. Rønningsen, *Viscosity of 'live'water-in-crude-oil emulsions: experimental work and validation of correlations.* Journal of Petroleum Science and Engineering, 2003. **38**(1): p. 23-36.

274. Bresme, F. *Pouring oil on troubled water* 2008 17.10.2014]; http://www3.imperial.ac.uk/newsandeventspggrp/imperialcollege/newssummary/news_4-8-2008-10-50-28:[

275. Mehta, N.S., N.J. Parekh, and R.K. Dayatar, *Improve the Thermal Efficiency of Gearbox Using Different Type of Gear Oils.* International Journal of Engineering and Advanced Technology (IJEAT), 2013. **2**(4): p. 120-123.

276. Ku, P., *Gear failure modes—importance of lubrication and mechanics.* ASLe Transactions, 1976. **19**(3): p. 239-249.

277. Lakes, S.C., *Automotive Gear Lubricants.* CHEMICAL INDUSTRIES-NEW YORK-MARCEL DEKKER-, 1999: p. 477-498.

278. Wu, S. and H. Cheng, *A friction model of partial-EHL contacts and its application to power loss in spur gears.* Tribology Transactions, 1991. **34**(3): p. 398-407.

279. Bai, Z.F., H. Zhang, and Y. Sun, *Wear prediction for dry revolute joint with clearance in multibody system by integrating dynamics model and wear model.* Latin American Journal of Solids and Structures, 2014. **11**(14): p. 2624-2647.

280. Oswald, F.B., E.V. Zaretsky, and J.V. Poplawski, *Effect of internal clearance on load distribution and life of radially loaded ball and roller bearings.* Tribology Transactions, 2012. **55**(2): p. 245-265.

281. Harris, T.A. and M.N. Kotzalas, *Advanced concepts of bearing technology: rolling bearing analysis, Fifth Edition*. 2006: CRC Press, Taylor & Francis Group.

282. Sheng, D.-p., et al., *Bifurcation and chaos study on transverse-torsional coupled 2K-H planetary gear train with multiple clearances.* Journal of Central South University, 2016. **23**(1): p. 86-101.

283. Thompson, R. and W. B. *Gear diagnostics and wear detection*. in *Mechanical Engineering*. 1969. ASME-AMER SOC MECHANICAL ENG 345 E 47TH ST, NEW YORK, NY 10017.

284. Randall, R., *A new method of modeling gear faults.* Journal of Mechanical Design-Trans.ASME104, 1982. **104**(2): p. 259-267.

Appendix A: Gearbox Modal Analysis

Mode shapes and frequencies can be used to understand the generation of vibration in a gearbox. In general, the vibration and noise are generated between the mating teeth and propagate through mechanical, air and oil lubricant to the casing of gearbox, as depicted in Figure (A-1). It is important to calculate the resonant excitation with gear mesh frequency, in certain that natural modes can lead to the highest vibrational and acoustic levels, which particularly occurs in a structure when the dynamic forces excite the natural frequencies, or modes of vibration.

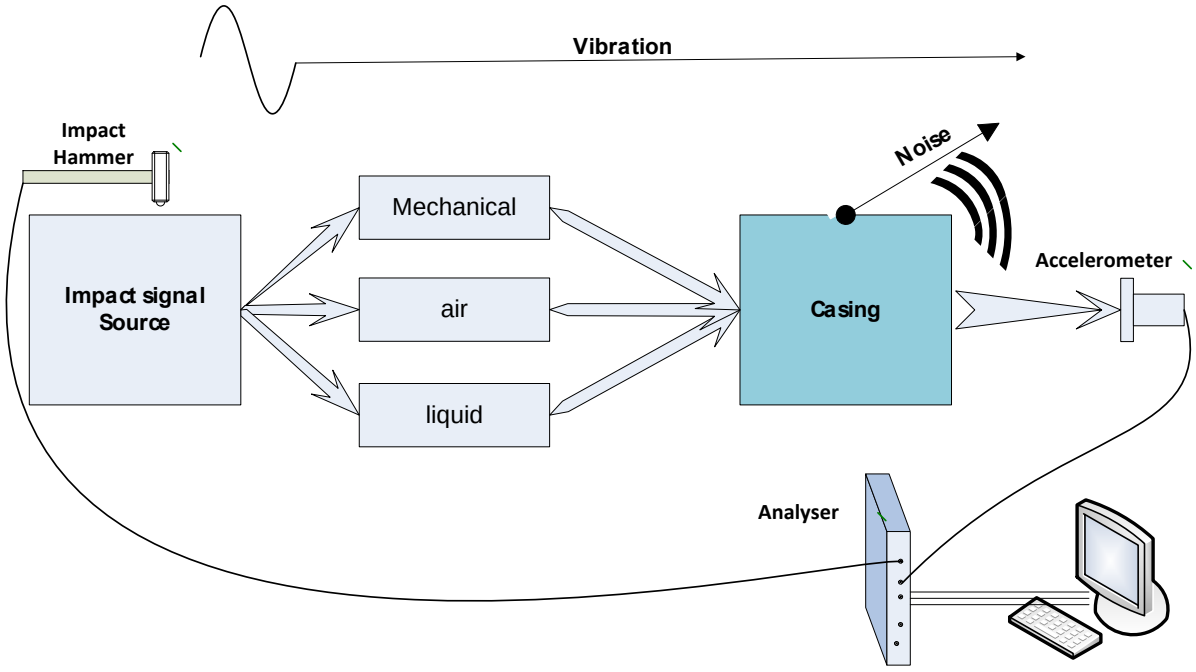

Figure (A-1) Sketch of impact test equipment's and the vibration transmission path of gearbox

FRF is a fundamental measurement of modal analysis that can be determined by either impact hammer testing or shaker testing. An impulse-force hammer (PCB–PIEZOTRONICS) was used to produce trigger force with the help of LMS-analyser and an accelerometer mounted on the gearbox housing was recorded the output signal within high frequency vibration measurements.

The FRF is mainly depend on: source-where the dynamic forces are generated, path-how the dynamic forces are transferred and receiver-how much noise/vibration can be tolerated. Figure (A-2) depicts the FRF signal of the gearbox housing at different input trigger points. The modal

parameters of the gearbox housing can be concluded, which can help to develop an accurate mathematical model of the gearbox complex structure.

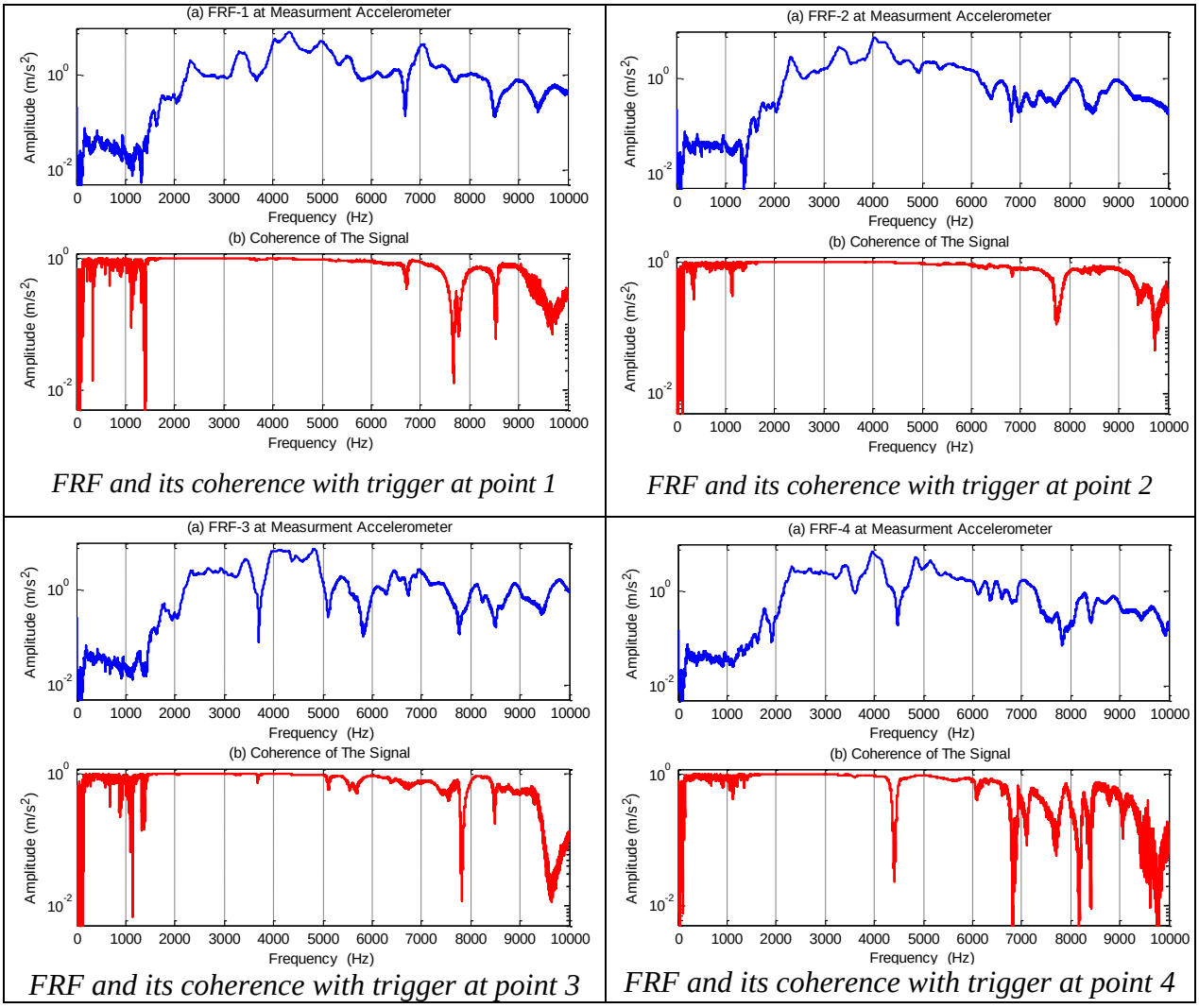

Figure (A-2) FRF and its coherence signals of the gearbox from different trigger points

Appendix B: FEM Modal Analysis of Gearbox Housing

To determine the natural frequencies and the associated eigen modes of gearbox housing, a numerical investigation was achieved based on 3D-FEM. An industrial gearbox model has been verified to measure the natural frequencies and mode shapes. The main part and the full gearbox housing modal were created in SolidWorks and implement in ANSYS Work bench R15.0 to calculate the natural frequencies in free condition. The first 44th natural frequencies of the full gearbox housing model are detailed in Table 1.

Table 2 Gearbox natural frequency

Mode No.	Frequency (Hz)	Mode No.	Frequency (Hz)	Mode No.	Frequency (Hz)
1-6	0	19.	2853.8	32.	3896.7
7.	1244.8	20.	2905.9	33.	3943.6
8.	1480.0	21.	3076.1	34.	3988.8
9.	1767.4	22.	3143.2	35.	4058.7
10.	1928.2	23.	3154.8	36.	4141.3
11.	2064.8	24.	3300.7	37.	4202.4
12.	2077.7	25.	3336.8	38.	4275.2
13.	2391.2	26.	3447.2	39.	4371.3
14.	2418.1	27.	3549.8	40.	4440.6
15.	2438.3	28.	3613.1	41	4474.2
16.	2594.1	29.	3673.7	42	4533.5
17.	2711.4	30.	3793.	43	4571.7
18.	2827.9	31.	3829.1	44	4598.3

The natural frequencies that are closed to the gearbox working frequencies are very important for avoiding resonance and reducing vibration and noise in their working life. Figure (B-1) and Figure (B-2) shows the main natural frequencies and their associated modes of the main part and the full gearbox housing, which can be show that the working frequency range is suitable to prevent maximum amplitude.

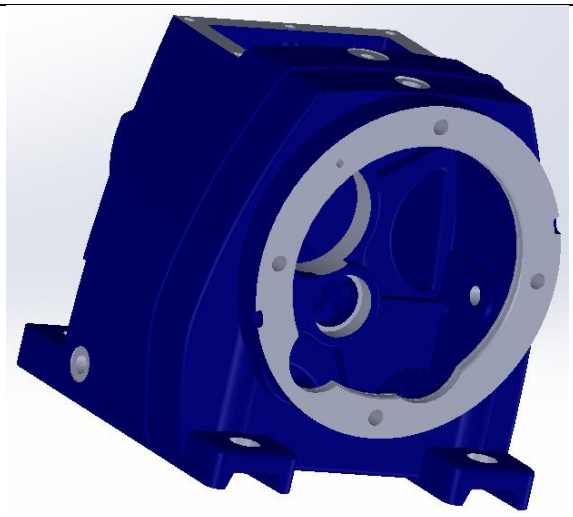

The main part of gearbox housing

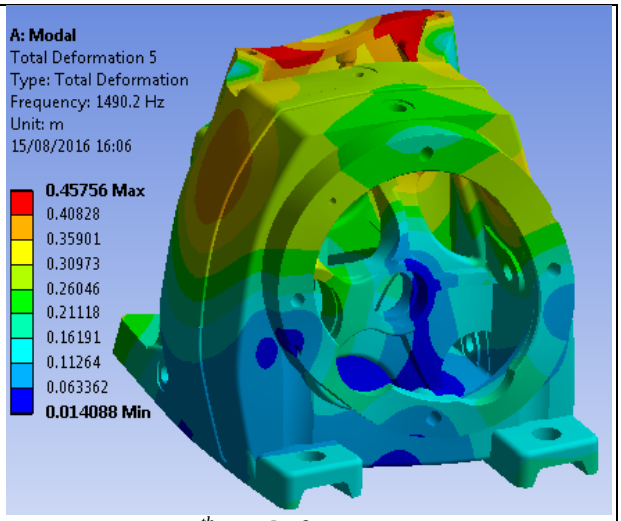

5th Mode f=1490 Hz

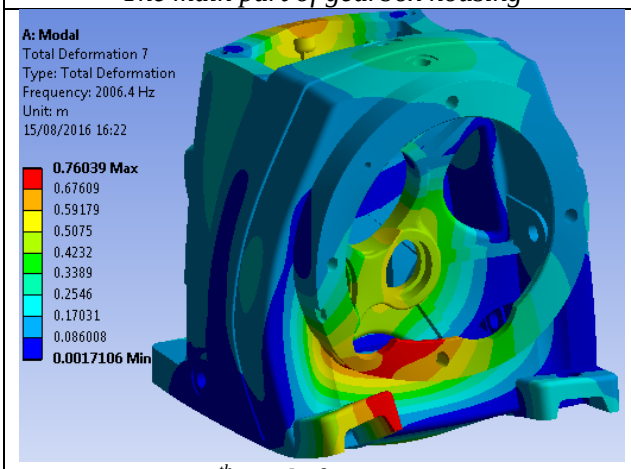

6th Mode f=2006 Hz

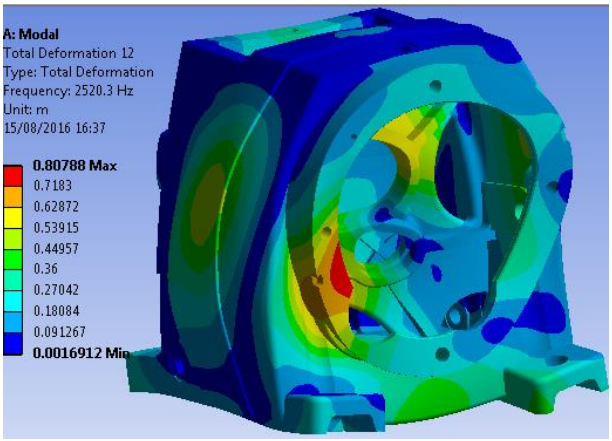

11th Mode f=2520 Hz

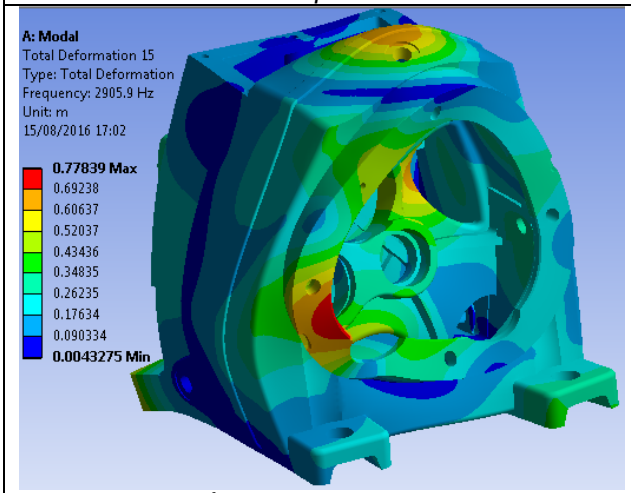

15th Mode f=2905.9 Hz

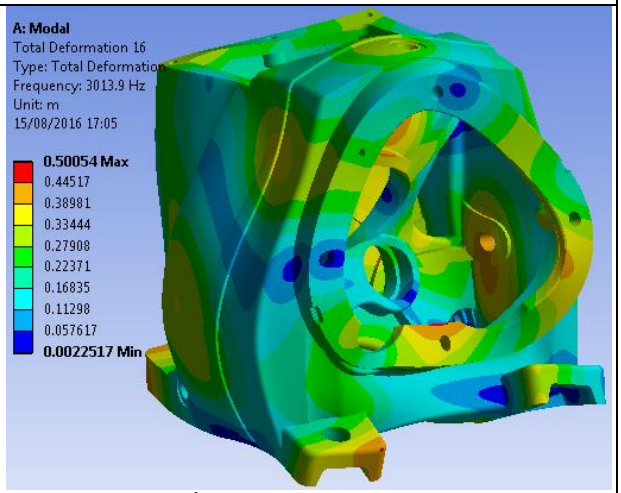

16th Mode f=3013.9 Hz

Figure (B-1) FEM of the main part of the gearbox housing

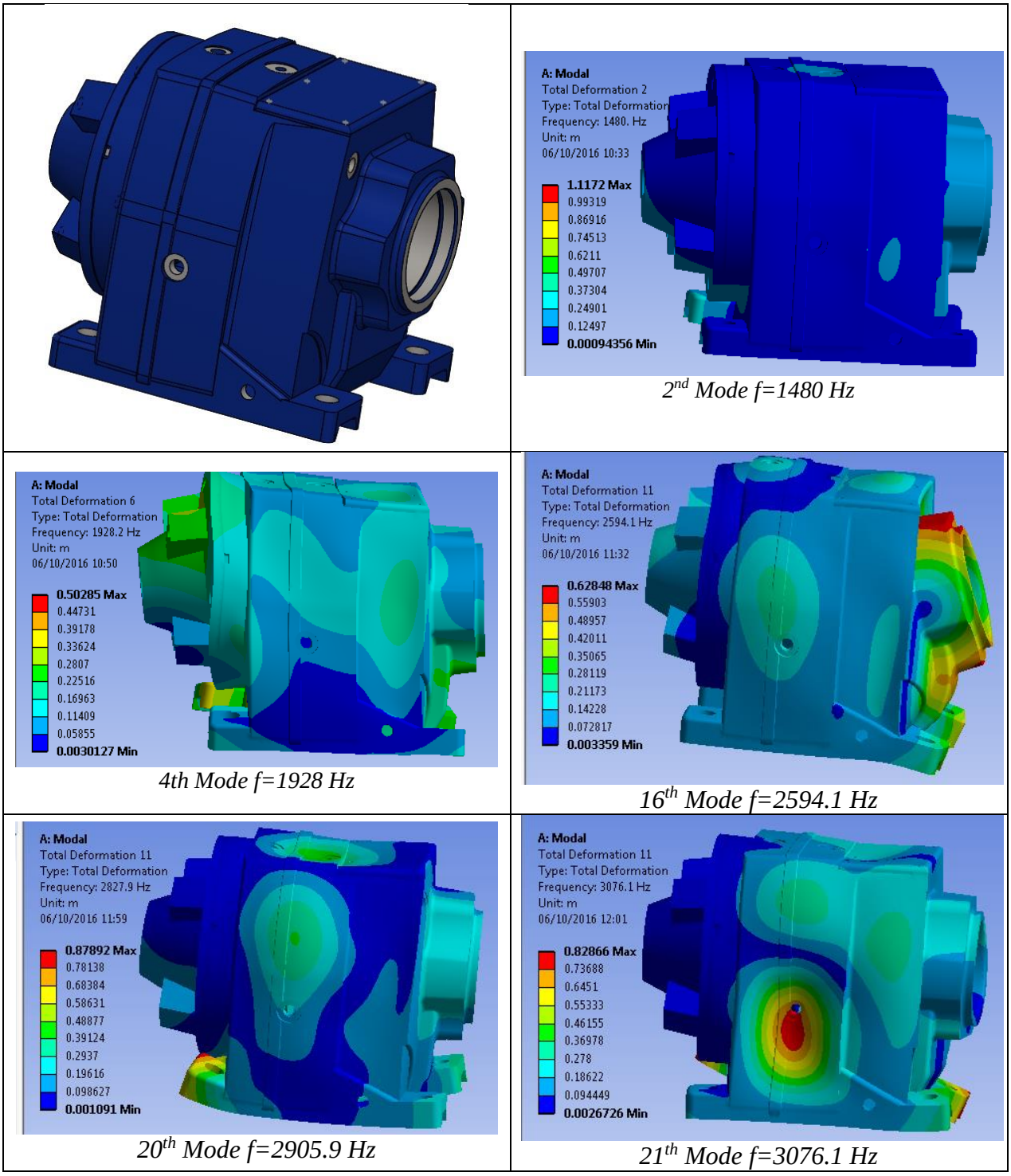

Figure (B-2) FEM of the full gearbox housing